

ENCAPSULATION OF L-CARVONE FOR BURST RELEASE IN CHEWING GUM APPLICATION

by

JULIETTE MARIE CAROLINE DELARUE

A thesis submitted to the University of Birmingham for the degree of

DOCTOR OF PHILOSOPHY

School of Chemical Engineering

University of Birmingham

September 2020

UNIVERSITY OF
BIRMINGHAM

University of Birmingham Research Archive

e-theses repository

This unpublished thesis/dissertation is copyright of the author and/or third parties. The intellectual property rights of the author or third parties in respect of this work are as defined by The Copyright Designs and Patents Act 1988 or as modified by any successor legislation.

Any use made of information contained in this thesis/dissertation must be in accordance with that legislation and must be properly acknowledged. Further distribution or reproduction in any format is prohibited without the permission of the copyright holder.

Abstract

It was desired to use microencapsulation to extend the perception of a spearmint flavour (L-carvone) in chewing gum products by providing a flavour burst delivery.

Core-shell capsules were first synthesised by complex coacervation using gum arabic in combination with chitosan. The stability of the emulsion was investigated by experimental design. It was identified that the best conditions were achieved for a polymer ratio of 6:1 (w/w), using highly concentrated gum arabic (12 wt%), without emulsifier, mixed at 3000 rpm, with a coacervation pH of 3.6, and using physical crosslinking (sodium tripolyphosphate).

The obtained capsules were further coated with an extra layer of gum arabic/chitosan 6:1 (w/w) by spray coating/drying. The final capsules with double coating were characterised by SEM, size distribution, UV-Vis and micromanipulation techniques to assess their mechanical stability. The capsules were finally incorporated in a chewing gum matrix and their release profile was quantified by UV measurements.

Capsules with different mechanical properties can have the potential to produce different bursting profiles, and release flavour at different times. It was proposed that zeta potential measurements should be used in association with turbidity measurements in order to efficiently identify the mixing polymer ratio and optimum coacervation pH for new polymer combinations. The use of corn starch combined with chitosan 3:2 (w/w) at pH 5.2 was identified as a promising alternative.

It is thought that this work offers a useful insight to understand better the critical steps which can influence the complex coacervation process. The proposed methodology of systematically using zeta potential measurements in association with turbidity measurements for investigating new polymer combinations for use in the complex coacervation process can be very beneficial for future work in the food industry as well as in other industrial fields, as it can reduce the necessity for time consuming trials.

Acknowledgements

I would like to express my sincere gratitude to my supervisors, Professor Zhibing Zhang and Professor Peter Fryer, for their invaluable guidance, precious help and advice, constant support as well as their patience, without which it would not have been possible to achieve this work.

I would like to acknowledge the financial support provided by the School of Chemical Engineering at the University of Birmingham, as well as the sponsor of this project, Mondelēz International. I wish to give special thanks to Dr Beth Green, Ms Alison Branch and Dr Barbara Suess from Mondelēz (Reading) for their continuous support throughout the project and their warm welcome at the company when I visited in August 2019, without forgetting Dr Thomas Curwen, Dr Andreas Czepa, Dr Michael Geary, Dr Inés Plasencia, Ms Suraksha Rajagopal and Dr Amir Saberi. I would also like to mention Mr Jean-François Halbardier, Ms Harriet Turner and Dr Haixia Xu for their technical assistance during my visit.

I am grateful to all past and present members of the Microencapsulation and Micromanipulation Group in the School of Chemical Engineering at the University and more specifically to Mr Daniele Baiocco, Dr Mingming Du, Mr Erick León Henneberg, Ms Yingying Li, Dr Javier Marques de Marino, Dr Iryna Mikheenko, Mr Abdullah Mustapha, Professor Colin Thomas, Ms Fanqianhui Yu, Dr Xiaotong Zhang and Dr Yan Zhang for sharing their knowledge and technical expertise with me.

My appreciation also goes to Dr Jie Chen, Dr Tom Mills, Ms Elaine Mitchell, Mr John Noon, Dr Mark Taylor and Dr Fideline Tchuenbou-Magaia for their technical assistance and trainings in FT-IR, Zetasizer, UV and Mastersizer measurements, and spray drying. I am also grateful to

Professor Jon Preece from the School of Chemistry for sharing his knowledge about molecule reactivity with me. Thanks are extended to the administration staff in the School of Chemical Engineering: Ms Jacqueline Deans, Ms Lynn Draper and Ms Mala Patel, for their support.

I want to express a special thank you to my parents and sister for their love, support and encouragement throughout this project.

Last but not least, I would like to thank my partner, Mr Tom Brennan, for his daily support and motivation.

Table of Contents

CHAPTER 1 – Introduction 1

1.1 A Growing Demand in the Food Industry 1

1.2 Chewing gums 2

1.2.1 A history of chewing gum 3

1.2.2 Chewing gum composition 3

1.3 Flavours 4

1.3.1 Definition 4

1.3.2 Most popular flavour compounds in gums 5

1.3.3 Flavour perception mechanism 7

1.4 Microencapsulation 8

1.5 Objectives 11

1.6 Thesis layout 12

CHAPTER 2 – Literature Review 14

2.1 Introduction 14

2.2 Core material: L-carvone 15

2.3 Encapsulation processes 16

2.3.1 Physico-mechanical processes 16

2.3.1.1 Spray drying 16

2.3.1.2 Spray cooling or spray chilling 18

2.3.1.2.1 Spray atomisation 19

2.3.1.2.2 Spinning disc or centrifugal suspension separation 20

2.3.1.2.3 Dripping, coextrusion or annular jet atomisation 21

2.3.1.2.3.1 Stationary nozzle 21

2.3.1.2.3.2 Vibrating nozzle 23

2.3.1.2.3.3 Centrifugal nozzle 24

2.3.1.2.3.4 Submerged nozzle 25

2.3.1.3 Freeze-drying 26
2.3.1.4 Encapsulation using glassy shell materials 27
2.3.1.4.1 Melt injection 27
2.3.1.4.2 Melt extrusion 28
2.3.1.5 Encapsulation by Rapid Expansion of Supercritical Solutions (RESS) 30
2.3.2 Physico-chemical processes 31
2.3.2.1 Emulsions with multilayers 31
2.3.2.2 Coacervation 32
2.3.2.3 Polymer-polymer incompatibility or segregative phase separation 35
2.3.2.4 In situ gelation 36
2.3.2.4.1 Thermal gelation 36
2.3.2.4.2 Ionic gelation or preparation of microspheres by emulsification 37
2.3.2.5 Emulsion phase inversion 37
2.3.2.6 Solvent evaporation 38
2.3.2.7 Co-crystallisation or co-precipitation 39
2.3.2.8 Molecular inclusion 40
2.3.2.9 Liposome entrapment 42
2.3.3 Processes comparison 43
2.3.3.1 Functionality of the particles in the end product 44
2.3.3.2 Nature of the active to be entrapped 45
2.3.3.3 Size of the capsules 46
2.3.3.4 Trigger mechanism for the release of the active 47
2.3.3.5 Cost constraints of the end product 48
2.3.3.6 Storage conditions of the final product 49
2.4 Shell materials 49
2.4.1 Regulations 49
2.4.1.1 Allergens 50
2.4.1.2 Other health risks 51
2.4.1.3 Culture 51
2.4.2 Special restrictions 52
2.4.3 Carbohydrates: polysaccharides 52

2.4.4 Available food grade shell materials for the previously selected techniques 54
2.5 Conclusions.....56
2.5.1 Selection of the encapsulation process.....52
2.5.2 Selection of the wall material.....52

CHAPTER 3 – Materials and Methods 68

3.1 Materials 69
3.1.1 Gum arabic (CAS# 9000-01-5).....69
3.1.2 Water (CAS# 7732-18-5).....70
3.1.3 Chitosan (CAS# 9012-76-4).....70
3.1.4 Acetic acid (CAS# 64-19-7).....71
3.1.5 Non-ionic emulsifiers.....71
3.1.6 L-carvone (CAS# 6485-40-1) 72
3.1.7 Nile red (CAS# 7385-67-3).....72
3.1.8 MCT oils 73
3.1.9 Sodium hydroxide (CAS# 1310-73-2).....73
3.1.10 Crosslinkers.....73
3.1.11 Ethanol (CAS# 64-17-5) 73
3.1.12 Maltodextrin (CAS# 9050-36-6).....73
3.1.13 Shellac coating 74
3.1.14 Chitosan grafting.....74
3.1.15 Nanoparticles.....74
3.1.16 Anionic gelling polysaccharides 75
3.1.16.1 Sodium alginate (CAS# 9005-38-3) 75
3.1.16.2 ι-Carrageenan (CAS# 9062-07-1).....77
3.1.16.3 Gellan gum (CAS# 71010-52-1).....79
3.1.16.4 Xanthan gum (CAS# 11138-66-2).....80
3.1.16.5 Pectin (CAS# 9000-69-5).....82
3.1.16.6 Karaya gum (CAS# 9000-36-6).....83
3.1.17 Guar gum (CAS# 9000-30-0).....84
3.1.18 Starch (CAS# 9005-25-8).....85
3.1.19 Whey protein (CAS# 977102-05-8).....87

3.1.20 Salts 88
3.1.21 Sugar 88
3.2 Methods 88
3.2.1 Mechanical agitation 88
3.2.1.1 Agitation devices 88
3.2.1.2 Stirred tank geometry 89
3.2.2 High-shear mixing 90
3.2.3 Size distribution measurement 91
3.2.4 Drop tensiometry 92
3.2.5 Optical microscopy 94
3.2.6 pH measurement 94
3.2.7 Centrifugation 95
3.2.8 UV-Vis spectroscopy 95
3.2.9 Scanning electron microscopy (SEM) 97
3.2.10 Micromanipulation 97
3.2.11 Zeta potential measurements 99
3.2.12 Turbidity measurements 103

CHAPTER 4 – Design of the Complex Coacervation Process 105

4.1 Introduction 105
4.2 Theoretical consideration of complex coacervation 106
4.2.1 Emulsion stability 106
4.2.1.1 Protein content 108
4.2.1.2 Viscosity 108
4.2.1.3 Emulsifiers 109
4.2.1.4 Stabilisation of the core 110
4.2.1.5 Emulsification speed 111
4.2.1.6 Type of emulsion (O/W or W/O) 111
4.2.2 Coacervation step 112
4.2.2.1 Polymer weight ratio 112
4.2.2.2 Total biopolymer concentration 112
4.2.2.3 Optimum pH 112

4.2.2.4 Agitation....114
4.2.2.5 Coacervation time....115
4.2.3 Hardening of the wall....115
4.2.3.1 Physical hardening....115
4.2.3.2 Chemical hardening....115
4.2.3.3 Crosslinking parameters....115
4.2.4 Gum arabic/chitosan combination....117
4.3 Experimental procedures....119
4.3.1 Preparation of polymer solutions....119
4.3.2 Preparation of emulsions....120
4.3.2.1 Emulsifier selection....120
4.3.2.1.1 Critical HLB determination....121
4.3.2.1.2 Dynamic interfacial tension (IFT)....122
4.3.2.1.3 Surfactant comparison....122
4.3.2.2 Mixing speed....123
4.3.2.3 Formulation optimisation....123
4.3.2.4 Type of emulsion....123
4.3.2.5 Stabilisation of the core....124
4.3.3 Coacervation step....124
4.3.4 Crosslinking....124
4.3.5 Sensory check of L-carvone in capsules....125
4.4 Results and discussion....126
4.4.1 Stability of the emulsion....126
4.4.1.1 Selection of an emulsifier....126
4.4.1.2 Mixing speed....133
4.4.1.3 Optimisation of the emulsion formulation....134
4.4.1.3.1 Identification of the different parameters of the study system....134
4.4.1.3.2 Construction of the experimental design....135
4.4.1.3.3 Study of the effects and interactions....137
4.4.1.4 Type of emulsion check....141
4.4.1.5 Core stabilisation....142

4.4.2 Coacervation step 143
4.4.2.1 Polymer ratio and optimal pH 143
4.4.2.2 Total biopolymer concentration 145
4.4.2.3 Polymer molecular weight 145
4.4.2.4 Coacervation time 145
4.4.3 Crosslinking 146
4.5 Conclusion 149

CHAPTER 5 – Engineering and Characterisation of Microcapsules 151

5.1 Introduction 151
5.2 Theoretical considerations for capsules engineering 152
5.2.1 Spray coating/drying 152
5.2.2 Chitosan grafting 153
5.3 Experimental procedures 154
5.3.1 Encapsulation by complex coacervation 155
5.3.2 Extra coating by spray drying 155
5.3.2.1 Encapsulation efficiency (EE) of wet capsules 155
5.3.2.2 Spray coating/drying process 156
5.3.3 Characterisation 157
5.3.3.1 Morphology 157
5.3.3.2 Size distribution 158
5.3.3.3 Payload 158
5.3.3.4 Mechanical strength 158
5.3.4 Study of the release profile 159
5.3.4.1 Preparation of the gum samples 159
5.3.4.2 Mastication experiment 160
5.3.4.3 Release quantification 161
5.3.5 Alternative engineering methods 162
5.3.5.1 Extra coating with shellac 162
5.3.5.2 Chitosan grafting 163
5.3.5.3 Nanoparticles 163

5.3.6 Statistical analysis 162
5.4 Results and discussion 165
5.4.1 Processing of the coacervated capsules in liquid phase 165
5.4.1.1 Entrapment efficiency 165
5.4.1.2 Mixing speed for the formation of the emulsion 165
5.4.1.3 Reproducibility 167
5.4.2 Characterisation 168
5.4.2.1 Morphology 168
5.4.2.2 Size 171
5.4.2.3 Payload 172
5.4.2.4 Mechanical strength 176
5.4.3 Release profile 185
5.4.4 Alternative engineering of the coacervated capsules 188
5.4.4.1 Shellac coating 188
5.4.4.2 Chitosan grafting 190
5.4.4.3 Nanoparticles 191
5.5 Conclusion 192

CHAPTER 6 – Development of a Technique to Investigate New Wall Material Combinations 194

6.1 Introduction 194
6.2 Theoretical considerations 195
6.3 Experimental procedures 197
6.3.1 Zeta potential measurements 197
6.3.2 Preparation of polymer solutions 197
6.3.3 Turbidity measurements 198
6.3.4 Complex coacervation with different wall material combinations 199
6.3.4.1 Combinations with chitosan 199
6.3.4.2 Combinations with whey protein 200
6.3.5 Spray drying 200
6.3.6 Characterisation 200
6.3.7 Statistical analysis 200

6.4 Results and discussion 201
6.4.1 Polymer mixing ratio 201
6.4.1.1 Gum arabic/chitosan combination checks 201
6.4.1.2 Ionic vs non-ionic polysaccharides 203
6.4.1.3 New anionic polysaccharide/chitosan combinations 205
6.4.1.4 Corn starch behaviour 212
6.4.2 Optimum pH 214
6.4.3 Promising combinations 218
6.4.3.1 Entrapment efficiency 218
6.4.3.2 Morphology 220
6.4.3.3 Payload 221
6.4.3.4 Mechanical strength 222
6.4.4 Trials with proteins (WPI) 228
6.4.4.1 Polymer mixing ratio 228
6.4.4.2 Optimum pH 235
6.4.4.3 Entrapment efficiency and morphology 241
6.4.4.4 Promising combination (corn starch/whey protein) 246
6.5 Conclusion 251

CHAPTER 7 – Overall Conclusions and Future Prospects 253

7.1 Overall conclusions 253
7.2 Recommendations and future work 257
7.2.1 Recommendations for the gum arabic/chitosan combination 257
7.2.1.1 Formulation 257
7.2.1.2 Strengthening of the capsules wall 258
7.2.1.3 Extend the release study to the gas phase 259
7.2.1.4 Storage stability studies 260
7.2.2 Recommendations for the investigation of new shell material combinations 260
7.2.2.1 Recommendations for investigating new shell material combinations 260
7.2.2.2 Composition characterisation of corn starch powder 260

7.2.2.3 Future work on the corn starch/chitosan and corn starch/whey protein combinations 261
7.2.2.4 Extend investigation to other polysaccharide materials 261
7.2.2.5 Extend the combinations to the use of proteins 262
7.2.3 Other recommendations 262
7.2.3.1 Reactivity of L-carvone 262
7.2.3.2 Non-ionic gelling polysaccharide 263

References 264

List of Figures

Figure 1.1: The 10 global leaders of the packaged food industry 2

Figure 1.2: Fruit flavour molecules in chewing gums 5

Figure 1.3: Mint flavour molecules in chewing gums 6

Figure 1.4: Cinnamon (spice) flavour molecule in chewing gums 6

Figure 1.5: The complex mechanism of flavour perception 8

Figure 1.6: Different morphologies of microparticles (a) reservoir microcapsule (b) matrix microsphere (c) multilayer microcapsule (d) multicore microcapsule (e) multi-layered multicore microcapsule (f) coated microsphere (g) multi-layered microsphere 9

Figure 2.1: Spray drying process 17

Figure 2.2: Spinning disc process 21

Figure 2.3: Coextrusion process with stationary nozzle 22

Figure 2.4: Coextrusion process with vibrating nozzle 23

Figure 2.5: Coextrusion process with centrifugal nozzle 24

Figure 2.6: Coextrusion process with submerged nozzle 25

Figure 2.7: Freeze-drying process 26

Figure 2.8: Melt extrusion process 29

Figure 2.9: RESS process 30

Figure 2.10: Double emulsion formation principle 31

Figure 2.11: Layer-by-layer coating process 32

Figure 2.12: Complex coacervation process 34

Figure 2.13: Polymer-polymer incompatibility process 36

Figure 2.14: Solvent evaporation process 38

Figure 2.15: Molecular inclusion structure 41

Figure 2.16: Liposome formation 43

Figure 2.17: Capsules size range depending on the encapsulation process 46

Figure 2.18: Cost trend of the different encapsulation processes depending on their production capacity and their complexity 48

Figure 3.1: Main repeating unit of gum arabic 69

Figure 3.2: Main repeating unit of chitosan 70

Figure 3.3: L-carvone structure 72

Figure 3.4: Example of the structure of alginate blocks composed of M and G repeating units 75

Figure 3.5: Gelling mechanism of alginates showing the “egg box” configuration 77

Figure 3.6: Main repeating units of ι-, κ- and λ-carrageenans 78

Figure 3.7: Main repeating units of gellan gum (a) high acyl (b) low acyl 79

Figure 3.8: Main repeating unit of xanthan gum 81

Figure 3.9: Main repeating unit of pectin 82

Figure 3.10: Main repeating unit of guar gum 85

Figure 3.11: Main repeating units of starch (a) amylose (b) amylopectin 86

Figure 3.12: Different flow patterns (a) axial mixing (pitched-blade impeller) (b) radial mixing (Rushton turbine) 89

Figure 3.13: Standard geometry of a stirred tank with the calculated values imposed by the diameter of a 500 mL jacketed beaker (H: height of liquid, D_T: diameter of the stirred tank, C: clearance from the bottom of the beaker, D_t: diameter of the turbine, h_b: height of the blade, l_b: length of the blade, w_B: width of the baffle) 90

Figure 3.14: Emulsor screens head for Silverson mixer 91

Figure 3.15: (A) Schematic presentation of the pendant drop method (B) Illustration of the calculation elements (P: point of pressure, r_c and r_c’: radii of the horizontal and vertical circles of curvature) 93

Figure 3.16: Calibration curve for UV-Vis measurements of L-carvone in ethanol at 320 nm 96

Figure 3.17: Schematic representation of the micromanipulation rig 98

Figure 3.18: Graphical method for the determination of polymer mixing ratio at a given pH for complex coacervation, based on an example from Espinosa-Andrews *et al.* (2013) presenting zeta potential data as a function of pH for gum arabic and chitosan: (1) determination of the optimal pH, (2) determination of the polymer ratio.....100

Figure 3.19: Folded capillary cell used for the measurement of electrophoretic mobility.....102

Figure 3.20: Phase evolution of polymer complexes in solution monitored by turbidity measurements observed as a function of pH.....103

Figure 4.1: Emulsion destabilisations.....107

Figure 4.2: Different types of coacervated complexes which can be observed by optical microscopy.....114

Figure 4.3: HLB range covered by different emulsifier combinations.....121

Figure 4.4: Schematic flow chart of the complex coacervation process for the encapsulation of L-carvone within a gum arabic/chitosan shell.....127

Figure 4.5: Influence of the HLB value of the Span 60/Tween 60 combination (based on mixing samples 1 – 7, see Table 4.9) on the size of emulsion droplets (the values of the plots were calculated by the software using the average size distribution data based on triplicate measurements, the standard deviation resulting from these average values should be negligible for a sample which is non-aggregating, which was the case for those emulsions).....127

Figure 4.6: Effect of 0.05 wt% of different lipophilic emulsifiers (Span 20, 60, 65, 80 and 85) on the dynamic interfacial tension (IFT) of an L-carvone O/W emulsion (the solid line was only traced to represent the trend of the reference).....129

Figure 4.7: Effect of 0.05 wt% of different hydrophilic emulsifiers (Tween 20, 60, 65, 80 and 85) on the dynamic interfacial tension (IFT) of an L-carvone O/W emulsion (the solid line was only traced to represent the trend of the reference).....130

Figure 4.8: Influence of the chemical family of emulsifiers at HLB = 8 (Span 20, Span 60/Tween 60, Span 80/Tween 80 and Span 85/Tween 85 mixes, see Table 4.10) on the droplet size of the fresh emulsions (the values of the plots were calculated by the software using the average size distribution data based on triplicate measurements, the standard deviation resulting from these average values should be negligible for a sample which is non-aggregating, which was the case for those emulsions).....132

Figure 4.9: Qualitative comparison of the droplet size of emulsions formed at different mixing speeds (500, 700, 900, 1100 and 2000 rpm) for 15 minutes (all scales represent 50 μm).....133

Figure 4.10: Study of the effects given by NemrodW software.....138

Figure 4.11: Interaction effects diagram between the amount of oil (U_2) and the emulsifier concentration (U_3), given by NemrodW software.....139

Figure 4.12: Interaction effects diagram between the amount of oil (U_2) and the gum arabic concentration (U_1), given by NemrodW software. 140

Figure 4.13: L-carvone stained with Nile red fluorescent dye (top) mixed with DI water (bottom). 141

Figure 4.14: Comparison of the emulsion made with L-carvone stained with Nile red by (a) light microscopy and (b) fluorescence microscopy (all scales represent 50 μm). 142

Figure 4.15: Comparison by light microscopy (left) and fluorescence microscopy (right) of dry capsules obtained by mixing L-carvone with different MCT oils: (a) coconut oil (b) palm oil (c) Miglyol 812 N (all scales represent 50 μm). 143

Figure 4.16: Observation of the coacervation step by light microscopy for different gum arabic/chitosan ratios (a) 2:1 (w/w) (pH = 4.1) (b) 4:1 (w/w) (pH = 3.9) (c) 6:1 (w/w) (pH = 3.6) (all scales represent 50 μm). 144

Figure 4.17: Observation of the coacervation phase by light microscopy after the addition of medium molecular weight chitosan (all scales represent 50 μm). 145

Figure 4.18: Observation of the dried capsules by light microscopy having used different crosslinkers (a) tannic acid (b) NaTPP (all scales represent 50 μm). 147

Figure 4.19: Observation of the dried capsules by light microscopy having used the 3-step NaTPP crosslinking modification (all scales represent 50 μm). 148

Figure 4.20: Observation of the dried capsules by (a) light microscopy and (b) fluorescence microscopy (all scales represent 50 μm). 149

Figure 5.1: Proposed mechanism for nanoparticles formed by chitosan grafting 153

Figure 5.2: Proposed mechanism for microcapsules formed by chitosan grafting 153

Figure 5.3: Schematic flow chart for the primary encapsulation of L-carvone within a gum arabic/chitosan shell using complex coacervation 166

Figure 5.4: Schematic illustration of the sample preparation for the quantification of total oil and free oil by UV-Vis spectroscopy 166

Figure 5.5: Schematic illustration of the double emulsion preparation prior to spray drying 166

Figure 5.6: Comparison of the mean EE and entrapment efficiency of two batches where the emulsion was formed with different mixing speeds (data are displayed with standard error bars). 166

Figure 5.7: Average encapsulation efficiency and entrapment efficiency obtained from 12 batches (data are displayed with standard error bars). 167

Figure 5.8: Light microscopy observations of dry powder coacervated capsules further coated with (a) gum arabic/chitosan 6:1 (w/w) (b) gum arabic (c) chitosan (d) gum arabic/maltodextrin 3:1 (w/w) (the blurry area corresponds to aggregated particles being in a different focus plan to the observed capsules) (e) gum arabic/maltodextrin 1:7 (w/w) (f) maltodextrin (all scales represent 50 μm) 169

Figure 5.9: Structure of coacervated capsules further coated by spray coating/drying with gum arabic/chitosan 6:1 (w/w) observed by FEG-SEM imaging, showing (a) the surface morphology and (b) the internal structure of particles. 170

Figure 5.10: Size distribution profile of coacervated capsules further coated with gum arabic/chitosan 6:1 (w/w) obtained with Mastersizer 2000 software. 171

Figure 5.11: Observation of the primary coacervated capsules in liquid phase by light microscopy (all scales represent 50 μm). 172

Figure 5.12: Comparison of capsules (a) directly spray dried and (b) spray coated (GA/Chi 6:1 (w/w)) observed by fluorescence microscopy (all scales represent 50 μm). 173

Figure 5.13: Comparison of the payloads of coacervated capsules further coated with different wall material combinations (GA/Chi 6:1 (w/w), GA, Chi, GA/MD 3:1 (w/w) and 1:7 (w/w), MD) by spray coating/drying (data are displayed with standard error bars) 174

Figure 5.14: Example of a force transducer compliance-like compression profile obtained for capsules which were too hard to rupture. 178

Figure 5.15: Compression profile of a 9 μm capsule with GA/Chi 6:1 (w/w) double coating showing a single rupture event, obtained by micromanipulation (1) rupture event (2) compression of the capsule debris and glass slide. 179

Figure 5.16: Comparison of the trends in average payload value and percentage of particles successfully ruptured by micromanipulation for coacervated capsules further coated with GA/Chi 6:1 (w/w), Chi, GA, GA/MD 3:1 (w/w), GA/MD 1:7 (w/w), or MD. 180

Figure 5.17: Compression profile of a 9 μm capsule with GA/Chi 6:1 (w/w) double coating showing two rupture events, obtained by micromanipulation (1) first rupture event (2) second rupture event (3) compression of the capsule debris and glass slide. 181

Figure 5.18: Rupture force versus particle diameter for coacervated capsules with GA/Chi 6:1 (w/w) double coating 182

Figure 5.19: Nominal rupture stress versus particle diameter for coacervated capsules with GA/Chi 6:1 (w/w) double coating.....184

Figure 5.20: Deformation at rupture versus particle diameter for coacervated capsules with GA/Chi 6:1 (w/w) double coating.....185

Figure 5.21: Average L-carvone cumulative release from the gum matrix with a 0.25 wt% load for two samples of coacervated capsules with different wall materials (GA/Chi or GA/GE) double coating compared with the release profile of free flavour oil in gum (displayed with standard error bars). 186

Figure 5.22: (a) Wet and (b) dry particles obtained from the chitosan grafting inspired protocol, observed by light microscopy (all scales represent 50 μm). 190

Figure 5.23: Dry particles observed by light microscopy obtained with $CaCO_3$ nanoparticles suspended (a) in the aqueous phase and (b) in the oil phase (all scales represent 50 μm). 191

Figure 6.1: Apparent zeta potential of gum arabic and chitosan plotted as a function of pH, displayed with the strength of their electrostatic interaction (SEI) at each pH value (apparent zeta potential data are displayed with standard error bars). 201

Figure 6.2: Apparent zeta potential of guar gum (data are displayed with standard error bars). 203

Figure 6.3: Apparent zeta potential of anionic polysaccharides: sodium alginate, ι-carrageenan, gellan gum, xanthan gum, citrus pectin, karaya gum (data are displayed with standard error bars). 204

Figure 6.4: Apparent zeta potential of sodium alginate and chitosan plotted as a function of pH, displayed with the strength of their electrostatic interaction (SEI) at each pH value (apparent zeta potential data are displayed with standard error bars). 206

Figure 6.5: Apparent zeta potential of ι-carrageenan and chitosan plotted as a function of pH, displayed with the strength of their electrostatic interaction (SEI) at each pH value (apparent zeta potential data are displayed with standard error bars). 207

Figure 6.6: Apparent zeta potential of gellan gum and chitosan plotted as a function of pH, displayed with the strength of their electrostatic interaction (SEI) at each pH value (apparent zeta potential data are displayed with standard error bars). 208

Figure 6.7: Apparent zeta potential of xanthan gum and chitosan plotted as a function of pH, displayed with the strength of their electrostatic interaction (SEI) at each pH value (apparent zeta potential data are displayed with standard error bars). 209

Figure 6.8: Apparent zeta potential of citrus pectin and chitosan plotted as a function of pH, displayed with the strength of their electrostatic interaction (SEI) at each pH value (apparent zeta potential data are displayed with standard error bars). 210

Figure 6.9: Apparent zeta potential of karaya gum and chitosan plotted as a function of pH, displayed with the strength of their electrostatic interaction (SEI) at each pH value (apparent zeta potential data are displayed with standard error bars). 211

Figure 6.10: Comparison of the apparent zeta potentials measured for guar gum, corn starch and gum arabic (data are displayed with standard error bars). 213

Figure 6.11: Measured apparent zeta potential of corn starch and chitosan plotted as a function of pH, displayed with the strength of their electrostatic interaction (SEI) at each pH value (apparent zeta potential data are displayed with standard error bars). 214

Figure 6.12: Macroscopic appearance of pure chitosan solution and its turbidity plotted as a function of pH (data are displayed with standard error bars). 215

Figure 6.13: Macroscopic appearance of gellan gum/chitosan mixture (9:4) as a function of pH. 216

Figure 6.14: Macroscopic appearance of the gum arabic/chitosan mixture 4.5:1 (w/w) and its turbidity plotted as a function of pH (data are displayed with standard error bars). 216

Figure 6.15: Macroscopic appearance of the karaya gum/chitosan mixture 6:5 (w/w) and its turbidity plotted as a function of pH (data are displayed with standard error bars). 217

Figure 6.16: Macroscopic appearance of the corn starch/chitosan mixture 3:2 (w/w) and its turbidity plotted as a function of pH (data are displayed with standard error bars). 218

Figure 6.17: Average entrapment efficiency of the wet capsules obtained by complex coacervation with karaya gum/chitosan and corn starch/chitosan combinations (data are displayed with standard error bars). 219

Figure 6.18: (a) Wet and (b) dry particles obtained with the karaya gum/chitosan 6:5 (w/w) combination, observed by light microscopy (all scales represent 50 μm). 220

Figure 6.19: (a) Wet and (b) dry particles obtained with the corn starch/chitosan 3:2 (w/w) combination, observed by light microscopy (all scales represent 50 μm). 220

Figure 6.20: Light microscopy observations of dry powder corn starch/chitosan coacervated capsules directly spray dried (all scales represent 50 μm). 221

Figure 6.21: Compression profile of a 13 μm coacervated capsule obtained with the corn starch/chitosan 3:2 (w/w) combination, showing a single rupture event when compressed by micromanipulation (1) rupture event (2) compression of the capsule debris and glass slide. 223

Figure 6.22: Compression profile of a 31 μm coacervated capsule obtained with the corn starch/chitosan 3:2 (w/w) combination showing several rupture events, obtained when compressed by micromanipulation. 224

Figure 6.23: Rupture force versus particle diameter for coacervated capsules obtained with the corn starch/chitosan 3:2 (w/w) combination 225

Figure 6.24: Nominal rupture stress versus particle diameter for coacervated capsules obtained with the corn starch/chitosan 3:2 (w/w) combination 226

Figure 6.25: Deformation at rupture versus particle diameter for coacervated capsules obtained with the corn starch/chitosan 3:2 (w/w) combination 227

Figure 6.26: Apparent zeta potential of sodium alginate and whey protein plotted as a function of pH, displayed with the strength of their electrostatic interaction (SEI) at each pH value (apparent zeta potential data are displayed with standard error bars). 229

Figure 6.27: Apparent zeta potential of ι-carrageenan and whey protein plotted as a function of pH, displayed with the strength of their electrostatic interaction (SEI) at each pH value (apparent zeta potential data are displayed with standard error bars). 230

Figure 6.28: Apparent zeta potential of gellan gum and whey protein plotted as a function of pH, displayed with the strength of their electrostatic interaction (SEI) at each pH value (apparent zeta potential data are displayed with standard error bars). 231

Figure 6.29: Apparent zeta potential of xanthan gum and whey protein plotted as a function of pH, displayed with the strength of their electrostatic interaction (SEI) at each pH value (apparent zeta potential data are displayed with standard error bars). 232

Figure 6.30: Apparent zeta potential of citrus pectin and whey protein plotted as a function of pH, displayed with the strength of their electrostatic interaction (SEI) at each pH value (apparent zeta potential data are displayed with standard error bars). 233

Figure 6.31: Apparent zeta potential of karaya gum and whey protein plotted as a function of pH, displayed with the strength of their electrostatic interaction (SEI) at each pH value (apparent zeta potential data are displayed with standard error bars). 234

Figure 6.32: Measured apparent zeta potential of corn starch and whey protein plotted as a function of pH, displayed with the strength of their electrostatic interaction (SEI) at each pH value (apparent zeta potential data are displayed with standard error bars)..... 235

Figure 6.33: Macroscopic appearance of pure whey protein solution and its turbidity plotted as a function of pH (data are displayed with standard error bars). 236

Figure 6.34: Macroscopic appearance of the sodium alginate/whey protein mixture 1:1 (w/w) and its turbidity plotted as a function of pH (data are displayed with standard error bars). .. 237

Figure 6.35: Macroscopic appearance of the ι-carrageenan/whey protein mixture 4:7 (w/w) and its turbidity plotted as a function of pH (data are displayed with standard error bars). 238

Figure 6.36: Macroscopic appearance of the gellan gum/whey protein mixture 1:1 (w/w) and its turbidity plotted as a function of pH (data are displayed with standard error bars). 239

Figure 6.37: Macroscopic appearance of the citrus pectin/whey protein mixture 1:1 (w/w) and its turbidity plotted as a function of pH (data are displayed with standard error bars). 240

Figure 6.38: Macroscopic appearance of the corn starch/whey protein mixture 12:5 (w/w) and its turbidity plotted as a function of pH (data are displayed with standard error bars). 241

Figure 6.39: Average entrapment efficiency of the wet capsules obtained by complex coacervation between whey protein isolate (WPI) and different gelling polysaccharides (ι-carrageenan, gellan gum, citrus pectin, corn starch) (data are displayed with standard error bars). 242

Figure 6.40: (a) Wet and (b) dry particles obtained with the sodium alginate/whey protein 1:1 (w/w) combination, observed by light microscopy (all scales represent 50 μm).....243

Figure 6.41: (a) Wet and (b) dry particles obtained with the ι-carrageenan/whey protein 4:7 (w/w) combination, observed by light microscopy (all scales represent 50 μm).....244

Figure 6.42: (a) Wet and (b) dry particles obtained with the gellan gum/whey protein 1:1 (w/w) combination, observed by light microscopy (all scales represent 50 μm). 244

Figure 6.43: (a) Wet and (b) dry particles obtained with the citrus pectin/whey protein 1:1 (w/w) combination, observed by light microscopy (all scales represent 50 μm). 244

Figure 6.44: (a) Wet and (b) dry particles obtained with the corn starch/whey protein 12:5 (w/w) combination, observed by light microscopy (all scales represent 50 μm). 245

Figure 6.45: Compression profile of a 12 μm coacervated corn starch/whey protein 12:5 (w/w) capsule showing a single rupture event, obtained by micromanipulation (1) rupture event (2) compression of the capsule debris and glass slide. 247

Figure 6.46: Compression profile of a 12 μm coacervated corn starch/whey protein 12:5 (w/w) showing two rupture events, obtained by micromanipulation (1) first rupture event (2) second rupture event (3) compression of the capsule debris and glass slide. 248

Figure 6.47: Rupture force versus particle diameter for coacervated particles obtained with the corn starch/whey protein 12:5 (w/w) combination 249

Figure 6.48: Nominal rupture stress versus particle diameter for coacervated capsules obtained with the corn starch/whey protein 12:5 (w/w) combination 249

Figure 6.49: Deformation at rupture versus particle diameter for coacervated capsules obtained with the corn starch/whey protein 12:5 (w/w) combination 250

List of Tables

Table 2.1: Comparison of particles morphology depending on the encapsulation process 44

Table 2.2: Nature of the core material depending on the encapsulation process 45

Table 2.3: Flavour release trigger mechanisms depending on the encapsulation process 47

Table 2.4: Carbohydrates classification 47

Table 2.5: Available materials for the liposome entrapment process..... 54

Table 2.6: Available materials for the coextrusion with vibrating nozzle process..... 55

Table 2.7: Available materials for the coacervation process. 55

Table 2.8: Comparison of the properties of the different available materials (✓ : yes, × : no, - : no data)..... 58

Table 2.9: pKa values of the remaining available materials 66

Table 4.1: Surfactant functionality groups depending on the HLB and according to the Griffin scale 110

Table 4.2: pKa of the polysaccharides gum arabic and chitosan..... 113

Table 4.3: Comparison of the crosslinking conditions used for pentasodium tripolyphosphate (NaTPP) and tannic acid (RT: room temperature) 117

Table 4.4: Comparison of the preparation of the chitosan solution from the literature. 117

Table 4.5: Comparison of the polymer concentrations from the literature. 118

Table 4.6: Comparison of the emulsification step from the literature. 118

Table 4.7: Comparison of the coacervation step from the literature. 118

Table 4.8: Comparison of the crosslinking step from the literature. 119

Table 4.9: Emulsifier combination 60 HLB spreadsheet. 122

Table 4.10: Emulsifier combinations for reaching a HLB of 8 135

Table 4.11: Parameters and domain values of the experimental design. 135

Table 4.12: Matrix of the model for 3 factors according to the construction of Plackett-Burman designs.....136

Table 4.13: Experimental matrix with experimental response Y (relative d_{32}). 136

Table 4.14: Table of the analysis of the variance calculated with NemrodW software 137

Table 4.15: Estimation of the coefficients calculated with NemrodW software. 137

Table 5.1: Coating solution compositions for spray coating/drying. 157

Table 5.2: Payloads of the different capsule samples to be incorporated in the gum matrix for the release study. 160

Table 5.3: Comparison of the payload data with the glass transition temperature (T_g) of coating materials involved in the spray coating/drying process. 176

Table 5.4: Size range and mean size observed for each sample with secondary coatings for 30 particles randomly selected to be compressed by micromanipulation. 177

Table 5.5: Percentage of capsules ruptured by micromanipulation among a sample of 30 randomly selected particles. 179

Table 6.1: pKa values for different anionic gelling polysaccharides. 195

Table 6.2: Key parameters for the complex interaction of chitosan with selected anionic polysaccharides (alginate, carrageenan, gellan gum, xanthan gum, pectin, karaya gum), based on the literature (v/v: volume ratio, w/w: weight ratio, w/v: weight per volume ratio) 196

Table 6.3: Complex coacervation conditions for the combination of whey protein with different gelling polysaccharides (sodium alginate, ι-carrageenan, gellan gum, citrus pectin, corn starch), based on zeta potential and turbidity measurements. 242

Table 6.4: Comparison of the different mechanical properties (rupture force, nominal rupture stress, deformation at rupture) obtained for the most promising batches (GA/Chi double coating, corn starch/chitosan single coating, and corn starch/WPI single coating). 250

Nomenclature

b_i	Coefficient of the model for parameter i
c	Dimensionless empirical constant
C	Clearance from the bottom of the beaker
$d_{0.1}$	Particle diameter below which 10% of the sample lies
$d_{0.5}$	Mean particle diameter
$d_{0.9}$	Particle diameter below which 90% of the sample lies
d_{32}	Sauter diameter (surface-weighted mean diameter)
d_i	Diameter of the particle i
d_p	Diameter of the particle
D_t	Diameter of the turbine
D_T	Diameter of the stirred tank
E	Mean energy dissipation rate per unit mass of fluid
f(κa)	Henry's function
F_R	Force at rupture
g	Gravitational acceleration
G	Shear rate
h_b	Height of the blade
H	Height of liquid
k	Stiffness
l_b	Length of the blade
n_0	Initial number of droplets per volume unit

n_i	Number of particles with the same d_i
N	Agitation speed
P	Pressure
ΔP	Difference of pressure
pH	Hydrogen potential
pH_{opt}	Optimal coacervation pH
pI	Isoelectric point
R^2	Coefficient of determination
R^2a	Adjusted coefficient of determination
r_c	Radius of curvature
r_d	Radius of the droplet
r_p	Radius of the particle
S_t	Sensitivity of the force transducer
T_g	Glass transition temperature
t_R	Time of rupture
U_i	Parameter i
ΔU_R	Change in voltage at rupture from the baseline
w_B	Width of the baffle
X_i	Factor i
x_R	Deformation at rupture
Y	Response parameter
Z	Collision frequency

Greek symbols

γ	Interfacial tension
δ_R	Displacement at rupture
ε	Dielectric constant
ζ	Zeta potential
η	Viscosity
η_Φ	Shear viscosity of the continuous phase
μ	Electrophoretic mobility
ν_c	Creaming velocity
ν_t	Velocity of the transducer
ρ_d	Density of the droplet
ρ_Φ	Density of the continuous phase
σ_R	Nominal rupture stress

Abbreviations

2D	Two-Dimensional
3D	Three-Dimensional
ANOVA	Analysis Of Variance
BC	Before Christ
BSA	Bovine Serum Albumin
BSE	Bovine Spongiform Encephalopathy
CA	Cellulose Acetate
CAB	Cellulose Acetate Butyrate

CAP	Cellulose Acetate Propionate
Chi	Chitosan
CMC	CarboxyMethyl Cellulose
DAG	DiAcylGlycerol
DE	Dextrose Equivalent
DI Water	DeIonised Water
DMSO	DiMethyl SulfOxide
DoE	Design of Experiments
EDX	Energy Dispersive X-ray
EE	Encapsulation Efficiency
EISA	Evaporation-Induced Self-Assembly
EU	European Union
FAA	Food Additives Amendment
FCSP	Fucosee-Containing Sulphated Polysaccharide
FDA	Food and Drug Administration
FTIR	Fourier Transform InfraRed
FTU	Formazin Turbidity Unit
GA	Gum Arabic
GC-FID	Gas Chromatography – Flame Ionisation Detector
GC-MS	Gas Chromatography – Mass Spectrometry
GE	Gelatine
GMO	Genetically Modified Organism
GRAS	Generally Recognised As Safe
HA	High Acyl

HDL	High Density Lipoproteins
HEC	HydroxyEthyl Cellulose
HLB	Hydrophilic-Lipophilic Balance
HM	High-Methoxyl
HPC	HydroxyPropyl Cellulose
HPMC	HydroxyPropyl Methyl Cellulose
IFT	InterFacial Tension
LA	Low Acyl
LbL	Layer-by-Layer
LDL	Low Density Lipoproteins
LM	Low-Methoxyl
MC	MethylCellulose
MCT	Medium-Chain Triglycerides
MD	MaltoDextrin
NaTPP	Sodium TriPolyPhosphate
NIOSH	National Institute for Occupational Safety and Health
O/W	Oil-in-Water
O/W/O	Oil-in-Water-in-Oil
PEG	Poly(Ethylene Glycol)
PES	Processed Eucheuma Seaweed
PGA	Propylene Glycol Alginate
PPI	Pea Protein Isolate
PVP	PolyVinylPyrrolidone
PTR-MS	Proton Transfer Reaction – Mass Spectrometry

RESS	Rapid Expansion of Supercritical Solutions
RT	Room Temperature
SEI	Strength of the Electrostatic Interaction
SEM	Scanning Electron Microscopy
SPI	Soybean Protein Isolate
TEM	Transmission Electron Microscopy
US	United States
USD	United States Dollar
UV-Vis	UltraViolet-Visible
v/v	Volume ratio
W/O	Water-in-Oil
W/O/W	Water-in-Oil-in-Water
w/v	Weight per volume ratio
w/w	Weight ratio
WPI	Whey Protein Isolate
wt%	Percentage based on weight

CHAPTER 1 – Introduction

This PhD was sponsored by Mondelēz International, which is one of the world's biggest multinational companies in the fields of confectionery, snacks and beverages, and is currently the 2nd global leader after Mars in the chewing gum sector, with 24.4% of the market share (Euromonitor, 2020).

1.1 A Growing Demand in the Food Industry

Consumers are becoming more and more demanding in general, and that is also true in the food industry, which is a market giant (Sobel *et al.*, 2014). The annual sales of the packaged food industry currently account for more than 2000 billion US dollars worldwide, and are expected to reach 3000 billion dollars by 2024 (Euromonitor, 2020). This sector can fall into several subcategories, among which: baby food; baked goods; breakfast cereals; confectionery; dairy products; edible oils; ice cream and frozen desserts; processed fruits and vegetables; processed meat and seafood; ready meals; rice, pasta and noodles; sauces, dressings and condiments; savoury snacks, sweet biscuits, snack bars and fruit snacks; soups; and sweet spreads. The 10 global leaders of this industry are Nestlé, PepsiCo, Mondelēz International, Danone, Kraft Heinz, Unilever, Mars, Lactalis, Ferrero, and Inner Mongolia Yili (see Figure 1.1) (Alexander *et al.*, 2011; Euromonitor, 2020).

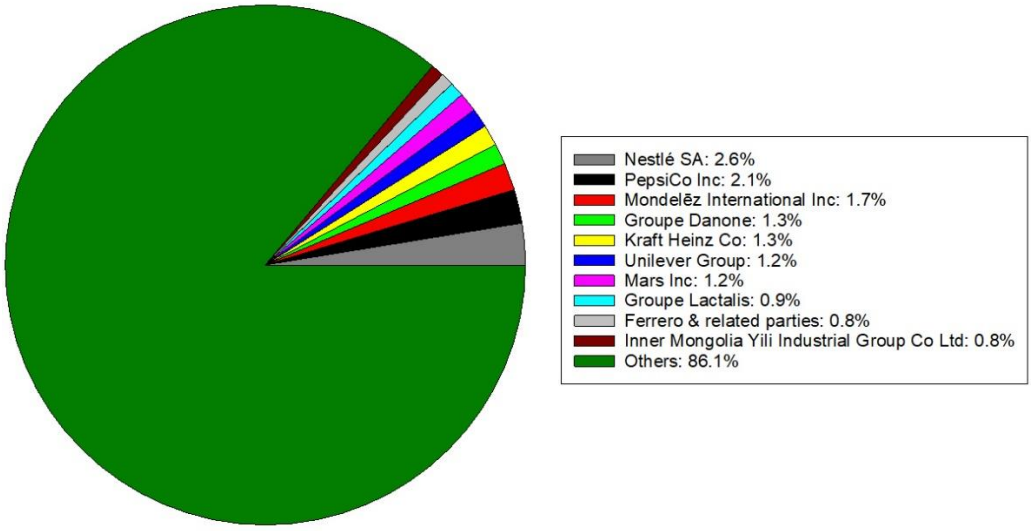


Figure 1.1: The 10 global leaders of the packaged food industry (adapted from Euromonitor, 2020).

Customers' needs are constantly changing and they are looking for affordable, innovative and fun products. Especially in snacks and confectionery, the food experience has to be enjoyable and creative since the objective is not to just satisfy a primary need here (Meyers, 2014; Klinjapo and Krasaekoopt, 2018).

It is a competitive market in which companies are striving to develop innovative products in order to thrive.

1.2 Chewing gums

Chewing gums belong to the confectionery category, which represented 8% of the total market size of the packaged food industry in 2019 (Euromonitor, 2020).

It is necessary to differentiate chewing gums and bubble gums. Bubble gums are more elastic than chewing gums due to a higher polymer content which makes it possible for them to form big bubbles (Edwards, 2003; Klinjapo and Krasaekoopt, 2018).

The term "chewing gum" will be used in what follows to represent either of these two products.

1.2.1 A history of chewing gum

Evidence of the use of chewing gum in Europe date as far back as the Middle Stone Age (from 7000 BC), in the form of tar, which was a sticky material coming from denatured birch bark, and used for making tools and weapons (Milov *et al.*, 1998; Gustaitis, 1998; Aveling and Heron, 1999).

John Bacon Curtis was the first one to start selling chewing gums in 1848, which he made from heated bark rolled into a slab and covered by corn starch to prevent stickiness. Those were later replaced by flavoured paraffin gum. In 1891, William Wrigley, Jr. entered the chewing gum industry and started using baking powder in his products (Gustaitis, 1998; Meyers, 2014). The first protocol to make chewing gum was patented in 1869 (Tyler, 1869).

Nowadays, gums are used not only as a recreational snack, but also for medicinal and hygiene purposes, such as teeth cleaning and breath freshening. Chewing has also been found to release stress and promote focus (Gustaitis, 1998; Aveling and Heron, 1999; Masumoto *et al.*, 2009; Mäkinen, 2014; Klinjapo and Krasaekoopt, 2018).

1.2.2 Chewing gum composition

Chewing gum is made of several main components. The hydrophobic gum base is made out of a blend of natural and synthetic gums and resins, which can be associated with antioxidants, elastomers, emulsifiers, fillers, humectants, plasticizers and softeners, leading to the final gum

matrix. The originally used natural latex chicle is now combined with a mixture of synthetic polymers, mostly polyvinyl esters. The taste is given by the addition of flavours. It can be enhanced by the presence of sugar or its derivatives, honey and corn syrup, although they are more and more replaced by other sweetener alternatives, such as acesulfame potassium, aspartame, saccharin, stevia, sucralose and sugar alcohols. Colouring can also be added for getting a colourful and attractive aspect. A coating like wax can optionally be applied (Milov *et al.*, 1998; Machiulskiene *et al.*, 2001; Edwards, 2003; Potineni and Peterson, 2008b; Mäkinen, 2014, Meyers, 2014; Sobel *et al.*, 2014; Klinjapo and Krasaekoopt, 2018).

1.3 Flavours

1.3.1 Definition

A flavour is usually the result of a blend of natural and/or synthetic organic compounds. The more than 1200 different flavours that are used in food products fall into three distinct categories: natural flavours, among which are essential oils, that can be extracted from plant ingredients or even animals and microbial fermentations; nature-identical flavours, which are chemically modified from natural raw materials; and artificial flavours, which are fully synthesised by the means of chemical processes and are not present in nature (Sobel *et al.*, 2014; Klinjapo and Krasaekoopt, 2018). Flavours are volatile and sensitive substances that can be affected by light, oxygen, temperature and processing conditions (Klinjapo and Krasaekoopt, 2018).

1.3.2 Most popular flavour compounds in gums

There are a few common flavours that are especially used in chewing gums. Some of them result from complex mixtures of compounds, such as liquorice and some fruit flavours: apple, blueberry, pineapple, strawberry and watermelon, which can be either natural extracts or nature-identical flavour mixtures. For some other simpler aroma, one main molecule is responsible for the flavour profile. This is the case for banana, cinnamon, grape, lemon, peppermint, raspberry, spearmint and wintergreen aroma (see Figures 1.2 to 1.4) (Gustaitis, 1998; Potineni and Peterson, 2008b; Wong *et al.*, 2009; Nogourani *et al.*, 2012; Meyers, 2014; Sobel *et al.*, 2014; Mostafa *et al.*, 2017; Klinjapo and Krasaekoopt, 2018; Li *et al.*, 2019).

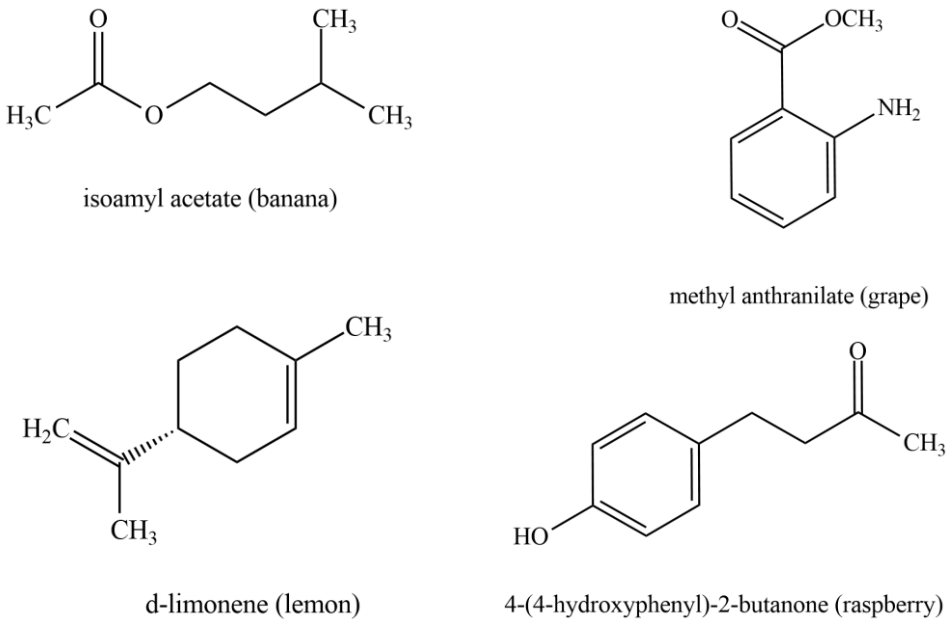
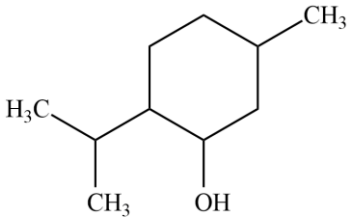
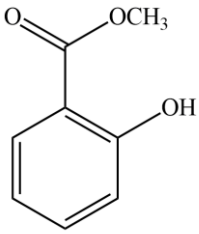


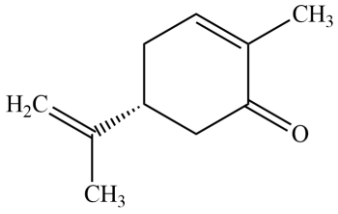
Figure 1.2: Fruit flavour molecules in chewing gums (adapted from Wong et al., 2009; Sobel et al., 2014; Klinjapo and Krasaekoopt, 2018; Merck, 2020).



menthol (peppermint)

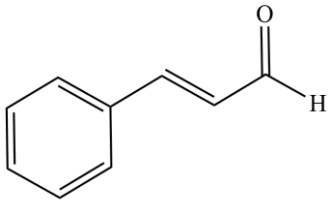


methyl salicylate (wintergreen)



L-carvone (spearmint)

Figure 1.3: Mint flavour molecules in chewing gums (adapted from Potineni and Peterson, 2008b; Wong *et al.*, 2009; Nogourani *et al.*, 2012; Meyers, 2014; Klinjapo and Krasaekoopt, 2018; Li *et al.*, 2019; Sigma Aldrich, 2020).



cinnamaldehyde (cinnamon)

Figure 1.4: Cinnamon (spice) flavour molecule in chewing gums (adapted from Nogourani *et al.*, 2012; Sigma Aldrich, 2020).

William J. White was the first to introduce mint flavour into his chewing gums, and used corn syrup to promote the flavour absorbance into the gum base (Gustaitis, 1998).

Many flavours are hydrophobic and will have a strong affinity for the gum base. Thus, the more hydrophilic the flavour compound, the better the release during mastication as it will be more

efficiently extracted in the saliva (Potineni and Peterson, 2008b; Meyers, 2014; Sobel *et al.*, 2014).

1.3.3 Flavour perception mechanism

Natural and synthetic flavours are responsible for the flavour in food. Flavour perception is multisensory and involves olfactory, gustatory and somatosensory senses. It starts with visual detection and the assimilation of colour with a particular known taste; this is the flavour expectation (Spence, 2015). Flavours are then perceived by a complex mechanism involving the activation of neuroreceptors in the mouth and the nose, which are then integrated in the orbitofrontal cortex (see Figure 1.5). Once released from the food bolus, flavour compounds partition between the water phase composed of the saliva, which contains binding proteins and enzyme, and the gas phase in the oral cavity, which is olfactory. The volatile aroma compounds in the breath are sent to the retronasal area during the swallowing step. The flavour intensity will depend both on the compound concentration in the food system and the chewing frequency and force to deliver it, as well as the volume of saliva secreted by the salivary glands during mastication, which will influence the dilution level of the volatiles. The non-volatile aroma molecules dissolved in the saliva are sensed thanks to taste buds located mainly on the tongue. There are five main taste qualities: bitter, salty, sour, sweet and umami (Laing and Jinks, 1996; Davidson *et al.*, 1999; van Ruth and Roozen, 2000; Delwiche, 2004; Haahr *et al.*, 2004; Pfeiffer *et al.*, 2005; Auvray and Spence, 2008; Salles *et al.*, 2011; Sobel *et al.*, 2014; Spence, 2015).

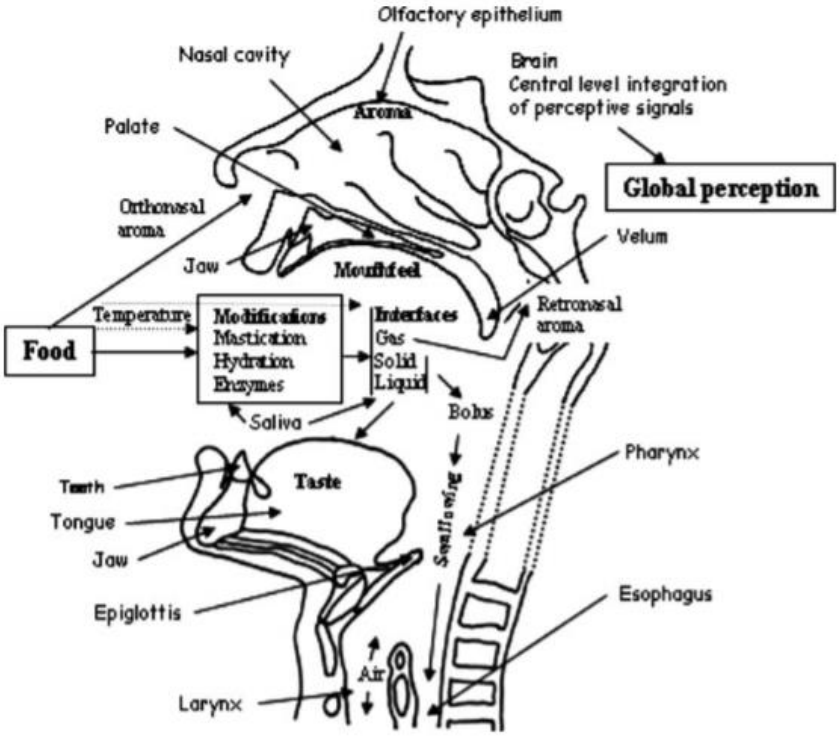


Figure 1.5: The complex mechanism of flavour perception (Salles *et al.*, 2011).

The perception of flavours can lead to sensory experiences of different natures, such as odour, taste and cooling sensation. Very often, the flavour profile will determine the main attribute of the product, to which the consumer will associate a preference. The flavour experience is linked to each individual's memories and feelings (Sobel *et al.*, 2014; Klinjapo and Krasaekoopt, 2018).

1.4 Microencapsulation

Encapsulation is a method which consists in entrapping an active ingredient (or core material or fill or internal phase or payload phase) inside an inert shell (or carrier or coating or encapsulant or external phase or matrix or membrane or wall material) (Nedovic *et al.*, 2011;

Sri *et al.*, 2012; Klinjapo and Krasaekoopt, 2018). It has been encountering a growing interest as it can give added value to products. It is particularly sought in a desire to answer the market needs, always looking for more innovative and convenient consumer goods.

Microparticles can be defined as spherical units with a size ranging from 1 µm to 1 mm in diameter (Parida *et al.*, 2013).

There are two main types of microparticles. Reservoir type or core-shell microcapsules have a gas, liquid or solid core containing the active agent, surrounded by a solid uniform shell. Matrix type particles, or microspheres, are presented as a solid porous matrix of wall material with embedded droplets of active ingredient, or even with the core material dissolved within the carrier. More complex systems can be obtained by modification of those two types of particles: such as having a multilayer coating, or having several cores, or even by combination of a matrix with a single or multi-layered coating (see Figure 1.6) (Uhlemann *et al.*, 2002; Zuidam and Shimoni, 2010; Sobel *et al.*, 2014; Klinjapo and Krasaekoopt, 2018).

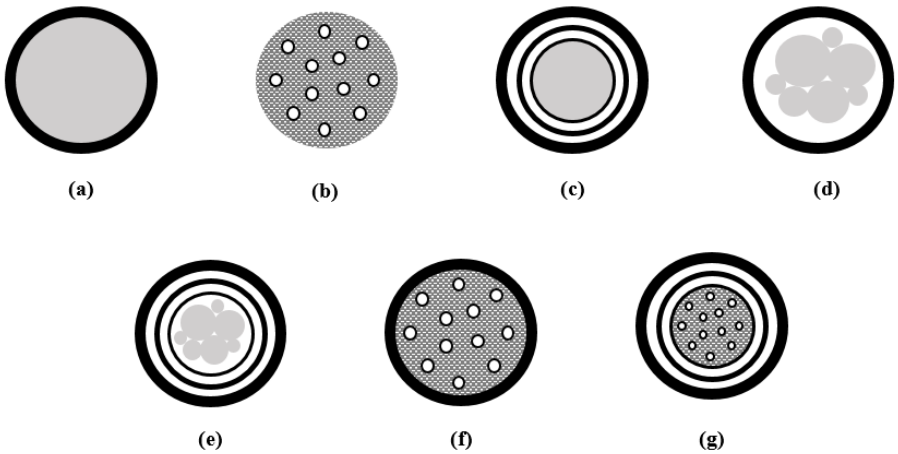


Figure 1.6: Different morphologies of microparticles (a) reservoir microcapsule (b) matrix microsphere (c) multilayer microcapsule (d) multicore microcapsule (e) multi-layered multicore microcapsule (f) coated microsphere (g) multi-layered microsphere (adapted from Zuidam and Shimoni, 2010; Nesterenko *et al.*, 2013; Klinjapo and Krasaekoopt, 2018).

The most common encapsulated components in foods are antioxidants, colours, essential oils, fatty acids, flavours, minerals, pharmaceutical actives, probiotics, sweeteners and vitamins (Nedovic *et al.*, 2011; Sri *et al.*, 2012; Nesterenko *et al.*, 2013; Meyers, 2014; Sobel *et al.*, 2014; Klinjapo and Krasaekoopt, 2018).

Microencapsulation can provide several advantages in the tuning of flavour performance in food products (Uhlemann *et al.*, 2002; Zuidam and Shimoni, 2010; Nesterenko *et al.*, 2013; Meyers, 2014; Sobel *et al.*, 2014; Klinjapo and Krasaekoopt, 2018):

- Provide an easier and safer handling (liquid active ingredient under a solid form, no dust)
- Protect volatile substances from evaporation, oxidation, moisture and light
- Prevent any chemical interaction with the food matrix
- Deliver an active with a controlled release
- Mask a bad odour or taste
- Increase the stability of the active ingredient
- Generate a desirable texture effect

There are several ways of triggering the release of the core material, such as dehydration, diffusion, dissolution, enzymatic effect, mechanical action, or melting. The temperature and pH of the medium also are influencing parameters (Uhlemann *et al.*, 2002; Madene *et al.*, 2006; Zuidam and Shimoni, 2010; Nesterenko *et al.*, 2013; Sobel *et al.*, 2014).

A main drawback of the use of flavour encapsulation for chewing gum application is that the high processing costs may increase the final price of the product, which needs to be taken into account when considering this technique (Meyers, 2014).

1.5 Objectives

The project focussed on the release of mint flavour, using L-carvone (spearmint) as a model flavour compound, for burst and sustained releases in chewing gum application. “Burst release” means a clear peak of flavour can be detected when breaking the capsules, which is usually obtained by mechanical trigger.

Encapsulation can, among other advantages, protect volatile substances from evaporation and oxidation, as well as deliver the active ingredient with a controlled release in time and space (Uhlemann *et al.*, 2002; Zuidam and Shimoni, 2010). As a matter of fact, it seemed to be the appropriate technology to reach the goals of this project.

Chewing gums usually have a strong initial flavour release which remains for around 5 minutes of mastication time (Meyers, 2014). Indeed, the sensory perception becomes lower and lower over time with a constant flavour release, which was suspected to be due to either a lack of sweetness perception or to adaptation (decrease responsiveness of the neuroreceptors) (Davidson *et al.*, 1999). The phenomenon that sweetness perception can be enhanced through pulsed delivery was studied by monitoring the taste perception in liquid solutions (Burseg *et al.*, 2010). The delivery of 2.5 seconds pulses of sucrose over a period of 40 seconds helped to enhance the taste perception, which could also be an interesting approach for chewing gum application. For this project, it was desired to deliver a technology that can release flavour as controlled bursts into the consumer’s mouth throughout the length of the chew, which was expected to be for a period of 10 minutes, although it can vary quite significantly from one consumer to the other. There is still no mature technology allowing to encapsulate L-carvone within a food grade shell capable to provide this prolonged flavour release to date, as flavour

delivery systems are specific to each food type, expensive and difficult to scale up (Bouquerand *et al.*, 2012; Sobel *et al.*, 2014a).

There were thus several objectives for this investigation. It was first intended to develop different sets of stable, food grade capsules which could survive the chewing gum processing step and achieve burst delivery at different timepoints during chewing. Ideally, the particles should be obtained as a low moisture, free-flowing powder, so that they could be easily incorporated into the gum matrix. Finally, it was planned to combine the different optimised technologies in a chewing gum matrix to obtain the desired final application.

Developing such a technology in the food industry is particularly challenging regarding the restricted choice of materials which can be used. Although some well-established systems have been used in other industry fields, they usually involve some efficient but toxic chemicals, and the stakes of this project is to achieve such high-performances with alternative food grade materials (Bouquerand *et al.*, 2012; Sobel *et al.*, 2014a).

1.6 Thesis layout

This thesis falls into seven chapters.

This chapter, **Chapter 1**, introduces the food industry and different elements involved in the research project, which are chewing gum applications and their composition, a focus on flavour ingredients in chewing gum and how they are perceived, and a general description of microencapsulation technique. The objectives are also detailed.

Chapter 2 presents a literature review of the state of the art, which is composed of three main parts. The core material to be encapsulated is first presented. Then the different encapsulation

processes available for food application are described in detail. Finally, the food grade encapsulation materials that can be used in the food industry are introduced, as well as the regulations which apply to food products.

In **Chapter 3**, the different materials used in the following work and their suppliers are presented, and the detailed procedures of preparing microcapsules and principles of the different characterisation techniques are explained.

Chapter 4 presents the tuning of each key step necessary to design the full complex coacervation process. A particular focus is given to the emulsion step, the shearing conditions, and the crosslinking step.

Chapter 5 describes the different characterisation methods used to evaluate the capsules obtained through the previously established process. It also considers some further engineering and modifications of the particles, following the complex coacervation process.

Chapter 6 shows a possible extension of the process to different and possibly new polymer combinations, which could even be broadened to other fields than the food applications, thanks to the definition of a method based on the combination of specific characterisation techniques.

Finally, **Chapter 7** aims at giving the general conclusions of this research work, and proposes some ideas and recommendations for future investigations on this subject.

CHAPTER 2 – Literature Review

2.1 Introduction

About 20 to 25% of commercialised flavours are sold in an encapsulated form (Gupta *et al.*, 2016). With a great number of encapsulation methods and available materials, designing an encapsulation process from scratch for a given application can prove to be quite challenging (Oxley, 2014).

A good knowledge of processes and materials is required to make an educated choice. Several parameters need to be taken into account when choosing an encapsulation process so as to suit the target application (Desai and Park, 2005; Zuidam and Shimoni, 2010; Mishra, 2015):

1) the desired functionality of the capsules in the end product
2) the physicochemical characteristics of the active to be entrapped
3) the processing conditions the capsules will have to undergo
4) the desired size of the capsules
5) the release mechanism to liberate the core material
6) the available coating materials for each technique
7) the legal issues to consider
8) the cost constraints of the end product
9) the storage conditions of the final product

In order to develop a suitable technology for burst delivery, a well-adapted encapsulation process first had to be determined according to the needs of the project. After that, an adequate

shell material had to be chosen in accordance with the selected technique, which respected the regulations imposed in the food industry.

This chapter is divided in three main parts. First the core material which should be encapsulated for sustained release in chewing gum is briefly presented. Then the different encapsulation processes available for use in food application are reviewed to identify the technique which would best fit the aims of the project and the nature of the core. Finally, the properties of food grade wall materials are compared for use with the selected encapsulation process.

2.2 Core material: L-carvone

L-carvone was proposed by Mondelēz as a reference spearmint flavour compound.

The nature and physicochemical properties of the core material are important information when designing an encapsulation process (Madene *et al.*, 2006; Vasisht, 2014; Mishra, 2015; Gupta *et al.*, 2016; Tolve *et al.*, 2016). Analysing those properties allows to make several observations. L-carvone is first and foremost found in liquid form. It should be safe to use it at temperatures up to 90ºC, as this is below its flash point. This flavour oil does not seem to be very volatile when comparing its boiling point (227-231ºC) and flash point (94ºC) values with other essential oils, such as limonene from which it is derived (respectively 176-178ºC and 48ºC) (Sobel *et al.*, 2014b). L-carvone is lipophilic and should be found in the oil phase as is practically immiscible with water (1.3-1.65 g/L) (Yalkowsky *et al.*, 2010). It is also less dense than water (0.959 at 25ºC) (Merck, 2020).

2.3 Encapsulation processes

There is a large variety of possible encapsulation processes of different natures: physico-mechanical or physico-chemical.

2.3.1 Physico-mechanical processes

2.3.1.1 Spray drying

It is one of the processes which is the most used in the food industry (80-95%). Spray drying leads to porous microspheres, with a size of 10 µm to 5 mm. It is used to encapsulate both polar and non-polar compounds (Uhlemann *et al.*, 2002; Desai and Park, 2005; Madene *et al.*, 2006; Gharsallaoui *et al.*, 2007; Zuidam and Shimoni, 2010; Nedovic *et al.*, 2011; Fang, 2012; Sri *et al.*, 2012; Meyers, 2014; Sobel *et al.*, 2014b; Mishra, 2015; Gupta *et al.*, 2016; Tolve *et al.*, 2016; Klinjapo and Krasaekoopt, 2018).

This technique consists of a shock-drying process which transforms a liquid active into a dry particle. The active ingredient is emulsified or put in suspension in an aqueous solution containing the dissolved carrier material. It is then uniformly atomised at high temperature and sprayed through a high-pressure nozzle or a spinning wheel in a hot cylinder, usually with a hot co-current flow of air (see Figure 2.1). In the chamber, the water droplets are evaporated by heat transfer in the hot air stream which instantaneously heats the particles to a temperature of about 100 ºC, while bigger molecules of active agent are retained in the oil phase droplets, which are coated by the formation of a semi-permeable fine film at their surface. For the encapsulation of food ingredients however, the use of a counter-current flow of air is more desirable as it allows a faster evaporation and thus a shorter exposure time to high temperatures. The dried particles go through a cyclone separator and are collected in a container at the end (Uhlemann *et al.*, 2002; Desai and Park, 2005; Madene *et al.*, 2006; Rosa, 2006; Gharsallaoui

et al., 2007; Zuidam and Shimoni, 2010; Fang, 2012; Sri *et al.*, 2012; Jacobs, 2014; Gupta *et al.*, 2016; Klinjapo and Krasaekoopt, 2018).

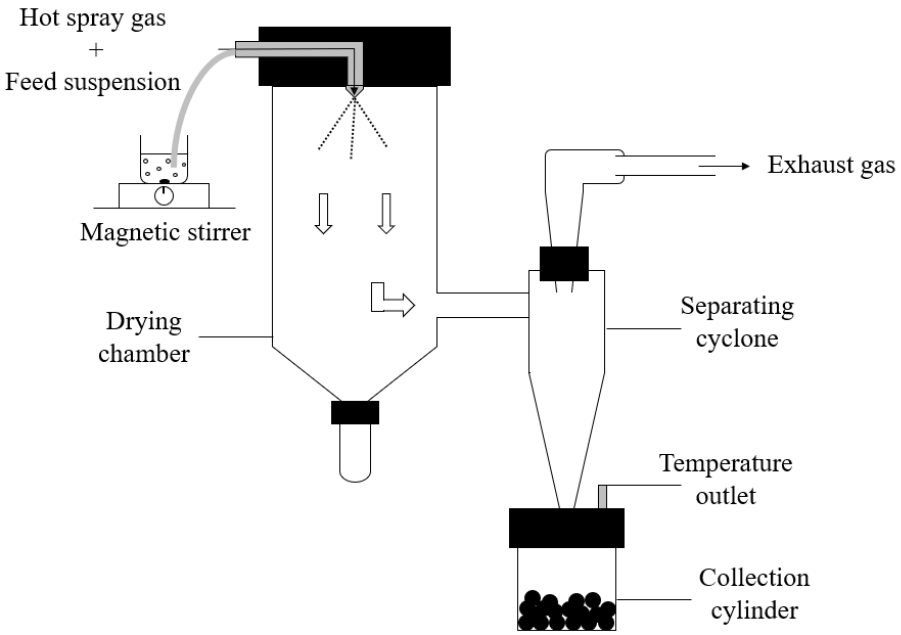


Figure 2.1: Spray drying process (adapted from Zuidam and Shimoni, 2010; Fang, 2012; Nesterenko *et al.*, 2013a; Jacobs, 2014).

The payload is typically 5 to 50%. The release mechanism of the active is based on dissolution; and this technique provides an upfront (fast and uniform) flavour release (Uhlemann *et al.*, 2002; Madene *et al.*, 2006; Zuidam and Shimoni, 2010; Meyers, 2014; Sobel *et al.*, 2014b; Mishra, 2015; Gupta *et al.*, 2016).

It is one of the well-established encapsulation techniques, it produces capsules with a good flowability, and presents the advantage of being cost-effective, the process can be run continuously, at a large scale, it is quite easy and fast to operate, and a wide variety of coating materials can be used with good results. However, there are also a few drawbacks of this process. Heat sensitive actives can be partially deteriorated by evaporation or oxidation during the process, especially flavours are likely to have a boiling point lower than the one of water.

The drying conditions in different parts of the heat chamber can vary slightly, controlling the size distribution of the particles is not simple, and the quality of the capsules obtained is not optimum as the encapsulation efficiency is low due to a considerable amount of product loss on the chamber wall (Uhlemann *et al.*, 2002; Desai and Park, 2005; Madene *et al.*, 2006; Rosa, 2006; Gharsallaoui *et al.*, 2007; Feng *et al.*, 2009; Zuidam and Shimoni, 2010; Nedovic *et al.*, 2011; Fang, 2012; Sri *et al.*, 2012; Nesterenko *et al.*, 2013a; Gupta *et al.*, 2016).

If larger particles are required, the further compaction granulation or agglomeration processes can be applied, as they lead to capsules of about 200 μm to 3 mm. For compaction granulation, the spray dried material is compressed under high pressure into chunks in presses, and pounded in smaller bits. The particles are stronger than those obtained by the sole spray drying process as they are less porous. For agglomeration, the spray dried material is introduced in a fluidised bed and a binding material is sprayed onto the particles so they can adhere together. The main drawback is that this further processing usually reduces the flavour load by four times (5 to 20%) (Uhlemann *et al.*, 2002; Madene *et al.*, 2006; Rosa, 2006; Zuidam and Shimoni, 2010; Meyers, 2014; Gupta *et al.*, 2016).

2.3.1.2 Spray cooling or spray chilling

In the food industry, 3 to 10% of particles are made using this technique. Spray cooling/chilling is used to obtain lipid-coated particles, which are thus insoluble in water. This method leads to microspheres or multicore microcapsules with a size of a few μm to several mm. It is used to encapsulate either polar or non-polar compounds (Oxley, 2012b; Sobel *et al.*, 2014b; Gupta *et al.*, 2016).

Spray cooling, or spray congealing, is similar to spray drying, but there is no drying involved since the process is carried out at a low temperature. It is more particularly employed when

release by heat is desired. There are different atomisation methods possible: spray atomisation (pressure nozzles, rotary atomisation, two-fluid nozzles, ultrasonic nozzles), spinning disc, or dripping technologies (Madene *et al.*, 2006; Zuidam and Shimoni, 2010; Nedovic *et al.*, 2011; Oxley, 2012b; Meyers, 2014).

2.3.1.2.1 Spray atomisation

This is the most common atomisation method for spray cooling or spray chilling. It leads to microspheres with a size between 20 and 200 μm (Uhlemann *et al.*, 2002; Desai and Park, 2005; Madene *et al.*, 2006; Zuidam and Shimoni, 2010; Nedovic *et al.*, 2011; Oxley, 2012b; Meyers, 2014; Mishra, 2015; Gupta *et al.*, 2016).

The active agent is dissolved or put in suspension in a molten lipid carrier material, such as vegetable or hydrogenated oils. The melting point of the lipids used for spray chilling is usually lower (32-42°C) than the ones used for spray cooling (45-122°C). The slurry is atomised through a nozzle and sprayed into a low temperature chamber this time, with a cold, co-current flow of air. The droplets of lipid solidify with the temperature drop, but there is no evaporation of water, and droplets of lipid can still adhere to already cooled solid particles while they are in the chamber. A fine suspension of free-flowing particles is finally obtained, which is usually collected in a cyclone and filter bags. The active ingredient is released above the melting point of the coating lipid material, so this technique is usually used for particles due to be used for cooking (Uhlemann *et al.*, 2002; Desai and Park, 2005; Madene *et al.*, 2006; Zuidam and Shimoni, 2010; Nedovic *et al.*, 2011; Oxley, 2012b; Gupta *et al.*, 2016).

The payload is 10 to 20%. The release mechanism of the active is based on diffusion, dissolution, heat (melting), mechanical breaking, or pH change; and this technique provides a flavour burst, visual and textural effects, as well as a long-lasting flavour (Uhlemann *et al.*,

2002; Madene *et al.*, 2006; Zuidam and Shimoni, 2010; Oxley, 2012b; Meyers, 2014; Sobel *et al.*, 2014b; Mishra, 2015; Gupta *et al.*, 2016).

This technique presents the advantage of being very cheap, high yields can be reached, and it is easy to scale up as it can be run as a continuous process. It is also a good alternative to spray drying for heat-sensitive actives. However, the size distribution range is quite large, the encapsulation efficiency is low, and the capsules are not very stable upon storage. It is not very suitable to produce particles that are due to be used in food which should have a long shelf-life, and particular handling may be needed. Furthermore, the bond between the active and the lipid material can be quite strong, which could lead to an ingredient loss if the fat matrix happened to melt during processing (Madene *et al.*, 2006; Nedovic *et al.*, 2011; Oxley, 2012b; Gupta *et al.*, 2016; Tolve *et al.*, 2016).

2.3.1.2.2 Spinning disc or centrifugal suspension separation

It is another atomisation method used to obtain porous lipid-coated microspheres, with a particle size of 5 μm to 2 mm (Senuma *et al.*, 2000; Zuidam and Shimoni, 2010; Sri *et al.*, 2012; Mishra, 2015; Gupta *et al.*, 2016).

The active ingredient is put in suspension in a molten lipid and spread on a horizontal disc rotating around its vertical axis (see Figure 2.2). The droplets are atomised at the edge of the disc, where they separate due to the rotation (centrifugal force and Rayleigh jet break up), and they solidify by cooling when they fall from the disc. This device can be equipped with a recycling system in order to collect pure coating wastes and reuse them. The melt temperature, shape and temperature of the disc, rotation speed and falling height can be controlled (Senuma *et al.*, 2000; Desai and Park, 2005; Madene *et al.*, 2006; Zuidam and Shimoni, 2010; Oxley, Sri *et al.*, 2012).

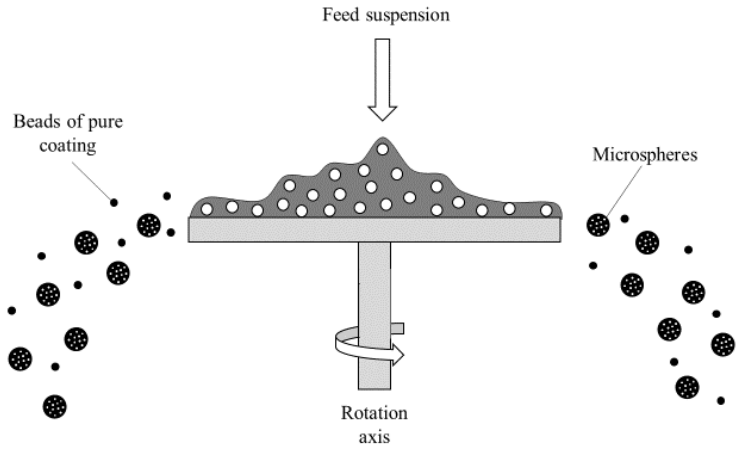


Figure 2.2: Spinning disc process (adapted from Desai and Park, 2005).

This technology is quite simple, fast, cheap and efficient, as it can be used in a continuous mode (Desai and Park, 2005; Sri *et al.*, 2012).

2.3.1.2.3 Dripping, coextrusion or annular jet atomisation

In the food industry, less than 1% of particles are made using this technique. Dripping is when the atomisation flow is too slow to form a jet. Coextrusion leads to core-shell particles with a size of 80 µm to 8 mm. It is more especially used to encapsulate non-polar compounds (Desai and Park, 2005; Zuidam and Shimoni, 2010; Nedovic *et al.*, 2011; Oxley, 2012a; Oxley, 2012b; Brandau, 2014; Sobel *et al.*, 2014b; Gupta *et al.*, 2016).

This technique relies on gravity or Rayleigh force. There are several nozzle design variations for the coextrusion process: stationary nozzle, vibrating nozzle, centrifugal nozzle, or submerged nozzle (Oxley, 2012a; Oxley, 2012b).

2.3.1.2.3.1 Stationary nozzle

This setup is the base for the other coextrusion variations. It leads to microcapsules with a size between 500 µm and 6 mm with a bimodal size distribution (Oxley, 2012a).

The active ingredient is dissolved or put in suspension in an oil medium. A concentric, multifluid nozzle, through which the two immiscible phases are squeezed simultaneously, is used to prepare core-shell particles with a lipophilic core (inner nozzle) and a shell made of an aqueous gel network or a fat coating (outer nozzle) (see Figure 2.3). A drop-by-drop laminar flow is generated, and the fluid jet is cut by gravity. The capsule wall hardens by congealing, interfacial gelation, or precipitation. There are different options for collecting the particles: liquid hardening baths, powdered beds, flash volatilisation chambers, misting chambers, refrigeration chambers, or cyclones (Desai and Park, 2005; Madene *et al.*, 2006; Zuidam and Shimoni, 2010; Oxley, 2012a; Brandau, 2014).

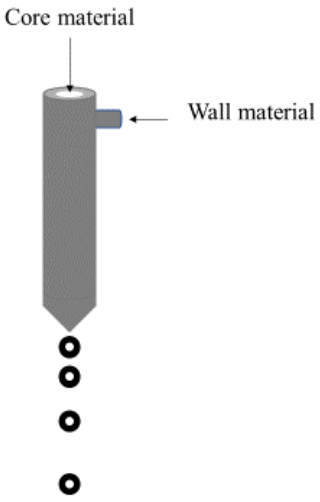


Figure 2.3: Coextrusion process with stationary nozzle (redrawn from Oxley, 2012a).

The payload is 70 to 95%. The release mechanism of the active is based on diffusion or heat (Zuidam and Shimoni, 2010; Oxley, 2012a; Oxley, 2012b; Sobel *et al.*, 2014b; Gupta *et al.*, 2016).

This kind of nozzle is easy to assemble and the process can be run continuously. This process also provides capsules with a good shelf-life stability. It is however an expensive process (Zuidam and Shimoni, 2010; Oxley, 2012a; Lazou and Krokida, 2017).

2.3.1.2.3.2 Vibrating nozzle

This technique, also called prilling, was made to decrease the size of capsules compared to the ones obtained with the stationary nozzle. This coextrusion method leads to capsules with a size of 30 μm to 8 mm (Whelehan and Marison, 2011; Oxley, 2012a; Brandau, 2014; Mishra, 2015).

This setup is the same as for the stationary technique, with the addition of a function generator, a vibrating source, a strobe light and a viewing system (see Figure 2.4). The vibration can either be co-current to the flow or perpendicular. It is also possible to apply heat to the system (Oxley, 2012a; Brandau, 2014).

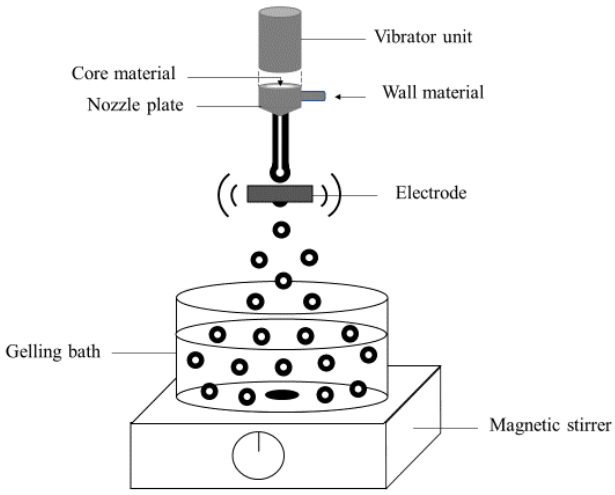


Figure 2.4: Coextrusion process with vibrating nozzle (adapted from Whelehan and Marison, 2011; Brandau, 2014).

The payload is 30 to 90% (Mishra, 2015).

The advantage of this setup is that it enables to obtain a monodisperse size distribution and more uniform particles due to a regular vibration frequency. It is also easy to scale up by the addition of multiple nozzles (Whelehan and Marison, 2011; Oxley, 2012a; Brandau, 2014).

2.3.1.2.3.3 Centrifugal nozzle

This is another coextrusion method. Centrifugal extrusion produces capsules with a size of 150 μm to 2 mm (Desai and Park, 2005; Madene *et al.*, 2006; Oxley, 2012a; Sri *et al.*, 2012; Mishra, 2015; Gupta *et al.*, 2016).

It consists in pumping the active ingredient through the inner orifice of a rotating cylinder, and the liquid carrier through its outer orifice (see Figure 2.5). Several nozzles consisting of concentric orifices are present on the outside of the cylinder, which is rotating around its vertical axis. The coextrudate which is coming out as a continuous flow is broken into particles by the rotation of the device (Rayleigh jet break up). The wall material is surrounding the core by effect of surface tension. The shell is hardened either by cooling, or dropping in a gelling bath or on a moving bed covered in fine-grained starch in order to cushion the fall and absorb moisture (Desai and Park, 2005; Madene *et al.*, 2006; Oxley, 2012b; Sri *et al.*, 2012; Gupta *et al.*, 2016).

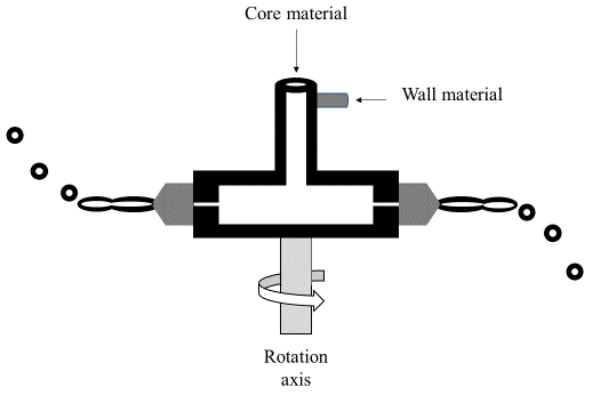


Figure 2.5: Coextrusion process with centrifugal nozzle (redrawn from Oxley, 2012a).

2.3.1.2.3.4 Submerged nozzle

This is a special coextrusion set-up. Submerged nozzle leads to core-shell particles with a size of 500 μm to 8 mm (Uhlemann *et al.*, 2002; Zuidam and Shimoni, 2010; Oxley, 2012a; Meyers, 2014).

Here the core and the shell materials are simultaneously pressed through a particular coextrusion nozzle, which is immersed in a co-currently flowing cooling medium, such as vegetable oil (see Figure 2.6). The droplets are formed by introduction of the external disruption (Uhlemann *et al.*, 2002; Zuidam and Shimoni, 2010; Oxley, 2012a; Brandau, 2014).

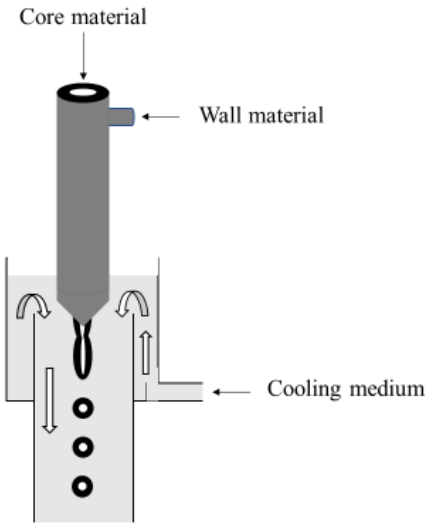


Figure 2.6: Coextrusion process with submerged nozzle (redrawn from Uhlemann *et al.*, 2002; Zuidam and Shimoni, 2010; Oxley, 2012a).

The payload is 70 to 95%. The release mechanism of the active is based on dissolution or mechanical breaking; and this technique provides an upfront flavour release, a flavour burst, visual and textural effects, as well as a long-lasting flavour (Uhlemann *et al.*, 2002; Zuidam and Shimoni, 2010; Meyers, 2014).

This technique provides capsules with a narrow size distribution and a regular shape. However, the technology is also very expensive and difficult to scale up (Brandau, 2014).

2.3.1.3 Freeze-drying

In the food industry, less than 1% of particles are made using this technique. This method, also called cryodesiccation or lyophilisation, leads to porous microspheres with a size of 20 μm to 5 mm. It is more especially used to encapsulate polar compounds (Nedovic *et al.*, 2011; Zuidam and Shimoni, 2010; Fang, 2012; Sobel *et al.*, 2014b; Mishra, 2015; Gupta *et al.*, 2016).

It is very similar to spray cooling and spray chilling atomisation, except that the emulsion is atomised at temperatures below 0ºC under vacuum. The sample is first frozen between -90 and -40ºC for dehydration, so that the crystallisation of water and soluble solids is maximal. Then it is dried by sublimation under low pressure while keeping the same low temperatures (see Figure 2.7). In a third step, the product undergoes a secondary drying to allow desorption of any remaining unfrozen water. Finally, the aggregated dry mass can be ground into smaller chunks (Desai and Park, 2005; Zuidam and Shimoni, 2010; Nedovic *et al.*, 2011; Fang, 2012; Gupta *et al.*, 2016; Klinjapo and Krasaekoopt, 2018).

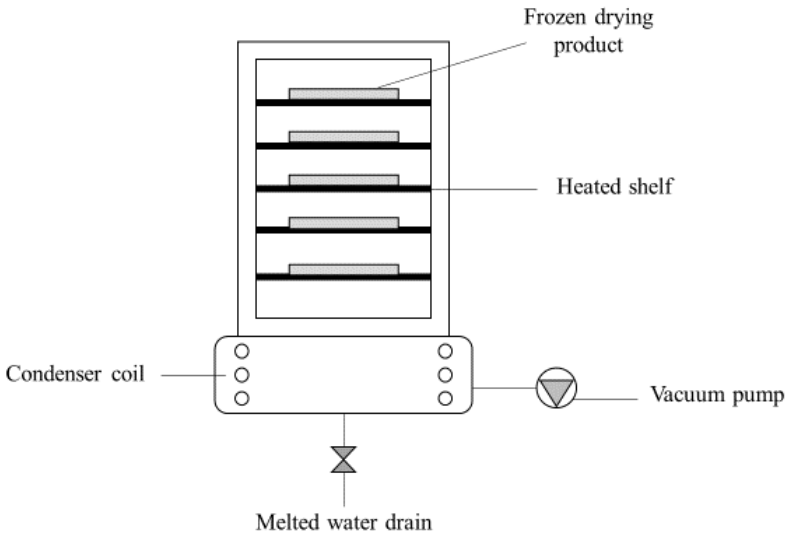


Figure 2.7: Freeze-drying process (redrawn from Fang, 2012).

This simple technique is quite useful for drying thermosensitive compounds which are unstable in solution. The product is convenient to handle. However, it is very expensive, with long processing times (20 hours), and energy costly. Also, due to its porous nature, the matrix does not provide very good barrier properties (Desai and Park, 2005; Madene *et al.*, 2006; Nedovic *et al.*, 2011; Fang, 2012; Gupta *et al.*, 2016; Klinjapo and Krasaekoopt, 2018).

2.3.1.4 Encapsulation using glassy shell materials

This method consists of encapsulating the active inside a glassy carbohydrate matrix, either by injection or extrusion. It is more especially used to encapsulate polar compounds (Rosa, 2006; Harrington and Schaefer, 2014; Sobel *et al.*, 2014b).

2.3.1.4.1 Melt injection

About 2% of encapsulation particles are prepared via this technology in the food industry. Melt injection leads to particles of the matrix type with a size of 200 μm to 2 mm (Uhlemann *et al.*, 2002; Madene *et al.*, 2006; Zuidam and Shimoni, 2010; Meyers, 2014; Sobel *et al.*, 2014b; Mishra, 2015; Gupta *et al.*, 2016).

It is a vertical extrusion process to encapsulate an active ingredient in a low moisture carbohydrate melt at a temperature above their glass transition, which is usually between 30 and 70°C. The core material is dissolved or put in suspension in the molten carbohydrate coating (> 100°C). Water or other plasticisers can be added to the molten carbohydrate. The melt is then pressed under high pressure through one or several filter(s), and an amorphous glass state entrapping the droplets of active agent is obtained by quenching with a cold, dehydrating solvent (usually isopropyl alcohol), at the contact of which the coating material hardens. The extrudate is then crushed into small pieces by vigorous mixing, and active ingredient wastes which might be left on the outside are washed away by the dehydrating solvent. This process

can be carried out under a nitrogen atmosphere as the core material might be sensitive to oxidation (Uhlemann *et al.*, 2002; Desai and Park, 2005; Madene *et al.*, 2006; Zuidam and Shimoni, 2010; Sobel *et al.*, 2014b; Gupta *et al.*, 2016).

The payload is 5 to 25%. The release mechanism of the active is based on dissolution; and this technique provides visual and textural effects (Uhlemann *et al.*, 2002; Desai and Park, 2005; Madene *et al.*, 2006; Zuidam and Shimoni, 2010; Meyers, 2014; Sobel *et al.*, 2014b; Mishra, 2015; Gupta *et al.*, 2016).

This technique provides stable capsules with a good protection against oxidation and a good shelf-life, but is quite expensive due to the low active load and the use of solvent. It is also quite difficult to scale up (Uhlemann *et al.*, 2002; Desai and Park, 2005; Madene *et al.*, 2006; Rosa, 2006; Meyers, 2014; Sobel *et al.*, 2014b; Gupta *et al.*, 2016).

2.3.1.4.2 Melt extrusion

In the food industry, 2 to 3% of encapsulation particles are made using this technique. Melt extrusion leads to particles of the matrix type with a size of 300 μm to 5 mm (Uhlemann *et al.*, 2002; Zuidam and Shimoni, 2010; Harrington and Schaefer, 2014; Meyers, 2014; Sobel *et al.*, 2014b; Mishra, 2015; Gupta *et al.*, 2016).

It is very similar to melt injection in the preparation, but the main difference lies in the fact that this is a horizontal extrusion process (see Figure 2.8). The melt is forced under high pressure through one or several screw(s), preferably a co-rotating twin-screw. This type of extruder is typically composed of a frame, a motor, a gearbox, a process section of variable size, an extrusion head, and a cutter. When using flavours as the active agent to be encapsulated, the latter can be added to the melt halfway of the screw in order to avoid a too long exposure to high temperatures. It is then quickly solidified by cooling, and the extrudate forms an

amorphous, glassy mass that encloses the active droplets. The geometry of the die at the end of the device sets the final shape of the extrudate and a cutting device can also be added. The other main difference is that there is no dehydrating solvent wash of the extrudate (Uhlemann *et al.*, 2002; Zuidam and Shimoni, 2010; Harrington and Schaefer, 2014; Sobel *et al.*, 2014b).

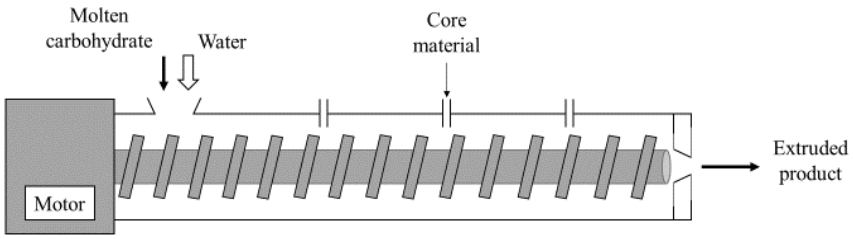


Figure 2.8: Melt extrusion process (redrawn from Uhlemann *et al.*, 2002; Zuidam and Shimoni, 2010).

The payload is 5 to 40%. The release mechanism of the active is based on swelling followed by dissolution, or heat; and this technique provides visual and textural effects (Uhlemann *et al.*, 2002; Zuidam and Shimoni, 2010; Meyers, 2014; Sobel *et al.*, 2014b; Mishra, 2015; Gupta *et al.*, 2016).

This process is easy to scale up as it can be run efficiently in a continuous mode, and it provides very stable capsules with a good protection against oxidation and a good shelf-life. However, the capsules obtained via this technique have a non-homogeneous size distribution, and are preferably used in dry products as they are unstable in water media. Moreover, this technology is also complex and quite expensive due to the low active load (usually < 10%), and the operation under high pressure may lead to significant active loss (Uhlemann *et al.*, 2002; Madene *et al.*, 2006; Rosa, 2006; Feng *et al.*, 2009; Zuidam and Shimoni, 2010; Harrington and Schaefer, 2014; Meyers, 2014; Sobel *et al.*, 2014b).

2.3.1.5 Encapsulation by Rapid Expansion of Supercritical Solutions (RESS)

In the food industry, less than 1% of particles are made using this technique. Encapsulation by Rapid Expansion of Supercritical Fluids leads to particles of the matrix type with a size of 10 to 400 μm (Zuidam and Shimoni, 2010; Sobel *et al.*, 2014b; Mishra, 2015).

When a material is brought above a certain critical temperature and pressure, it does not have two distinct liquid and gas phases anymore. This is called supercritical fluid state. Thus, in this state, the material displays different properties of either the liquid or gas. The active ingredient is dispersed in a supercritical fluid containing the dissolved or swollen carrier material. When this dispersion is liberated through a small nozzle, the wall material precipitates onto the active agent as the supercritical fluid evaporates or changes into a much poorer solvent due to the sudden pressure drop (see Figure 2.9). Supercritical carbon dioxide and nitrous oxide are the two most widely used supercritical fluids (Zuidam and Shimoni, 2010; Sri *et al.*, 2012).

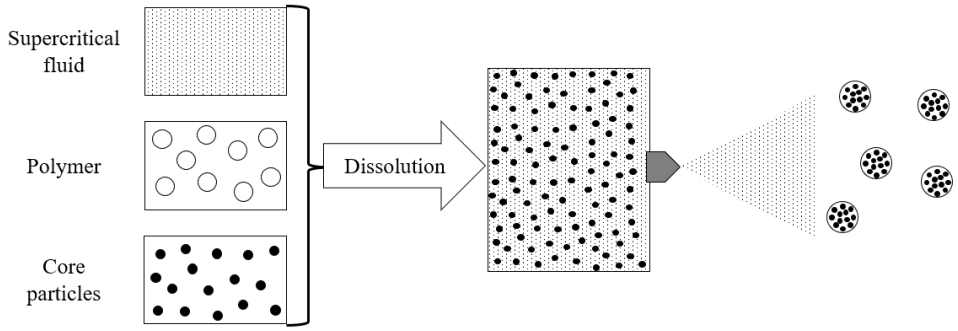


Figure 2.9: RESS process (redrawn from Sri *et al.*, 2012).

The payload is 20 to 50% (Zuidam and Shimoni, 2010; Sobel *et al.*, 2014b; Mishra, 2015).

A good amount of compounds can be used for this method. However, the challenge is to find an active and carrier material that can both dissolve in the supercritical fluid (Zuidam and Shimoni, 2010; Sri *et al.*, 2012).

2.3.2 Physico-chemical processes

Emulsions are immiscible two-phase systems in equilibrium. There can be different kinds of emulsions: water-in-oil (W/O), oil-in-water (O/W); or even double emulsions: water-in-oil-in-water (W/O/W) or oil-in-water-in-oil (O/W/O). The active is dissolved in an oil or water medium. Then the oil and water phases are mixed together under high shear thanks to a colloid mill, a high shear mixer, a homogeniser, or a stirred tank equipped with baffles. An emulsifier can optionally be added to help the formation and stabilisation of the emulsion in the desired way (Zuidam and Shimoni, 2010).

Double emulsions are formed in two steps. For a W/O/W emulsion for example, a simple W/O emulsion first needs to be formed, with a lipophilic emulsifier (low hydrophilic-lipophilic balance, HLB) in the oil phase (see Figure 2.10). Then, a second emulsion is formed by dispersing the previous W/O emulsion in an aqueous phase containing a hydrophilic emulsifier (high HLB) (Pal, 1996; Duque Estrada *et al.*, 2017).

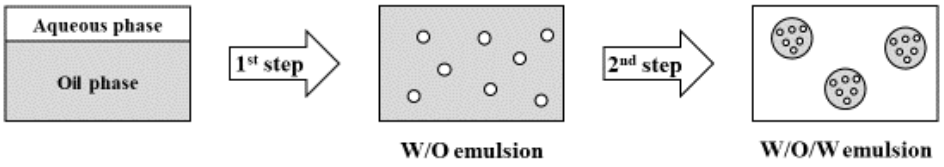


Figure 2.10: Double emulsion formation principle (adapted from Duque Estrada *et al.*, 2017).

For an O/W/O emulsion, the phases and emulsifier affinities are reversed (Pal, 1996).

2.3.2.1 Emulsions with multilayers

Emulsions with multilayers lead to core-shell particles with a size of 0.2 μm to 5 mm (Zuidam and Shimoni, 2010; Mishra, 2015).

To form an emulsion with multilayers, also called layer-by-layer (LbL) electrostatic deposition technique, an ionic emulsifier can be added to a simple emulsion. The whole can be mixed with an aqueous solution containing an oppositely charged polyelectrolyte to form a "secondary" emulsion. Thus, a layer would be formed around the "primary" emulsion (see Figure 2.11). The excess of free polyelectrolyte can be optionally removed, and this process can be subsequently reproduced several times, alternating cationic and anionic polymers, to obtain several layers (Zuidam and Shimoni, 2010; Thies, 2012).

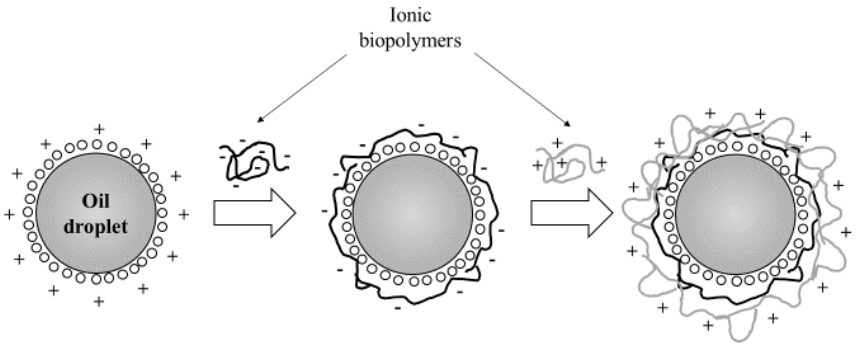


Figure 2.11: Layer-by-layer coating process (redrawn from Southwest Research Institute, 2015).

The payload ranges from 1 to 90% (Zuidam and Shimoni, 2010; Mishra, 2015).

This technique is still quite new, and although it is quite easy to carry out at a lab scale, it is time-consuming and much more challenging for scale-up application (Zuidam and Shimoni, 2010).

2.3.2.2 Coacervation

Coacervation was the first encapsulation process to be studied in 1955 for carbonless copy paper application. However, less than 1% of encapsulation particles are prepared via this technology in the food industry (Madene *et al.*, 2006; Zuidam and Shimoni, 2010; Sobel *et al.*, 2014b).

A coacervate is a tiny droplet of concentrated polyelectrolyte(s) which forms spontaneously due to hydrophobic forces with the surrounding medium. Coacervation consists of a phase separation between a highly concentrated polymer phase and the more diluted solution medium, also called the equilibrium solution. There are two types of coacervation: simple and complex. Only one polymer is involved in simple coacervation and a desolvation agent is used, while complex coacervation is based on several interactions between two or more oppositely charged polymers: electrostatic interaction, hydrogen bonding, hydrophobic interaction and polarisation-induced attractive interaction. This second technique is more efficient as it leads to higher payloads. The term "coacervation" will be used to refer to "complex coacervation" in what follows, as focus will be put on this process (Madene *et al.*, 2006; Zuidam and Shimoni, 2010; Sri *et al.*, 2012; Xiao *et al.*, 2014; Klinjapo and Krasaekoopt, 2018).

Complex coacervation, also called associative phase separation, leads to core-shell particles with a size of 2 μm to 1.2 mm (Uhlemann *et al.*, 2002; Madene *et al.*, 2006; Barrow *et al.*, 2007; Zuidam and Shimoni, 2010; Sri *et al.*, 2012; Thies, 2012; Meyers, 2014; Sobel *et al.*, 2014b; Mishra, 2015; Gupta *et al.*, 2016).

This controlled desolvation technique comprises three main steps: emulsification, coacervation and wall hardening (see Figure 2.12). First, an O/W emulsion is formed, with the active ingredient in the oil phase and an ionic hydrocolloid in the aqueous phase. A solution containing an oppositely charged hydrocolloid is then added to the emulsion to form a three-immiscible chemical phase (the continuous phase, the emulsion droplets and the coacervates). The second step consists of adjusting the pH of the solution, so that the two hydrocolloids are of clearly opposite charges. The droplets of coacervate (polymer-rich solution) will slowly migrate and adsorb at the surface of the emulsion droplets, due to hydrophobic forces, until it forms a regular coating by coalescence. The formation of a thin shell results from the precipitation of the two

electrolytes, which get adsorbed at the interface between oil and water. When the appropriate pH is reached, the shell is hardened in the third step by thermal gelation or chemical crosslinking. Finally, the suspension may need to be purified and the capsules are usually isolated by decantation, filtration or centrifugation. An additional drying step may be required, usually by spray drying. Gum arabic and gelatine are often used as the preferred polymer combination (Uhlemann *et al.*, 2002; Desai and Park, 2005; Madene *et al.*, 2006; Barrow *et al.*, 2007; Zuidam and Shimoni, 2010; Sri *et al.*, 2012; Thies, 2012; Nesterenko *et al.*, 2013a; Sobel *et al.*, 2014b; Yan and Zhang, 2014; Gupta *et al.*, 2016).

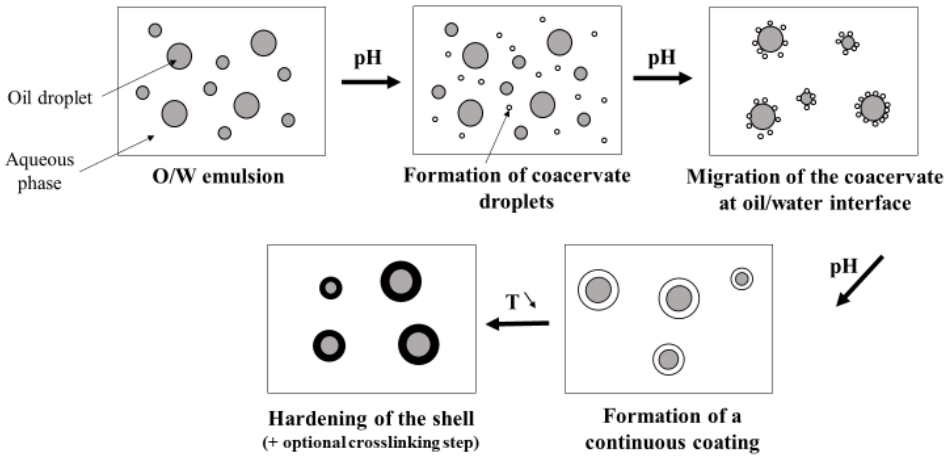


Figure 2.12: Complex coacervation process (adapted from Madene *et al.*, 2006; Sri *et al.*, 2012; Nesterenko *et al.*, 2013a).

The payload is 20 to 95%. The release mechanism of the active is based on dissolution, pH change, pressure, diffusion, dehydration or enzymatic effect; and this technique provides a flavour burst, visual and textural effects, as well as a long-lasting flavour (Uhlemann *et al.*, 2002; Madene *et al.*, 2006; Zuidam and Shimoni, 2010; Thies, 2012; Meyers, 2014; Sobel *et al.*, 2014b; Mishra, 2015; Gupta *et al.*, 2016).

This technique presents many advantages such as ease to control the size distribution, high payload and encapsulation efficiency. It provides capsules with good barrier properties and a good shelf-life stability. It is also possible to scale it up. The amount of surface oil is extremely low compared to some other techniques. Moreover, it is an encapsulation method which provides capsules with a consistent shell and which have optimal controlled-release properties. However, a few drawbacks can also be listed. It is a complicated technique as a lot of parameters can have a significant influence on the final product and its stability, it must be carried out in a quite narrow pH range, and it exhibits a multi-dispersed size distribution. Furthermore, it is a long process which involves several steps. For all those reasons it is obviously quite expensive. Complex coacervation also poses the concern of the toxicity of its commonly used crosslinkers (glutaraldehyde and formaldehyde) (Desai and Park, 2005; Madene *et al.*, 2006; Barrow *et al.*, 2007; Feng *et al.*, 2009; Zuidam and Shimoni, 2010; Sri *et al.*, 2012; Thies, 2012; Nesterenko *et al.*, 2013a; Xiao *et al.*, 2014; Yan and Zhang, 2014; Klinjapo and Krasaekoopt, 2018).

2.3.2.3 Polymer-polymer incompatibility or segregative phase separation

This technique leads to microcapsules with a size of 0.5 μm to 1 mm. It is mostly used to encapsulate polar solids (Mark, 2007; Sri *et al.*, 2012; Mishra, 2015).

Two immiscible polymers are dissolved in a common solvent, which is usually non-aqueous. The solution forms two immiscible polymer-rich phases driven by an endothermic mixing heat, only one of which is intended to form the particle shell (see Figure 2.13). An active, which is insoluble in the solvent, is dispersed in the mixture, and the polymer which has a preferred adsorption behaviour for the selected core material surrounds it by a thin film (Mark, 2007; Sri *et al.*, 2012; Thies, 2012).

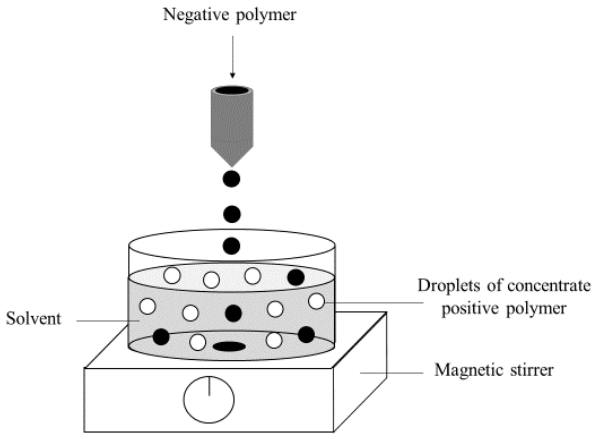


Figure 2.13: Polymer-polymer incompatibility process (redrawn from Sri *et al.*, 2012).

2.3.2.4 In situ gelation

This is the second method used to prepare microspheres by dropping. In the food industry, about 1% of particles are made using this technique. The preparation of microspheres via emulsification leads to particles of the matrix type with a size of 0.2 μm to 5 mm (Zuidam and Shimoni, 2010; Sobel *et al.*, 2014b).

This technique consists of forming a W/O emulsion. Both a gelling polymer and the active ingredient are dissolved (hydrophilic active) or dispersed (active under solid form) in the aqueous phase, and the continuous phase is composed of an edible oil. An appropriate emulsifier can optionally be added to either of these phases. The aqueous droplets are then gelled by ionic or thermal gelation. The gelled beads are finally separated, washed and dried (Thies, 2012).

2.3.2.4.1 Thermal gelation

Here, the beads are formed using the gelling properties of the polymers, simply by cooling down (Thies, 2012).

2.3.2.4.2 Ionic gelation or preparation of microspheres by emulsification

This technique consists of making particles from emulsions. Calcium-alginate gel is the most used system for this technique. The addition under shear of calcium-chloride to an emulsion made of an alginate solution and active ingredient in vegetable oil will lead to a destabilisation of the emulsion. The formation of the particles results from the gelation of the alginate droplets in the presence of divalent cations. Another option consists of having both the alginate and the calcium, in a salt form so that it is not soluble, already in presence in the aqueous phase of the emulsion. Adding a lipophilic acid to the mixture will enable to free the calcium in its cationic form and undergo a gelation step with alginate. An optional colloid, such as xanthan gum, can also be added to strengthen the gel. Depending on the processing conditions, it is possible to witness either agglomeration or deagglomeration. Finally, the gel network forming the shell is hardened at high temperature (about 75ºC) (Zuidam and Shimoni, 2010).

The payload is 20 to 50%. The release mechanism of the active is based on diffusion or dissolution (Zuidam and Shimoni, 2010).

This process is easier to apply at industrial scale than the preparation of microspheres via extrusion or dropping. However, it is also much more expensive as a step of waste disposal needs to be considered (Zuidam and Shimoni, 2010).

2.3.2.5 Emulsion phase inversion

This is a modified version of the preparation of microspheres by emulsification. This technique leads to particles with a size of 0.5 to 5 μm (Zuidam and Shimoni, 2010; Sri *et al.*, 2012; Mishra, 2015).

A W/O emulsion is first prepared in edible oil, with the active either in the oil or water phase, and calcium ions in the aqueous phase. The further addition of an aqueous alginate solution

under shear is going to destabilise the emulsion and provoke a change of continuous phase, leading to the phase inversion. The calcium-alginate gel will deposit at the surface of the oil droplets containing the primary emulsion water droplets. The microspheres can be further coated by a colloid layer, and the size of the inner water droplets can be minimised by the addition of a surfactant (Casana Giner *et al.*, 2006; Zuidam and Shimoni, 2010).

2.3.2.6 Solvent evaporation

This technique leads to microspheres with a size of 0.5 μm to 1 mm (Sri *et al.*, 2012; Mishra, 2015).

This process enables to use water-insoluble materials for the shell of the particles. Here, the coating polymer is dissolved in a volatile solvent which is immiscible with water, and the active ingredient is dissolved or dispersed in this organic phase. Then this mixture is added under shear into a water phase, until the obtention of the desired droplet size (see Figure 2.14). The batch is then heated and stirred until all the solvent is evaporated, thus the polymer will shrink around the droplets containing the active ingredient. The particles are finally washed and dried (Das *et al.*, 2011; Sri *et al.*, 2012; Klinjapo and Krasaekoopt, 2018).

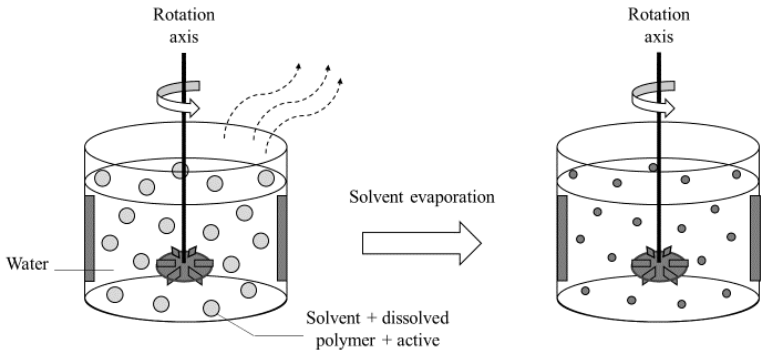


Figure 2.14: Solvent evaporation process (adapted from Sri *et al.*, 2012).

An alternative to this technique is the Evaporation-Induced Self-Assembly (EISA), where the encapsulating material is amphiphilic. The shell material undergoes self-assembly and forms micelles, similarly to the liposome entrapment mechanism, due to hydrophobic interactions resulting from the solvent evaporation. It is used to encapsulate non-polar compounds. A dry powder is finally obtained by water evaporation (Sobel *et al.*, 2014b).

This process is advantageous as it is relatively easy, it does not require any heat and provides capsules with a good size distribution. However, this method involves the use of toxic solvents, which is not desirable for food application. The encapsulation efficiency is not very good either (Das *et al.*, 2011; Sobel *et al.*, 2014b; Klinjapo and Krasaekoopt, 2018).

2.3.2.7 Co-crystallisation or co-precipitation

This technique leads to crystals of various sizes (Gupta *et al.*, 2016).

This technique consists of encapsulating a compound by entrapment due to spontaneous crystallisation, or by inclusion due to precipitation inside carbohydrate crystals. Usually, the active ingredient and high temperature supersaturated sucrose syrup are mechanically mixed together under high shear, causing the mixture to crystallise by nucleation when the syrup reaches its crystallisation temperature. The obtained product can optionally be further dried to obtain a desired moisture level (Uhlemann *et al.*, 2002; Desai and Park, 2005; Madene *et al.*, 2006; Gupta *et al.*, 2016).

The payload is very variable. The active is released by dissolution (Gupta *et al.*, 2016).

This process is quite economical, easy to operate, and leads to particles with a good flowability. However, the high temperature of the process may damage heat sensitive actives (Madene *et al.*, 2006).

2.3.2.8 Molecular inclusion

In the food industry, less than 1% of particles are made using this technique. Inclusion complexation leads to particles with a size of 1 nm to 100 μm (Uhlemann *et al.*, 2002; Madene *et al.*, 2006; Meyers, 2014; Sobel *et al.*, 2014b; Mishra, 2015; Gupta *et al.*, 2016).

This method consists of encapsulating an active ingredient which is less polar than water, in suspension in an aqueous medium, by precipitation in a cavity-based material at molecular level. Cyclodextrins (mostly α- and β-cyclodextrins in the food industry), which are cyclic oligosaccharides obtained from enzymatically modified starch, are commonly used for this technique. Those sugar molecules are hydrophilic on their outer surface, but have an inner lipophilic cavity which can, when hydrated in a solution, entrap the active by precipitation due to hydrophobic interactions (see Figure 2.15). Their central cavity measures around 0.5 to 0.8 nm in diameter. The inclusion complex that results from this process is in crystalline form and can be collected by filtration. It can also be mixed with dry cyclodextrin molecules in the presence of a minimum of water so that it constitutes a pasty complex under high shear. The duration of the process depends on the nature of the compound to encapsulate, and the complexation efficiency is temperature dependent (Uhlemann *et al.*, 2002; Desai and Park, 2005; Madene *et al.*, 2006; Rosa, 2006; Zuidam and Shimoni, 2010; Nedovic *et al.*, 2011; Sobel *et al.*, 2014b; Gupta *et al.*, 2016).

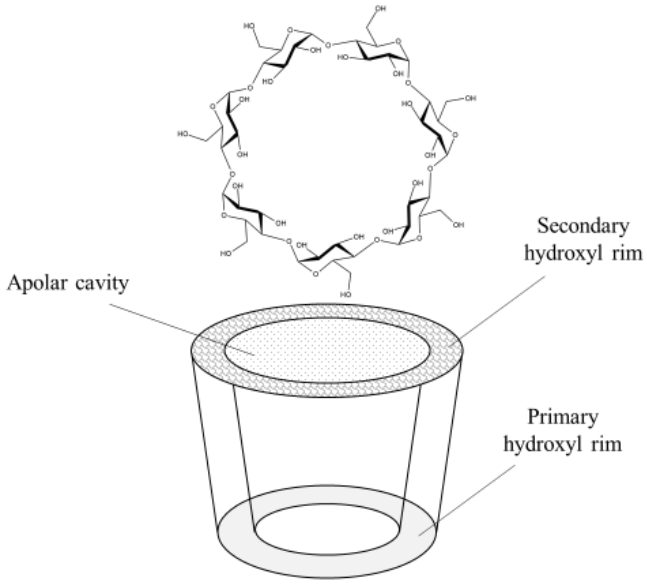


Figure 2.15: Molecular inclusion structure (redrawn from Desai and Park, 2005; Madene *et al.*, 2006).

The payload is 5 to 20%. The release mechanism of the active is based on dissolution, or melting; and this technique provides an upfront flavour release and a long-lasting flavour (Uhlemann *et al.*, 2002; Madene *et al.*, 2006; Zuidam and Shimoni, 2010; Meyers, 2014; Sobel *et al.*, 2014b; Mishra, 2015; Gupta *et al.*, 2016).

This method provides capsules which are stable upon storage, well protected against evaporation and oxidation, and which also offer the advantage of having a long-lasting effect in chewing gum. And yet, it is not very suitable for industrial scale. It is an expensive process due to the high cost of cyclodextrins and to a low loading capacity (Uhlemann *et al.*, 2002; Desai and Park, 2005; Madene *et al.*, 2006; Zuidam and Shimoni, 2010; Nedovic *et al.*, 2011; Meyers, 2014; Sobel *et al.*, 2014b; Gupta *et al.*, 2016).

2.3.2.9 Liposome entrapment

In the food industry, less than 1% of particles are made using this technique. Liposome entrapment leads to particles of various morphologies with a size of 20 nm to 10 mm (Uhlemann *et al.*, 2002; Desai and Park, 2005; Zuidam and Shimoni, 2010; Nedovic *et al.*, 2011; Singh *et al.*, 2012; Meyers, 2014; Mirafzali *et al.*, 2014; Sobel *et al.*, 2014b; Liu *et al.*, 2015b; Mishra, 2015; Gupta *et al.*, 2016).

Liposomes are non-toxic, thermodynamically-stable, closed vesicles, which comprise a phospholipid membrane of one or more bilayer(s). Phospholipids consist of a polar head and a fatty acid chain. The formation of liposomes relies on hydrophilic-hydrophobic interactions. They are likely to form aggregates to minimise the contact between the medium and its fatty acid chains, which can be prevented by electrostatic repulsion or steric stabilisation (see Figure 2.16). The size of the vesicles depends on the energy input. The structure of the membrane will lead to a size classification: 20-400 nm (unilamellar vesicles), 400 nm to 1 µm (multilamellar vesicles), and > 1 µm (multivesicular vesicles). Either hydrophilic or hydrophobic active ingredients can be encapsulated in liposomes, either in the aqueous compartment of the vesicle at a low yield, or it can be linked to the lipophilic membrane at a high yield. The lipid is dispersed in water under low shear, with the active in either the lipid molecules or the water phase (Desai and Park, 2005; Zuidam and Shimoni, 2010; Nedovic *et al.*, 2011; Singh *et al.*, 2012; Mirafzali *et al.*, 2014; Liu *et al.*, 2015b).

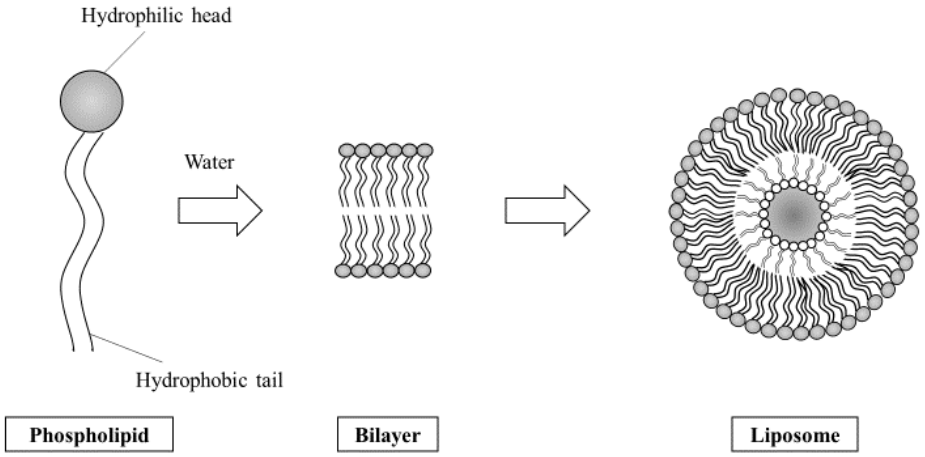


Figure 2.16: Liposome formation (redrawn from Mirafzali *et al.*, 2014; Liu *et al.*, 2015b).

The payload is 5 to 50%. The release mechanism is based on melting, diffusion, or pH change; and this technique provides an upfront flavour release and a long-lasting flavour (Desai and Park, 2005; Zuidam and Shimoni, 2010; Singh *et al.*, 2012; Meyers, 2014; Sobel *et al.*, 2014b; Mishra, 2015).

This simple method uses very mild processing conditions and it is possible to scale it up. Unfortunately, the encapsulation efficiency is rather low and this technique is quite costly. What is more, the liposomes are unstable upon storage at room temperature and can undergo leakage (Desai and Park, 2005; Zuidam and Shimoni, 2010; Nedovic *et al.*, 2011; Singh *et al.*, 2012; Mirafzali *et al.*, 2014; Liu *et al.*, 2015b).

The use of liposomes in the food industry is mainly limited to cheeses (Zuidam and Shimoni, 2010; Singh *et al.*, 2012; Gupta *et al.*, 2016).

2.3.3 Processes comparison

The process design parameters which were listed in the introduction will serve as a guideline for the selection of an appropriate method. Going through this list of parameters for each

process will enable to proceed by elimination in order to identify the most suitable options for the desired application.

2.3.3.1 Functionality of the particles in the end product

The morphology of the particles that can be obtained via the different encapsulation processes were compared (see Table 2.1). As explained in **Chapter 1**, there are two main types of primary particles: core-shell or matrix particles. Furthermore, it is important to note that processes leading to core-shell microcapsules can either be used with a liquid or solid core. Differentiation was made between methods providing core-shell capsules suitable for the use of L-carvone (liquid core) and those offering a coating (solid core).

Table 2.1: Comparison of particles morphology depending on the encapsulation process.

Processes	Core-shell (liquid core)	Coating (solid core)	Matrix
Spray drying		✓	✓
Spray cooling atomisation		✓	✓
Spinning disc		✓	✓
Stationary nozzle coextrusion	✓		
Vibrating nozzle coextrusion	✓		
Centrifugal nozzle coextrusion	✓		
Submerged nozzle coextrusion	✓		
Freeze-drying			✓
Melt injection			✓
Melt extrusion			✓
Supercritical fluid			✓
Emulsions with multilayers	✓	✓	
Coacervation	✓		
Polymer-polymer incompatibility	✓	✓	
Thermal gelation			✓
Microspheres by emulsification			✓
Phase inversion			✓
Solvent evaporation			✓
Co-crystallisation			Crystals
Molecular inclusion			Crystals
Liposome entrapment	✓		

In the case of chewing gum, the flavour should be released fast upon chewing (burst) (Uhlemann *et al.*, 2002). This means a core-shell structure would be more adapted in order to obtain a flavour burst rather than a slow release by diffusion through a matrix.

As a consequence, only the processes leading to core-shell microcapsules with a liquid core (coextrusion methods, emulsions with multilayers, coacervation, polymer-polymer incompatibility and liposome entrapment) were kept for further considerations.

2.3.3.2 Nature of the active to be entrapped

L-carvone is a lipophilic liquid. So in addition to the encapsulated form which is allowed by each process, the nature of the active to be encapsulated should also be checked for those processes (see Table 2.2).

Table 2.2: Nature of the core material depending on the encapsulation process.

Processes	Polar	Non-polar
Stationary nozzle coextrusion		✓
Vibrating nozzle coextrusion		✓
Centrifugal nozzle		✓
Submerged nozzle		✓
Emulsions with multilayers		✓
Coacervation		✓
Polymer-polymer incompatibility	✓	
Liposome entrapment	✓	✓

Only the methods which permitted to entrap non-polar cores in an oil phase (coextrusion methods, emulsions with multilayers, coacervation and liposome entrapment) were given further consideration.

2.3.3.3 Size of the capsules

During the chewing gum making process, the capsules are going to undergo shearing while in the gum matrix, which may damage them. At equivalent shell thickness, the bigger the capsules, the easier they can be broken (Keller and Sottos, 2006). So ideally they would need to be small enough not to be crushed during the chewing gum processing step, but still be big enough to be ruptured by chewing. It was thus agreed that the desired capsules should be smaller than 100 µm. Furthermore, particles smaller than 30 µm were feared to get stuck between the teeth and not be efficiently crushed during chewing.

The size of the obtained particles was compared for the previously selected processes (see Figure 2.17).

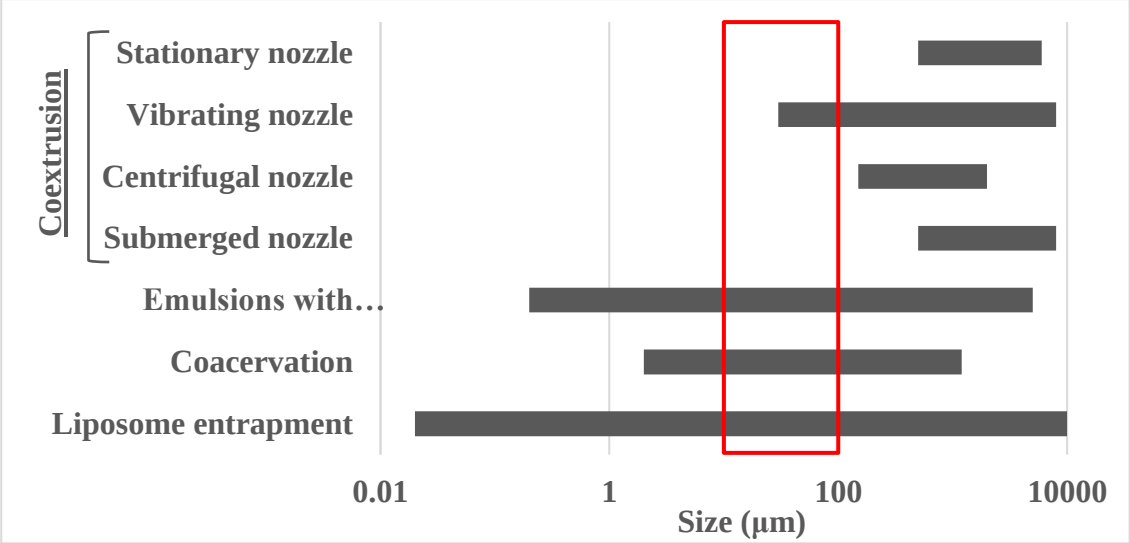


Figure 2.17: Capsules size range depending on the encapsulation process (Uhlemann *et al.*, 2002; Desai and Park, 2005; Madene *et al.*, 2006; Zuidam and Shimoni, 2010; Nedovic *et al.*, 2011; Whelehan and Marison, 2011; Oxley, 2012a; Singh *et al.*, 2012; Sri *et al.*, 2012; Brandau, 2014; Meyers, 2014; Mirafzali *et al.*, 2014; Sobel *et al.*, 2014b; Liu *et al.*, 2015b; Mishra, 2015; Gupta *et al.*, 2016).

Only the methods leading to capsules with a size between 30 and 100 μm (vibrating nozzle coextrusion, emulsions with multilayers, coacervation and liposome entrapment) were kept for further considerations.

2.3.3.4 Trigger mechanism for the release of the active

For chewing gum application, release by either mechanical trigger (chewing), dissolution or heat (melting in the mouth at 37ºC) were acceptable. Mechanical breaking would however be preferred in order to obtain a clear burst rather than a slow release by dissolution (see Table 2.3). The emulsions with multilayers process was not further considered due to lack of information.

Table 2.3: Flavour release trigger mechanisms depending on the encapsulation process.

Processes	**Release mechanism**	**Flavour effect**
Vibrating nozzle coextrusion	Diffusion Heat	-
Coacervation	Dissolution pH Mechanical Diffusion Dehydration Enzymatic effect	Flavour burst Long-lasting flavour
Liposome entrapment	Diffusion Heat pH	Upfront flavour Long-lasting flavour

None of the remaining options could really be set aside based on this parameter.

2.3.3.5 Cost constraints of the end product

The technology is due to be used for production at a large scale and involves a lot of other compounds in addition to the capsules. Yet, chewing gums are not expensive goods, so the cost of the process should try to be minimised.

It is possible to have an idea of the cost trend of the processes as being dependent on their complexity and productivity (see Figure 2.18). We can see that liposome entrapment is one of the most expensive methods. Coacervation and vibrating nozzle coextrusion are not among the cheapest processes but they should not be too far from each other in price.

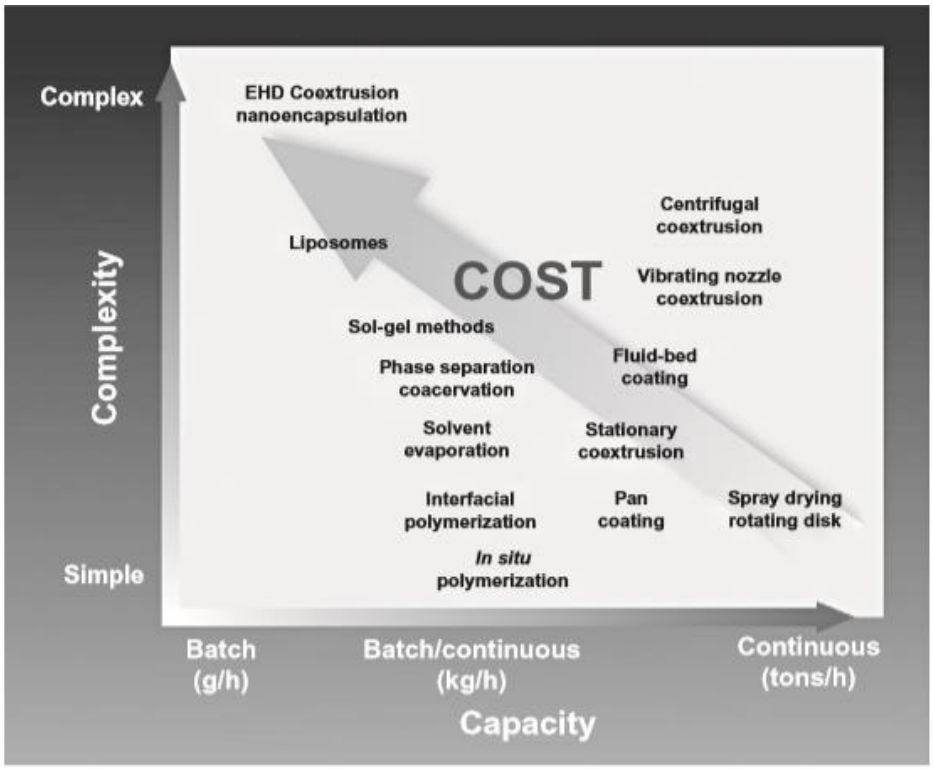


Figure 2.18: Cost trend of the different encapsulation processes depending on their production capacity and their complexity (Oxley, 2014).

2.3.3.6 Storage conditions of the final product

Chewing gum is not a food that really expires quickly and it is likely to stay on the consumers' shelf at room temperature from a few months to a couple of years. The capsules should thus remain stable in those conditions.

2.4 Shell materials

2.4.1 Regulations

Although non-food materials could have been considered as a proof of principle before being replaced by food grade alternatives, it was decided, in accordance with the sponsor, to strictly focus on food grade materials approved by Mondelez Regulatory Department.

Food materials which have been approved for use in food in the EU are identified by an E-number. In the US, they are qualified of Generally Recognised As Safe (GRAS) materials. Those chemicals are substances which are "generally recognized, among qualified experts, as having been adequately shown to be safe under the conditions of their intended use" as defined by the American Food and Drug Administration (FDA) (Taggart and Mitchell, 2009; Hoffmann, 2014; Food and Drug Administration, 2018).

The available materials fall into four main categories: carbohydrates, proteins, lipids and synthetic polymers. Particular interest has been shown in the use of polysaccharide-protein combinations due to their possible electrostatic interactions as well as the occurrence of Maillard reaction under mild heating, which can lead to complexes. The association of hydrocolloids has also been used to obtain new improved rheological properties (Turgeon and Laneuville, 2009; Williams and Phillips, 2009b). Seeing the hydrophobic character of L-

carvone lipids would retain the flavour oil and may lead to matrix particles, which was not desired for release with a clear burst. As a consequence fats and waxes were set aside.

However, some extra regulations (allergens, health concerns) as well as other cultural considerations, are limiting even more the choice of possible shell components among food grade materials. It is also important to note that many synthetic polymers which are authorised for pharmaceutical applications are not allowed in food (Augustin and Oliver, 2014).

2.4.1.1 Allergens

Any food additive known to have an allergenic effect needs to be properly displayed on the label of the food product where it appears (Food and Drug Administration, 2004).

90% of food allergies worldwide have been identified to be due to one of the eight following food groups: eggs, milk, crustaceans, fish, peanuts, soybean, tree nuts or wheat. Proteins are usually responsible for those food allergies. The main groups of allergen proteins are albumins, globulins and prolamins (González-Pérez and Arellano, 2009; Aider and Barbana, 2011; Hoffmann, 2014).

Egg proteins are considered as allergens and are the second most common cause of food allergies among children (Mine and Yang, 2011; Strixner and Kulozik, 2011).

Milk proteins have been identified as allergenics. More especially β-lactoglobulin has been identified as a major source of allergies in milk and is preferably removed from whey protein (Fee *et al.*, 2010; Boland, 2011; Deeth and Bansal, 2019).

A lot of plant proteins, such as canola, chickpea, soybean and sunflower proteins, contain a 2S albumin storage protein, or napin, which makes them allergens (Moreno and Clemente, 2008;

Aider and Barbana, 2011; Fukushima, 2011; Tan *et al.*, 2011; Meng and Cloutier, 2014; Ariyarathna and Karunaratne, 2015; González-Pérez, 2015).

Wheat proteins are major allergens, especially with the growing sensitivity to gluten in the population. Starches and maltodextrins can be derived from wheat cereals for example and can also pose a concern. Pea protein is a potential allergen. Rice protein is highly hypoallergenic. Potato protein is not an allergen (Sandberg, 2011; Vicente *et al.*, 2011; Islam *et al.*, 2012; Hoffmann, 2014; Wang *et al.*, 2020).

Sensitisers also need to be reported, such as sulphites which can be found in many modified starch materials (Hoffmann, 2014).

2.4.1.2 Other health risks

Although it has a GRAS status, gelatine has been suspected to present a potential risk of transmitting animal diseases, such as the bovine spongiform encephalopathy (BSE), or mad cow disease. For safety reasons, materials from meat or fish origin may need government inspection prior to exportation (Haug and Draget, 2009; Tarté, 2011; Hoffmann, 2014; Meng and Cloutier, 2014).

There are also some concerns regarding ingredients from crop origin with the uncertainty of the safety of Genetically Modified Organisms (GMO), such as starches, dextrin and maltodextrin (Hoffmann, 2014).

2.4.1.3 Culture

Materials from animal origin may not suit everyone's diet arrangements, such as vegetarians or vegans (Hoffmann, 2014).

Animal derivatives can also pose religion issues as some communities require halal or kosher products (Hoffmann, 2014).

2.4.2 Special restrictions

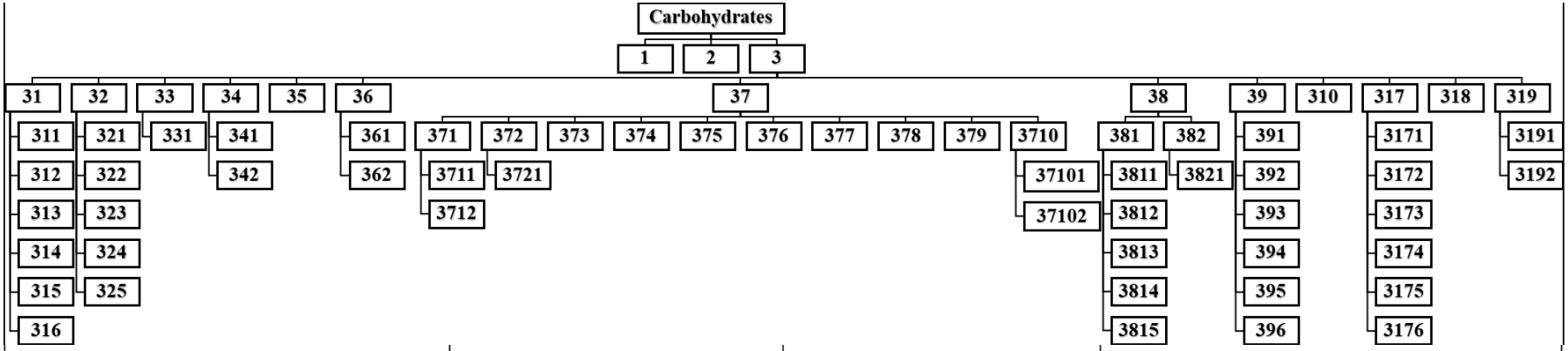
Preliminary trials were initially made with the gelatine type B/chitosan and the pea protein isolate/pectin combinations, only taking into account the fact that the materials needed to be food grade. However, developing capsules for use in foods appropriate for a wide range of consumers proved to be much more complicated than that.

After communicating with the Regulatory Department of the sponsor of the project, it was proposed that only materials from non-animal origins, and not posing any allergenic concerns should be considered. Hence the choice of the final combination was limited by these guidelines.

2.4.3 Carbohydrates: polysaccharides

Carbohydrates offer a wide range of materials which are organised according to a quite complex classification (see Table 2.4). Polysaccharides are biopolymers composed of several monosaccharide units linked by glycosidic binding (Wandrey *et al.*, 2010).

Table 2.4: Carbohydrates classification (adapted from MeSH database, 2020).



1 ***Monosaccharides***	**34 Fructans**	**378 Schizophyllan**	**393 Gellan gum**
2 ***Oligosaccharides***	**341 Inulin**	**379 Scleroglucan**	**394 Kefiran**
3 ***Polysaccharides***	**342 Levan**	**3710 Starches**	**395 Welan gum**
31 Alginates	**35 Fucoidan**	**37101** Starch	**396 Xanthan gum**
311 Alginic acid	**36 Galactans**	**37102** Modified starches	**310 Pectin**
312 Ammonium alginate	**361 Agar**	**38 Mannans**	**317 Plant gums**
313 Calcium alginate	**362 Larch gum**	**381 Galactomannans**	**3171 Flaxseed gum**
314 Potassium alginate	**37 Glucans**	**3811** Cassia gum	**3172 Gum arabic**
315 Sodium alginate	**371 Cellulosics**	**3812** Fenugreek gum	**3173 Gum ghatti**
316 Propylene glycol alginate	**3711** Cellulose	**3813** Guar gum	**3174 Gum tragacanth**
32 Carrageenans	**3712** Cellulose derivatives	**3814** Locust bean gum	**3175 Karaya gum**
321 ι-Carrageenan	**372 Cereal β-glucans**	**3815** Tara gum	**3176 Mesquite gum**
322 κ-Carrageenan	**3721** Oat gum	**382 Glucomannans**	**318 Soluble soybean polysaccharide**
323 λ-Carrageenan	**373 Curdlan**	**3821** Konjac mannan	**319 Xylans**
324 Furcellaran	**374 Dextran**	**39 Other microbial polysaccharides**	**3191 Psyllium**
325 Processed Eucheuma Seaweed	**375 Elsinan**		**3192 Tamarind gum**
33 Chitin	**376 Lentinan**	**391 Acetan**	
331 Chitosan	**377 Pullulan**	**392 Emulsan**	

Wall materials destined to flavour encapsulation should present a number of specific properties: be non-toxic, non-allergenic, biocompatible and biodegradable, have a GRAS status, be soluble or at least dispersible in a GRAS solvent, have film-forming and/or emulsifying properties, have good barrier properties, be tasteless so as not to interfere with the flavour that is intended to be released by creating an off-taste, be chemically inert and relatively cheap. The shell material should also be able to provide a continuous coating and form a film which is cohesive with the active ingredient (Uhlemann *et al.*, 2002; Fang, 2012; Sri *et al.*, 2012; Sobel *et al.*, 2014b; Vasisht, 2014; Mishra, 2015; Gupta *et al.*, 2016; Tolve *et al.*, 2016).

Depending on the selected encapsulation process, different properties can be of interest and will be listed for each compound to help select suitable shell materials.

2.4.4 Available food grade shell materials for the previously selected techniques

Liposome entrapment limits its available materials to a small number of lipids (see Table 2.5).

Table 2.5: Available materials for the liposome entrapment process.

LIPOSOME ENTRAPMENT	
Wall materials	**References**
Modified starches	(Tolve *et al.*, 2016)

Coextrusion with a vibrating nozzle also offers a limited number of possibilities (see Table 2.6), but complex coacervation presents a very large range of available materials (see Table 2.7), and this choice can even be enlarged by the combination of those compounds.

Table 2.6: Available materials for the coextrusion with vibrating nozzle process.

COEXTRUSION WITH VIBRATING NOZZLE	
Wall materials	**References**
Agar	(Brandau, 2014)
Alginate	(Whelehan and Marison, 2011; Brandau, 2014)
Carrageenan	(Brandau, 2014)
Chitosan	(Whelehan and Marison, 2011)
Gellan gum	(Brandau, 2014)
Modified celluloses	(Brandau, 2014)
Pectin	(Brandau, 2014)
Starch	(Brandau, 2014)

Table 2.7: Available materials for the coacervation process.

COACERVATION	
Wall materials	**References**
Acetylcellulose	(Sobel *et al.*, 2014b)
Agar	(Sobel *et al.*, 2014b)
Alginate	(Nesterenko *et al.*, 2013; Sobel *et al.*, 2014b; Gupta *et al.*, 2016)
Carboxymethyl cellulose	(Desai and Park, 2005; Nesterenko *et al.*, 2013; Wallick, 2014; Sobel *et al.*, 2014b; Gupta *et al.*, 2016)
Carrageenan	(Desai and Park, 2005; Sobel *et al.*, 2014b; Gupta *et al.*, 2016)
Cellulose derivatives	(Das *et al.*, 2011)
Chitosan	(Desai and Park, 2005; Das *et al.*, 2011; Gupta *et al.*, 2016)
Corn syrup solids	(Desai and Park, 2005; Gupta *et al.*, 2016)
Dextran	(Desai and Park, 2005; Gupta *et al.*, 2016)
Dextrin	(Gupta *et al.*, 2016)
Ethyl cellulose	(Desai and Park, 2005; Sobel *et al.*, 2014b; Gupta *et al.*, 2016)
Fucoidan	(Citkowska *et al.*, 2019)
Guar gum	(Desai and Park, 2005; Gupta *et al.*, 2016)
Gum Arabic	(Uhlemann *et al.*, 2002; Desai and Park, 2005; Das *et al.*, 2011; Nesterenko *et al.*, 2013; Sobel *et al.*, 2014b; Mishra, 2015; Gupta *et al.*, 2016)
HPMC	(Wallick, 2014)
Maltodextrin	(Desai and Park, 2005; Gupta *et al.*, 2016)
Methyl cellulose	(Desai and Park, 2005; Sobel *et al.*, 2014b; Gupta *et al.*, 2016)
Modified starch	(Desai and Park, 2005; Gupta *et al.*, 2016)
Pectin	(Nesterenko *et al.*, 2013; Gupta *et al.*, 2016; Klinjapo and Krasaekoopt, 2018)
Starch	(Desai and Park, 2005; Gupta *et al.*, 2016)

2.5 Conclusions

2.5.1 Selection of the encapsulation process

Based on the study of the parameters obtained for the different methods (particle morphology, nature of the active, particle size, trigger mechanism, processing costs, and available wall materials), complex coacervation seemed to be the best option for this project and was thus selected as the encapsulation process.

Coacervation is used for the encapsulation of essential oils and produces capsules with good controlled release properties (Burnside, 2014; Martins *et al.*, 2014). More specifically, it is one of the processes of choice for the encapsulation of flavours in confectionery (Klinjapo and Krasaekoopt, 2018).

2.5.2 Selection of the wall material

The oldest and most studied system for complex coacervation is the gelatine/gum arabic combination (Burnside, 2014; Xiao *et al.*, 2014).

The idea here is to combine two compounds with different properties to create a new composite shell material. Due to consumer acceptance and safety regulation concerns regarding materials from animal origin and the allergenic tendency of plant proteins, it was decided that the use of proteins in general would be best avoided. Instead of protein/polysaccharide combinations, complex coacervation can also occur between two oppositely charged polysaccharides (Xiao *et al.*, 2014). Hydrocolloid films provide a good barrier against oxygen and have excellent mechanical properties, although proteins can form films with even better properties (Shit and Shah, 2014).

Different properties of interest for complex coacervation were compared (see Table 2.8, the references are listed per material after the table).

The following table is organised in three main categories of parameters, considered by degree of importance. First it was checked whether the materials possessed the required characteristics to undergo complex coacervation: 1) the materials used to produce a shell need to be in the continuous phase so they need to be soluble or at least dispersible in water; 2) since complex coacervation is based on the electrostatic charge interaction between two polymers, the compounds also need to be ionic. Then the capacity of the materials to form a proper wall were considered: it should be desired that at least one of the two polysaccharides has gelling or film-forming properties. Finally, a few aspects for the use of compounds in food application were also taken into account: no off-taste, ingredient recognised as a food additive in Europe and/or with a GRAS status in the US.

Table 2.8: Comparison of the properties of the different available materials (✓ : yes, × : no, - : no data).

Polysaccharides	Solubility/ Dispersibility in water	Ionic	Gelling agent	Film-forming properties	Tasteless	Food additive	GRAS
Alginic acid[1]	×	×	×	✓	✓	✓	✓
Ammonium alginate[2]	✓	✓	×	✓	✓	✓	✓
Calcium alginate[3]	×	✓	✓	✓	✓	✓	✓
Potassium alginate[4]	✓	✓	×	✓	✓	✓	✓
Sodium alginate[5]	✓	✓	✓	✓	✓	✓	✓
Propylene glycol alginate[6]	✓	✓	×	✓	✓	✓	×
ι-Carrageenan[7]	✓	✓	✓	✓	✓	✓	×
κ-Carrageenan[8]	✓	✓	✓	✓	✓	✓	×
λ-Carrageenan[9]	✓	✓	×	✓	✓	✓	×
Furcellaran[10]	✓	✓	✓	✓	✓	✓	×
Processed Eucheuma Seaweed[11]	✓	✓	✓	✓	✓	✓	×
Chitosan[12]	✓	✓	×	✓	✓	×	×
Inulin[13]	✓	×	✓	✓	✓	×	×
Levan[14]	✓	×	×	✓	-	×	×
Fucoidan[15]	✓	✓	×	✓	-	×	✓
Agar[16]	✓	×	✓	✓	✓	✓	✓
Larch gum[17]	✓	×	✓	✓	✓	✓	×
Cellulose[18]	×	×	✓	✓	✓	✓	✓
Carboxymethyl cellulose[19]	✓	✓	×	✓	✓	✓	×

Table 2.8: Comparison of the properties of the different available materials (✓ : yes, × : no, - : no data) (continued).

Polysaccharides	Solubility/ Dispersibility in water	Ionic	Gelling agent	Film-forming properties	Tasteless	Food additive	GRAS
Ethyl cellulose[20]	×	×	×	✓	✓	✓	×
Ethyl hydroxyethyl cellulose[21]	✓	×	×	-	✓	✓	✓
Hydroxypropyl cellulose[22]	✓	×	×	✓	✓	✓	×
Hydroxypropyl methyl cellulose[23]	✓	×	✓	✓	✓	✓	×
Methyl cellulose[24]	✓	×	✓	✓	✓	✓	✓
Methyl ethyl cellulose[25]	✓	×	×	-	✓	✓	×
Cereal β-glucan[26]	✓	×	✓	✓	✓	✓	✓
Curdlan[27]	✓	×	✓	✓	✓	✓	×
Dextran[28]	✓	×	✓	-	✓	×	✓
Elsinan[29]	✓	×	-	✓	✓	×	×
Lentinan[30]	✓	×	-	-	-	×	×
Pullulan[31]	✓	×	-	✓	✓	✓	✓
Schizophyllan[32]	✓	×	-	✓	-	×	×
Scleroglucan[33]	✓	×	✓	✓	-	×	✓
Starch[34]	✓	×	✓	✓	✓	×	✓
Dextrin[35]	✓	×	×	✓	-	✓	✓
Cyclodextrin[36]	✓	✓	×	×	-	✓	×
Maltodextrin[37]	✓	×	✓	✓	✓	×	✓

Table 2.8: Comparison of the properties of the different available materials (✓ : yes, × : no, - : no data) (continued).

Polysaccharides	Solubility/ Dispersibility in water	Ionic	Gelling agent	Film-forming properties	Tasteless	Food additive	GRAS
Starch sodium octenyl succinate[38]	✓	✓	×	✓	-	✓	×
Cassia gum[39]	✓	×	×	✓	-	✓	✓
Fenugreek gum[40]	✓	✓	×	✓	×	×	✓
Guar gum[41]	✓	×	✓	✓	✓	✓	✓
Locust bean gum[42]	✓	×	✓	✓	-	✓	✓
Tara gum[43]	✓	×	×	✓	✓	✓	✓
Konjac mannan[44]	✓	×	✓	✓	✓	✓	✓
Acetan[45]	✓	✓	✓	-	-	×	×
Emulsan[46]	✓	✓	✓	✓	-	×	×
Gellan gum[47]	✓	✓	✓	✓	-	✓	×
Kefiran[48]	✓	×	✓	✓	-	×	×
Welan gum[49]	✓	✓	✓	✓	-	×	×
Xanthan gum[50]	✓	✓	✓	✓	✓	✓	×
Pectin[51]	✓	✓	✓	✓	-	✓	✓
Flaxseed gum[52]	✓	✓	✓	✓	-	×	×
Gum arabic[53]	✓	✓	×	✓	✓	✓	✓
Gum ghatti[54]	✓	✓	×	✓	✓	✓	✓
Gum tragacanth[55]	✓	✓	✓	✓	✓	✓	✓
Karaya gum[56]	✓	✓	✓	✓	✓	✓	✓
Mesquite gum[57]	✓	×	×	✓	-	×	×
Soluble soybean polysaccharide[58]	✓	✓	×	✓	-	×	✓
Psyllium[59]	✓	✓	✓	✓	-	×	×
Tamarind gum[60]	✓	×	×	✓	✓	×	✓

1 (Draget, 2009; Williams and Phillips, 2009b; Wandrey *et al.*, 2010; Wüstenberg, 2015; Food and Drug Administration, 2020)

2-4 (Hawley, 1977; Draget, 2009; Williams and Phillips, 2009b; Wüstenberg, 2015; Food and Drug Administration, 2020)

5 (Draget, 2009; Williams and Phillips, 2009b; Wandrey *et al.*, 2010; Wüstenberg, 2015; Food and Drug Administration, 2020)

6 (Fallourd and Viscione, 2009; Williams and Phillips, 2009b; Wüstenberg, 2015; Food and Drug Administration, 2020)

7-11 (Imeson, 2009; Williams and Phillips, 2009b; Wandrey *et al.*, 2010; Wüstenberg, 2015; Gawai *et al.*, 2017; Food and Drug Administration, 2020)

12 (Muzzarelli, 2009; Wandrey *et al.*, 2010; Khan and Marya, 2019; Food and Drug Administration, 2020)

13 (Grandtner *et al.*, 2005; Fallourd and Viscione, 2009; Meyer and Blaauwhoed, 2009; BeMiller, 2019b; BeMiller, 2019d; Food and Drug Administration, 2020)

14 (Fett *et al.*, 1995; Park and Khan, 2009; Giavasis, 2013; Food and Drug Administration, 2020)

15 (Hifney *et al.*, 2016; Citkowska *et al.*, 2019; Food and Drug Administration, 2020)

16 (Budavari, 1996; Williams and Phillips, 2009b; Wüstenberg, 2015; BeMiller, 2019d; Food and Drug Administration, 2020)

17 (López-Franco *et al.*, 2009; Williams and Phillips, 2009b; BeMiller, 2019d; Food and Drug Administration, 2020)

18 (Williams and Phillips, 2009b; Wandrey *et al.*, 2010; Wang *et al.*, 2012a; Wüstenberg, 2015; BeMiller, 2019d)

19-20 (Williams and Phillips, 2009b; Wandrey *et al.*, 2010; Wüstenberg, 2015; BeMiller, 2019d; Food and Drug Administration, 2020)

21 (Carlsson *et al.*, 1986; Williams and Phillips, 2009b; Wandrey *et al.*, 2010)

22 (Williams and Phillips, 2009b; Wandrey *et al.*, 2010; BeMiller, 2019d; Food and Drug Administration, 2020)

23 (Klemm *et al.*, 2005; Williams and Phillips, 2009b; Wandrey *et al.*, 2010; Wallick, 2014; BeMiller, 2019d; Food and Drug Administration, 2020)

24 (Williams and Phillips, 2009b; Wandrey *et al.*, 2010; Wallick, 2014; BeMiller, 2019d; Food and Drug Administration, 2020)

25 (Williams and Phillips, 2009b; Wandrey *et al.*, 2010; BeMiller, 2019d; Food and Drug Administration, 2020)

26 (Stevenson, 2009; Williams and Phillips, 2009b; Viscione, 2013; BeMiller, 2019d; Food and Drug Administration, 2020)

27 (Nishinari *et al.*, 2009b; Williams and Phillips, 2009b; Giavasis, 2013; Jindal and Khattar, 2018; BeMiller, 2019d; Food and Drug Administration, 2020)

28 (Park and Khan, 2009; Giavasis, 2013; Jindal and Khattar, 2018; BeMiller, 2019d; Food and Drug Administration, 2020)

29 (Park and Khan, 2009; Giavasis, 2013; Food and Drug Administration, 2020)

30 (Giavasis, 2013; Nandi *et al.*, 2013; Food and Drug Administration, 2020)

31 (Giavasis, 2013; Jindal and Khattar, 2018; BeMiller, 2019d)

32 (Giavasis, 2013; Zhang *et al.*, 2013; Food and Drug Administration, 2020)

33 (Park and Khan, 2009; Giavasis, 2013; Jindal and Khattar, 2018)

34 (Parker and Ring, 2001; Taggart and Mitchell, 2009; Wandrey *et al.*, 2010; Wüstenberg, 2015; BeMiller, 2019d; Food and Drug Administration, 2020)

35 (Taggart and Mitchell, 2009; Wandrey *et al.*, 2010; Food and Drug Administration, 2020)

36 (Mentink, 1999; Wandrey *et al.*, 2010; Food and Drug Administration, 2020; Merck, 2020)

37 (Loret *et al.*, 2004; Taggart and Mitchell, 2009; Wandrey *et al.*, 2010; Wüstenberg, 2015; Food and Drug Administration, 2020)

38 (McClements, 2009; Williams and Phillips, 2009b; Chen, 2015; Wüstenberg, 2015; Food and Drug Administration, 2020)

39 (Hallagan *et al.*, 1997; Cao *et al.*, 2018; BeMiller, 2019d; Food and Drug Administration, 2020)

40 (BeMiller, 2019d; Salarbashi *et al.*, 2019; Food and Drug Administration, 2020)

41 (Williams and Phillips, 2009b; Wüstenberg, 2015; Gupta and Variyar, 2018; BeMiller, 2019d; Food and Drug Administration, 2020)

42 (Fallourd and Viscione, 2009; Williams and Phillips, 2009b; Wüstenberg, 2015; BeMiller, 2019d; Food and Drug Administration, 2020; Liu *et al.*, 2020)

43 (Garti *et al.*, 1997; Williams and Phillips, 2009b; BeMiller, 2019d; Santos *et al.*, 2019; Liu *et al.*, 2020)

44 (Takigami, 2009; Williams and Phillips, 2009b; Wüstenberg, 2015; BeMiller, 2019b; BeMiller, 2019d)

45 (Ishida *et al.*, 2003; Giavasis, 2013; Jindal and Khattar, 2018; Food and Drug Administration, 2020)

46 (Gutnick *et al.*, 1982; Gutnick, 1987; Jindal and Khattar, 2018; Food and Drug Administration, 2020)

47 (Sworn, 2009a; Williams and Phillips, 2009b; Jindal and Khattar, 2018; Soni and Ghosh, 2018; BeMiller, 2019d; Food and Drug Administration, 2020)

48 (Piermaria *et al.*, 2015; Moradi and Kalanpour, 2019; Food and Drug Administration, 2020)

49 (Kaur *et al.*, 2014; Wang *et al.*, 2019; Food and Drug Administration, 2020)

50 (Williams and Phillips, 2009b; Giavasis, 2013; Abson *et al.*, 2014; Wüstenberg, 2015; Jindal and Khattar, 2018; BeMiller, 2019d; Food and Drug Administration, 2020)

51 (Williams and Phillips, 2009b; Wandrey *et al.*, 2010; Wüstenberg, 2015; BeMiller, 2019d; Food and Drug Administration, 2020)

52 (Izydorczyk *et al.*, 2005; Hu *et al.*, 2017; Food and Drug Administration, 2020)

53 (Williams and Phillips, 2009a; Williams and Phillips, 2009b; Wandrey *et al.*, 2010; BeMiller, 2019d; Food and Drug Administration, 2020)

54 (Izydorczyk *et al.*, 2005; Williams and Phillips, 2009b; Wüstenberg, 2015; BeMiller, 2019d; Food and Drug Administration, 2020)

55 (López-Franco *et al.*, 2009; Williams and Phillips, 2009b; Wandrey *et al.*, 2010; Wüstenberg, 2015; BeMiller, 2019d; Food and Drug Administration, 2020)

56 (López-Franco *et al.*, 2009; Williams and Phillips, 2009b; BeMiller, 2019d; Food and Drug Administration, 2020)

57 (López-Franco *et al.*, 2009; Wandrey *et al.*, 2010; Food and Drug Administration, 2020)

58 (Maeda and Nakamura, 2009; Wandrey *et al.*, 2010)

59 (Izydorczyk, 2009; Swaroop *et al.*, 2017; Nie *et al.*, 2018; BeMiller, 2019d; Food and Drug Administration, 2020)

60 (Wüstenberg, 2015; BeMiller, 2019d; Dey *et al.*, 2019; Food and Drug Administration, 2020)

Given the previously explained considerations for the comparison of materials, suitable compounds had to fulfil both parameters for the first two columns (be soluble or dispersible in water, and be ionic) as well as at least one parameter between the third and fourth columns (gelling and/or film-forming properties) to be used for complex coacervation encapsulation. It was also important that the ingredients were tasteless so as not to mask the encapsulated flavour when released. The remaining possible materials remaining for this method (highlighted in green in the "Polysaccharides" column) were therefore: alginate salts (except calcium alginate), carrageenans, furcellaran, Processed Eucheuma Seaweed, fucoidan, carboxymethyl cellulose, starch sodium octenyl succinate, gellan gum, xanthan gum, pectin, gum arabic, gum ghatti, gum tragacanth, karaya gum and soluble soybean polysaccharide.

With the new opportunity of using a vegetable chitosan alternative, chitosan could still be considered as a potential material.

Even though some starch derivatives seemed to be good candidates, they were not considered for this project as they could be potential allergens or contain sensitisers, as mentioned in the "Regulations" section.

Sought after properties for the wall material in this project were to have a quite brittle shell in order to create a clear burst upon chewing, as well as provide a good barrier against moisture. Brittleness means that a material has little tendency to deform, when subjected to stress, before it is ruptured. This information is characterised by a low tensile strength and a low elongation at break percentage (Zhang, 2011).

Chitosan is a rather interesting material as it is one of the only cationic polysaccharides and enables a large choice of combinations with other polysaccharides at pH above their pKa. It is chemically inert, non-toxic, very abundant, and does not need the addition of any additive to

form films with good mechanical and barrier properties. Indeed, it can have reasonably low tensile strength and elongation at break values (respectively 10-100 MPa and 20-80%) (Shit and Shah, 2014), which makes it a good candidate for the brittleness characteristic. It also has a very low Water Vapour Permeability (3.66-4.80 x 10^{-11}) at a 2% concentration, which makes it an efficient barrier against moisture.

In order to choose another material to combine with chitosan, the comparison of the pKa of the polysaccharides needed to be done to check that there could be a pH window below the pKa of chitosan and above the pKa of other polyelectrolytes so that they could be oppositely charged in solution.

Among the remaining polysaccharide options, even there were some missing pKa values, they all seemed to be a possible combination material for chitosan as they are all anionic (see Table 2.9).

Table 2.9: pKa values of the remaining available materials.

Polysaccharides	pKa	References
Alginates	3.0 - 4.4	(Rinaudo, 2006a; Draget, 2009; Shinde and Nagarsenker, 2009)
Carrageenans	4.9	(Sadeghi, 2012)
Furcellaran	Anionic	
Chitosan	5.5 - 7.0	(Muzzarelli, 2009; Santiago de Alvarenga, 2011; Xiao *et al.*, 2014)
Fucoidan	1.0 - 2.5	(Ho, 2015)
Carboxymethyl cellulose	3.2 - 3.8	(Zhivkov, 2013)
Gellan gum	3.0 - 3.6	(Fasolin *et al.*, 2013; Yang *et al.*, 2013; Würstenberg, 2015)
Xanthan gum	3.1	(Oprea *et al.*, 2013)
Pectin	3.5 - 4.0	(Chen *et al.*, 2012; Xiao *et al.*, 2014)
Gum arabic	2.0	(Gulão *et al.*, 2016)
Gum ghatti	Anionic	
Gum tragacanth	3.6	(Comert *et al.*, 2016)
Karaya gum	Anionic	(Pegg, 2012)
Soluble soybean polysaccharide	Anionic	

However, fucoidan and gum arabic have the lowest pKa values and would allow a larger pH range to enable the charge interaction, they should thus be a privileged choice. Furthermore, fucoidan has not been widely studied and is not recognised as a food additive in Europe.

Gum arabic possesses unique properties and is a material of choice for coacervation (Burnside, 2014). It is also a commonly used polysaccharide in confectionery (Klinjapo and Krasaekoopt, 2018).

Finally, after reviewing a few patents, it was found that the combination of chitosan and gum arabic through complex coacervation did not seem to have been claimed for chewing gum application (Elabbadi and Erni, 2019). Especially the use of vegetable chitosan would also be quite innovative.

After all those considerations, the combination **gum arabic/chitosan** was selected as the starting wall material to be used in **complex coacervation** for this project.

CHAPTER 3 – Materials and Methods

Following a thorough literature review, the complex coacervation process was first selected to encapsulate L-carvone flavour oil within a gum arabic/chitosan composite shell for chewing gum application. It was first desired to produce physically stable capsules which would keep their integrity in time after the drying step and when incorporated to the gum matrix. Secondly, it was expected to obtain a flavour burst during chewing. Several methods were thereby used to characterise the particles physical, structural and mechanical properties, as well as the flavour release profile.

In a desire to improve their performance, the previous capsules were engineered through further processes, using additional shell materials for the gum arabic/chitosan combination. Later on, alternative ionic polymer combinations were also investigated for complex coacervation in an effort to surpass the quality of the gum arabic/chitosan capsules which were previously obtained.

This chapter is composed of two parts. In the first section, all food grade materials involved in the following work are presented, with their properties and suppliers. The second part focuses on the experimental techniques and procedures involved in the preparation and characterisation of the capsules.

3.1 Materials

3.1.1 Gum arabic (CAS# 9000-01-5)

Gum arabic, or gum *Acacia*, is the most used food hydrocolloid, and is extracted from the *Acacia* tree. It is supplied under the form of an odourless and tasteless, beige powder (Williams and Phillips, 2009a; Wandrey *et al.*, 2010).

Gum arabic is a complex, highly branched polysaccharide. Its principal chemical structure is composed of β-1,3-, β-1,6-D-galactopyranosyl, and β-1,6-D-glucuronopyranosyl units, with side chains of β-1,6-D-galactopyranose, α-L-arabinofuranose, α-L-rhamnopyranose, β-D-glucopyranuronic acid and 4-O-methyl-β-D-glucopyranuronic acid residues (see Figure 3.1) (Izydorczyk *et al.*, 2005; Wandrey *et al.*, 2010). It also has about 2-3% (the author did not specify the basis of the percentage) of protein content (Williams and Phillips, 2009b). The gum arabic molecule takes a disc-like conformation (Williams and Phillips, 2009a).

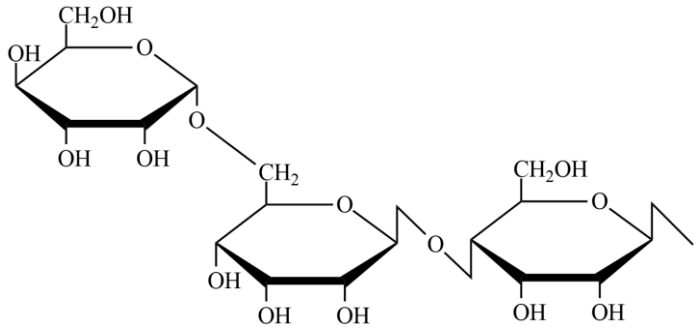


Figure 3.1: Main repeating unit of gum arabic (redrawn from Mariod, 2018).

Gum arabic from ACROS Organics was purchased from Fisher Scientific UK Ltd. (Leicestershire, United Kingdom). It has a molecular weight between 200 and 800 kDa. It is highly soluble in water and assumes a random coil conformation in solution (Williams and Phillips, 2009a; Masuelli, 2013). It leads to low viscosity, acidic solution (pH 4.5).

3.1.2 Water (CAS# 7732-18-5)

Deionised (DI) water was used as the presence of ions can modify the complex coacervation process. Furthermore, the presence of salts can even completely inhibit the phenomenon as it exhibits a dissociating effect on complexes (de Kruif *et al.*, 2004; Schmitt, 2009).

The water was purified directly from the tap using a Arium® Mini Plus from Sartorius (Surrey, United Kingdom).

3.1.3 Chitosan (CAS# 9012-76-4)

Chitosan is an abundant, non-toxic, biocompatible, biodegradable food hydrocolloid from animal or vegetable origin (Muzzarelli, 2009). It comes from the alkaline partial deacetylation of chitin, which can be found in the shell of crustaceans, the cell wall of fungi, and the exoskeleton of insects. It is supplied under the form of a beige powder, which has a slight bitter taste.

Chitosan is a cationic semi-crystalline linear copolymer (Muzzarelli, 2009). Its principal chemical structure is composed of β-1,4-linked N-acetyl-D-glucosamine and D-glucosamine units (see Figure 3.2) (Wandrey *et al.*, 2010). The molecule is semi-rigid (Rinaudo, 2006b).

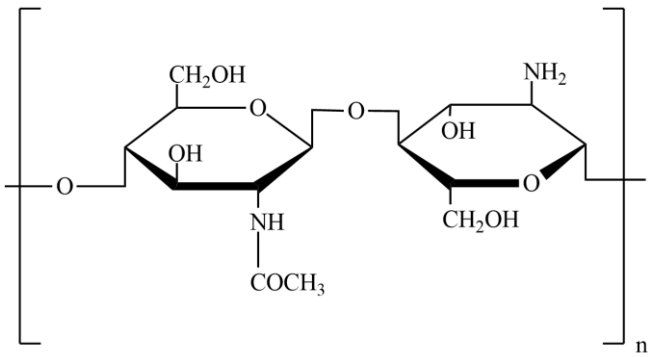


Figure 3.2: Main repeating unit of chitosan (redrawn from Wandrey *et al.*, 2010).

Chitosan can be purchased in low, medium, or high molecular weight grades (Merck, 2020). Low molecular weight chitosan (75-85% deacetylated, M_w = 50-190 kDa) was purchased from Sigma-Aldrich Company Ltd. (Dorset, United Kingdom) and was used for most experiments. High molecular weight chitosan (>75% deacetylated, M_w = 310-375 kDa) and medium molecular weight chitosan (75-85% deacetylated) from Sigma-Aldrich Company Ltd. (Dorset, United Kingdom) were also used for one-off trials. Complex coacervation is influenced by the molecular weight and concentration of the wall materials. Low molecular weight chitosan exhibits a molecular weight of the same order of that of gelatine type B (about 46 kDa) which has been used in the extensively studied gelatine/gum arabic combination for complex coacervation (Burgess and Carless, 1984; Burgess, 1990). This material could indeed be used as proof of principle but vegetable-derived chitosan could be used in future work.

Chitosan is insoluble in water and organic solvents (Muzzarelli, 2009). It is soluble in aqueous acidic media, such as formic acid or acetic acid, after the protonation of its amino groups and thanks to the formation of water-soluble salts (Mourya and Inamdar, 2008; Muzzarelli, 2009). It precipitates around pH 7.0 (Yan and Zhang, 2014). Chitosan can lead to strong, flexible and tear-resistant films (Muzzarelli, 2009). It is brittle when dry (Khan and Marya, 2019). It also has antimicrobial properties (Muzzarelli, 2009).

3.1.4 Acetic acid (CAS# 64-19-7)

Glacial acetic acid (100%, ACS reagent) was purchased from Sigma-Aldrich Company Ltd. (Dorset, United Kingdom).

3.1.5 Non-ionic emulsifiers

Span® 20 (sorbitan monolaurate, CAS# 1338-39-2), Polysorbate 20 (Tween® 20, CAS# 9005-64-5, grade FG), Span® 60 (sorbitane monostearate, CAS# 1338-41-6), Tween® 60 (CAS#

9005-67-8), Span® 65 (sorbitan tristearate, CAS# 26658-19-5), Tween® 65 (polyoxyethylenesorbitan tristearate, CAS# 9005-71-4), Span® 80 (sorbitane monooleate, CAS# 1338-43-8), Polysorbate 80 (Tween® 80, CAS# 9005-65-6, grade FG), Span® 85 (sorbitane trioleate, CAS# 26266-58-0) and Tween® 85 (CAS# 9005-70-3) were all obtained from Sigma-Aldrich Company Ltd. (Dorset, United Kingdom).

3.1.6 L-carvone (CAS# 6485-40-1)

L-carvone (≥ 97%, FCC, FG) from Sigma-Aldrich was kindly provided by Mondelēz International (New Jersey, United States). It should be used below 94ºC (flash point) (Merck, 2020). This flavour oil (see Figure 3.3) is practically insoluble in water (1.3-1.65 g/L) (Yalkowsky *et al.*, 2010). It is miscible with alcohol and soluble in propylene glycol and most fixed oils (Burdock, 2005). It has a refractive index of 1.497 at 20ºC, a density of 0.959 at 25ºC, and a vapour pressure of 50 Pa at 20ºC (Burdock, 2005; Merck, 2020).

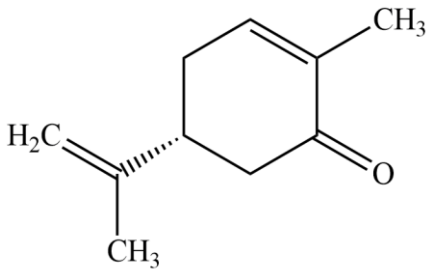


Figure 3.3: L-carvone structure (redrawn from Merck, 2020).

3.1.7 Nile red (CAS# 7385-67-3)

Nile red (technical grade) was purchased from Sigma-Aldrich Company Ltd. (Dorset, United Kingdom).

3.1.8 MCT oils

Coconut oil from *Cocos crucifera* (CAS# 8001-31-8, low-melting solid) and palm oil (CAS# 8002-75-3, analytical standard) were both supplied by Sigma-Aldrich Company Ltd. (Dorset, United Kingdom).

Miglyol® 812 N (CAS# 73398-61-5) was a gift from KemCare Ltd (Greater London, United Kingdom).

3.1.9 Sodium hydroxide (CAS# 1310-73-2)

Sodium hydroxide (K <0.02%) pellets (≥ 98%, ACS reagent) were obtained from Fluka (Fisher Scientific UK Ltd., Leicestershire, United Kingdom).

3.1.10 Crosslinkers

Tannic acid (CAS# 1401-55-4, ACS reagent) was purchased from Sigma-Aldrich Company Ltd. (Dorset, United Kingdom).

Sodium tripolyphosphate (NaTPP, CAS# 7758-29-4, granular) from Alfa Aesar was purchased from Fisher Scientific UK Ltd. (Leicestershire, United Kingdom).

3.1.11 Ethanol (CAS# 64-17-5)

Ethanol, absolute (analytical reagent grade) was obtained from Fisher Scientific UK Ltd. (Leicestershire, United Kingdom).

3.1.12 Maltodextrin (CAS# 9050-36-6)

Maltodextrin (dextrose equivalent 4.0-7.0) was purchased from Sigma-Aldrich Company Ltd. (Dorset, United Kingdom).

3.1.13 Shellac coating

Shellac is a natural, non-toxic and biodegradable resin (Xue and Zhang, 2008; Farag and Leopold, 2009). It is extracted from the lac bug (*Kerria lacca*) and is usually supplied under the form of translucid, orange to brown flakes. It is a GRAS food additive and has been used as a coating agent in the food industry (Farag and Leopold, 2009).

A 25 wt% solution from shellac ammonium salt (CAS# 68308-35-0), SWANLAC® ASL 10, was a kind gift from A.F. Suter & Co. Ltd (Essex, United Kingdom). Shellac is a hydrophobic oligomer which can however be dissolved in alkali conditions (above pH 7) (Farag and Leopold, 2009; Long *et al.*, 2015). It exhibits good barrier and mechanical properties, and also has film-forming properties.

Sunflower oil was purchased from a local supermarket and used as such.

3.1.14 Chitosan grafting

Gallic acid (CAS# 149-91-7, 97.5-102.5% (titration)), L-ascorbic acid (CAS# 50-81-7, puriss. p.a., ACS reagent, reag. ISO, reag. Ph. Eur., 99.7-100.5% (oxidimetric)), and PERDROGEN™ 30% H_2O_2 (w/w) (CAS# 7722-84-1, puriss. p.a., reag. ISO, reag. Ph. Eur., ≥30%) were all purchased from Sigma-Aldrich Company Ltd. (Dorset, United Kingdom).

3.1.15 Nanoparticles

Calcium carbonate nanoparticles (CAS# 471-34-1, product 1951RH, 98+%, 15~40 nm) were purchased from Skyspring Nanomaterials, Inc. (Texas, United States).

Calcium chloride dihydrate (CAS# 10035-04-8, 99.0-103.0%, AnalaR NORMAPUR® ACS, Reag. Ph. Eur. analytical reagent) and sodium carbonate anhydrous (CAS# 497-19-8) were

respectively obtained from VWR International Ltd (Leicestershire, United Kingdom) and Sigma-Aldrich Company Ltd. (Dorset, United Kingdom).

3.1.16 Anionic gelling polysaccharides

3.1.16.1 Sodium alginate (CAS# 9005-38-3)

Alginates are quite abundant food hydrocolloid gums, and more precisely phycocolloids as they are extracted from brown seaweeds (*Phaeophyceae*) (Draget, 2009). They are non-toxic, biocompatible, biodegradable polysaccharides (Paques, 2015). They are supplied under the form of a clear-coloured, odourless powder.

Alginates are unbranched, anionic polysaccharides (Wandrey *et al.*, 2010). Their principal chemical structure is composed of linear binary copolymers of β-1,4-D-mannuronic acid (M) and α-1,4-L-guluronic acid (G), linked by 1,4-glycosidic linkages and arranged in homopolymeric blocks, with several possible modifications (see Figure 3.4). However, the distribution of the monomers is not repeating itself as a regular sequence. The sequential parameters, and thus properties, are dependent on the algae source, the extraction process, the season and the growth conditions (Paques, 2015). G blocks are more rigid than M blocks due to steric hindrance.

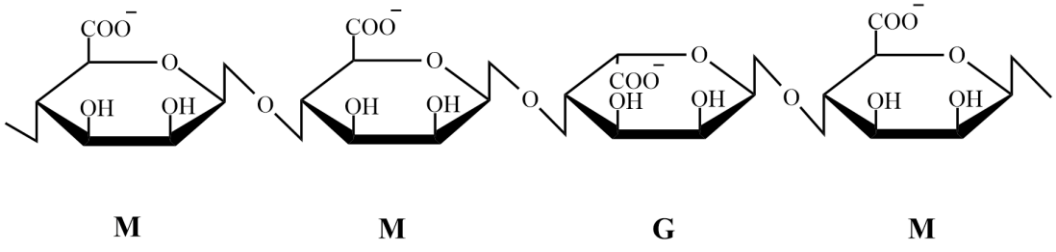


Figure 3.4: Example of the structure of alginate blocks composed of M and G repeating units (redrawn from Wandrey *et al.*, 2010).

Sodium alginate (halal grade) was purchased from Sigma-Aldrich Company Ltd. (Dorset, United Kingdom). It is soluble in water, but its solubility depends on the pH, the total ionic strength and the hardness of the water (Draget, 2009). Alginates can precipitate at pH below their pKa (Fallourd and Viscione, 2009). The exact value varies with the alternating block sequence (Draget, 2009).

Alginates can lead to the formation of cold set thermo-irreversible gels in the presence of divalent cations, except magnesium, the most commonly used one being calcium. Ionic crosslinking can be done either by outer diffusion (or external gelation), or by internal setting (or internal gelation), using inert calcium and adjusting the pH. Their gelling properties are mostly independent of temperature, but too high temperatures (above 200°C) can degrade the polysaccharide. A three-dimensional (3D) gel network is instantaneously formed resulting from a sol/gel transition due to an ion exchange between the divalent cation and the molecule counter ions. This phenomenon causes a gathering of the G blocks around the cations in a saw-tooth conformation, leading to a characteristic "egg box" configuration (see Figure 3.5). Alginates with a high G block content thus lead to rigid, porous, brittle gels, whereas alginates with a high M block content lead to more elastic weaker gels. The gelling behaviour is however difficult to forecast since the block sequence can vary from one batch to the other (Izydorczyk *et al.*, 2005; Draget, 2009; Paques, 2015; dos Santos Araújo *et al.*, 2019).

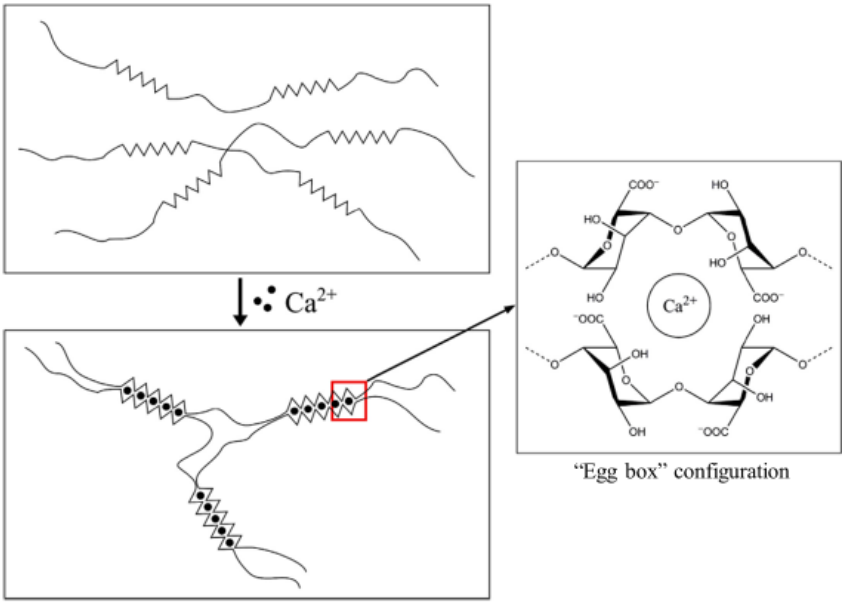


Figure 3.5: Gelling mechanism of alginates showing the "egg box" configuration (Paques, 2015).

3.1.16.2 ι-Carrageenan (CAS# 9062-07-1)

Carrageenan is a food hydrocolloid gum, and more precisely a phycocolloid as it is extracted from red seaweeds (*Rhodophyceae*) (Imeson, 2009). It is supplied under the form of a tasteless, beige powder (Gawai *et al.*, 2017).

It is a linear, anionic polysaccharide, whose main chemical structure is composed of repeating units of β-1,3-D-galactopyranose and 3,6-anhydro-α-1,4-D-galactopyranose (3,6 AG), alternatively linked by α-1,3- and β-1,4-glycosidic segments (Imeson, 2009; Wandrey *et al.*, 2010). There are three types of carrageenans: ι-carrageenan, κ-carrageenan and λ-carrageenan, depending on the number and position of their sulphate groups (see Figure 3.6). Carrageenans have high sulphate contents (24 to 53%, the authors did not specify the basis of this percentage) (Armisén and Galatas, 2009).

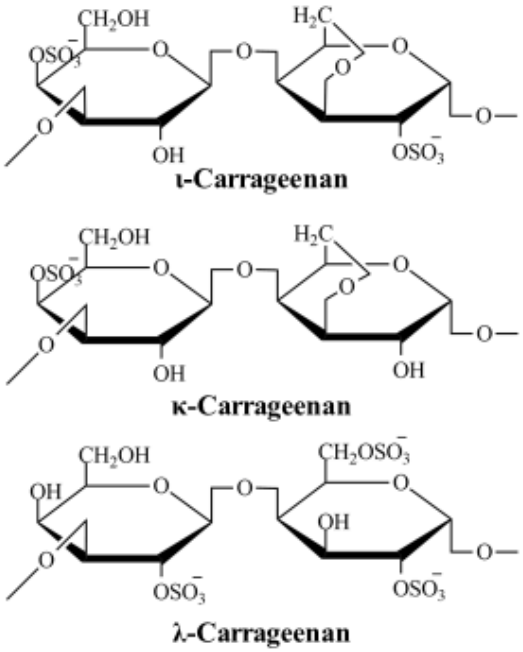


Figure 3.6: Main repeating units of ι-, κ- and λ-carrageenans (redrawn from Imeson, 2009; Wandrey *et al.*, 2010; Xiao *et al.*, 2014).

Carrageenan, iota type (powder) from Alfa Aesar was obtained from Fisher Scientific UK Ltd. (Leicestershire, United Kingdom). It is soluble in hot water at a concentration of 0.5 to 1% (the author did not specify the basis of this percentage) (Imeson, 2009). It usually hydrates above 40-60ºC. Carrageenan solutions lose their viscosity when heated, at pH below 4.3.

Carrageenans lead to thermo-reversible cold set gels upon cooling below 70-40ºC, depending on the type of carrageenan. The different types of carrageenans also have different texture properties: ι-carrageenan leads to soft and elastic gels in the presence of calcium ions, while κ-carrageenan results in rigid and brittle ones in the presence of potassium ions as the molecule adopts a helix conformation upon cooling, and λ-carrageenan does not gel. It was also noted that in the particular example of polyelectrolyte complexes formed with chitosan, the gel exhibited a higher mechanical strength when ι-carrageenan was used rather than κ-carrageenan. The gel network results from a coil to double helix transition, which leads to aggregation.

Solutions however lose their gel strength at pH below 4.3 due to hydrolysis so it would be desirable to use alginate above this pH when gelling properties are sought (Izydorczyk *et al.*, 2005; Imeson, 2009; Hamman, 2010; Wandrey *et al.*, 2010; Wu and McClements, 2015; Du *et al.*, 2016).

3.1.16.3 Gellan gum (CAS# 71010-52-1)

Gellan gum is an extracellular food hydrocolloid from bacterial origin (*Sphingomonas elodea*) (Sworn, 2009a). It is supplied under the form of a clear-coloured powder.

Gellan gum is an anionic polysaccharide (Sworn, 2009a; Wandrey *et al.*, 2010). Its principal chemical structure is composed of a linear tetrasaccharide made of a β-1,4-D-glucopyranosyl, a β-1,4-D-glucuronopyranosyl, a β-1,4-D-glucopyranosyl and an α-1,3-L-rhamnopyranosyl units, with acyl substituents (see Figure 3.7). It can either be in the high acyl (HA) or low acyl (LA) form. The molecule takes a double helix conformation (Izydorczyk *et al.*, 2005).

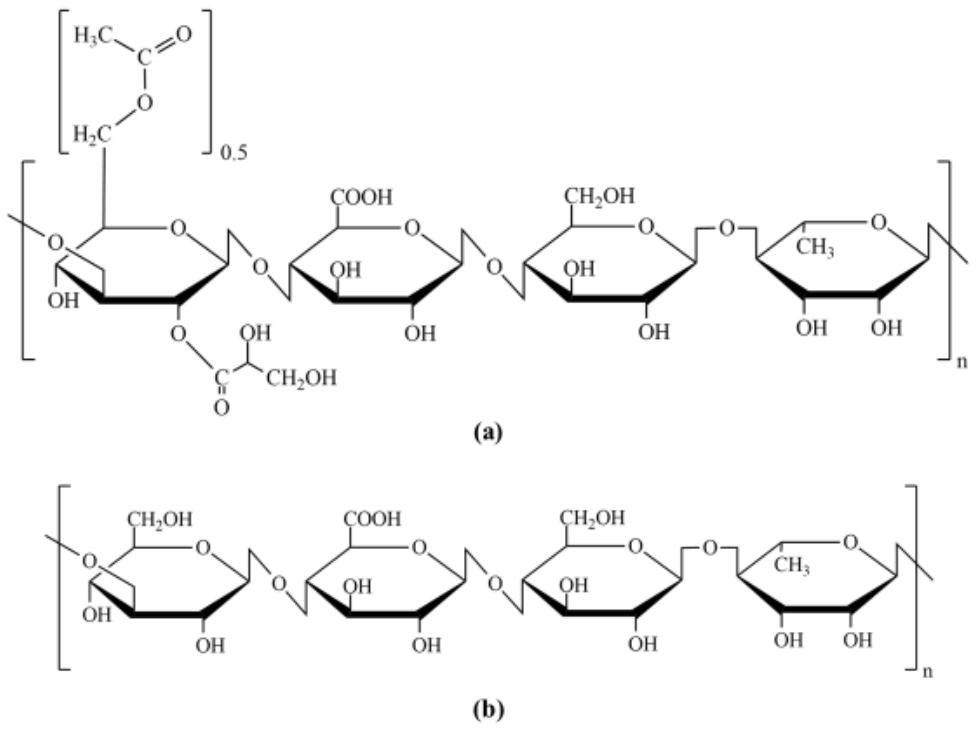


Figure 3.7: Main repeating units of gellan gum (a) high acyl (b) low acyl (redrawn from Sworn, 2009a; Giavasis, 2013).

Gellan gum (powder) from Alfa Aesar was purchased from Fisher Scientific UK Ltd. (Leicestershire, United Kingdom). It is insoluble in cold water but swells when dispersed (Sworn, 2009a). As it was unsure which was the form of the supplied gellan gum (HA or LA), it was desired to use it in temperature conditions that could suit either type. For HA gellan gum, the temperature of hydration depends on the ion content of the water but should be around 75ºC in DI water. LA gellan gum is fully hydrated around 85-90ºC. The hydration is incomplete if the pH is maintained below 4.0.

Gellan gum can form thermo-reversible transparent gels at low concentration upon cooling down to 70-10ºC, depending on the acyl level. A three-dimensional gel network is formed due to the occurrence of junction zones between the polymer chains during a coil to helix transition when cooling down. The high acyl form leads to soft, elastic gels whereas the low acyl form leads to hard, brittle ones in the presence of calcium, magnesium, sodium, potassium or hydrogen ions. The nature and concentration of the cations also influence the setting temperature (Izydorczyk *et al.*, 2005; Sworn, 2009a; Oxley, 2012b).

3.1.16.4 Xanthan gum (CAS# 11138-66-2)

Xanthan gum is a natural food hydrocolloid from bacterial origin (*Xanthomonas campestris*) (Sworn, 2009b). It is supplied under the form of a tasteless, cream-coloured powder (Abson *et al.*, 2014).

Xanthan gum is a long-chain, anionic heteropolysaccharide (Wandrey *et al.*, 2010). Its principal chemical structure is a repeating pentasaccharide composed of two linear chains of β-1,4-D-glucopyranosyl units linked to a trisaccharide side chain made of a α-1,3-D-mannopyranosyl unit followed by a β-1,2-D-glucuronopyranosyl unit and terminated by a β-1,4-D-mannopyranosyl unit (see Figure 3.8) (García-Ochoa *et al.*, 2000; Izydorczyk *et al.*, 2005;

Sworn, 2009b; Wandrey *et al.*, 2010). The first mannose residue of the side chain usually carries an acetyl group and about half of the end chain mannose residues carry a pyruvyl group (Sworn, 2009b). At room temperature, the molecule takes a rigid double helix conformation (Wandrey *et al.*, 2010).

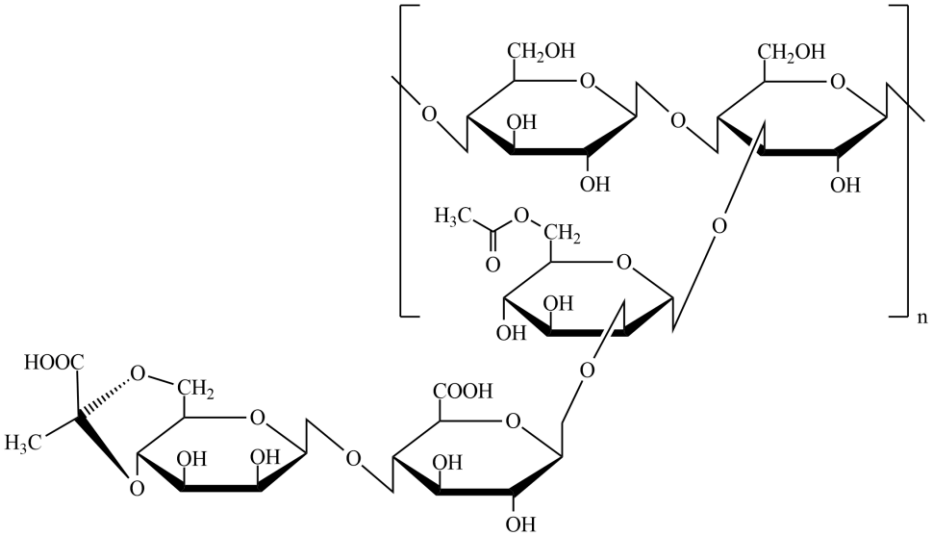


Figure 3.8: Main repeating unit of xanthan gum (redrawn from García-Ochoa *et al.*, 2000; Izydorczyk *et al.*, 2005; Sworn, 2009b; Giavasis, 2013).

Xanthan gum from *Xanthomonas campestris* was purchased from Sigma-Aldrich Company Ltd. (Dorset, United Kingdom). It is highly soluble in water and is usually used in solution at concentrations between 0.1 and 1% (w/w), and those solutions are stable upon heat and pH change in the range 2.5-11 (García-Ochoa *et al.*, 2000; Fallourd and Viscione, 2009). The viscosity depends on biopolymer concentration, temperature (the dissolution temperature also has an influence), pH below 4.0, and the addition of salts (García-Ochoa *et al.*, 2000; Sworn, 2009b).

Although it is considered as mainly non-gelling, xanthan gum can form weak gels at high concentration in the presence of calcium ions due to inter-polymer interactions caused by

charge screening and the resulting lower interaction with water molecules (Baumgartner *et al.*, 2008; Wandrey *et al.*, 2010; Wu and McClements, 2015).

3.1.16.5 Pectin (CAS# 9000-69-5)

Pectin is a food hydrocolloid extracted from the cell wall of plants, and more especially fruits, such as apples, citrus fruits, grapes or oranges (Endreß and Christensen, 2009). It is supplied under the form of a light brown powder.

Pectin is an anionic heteropolysaccharide organised in linear blocks (Xiao *et al.*, 2014). Its principal chemical structure is composed of α-1,4-D-galacturonic acid units (see Figure 3.9). It also includes a few neutral sugars, such as L-arabinose, D-galactose, L-rhamnose and D-xylose, depending on the origin of the pectin (Wandrey *et al.*, 2010). The molecule takes a helical conformation in its solid state due to hydrogen bondings (Izydorczyk *et al.*, 2005).

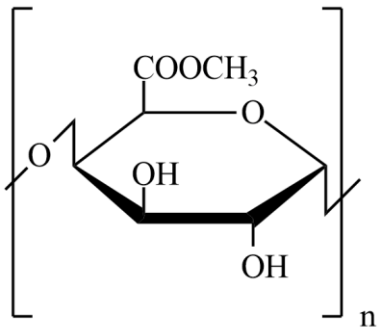


Figure 3.9: Main repeating unit of pectin (adapted from BeMiller, 2019c).

Depending on the degree of esterification of the galacturonic acid, pectins are classified as high-methoxyl (HM or "regular" pectin: > 50% of esterification), which is usually found in citrus fruits, or low-methoxyl (LM pectin: < 50% of esterification), which is found in sugar beet (Izydorczyk *et al.*, 2005; Wu and McClements, 2015; Featherstone, 2016). Pectin from citrus peel (Galacturonic acid, ≥74.0% (dried basis)) (HM pectin) was purchased from Sigma-Aldrich

Company Ltd. (Dorset, United Kingdom). Pectin is soluble in water between 60ºC and 100ºC, where it adopts a random coil conformation, but usually insoluble in organic solvents (Izydorczyk *et al.*, 2005; Wandrey *et al.*, 2010; Featherstone, 2016). It has to be dissolved not too close to its gelling conditions otherwise it will not hydrate properly. It leads to low viscosity solutions which are highly stable at low pH. The physicochemical properties of pectins vary with the source (Endreß and Christensen, 2009).

Pectin can lead to spreadable gels at concentrations above 0.5-1% (although it was not specified by the authors if this value referred to a weight, volume or molar percentage), whose formation is dependent on the temperature, pH and presence of cationic ions, as well as the pectin type. HM pectin gels are thermo-irreversible and need the presence of sugar (more than 55 wt%) in acidic conditions (2.4<pH<3.6) and heat (with a gelling temperature around 68-42ºC). A gel network is formed during a sol/gel transition resulting from the precipitation of the polysaccharide due to the dehydrating effect of sugar, and strengthened by hydrogen bonding in acidic medium (Izydorczyk *et al.*, 2005; Endreß and Christensen, 2009; Oxley, 2012b; Featherstone, 2016).

3.1.16.6 Karaya gum (CAS# 9000-36-6)

Karaya gum is a food hydrocolloid coming from the gum exudate of *Sterculia urens* trees (López-Franco *et al.*, 2009). It is supplied under the form of granules or a white to pinkish-grey powder with a slight vinegar odour and taste.

Karaya gum is a complex mixture of anionic acetylated polysaccharides, such as rhamnogalacturonan (López-Franco *et al.*, 2009; Pegg, 2012). Its principal chemical structure is composed of α-1,4-D-galacturonic acid units with alternating units of α-1,2-L-rhamnosyl and

α-1,2-L-rhamnopyranosyl units in between, and β-1,4-D-galactose, β-1,3-D-glucopyranuronate and β-1,2-D-galactopyranosyl branched units (Izydorczyk *et al.*, 2005).

Karaya gum (powder) from Alfa Aesar was obtained from Fisher Scientific UK Ltd. (Leicestershire, United Kingdom). It has a very low solubility in water (under 0.02% in cold water and about 0.06% in hot water, the authors did not specify the basis for these percentage values), but it swells (López-Franco *et al.*, 2009). It is commonly used in solution at concentrations of 1 to 4% (the author did not specify the basis of this percentage) and leads to acidic, highly viscous dispersions, which are unstable upon heat exposure.

Karaya gum can form spreadable gels above 4% (although it was not specified by the authors if this value referred to a weight, volume or molar percentage) (Izydorczyk *et al.*, 2005; López-Franco *et al.*, 2009).

3.1.17 Guar gum (CAS# 9000-30-0)

Guar gum is a food hydrocolloid extracted from the seeds of *Cyamopsis tetragonolobus*. It is supplied under the form of a tasteless and nearly odourless, beige powder (Gupta and Variyar, 2018; Merck, 2020).

Guar gum is a non-ionic, heterogeneous polysaccharide. Its chemical structure is composed of a linear chain of β-1,4-D-mannopyranose units among which about half of them have a α-1,6-D-galactopyranose unit randomly attached to it (see Figure 3.10). It also has about 5% of protein content. The molecule takes a rigid ribbon-like conformation (BeMiller, 2008; Williams and Phillips, 2009b; Gupta and Variyar, 2018; Liu *et al.*, 2020).

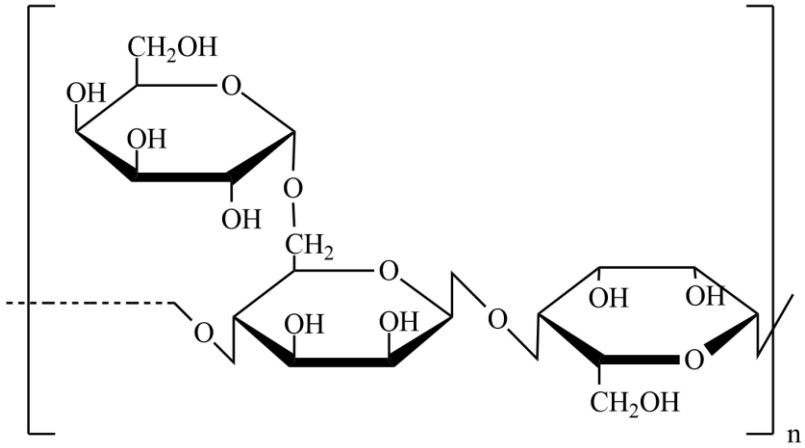


Fig. 3.10: Main repeating unit of guar gum (redrawn from Rayment and Ellis, 2003; Wandrey *et al.*, 2010; Gadkari *et al.*, 2018; Gupta and Variyar, 2018).

Guar gum was purchased from Sigma-Aldrich Company Ltd. (Dorset, United Kingdom) and was used as a proof of principle in comparison with other ionic gelling polysaccharides. It is soluble in water and in polar solvents, but insoluble in non-polar organic solvents. It is generally used in solution at concentrations of 1% or below. It swells and has a good water-binding capacity. Its viscosity exhibits a temperature-thinning effect and can be lost at high temperature (above 80ºC) or at extreme pH values (outside the pH range 3.5-7) (Wielinga, 2009; Gupta and Variyar, 2018).

3.1.18 Starch (CAS# 9005-25-8)

Starch is the second most abundant food hydrocolloid after cellulose (Taggart and Mitchell, 2009). It serves as energy storage in plants, such as cassava (tapioca starch), corn, maize, potato, rice or wheat. It is biocompatible, biodegradable and of low toxicity (Yang *et al.*, 2015). It is supplied under the form of odourless and tasteless, white, semi-crystalline granules with varying sizes, shapes and crystallinity (Taggart and Mitchell, 2009; Wandrey *et al.*, 2010; Bello Perez and Agama-Acevedo, 2017).

Starch is a non-ionic polysaccharide (BeMiller, 2019d). It is made of a mixture of a linear helical polysaccharide, amylose (25-30%), and another highly branched polysaccharide, amylopectin (70-75%) (the authors did not specify the basis of these percentage values) (Bello Perez and Agama-Acevedo, 2017). It also contains minor amounts of lipids and proteins. Its principal chemical structure is composed of α-1,4-anhydro-D-glucopyranosyl units with some α-1,6-D-glucopyranose branching (see Figure 3.11) (Wandrey *et al.*, 2010; Bello Perez and Agama-Acevedo, 2017). The molecule takes a helical conformation.

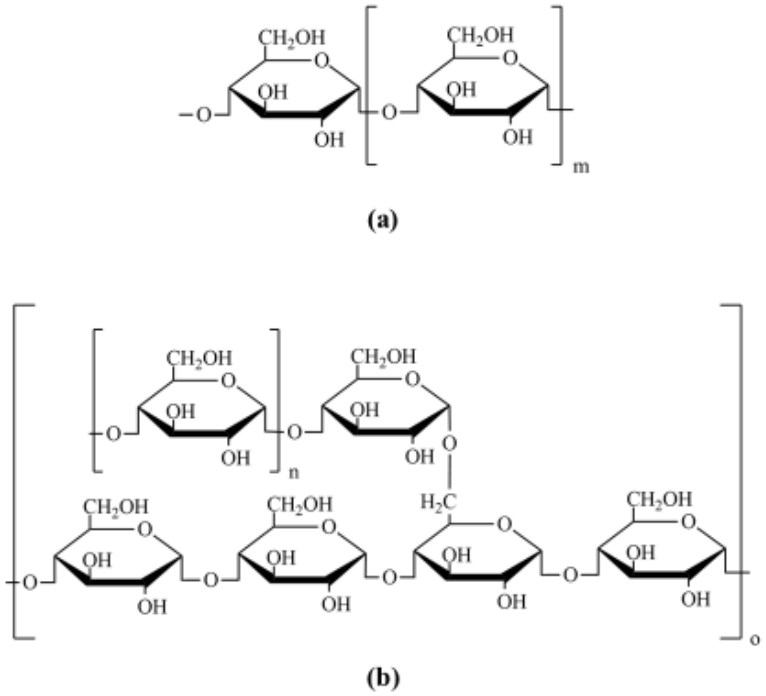


Figure 3.11: Main repeating units of starch (a) amylose (b) amylopectin (redrawn from Wandrey *et al.*, 2010; Li, 2014; Bello Perez and Agama-Acevedo, 2017).

Starch from corn (practical grade) was obtained from Sigma-Aldrich Company Ltd. (Dorset, United Kingdom). It is insoluble in cold water, but swells, as well as in alcohols and most organic solvents (Wandrey *et al.*, 2010). It dissolves in hot water between 60ºC and 150ºC, depending on the molecular weight and the nature of the source (Parker and Ring, 2001). Starch

swells to form a paste when suspended in an excess of hot water (Parker and Ring, 2001; Wandrey *et al.*, 2010). This leads to gelatinisation due to the formation of a network which increases the viscosity of the solution. Starch undergoes a structural retrogradation upon cooling (Bello Perez and Agama-Acevedo, 2017). Its properties can vary a lot depending on its source and even within the same plant origin. It is also possible to cationise starch in order to make it interact with negatively charged compounds (Yang *et al.*, 2015).

3.1.19 Whey protein (CAS# 977102-05-8)

Whey protein is a food hydrocolloid from animal origin (milk) (Boland, 2011). It is a by-product from the processing of other dairy products, mainly caseins and cheese. It is composed of a mix of globular proteins: β-lactoglobulin (about 58%), α-lactalbumin (about 13%), bovine serum albumin (about 8%), immunoglobulins and other minor components (Kilara and Vaghela, 2018; Deeth and Bansal, 2019). It is supplied under concentrate or isolate powder form, including respectively 35-85% or 90-95% of protein content.

Whey protein isolate (WPI, Pure Whey Isolate™ 97 Unflavoured) was purchased from BULK POWDERS™ (Essex, United Kingdom). It is soluble in water on a large pH range in the absence of salts, except close to its isoelectric point (pI, around pH 5) (O'Regan *et al.*, 2009; Kilara and Vaghela, 2018). Its pI is between 4.4 and 5.2 (Ju and Kilara, 1998; Guimarães and Gasparetto, 2005; Chen *et al.*, 2012). It can lead to cold-set gels at a concentration of about 10% (the authors did not specify the basis of this percentage) and at pH 7.0, following denaturation by heating at 80ºC for 30 min (Ju and Kilara, 1998; O'Regan *et al.*, 2009; Deeth and Bansal, 2019). Alternatively, gelation can also be induced by the addition of salts producing calcium or sodium ions (Kilara and Vaghela, 2018).

3.1.20 Salts

Potassium chloride (CAS# 7447-40-7, ACS reagent, 99.0-100.5%) and calcium chloride (CAS# 10043-52-4, anhydrous powder Reag. Ph Eur) were both obtained from Sigma-Aldrich Company Ltd. (Dorset, United Kingdom).

3.1.21 Sugar

White granulated sugar was purchased from a local supermarket and used as such.

3.2 Methods

3.2.1 Mechanical agitation

The use of mechanical agitation was required both for the preparation of the polymer solutions and for the mixing of the batch medium during complex coacervation.

3.2.1.1 Agitation devices

There are two main flow patterns for agitation: axial or radial. Axial flow consists of pumping down the liquid, providing a bottom to top mixing (see Figure 3.12). It is typically produced by marine propellers with inclined blades or pitched-blade impellers. Radial flow involves the propulsion of liquid from the centre to the periphery of the agitation pattern, leading to an "8-shaped" flow profile. Rushton turbines are known to give this second type of flow (Ibrahim, 2007).

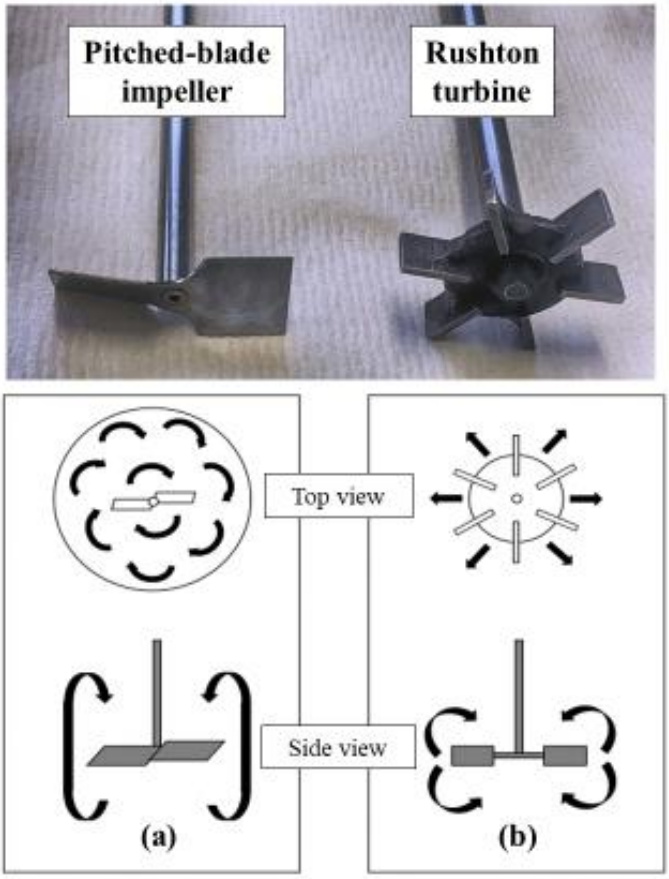


Figure 3.12: Different flow patterns (a) axial mixing (pitched-blade impeller) (b) radial mixing (Rushton turbine) (adapted from Ibrahim, 2007).

Rushton turbines were suggested to be well adapted for complex coacervation (Zuidam and Shimoni, 2010; Ach *et al.*, 2015). Therefore a six-blade Rushton turbine was used with an IKA EUROSTAR overhead stirrer (speed range: 0/50 – 2000 rpm) for all experiments.

3.2.1.2 Stirred tank geometry

The standard stirred tank geometry was established from the literature (see Figure 3.13).

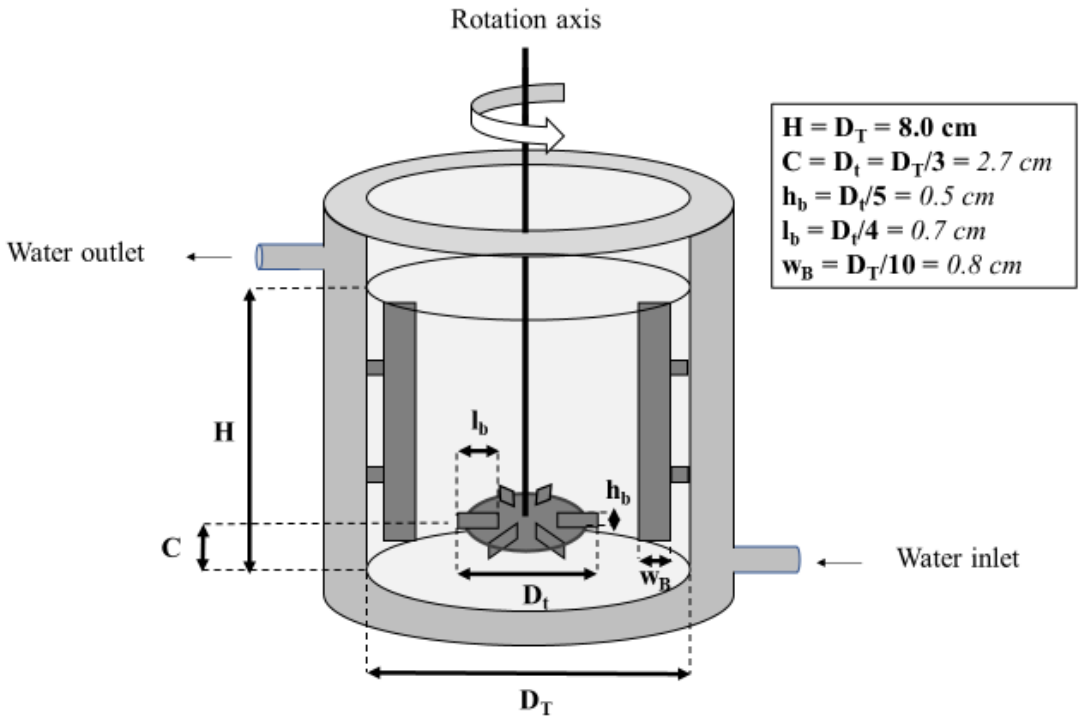


Figure 3.13: Standard geometry of a stirred tank with the calculated values imposed by the diameter of a 500 mL jacketed beaker (H: height of liquid, D_T: diameter of the stirred tank, C: clearance from the bottom of the beaker, D_t: diameter of the turbine, h_b: height of the blade, l_b: length of the blade, w_B: width of the baffle) (adapted from Delafosse *et al.*, 2008; Cekinski *et al.*, 2010 ; Zuidam and Shimoni, 2010).

An R 3004 Rushton turbine (diameter: 30 mm) was purchased from Fisher Scientific UK Ltd. (Leicestershire, UK) to suit the dimensions of a 500 mL jacketed beaker (D_T = 8.0 cm) and stainless steel baffles were designed.

3.2.2 High-shear mixing

High-shear mixing is a method used to form emulsions. It enables to bring the desired input energy (disruptive force) for breaking up drops bound by interfacial forces into smaller droplets (McClements, 2009).

A high-shear mixer of the Silverson type L5M-A (speed range: 0 – 8000 rpm) equipped with an emulsor screens head (see Figure 3.14) was used (Silverson, 2020).



Figure 3.14: Emulsor screens head for Silverson mixer (Silverson, 2020).

An upward suction is created at the base of the head of the mixer due to the high rotation speed of the rotor blades. The two liquid phases enter the centre of the emulsor screen via the bottom. They are pumped out through the peripheral holes as a result of centrifugal forces, which produces small droplets propelled radially (Silverson, 2020).

3.2.3 Size distribution measurement

Droplet (or particle) size distribution is measured by laser diffraction technique where the emulsion goes through a focused monochromatic red laser beam (He-Ne, λ = 633 nm). The light is diffracted by the emulsion droplets (or suspended particles) following an angle which is inversely proportional to their size, and this angular intensity is measured by photosensitive detectors (Huang *et al.*, 2001; Malvern Instruments Ltd., 2005; Malvern Instruments Ltd., 2007).

Light-scattering can rely on two different optical theories: the Fraunhofer approximation or the Mie theory. The Fraunhofer approximation assumes that all sizes of droplet (or particle) scatter light with equal efficiency, and that the droplets (or particles) are opaque and do not transmit light. This is not true for L-carvone oil droplets as they are transparent. The Mie scattering theory is derived from Maxwell's equations of electromagnetism and assumes that droplets (or particles) are homogeneous and spherical. It requires the refractive index values of the droplet

phase (or particle wall material) and dispersion medium (Malvern Instruments Ltd., 2007; Senoo and White, 2017).

The surface-weighted mean diameter (or Sauter diameter, d_{32}) and the span of the size distribution were the parameters of interest to study the stability of emulsions:

$$d_{32} = \frac{\sum n_i d_i^3}{\sum n_i d_i^2} \quad \textbf{(Eq. 3.1)}$$

$$\text{Span} = \frac{d_{0.9} - d_{0.1}}{d_{0.5}} \quad \textbf{(Eq. 3.2)}$$

where d_i is the diameter of the droplet (or particle) i, n_i is the number of droplets (or particles) with the same d_i, $d_{0.1}$ is the droplet (or particle) diameter below which 10% (v/v) of the sample lies, $d_{0.5}$ is the mean diameter, and $d_{0.9}$ is the droplet (or particle) diameter below which 90% (v/v) of the sample lies (Sánchez *et al.*, 1998; Malvern Instruments Ltd., 2007).

The size distribution measurements were performed by a Mastersizer 2000 from Malvern Instruments Ltd. (Worcestershire, United Kingdom) with the Mastersizer 2000 software. This instrument uses the Mie theory and the reference refractive indexes of 1.497 and 1.333 were used for L-carvone dispersed in water respectively. All measurements were made in triplicate with a precision of 0.02 μm.

3.2.4 Drop tensiometry

The interfacial tension corresponds to intermolecular attractive forces between two liquid phases in contact. It is commonly measured experimentally using the du Noüy ring, capillary rise or pendant drop method (Gholami and Fakhari, 2017; Belyadi *et al.*, 2019).

A drop tensiometer enables to optically analyse the shape of a drop, via the pendant drop method (see Figure 3.15) when the inner phase has a higher density than the surrounding phase, or its

equivalent rising drop method when on the contrary the former is less dense than the latter. The interfacial tension (γ) is linked to the interface properties by Laplace's law:

$$\Delta P = \gamma \times \left(\frac{1}{r_c} + \frac{1}{r_c'}\right) \qquad \textbf{(Eq. 3.3)}$$

where ΔP is the difference of pressure between the phases on each side of the interface, r_c and r_c' are the radii of the horizontal and vertical circles of curvature (KRÜSS GmbH, 2010; Belyadi *et al.*, 2019).

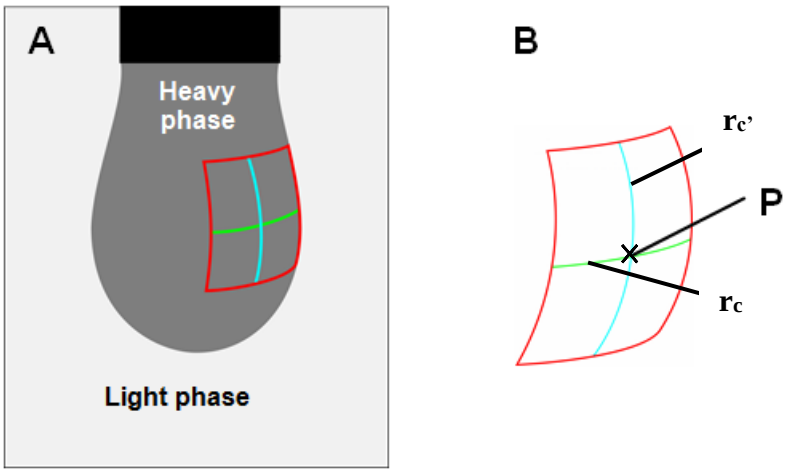


Figure 3.15: (A) Schematic presentation of the pendant drop method (B) Illustration of the calculation elements (P: point of pressure, r_c and r_c': radii of the horizontal and vertical circles of curvature) (KRÜSS GmbH, 2010).

The dynamic interfacial tension measurements were made using a drop shape analyser (model DSA30) from KRÜSS (Bristol, UK). DI water containing 0.05 wt% of emulsifier was placed in an optical glass cuvette (model SC02, dimensions: 36 x 36 x 30 mm). A rising drop of pure L-carvone was generated in the water phase ($d_{L\text{-carvone}}$ = 0.959) using a 500 µL glass gas-tight syringe with Luer-Lock connector (model SY20) with a 1.0 mm stainless steel J-shaped needle (model NE72). The measurements were recorded by applying the pendant drop method via the

KRÜSS ADVANCE software with values collected every minute for 6h to allow stabilisation. The interfacial tension values are given with a 0.3 mN/m accuracy.

3.2.5 Optical microscopy

Light microscopy is an imaging technique allowing direct observation of microscopic systems. It enables to examine the general 2D appearance of emulsion and capsules, and to estimate their size thanks to the scale display. This technique is particularly essential to investigating the optimal pH of the complex coacervation process since the latter is characterised by the deposition of a coacervate layer which can be visually identified around the emulsion droplets.

A Leica DMRBE trinocular optical microscope (objective x10, aperture 1.6) equipped with a 100 W transmitted light source was operated. A Moticam Pro 252B camera was fitted on the microscope and was used with the Motic Images Advanced 3.2 software (a 50 μm scale is indicated on all optical microscopy views). Fluorescence microscopy observations could also be performed thanks to a CoolLED pE-300 LED illumination system used with a blue light excitation peaking around $\lambda = 460$ nm. Plain glass microscope slides (dimensions: 76 x 26 mm, thickness: 1 – 1.2 mm) from Thermo Scientific were used.

3.2.6 pH measurement

The pH (hydrogen potential) is used to indicate the acidity of aqueous media on a scale from 1 to 14. The medium is considered neutral at pH 7 (pH of pure water); it is qualified as acidic below this value and alkaline above (Karastogianni *et al.*, 2016).

There are two options for determining the pH of a solution experimentally: by colorimetry (qualitative method) which uses colour indicator paper, or by electrochemical measurement with a pH meter (quantitative method) which usually involves a glass electrode and a millivoltmeter. The measurement is given with a 0.1 precision (Webster, 2003).

A FiveEasy^{TM} F20 pH meter purchased from Mettler-Toledo Ltd (Leicestershire, United Kingdom) was used for all pH measurements. A two-point calibration was realised with colour-coded buffer solutions pH 4.00 (phthalate, pink) and pH 10.00 (borate, blue), which were purchased from Fisher Scientific UK Ltd (Leicestershire, United Kingdom). The glass electrode was stored in a 3M potassium chloride (KCl) solution.

3.2.7 Centrifugation

Centrifugation is a mechanical method which enables to separate phases of different densities by applying a centrifugal force field (Taulbee and Maroto-Valer, 2000).

Unless stated otherwise, centrifugation was carried out using a Hermle compact benchtop centrifuge (Z206-A) from Labnet, equipped with a 6 × 50 mL conical rotor.

3.2.8 UV-Vis spectroscopy

L-carvone presents several unsaturated functional groups and therefore possesses chromophores which can absorb light (Chakraborty, 2014). Ultraviolet-Visible (UV-Vis) spectroscopy is a method which can quantify the light absorption of an analyte in the UV and visible light spectra within the wavelength range 180-750 nm. The concentration of the compound can be deduced from the absorbance value (Rakhee *et al.*, 2018).

A CECIL CE 2021 spectrophotometer from Cecil Instruments Limited was used for the measurements with a quartz cuvette (semi-micro cell, light path: 10 mm) from Hellma UK Ltd (Essex, United Kingdom).

A calibration curve was made by diluting pure L-carvone in ethanol at different concentrations (see Figure 3.16). For the first measurement the full UV-Vis range was scanned with the DataStream software in order to identify at which wavelength L-carvone was absorbing. Two

peaks could be observed: a major one around 240 nm and a minor one at 320 nm. The main absorbance peak of L-carvone was very close to the cut-off wavelength of ethanol (210 nm), which was not desirable for quantitative measurements (Haynes, 2010). The second, less intense peak at 320 nm was preferred for the UV-Vis measurements.

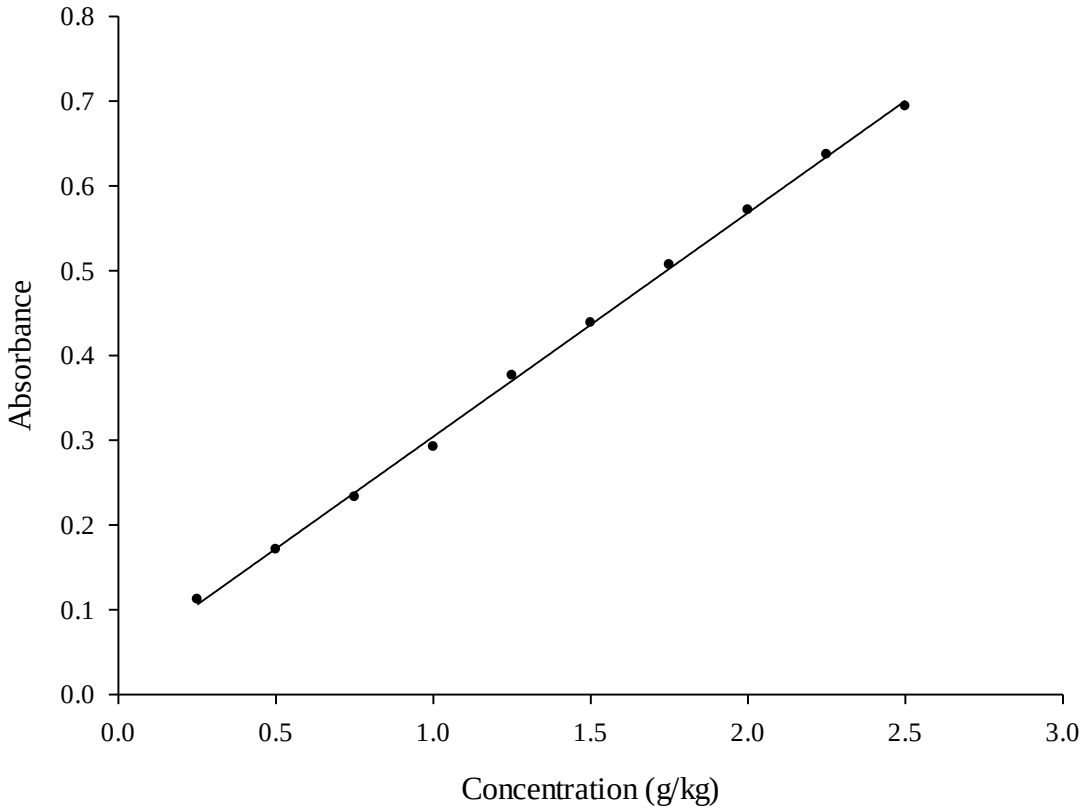


Figure 3.16: Calibration curve for UV-Vis measurements of L-carvone in ethanol at 320 nm.

The calibration gave the equation:

$$\text{Absorbance} = 0.040 + 0.264 \times \text{Concentration} \qquad \textbf{(Eq. 3.4)}$$

with a coefficient of determination $R^2 = 0.9991$, which attests of an excellent linearity. This equation was therefore further used for determining the amount of L-carvone present in

different samples via UV-Vis spectroscopy. All measurements were made in triplicate and the mean value was calculated.

3.2.9 Scanning electron microscopy (SEM)

Scanning electron microscopy (SEM) is a high-resolution imaging technique which enables to observe the 3D shape, surface morphology and wall structure of solid materials. Samples are scanned by a fine electron beam and should therefore be electrically conductive at their surface. A signal is then shown on the screen of a cathode ray tube resulting from the interaction of the electrons with the conductive surface of the particles (Ray, 2013; Rennie *et al.*, 2014; Amidon *et al.*, 2017).

The measurements were carried out in Mondelēz International laboratories (RSSL, Reading), by Dr Haixia Xu. A small amount of powder was deposited on a self-adhesive carbon tab glued on a specimen stub. The sample was coated by a thin gold-palladium layer (10 nm) under high vacuum, using a Leica EM ACE600 sputter coater, in order to make the particles electrically conductive without disrupting the measurement by the charge of the polymeric shell and to enhance imaging contrast (Ray, 2013). The SEM images were captured using a ZEISS Sigma Field Emission Gun Scanning Electron Microscope (FEG-SEM), with a secondary electron (SE) detector at an acceleration voltage of 5 kV.

3.2.10 Micromanipulation

Micromanipulation is a characterisation technique which enables to evaluate the mechanical properties of microparticles including capsules. It consists of a direct measurement obtained by compressing a single particle between a glass surface and a cylindrical glass probe with a diameter greater than the one of the capsule. This leads to either rupture or deformation of the microparticle. From the collected data, force-displacement curves can be established, which

enables to characterise the mechanical strength of the capsules (Zhang *et al.*, 1999; Zhang and Adams, 2014; Gray *et al.*, 2016).

The samples were prepared by gently blowing the dry capsules with a pipette on a microscope glass slide cut to fit the desired size of the equipment. Micromanipulation measurements were carried out with a self-built micromanipulator compression rig (see Figure 3.17) monitored by a CCD camera. A force transducer (model: 403A, serial number: 1529011, sensitivity: 0.453 mN/V) from Aurora Scientific Ltd. (Bristol, UK) was mounted on the device and equipped with a polished glass probe tip with a diameter of about 70 μm (Zhang *et al.*, 2020).

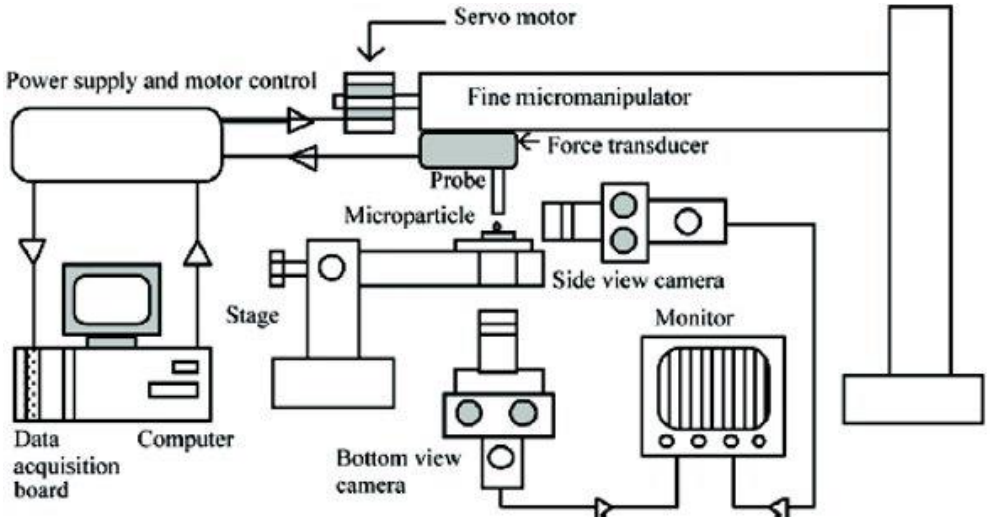


Figure 3.17: Schematic representation of the micromanipulation rig (Zhang and Adams, 2014).

The manipulations were operated using MA 6000 software. In order to evaluate the measurement baseline, the compliance of the system was tested 5 times, averaged and subtracted from further measurements. Following the standard measurement procedure, 30 capsules were randomly selected for each sample and squeezed at a compression speed of 2 μm/s. The measurements were stopped when the voltage reached a maximum of 10 V.

The force at rupture (F_R) is calculated by the following equation:

$$F_R = \Delta U_R \times S_t \quad \textbf{(Eq. 3.5)}$$

where ΔU_R is the change in voltage at rupture from the baseline, and S_t is the sensitivity of the force transducer.

The nominal rupture stress (σ_R) is given by:

$$\sigma_R = \frac{F_R}{\pi {r_p}^2} \quad \textbf{(Eq. 3.6)}$$

where r_p is the initial radius of the particle.

Finally, the deformation at rupture (x_R) is calculated as follows:

$$\delta_R = \nu_t \times t_R - F_R \times \frac{1}{k} \quad \textbf{(Eq. 3.7)}$$

$$x_R = \frac{\delta_R}{d_p} \quad \textbf{(Eq. 3.8)}$$

where δ_R is the displacement at rupture, ν_t is the velocity of the transducer, t_R is the time of rupture, k is the stiffness and $\frac{1}{k}$ is the compliance, d_p is the initial diameter of the particle.

3.2.11 Zeta potential measurements

The zeta potential is the surface charge of particles in colloidal solution. It is usually expressed in millivolts (mV) and evaluated from electrophoretic mobility measurements (Shnoudeh *et al.*, 2019).

It was found in the literature that zeta potential measurements could prove to be a powerful tool to study the possible interaction of oppositely charged polymers for use in complex

coacervation (Prata and Grosso, 2015). Plotting the zeta potential of the polymers could indeed help to determine the required polymer ratio (see Figure 3.18).

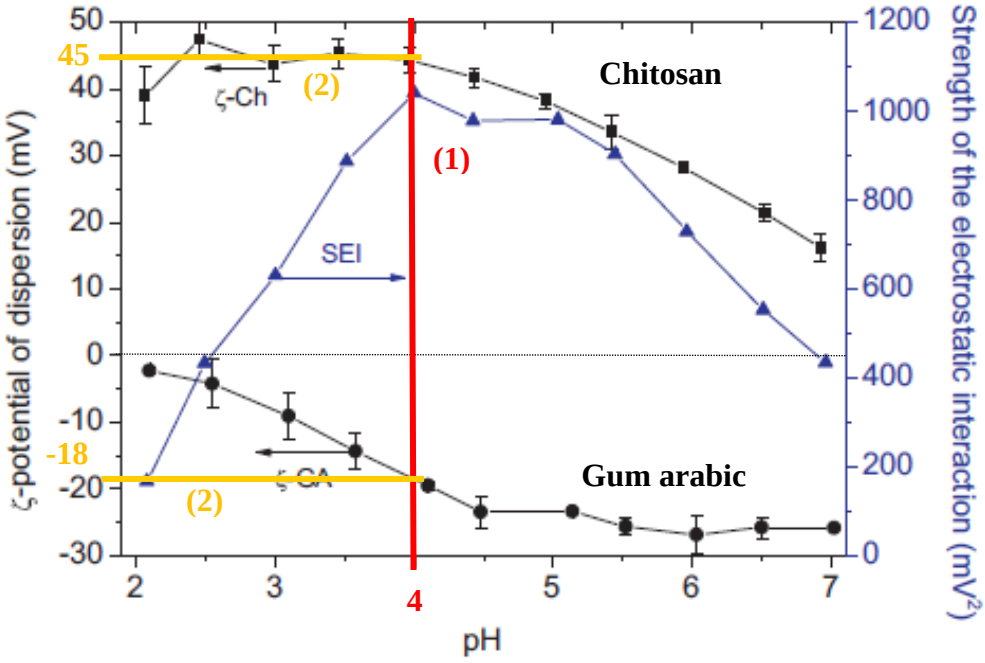


Figure 3.18: Graphical method for the determination of polymer mixing ratio at a given pH for complex coacervation, based on an example from Espinosa-Andrews *et al.* (2013) presenting zeta potential data as a function of pH for gum arabic and chitosan: (1) determination of the optimal pH, (2) determination of the polymer ratio.

The strength of the electrostatic interaction (SEI) at a given pH can be calculated by the product of the absolute value of the zeta potential of each polymer. The maximum given by this plot should indicate the pH value at which the interaction between the two polyelectrolytes is the strongest (Espinosa-Andrews *et al.*, 2013). The optimum pH is determined by tracing a vertical line (1) where the SEI reaches a maximum (see Figure 3.18). From there, two horizontal lines (2) are drawn at the intersection between the optimum pH line (1) and the zeta potential curves of the two polymers.

Two polyelectrolytes can interact when they are oppositely charged, and optimal interaction happens when a neutrality of charges is reached. In the example from Espinosa-Andrews *et al.* (2013), the SEI is at its highest at pH 4, which is determined as the optimum pH by (1) (see Figure 3.18). Drawing the two horizontal lines (2) gives zeta potential values of +45 mV and -18 mV for chitosan and gum arabic respectively. The ratio of the zeta potential values is then used to determine the optimum polymer ratio required to obtain the neutrality of charges. In this example, the gum arabic/chitosan ratio should be of 5:2 (w/w) for an identified optimum pH of 4. This data also explains why the polymer ratio is dependent on the pH since the electrical charge of each polymer changes with the pH.

It will be noted that, although the notion of "zeta potential" for polymer solutions was found in several articles, it is not correct to use it in this case as molecules do not have an interface, unlike particles. They do however have a measurable electrophoretic mobility if they are charged, and "zeta potential" values will be rather referred to as "apparent zeta potential" of polymers in what follows.

The samples for each polymer solution were shaken by hand and introduced in a folded capillary cell with electrodes (DTS1070) (see Figure 3.19) from Malvern Instruments Ltd. (Worcestershire, United Kingdom), making sure there was no air bubble in the sample.

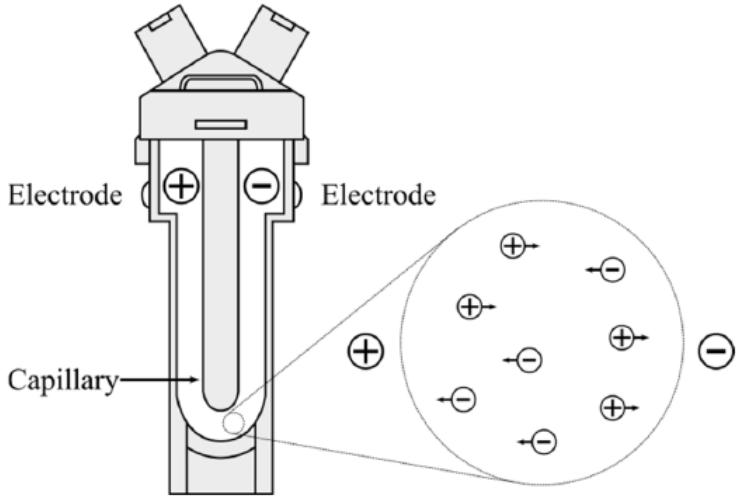


Figure 3.19: Folded capillary cell used for the measurement of electrophoretic mobility (Malvern Intruments Ltd., 2013).

The electrophoretic mobility was measured at 25°C using a Zetasizer Nano ZS from Malvern Instruments Ltd. (Worcestershire, United Kingdom), belonging to the Food and Manufacture Engineering group, under the care of Dr Tom Mills. For this method, an electrical potential is applied to the electrodes of the folded capillary cell, and the charged molecules move towards the oppositely charged electrode (see Figure 3.19). The electrophoretic mobility is determined by an electrophoresis experiment performed on the sample, associated with a Laser Doppler Velocimetry measurement (Malvern Instruments Ltd., 2013). The software is using the Henry equation to calculate the zeta potential value (called "apparent zeta potential" here):

$$\mu = \frac{2\varepsilon \times \zeta \times f(\kappa a)}{3\eta} \qquad \textbf{(Eq. 3.9)}$$

where μ is the electrophoretic mobility, ε is the dielectric constant, ζ is the zeta potential, f(κa) = 1.5 is Henry's function based on the Smoluchowski approximation for aqueous samples, and η is the viscosity which is deduced from the nature of the dispersant (water here) (Malvern Intruments Ltd., 2013). All measurements were made in triplicate.

3.2.12 Turbidity measurements

Turbidity is a visual parameter characterising the clarity of a solution. More specifically, it corresponds to the light scattering ability of a liquid sample (Woodard & Curran, Inc., 2006).

It was reported in the literature that turbidity measurements could help identifying the key phase transitions of polyelectrolyte complexes interaction (Turgeon and Laneuville, 2009). A slow increase in turbidity corresponds to the apparition of soluble complexes and is characterised by the critical pH (pH_c) (see Figure 3.20). Then interpolymeric interactions are observed from pH_Φ, where complexes start to form. A maximum in turbidity is reached when the electrostatic interaction is the highest (pH_{opt}), after which it decreases and the complexes dissociate until the polymers remain in solution separately again at $pH_{\Phi 2}$.

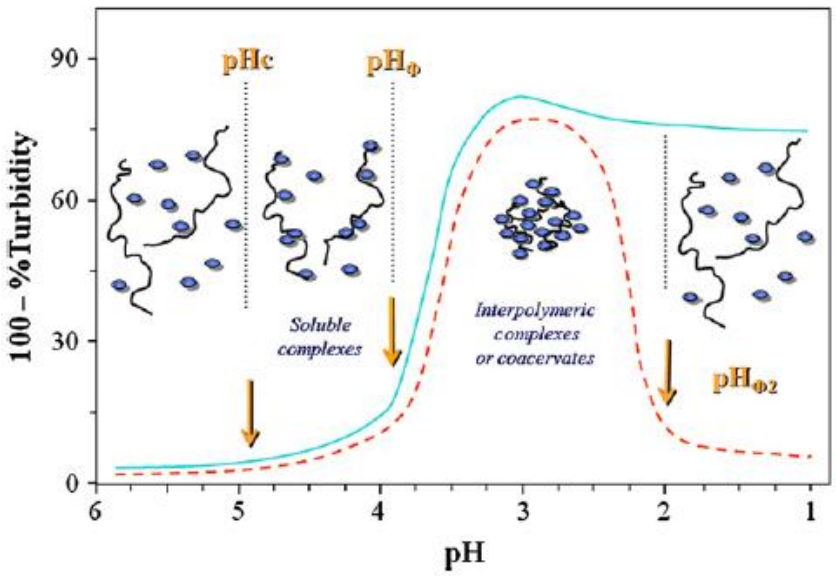


Figure 3.20: Phase evolution of polymer complexes in solution monitored by turbidity measurements observed as a function of pH (Turgeon and Laneuville, 2009).

In this case, identifying the pH at which a maximum turbidity was observed was useful for confirming the optimal pH for complex coacervation of different polysaccharide combinations at a given polymer ratio.

A portable turbidity meter (HI-93703), equipped with an Infrared LED emitting at 890 nm, from HANNA Instruments Ltd (Bedfordshire, United Kingdom) was used. A three-point calibration was made using calibrating solutions at 0, 10 and 500 Formazin Turbidity Units (FTU). The samples were placed in the cylindrical glass cuvette and their turbidity was measured at room temperature (RT). All measurements were made in triplicate.

CHAPTER 4 – Design of the Complex Coacervation Process

4.1 Introduction

Complex coacervation results from the attractive interaction of two oppositely charged hydrocolloids (see **Chapter 2**). This process is composed of three specific steps (see Figure 2.12): 1) formation of an O/W emulsion, 2) pH adjustment, which generates the coacervate coating layer, 3) physical and/or chemical hardening of the wall.

First and foremost, it is important to form a stable emulsion, as it will be the base of the coacervation process, and will influence the flavour release intensity as more stable emulsions were reported to lead to a higher encapsulation efficiency (Carneiro *et al.*, 2013; Mao *et al.*, 2017).

During the coacervation step, the pH of the solution is the crucial parameter as the phenomenon is mostly ruled by the charge density of the polyelectrolytes, and the target value depends on the chosen biopolymer ratio (de Kruif *et al.*, 2004).

Finally, the wall must be hardened, either by gelation or through crosslinking, and without changing the pH as the coacervate phase formation can be otherwise reversible (Burgess, 1990; Comert *et al.*, 2016).

In this chapter, the theory involved in the different steps of the complex coacervation process will be explained, then the experimental protocol for complex coacervation with the gum arabic/chitosan combination as wall material and L-carvone oil as the core will be described, and finally the results of those investigations will be presented and discussed.

4.2 Theoretical consideration of complex coacervation

4.2.1 Emulsion stability

Emulsions are thermodynamically unstable systems which tend to go back to two distinct phases. They can undergo different destabilisation behaviours such as creaming, sedimentation, Brownian flocculation, coalescence, Ostwald ripening or phase inversion (see Figure 4.1). Creaming (O/W emulsions) and sedimentation (W/O emulsions) are two phenomena linked to gravity; depending on the relative density of the droplets compared to the continuous phase they tend to respectively either float or sink. Flocculation is when the emulsion droplets aggregate together because they collide due to attractive and adhesive forces while staying as individual entities. If they however merge to form a bigger drop, this is called coalescence. Ostwald ripening is a bit more complex as there is a mass transfer between two droplets due to Laplace pressure, meaning one grows bigger at the expense of the other, without merging together. Phase inversion is quite self-explanatory: it involves a change in continuous phase, meaning an O/W emulsion would become a W/O emulsion (Huang *et al.*, 2001; Dickinson, 2009; McClements, 2009; Balcão *et al.*, 2015).

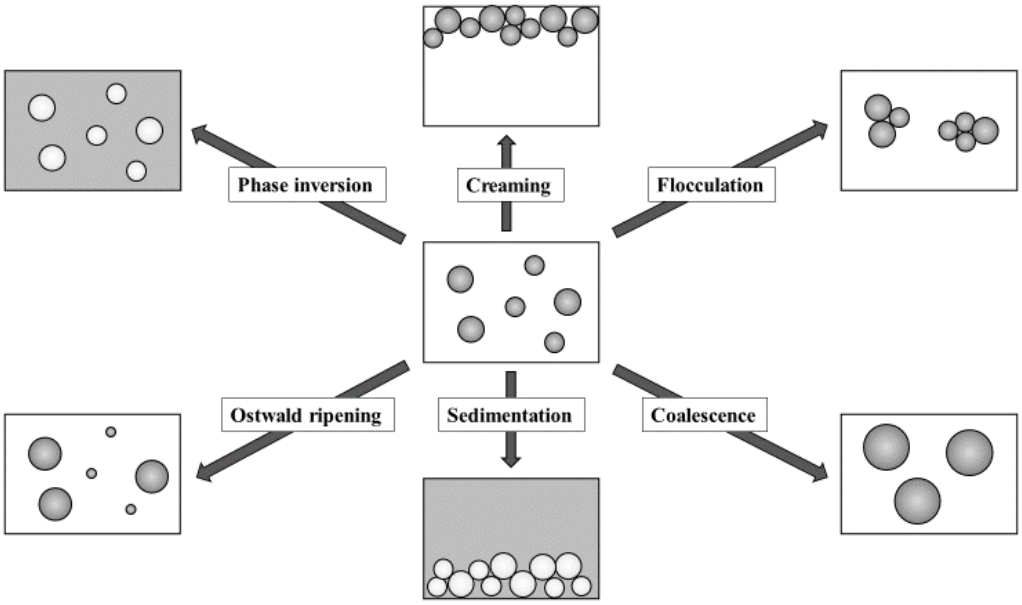


Figure 4.1: Emulsion destabilisations (adapted from McClements, 2009; Balcão *et al.*, 2015).

It is important to obtain stable emulsions at first as it will be determinant for the quality of the encapsulation, as well as for the size and morphology of the microcapsules. The emulsion should remain stable during the full time of the coacervate deposition step until crosslinking, which should take two hours.

According to Stokes' law, the gravitational velocity of a spherical object in a viscous solution is proportional to the square of its radius:

$$\nu_c = -\frac{2gr_d^2(\rho_d - \rho_\Phi)}{9\eta_\Phi} \quad \textbf{(Eq. 4.1)}$$

where ν_c is the creaming velocity, g is the gravitational acceleration, r_d is the radius of the droplet, ρ_d is the density of the droplet, ρ_Φ is the density of the continuous phase, and η_Φ is the shear viscosity of the continuous phase (McClements, 2009).

The collision frequency for simple shear in a stirred vessel, which leads to flocculation and coalescence, is furthermore proportional to the cubic radius of the droplets:

$$Z = \frac{16}{3} G r_d^3 n_0^2 \quad \textbf{(Eq. 4.2)}$$

where Z is the collision frequency, G is the shear rate, and n_0 is the initial number of droplets per volume unit (McClements, 2009).

It is therefore possible to characterise the stability of an emulsion by size distribution measurements (Huang *et al.*, 2001). This stability can also be assessed visually as a secondary method if no phase separation is witnessed (Züge *et al.*, 2013).

This stability is influenced by several parameters such as the content in surface-active proteins (amphiphilic) of the polysaccharide which can reduce the interfacial tension of the emulsion, the concentration of biopolymer in the aqueous phase which affects the viscosity, the use of emulsifier or not, the physical stabilisation of the core in order to increase the flavour retention, and the mixing speed to form the emulsion which is inversely proportional to the size of the droplets (Burgess, 1990; Jégat and Taverdet, 2000; Huang *et al.*, 2001; Lam and Nickerson, 2013).

4.2.1.1 Protein content

Gum arabic has a content of about 2-3% (the author did not specify the basis of the percentage) in surface active protein (Williams and Phillips, 2009b), which can partially explain some attractive properties of this hydrocolloid, like emulsifying and stabilising capacities (Food and Drug Administration, 2020).

4.2.1.2 Viscosity

Viscosity is suspected to reduce the mobility of emulsion droplets (see Equation 4.1). Gum arabic reaches its maximum viscosity for application in emulsions at a concentration of 12.5 wt% (Huang *et al.*, 2001).

4.2.1.3 Emulsifiers

Emulsifiers are surface active ingredients which can adsorb at the oil-water interface and fulfil two main roles. First, they permit to decrease the interfacial tension at the oil-water interface which makes the drops break-up easier during emulsification. Secondly, they create a protective layer around the newly formed droplets which prevents them from coalescing together again due to the turbulences created during mixing (Dickinson, 2009; McClements, 2009).

Small molecule surfactants, comprising monoglycerides (e.g. glycerol monostearate), phospholipids (e.g. lecithin), polysorbates (Tweens) and sorbitan esters (Spans) are the most commonly used emulsifiers for food application. Amphiphilic biopolymers can also be used as emulsifying agents (Dickinson, 2009; McClements, 2009; Sessa and Donsì, 2015).

The hydrophilic-lipophilic balance (HLB) is a good indicator to characterise the nature of surfactants. Hydrophilic emulsifiers (HLB > 10) are known to lead to O/W emulsions and should be used in low concentrations (0.5 – 5 wt%) in the aqueous phase, whereas W/O emulsions are stabilised by lipophilic emulsifiers (HLB < 10). Emulsifiers can be further organised in five functionality groups depending on their HLB value (see Table 4.1) (ICI Americas Inc., 1976; Balcão *et al.*, 2015; Komaiko and McClements, 2016). An appropriate choice of emulsifier should help to direct the emulsion in the desired way and avoid the inversion phenomenon.

Table 4.1: Surfactant functionality groups depending on the HLB and according to the Griffin scale (Chen, 2015; Komaiko and McClements, 2016).

HLB value ranges	Applications
3 - 6	W/O emulsifier
7 - 9	Wetting agent
8 - 18	O/W emulsifier
13 - 15	Detergent
15 - 18	Solubilisation

Furthermore, each emulsion system is unique and there should be an ideal HLB (HLB_{crit}) with which the emulsion is most stable. The ideal emulsifying agent should then be determined by investigating different surfactant systems at the previously identified critical HLB value. The combination of two emulsifiers can lead to a brand new emulsifying agent with a customised HLB (ICI Americas Inc., 1976; Macedo *et al.*, 2006; Balcão *et al.*, 2015).

Identifying a good emulsifier is important for the stability of the emulsion, which can have a significant impact on the encapsulation efficiency (Rabišková and Valášková, 1998). Spans and Tweens are food grade surfactants and are also non-ionic, which presents the advantage of avoiding any influence in the coacervation process (Garti and Aserin, 2012).

4.2.1.4 Stabilisation of the core

The flavour oil, although it may also be used alone, can optionally be mixed with a stabilising flavour solvent (triacetin, propylene glycol) or with a carrier oil such as medium-chain triglycerides (MCT), which are saturated fatty acid chains composed of 6 to 12 carbons each (e.g. coconut oil, palm oil) (Kupongsak and Sathitvorapojjana, 2017), in order to limit the flavour reactivity (Potineni and Peterson, 2008a; Choi *et al.*, 2009; Sobel *et al.*, 2014b; Komaiko and McClements, 2016). Flavour solvents are however used in chewing gums for the

addition of the free flavour oil directly into the gum matrix, not within capsules, therefore only MCT will be further considered for the stabilisation of the core.

4.2.1.5 Emulsification speed

The mixing speed should be high enough to generate the emulsion and further adapted to meet the droplet size requirements (McClements, 2009). The higher the speed, the smaller the droplets as the Kolmogorov law of turbulence applied to dispersed phase can lead to infer an inverse proportionality between the Sauter diameter (d_{32}) of emulsion droplets and the agitation speed (N) (Jégat and Taverdet, 2000):

$$d_{32} \propto (N)^{-6/5} \quad \textbf{(Eq. 4.3)}$$

4.2.1.6 Type of emulsion (O/W or W/O)

In order to make sure there is no destabilisation by phase inversion, it is also necessary to check the type of the emulsion. This can easily be done by colouring one of the two phases with a selective staining dye, or by electrical conductivity measurement, as O/W emulsions display higher conductivities than W/O ones (Chang, 2016).

The use of a lipophilic solvatochromic fluorophore which is insoluble in the aqueous phase is a non-destructive way to check both the type of emulsion and the success of encapsulation. Solvatochromic dyes can reversibly change their absorption or emission spectrum depending on their surrounding medium. Nile red is an example of a lipophilic push-pull solvatochromic dye. It is activated in the blue region but emits from green (non-polar solvents) to red colour (polar solvents and air) (Rijavec and Bračko, 2007; Klymchenko, 2017; Zhang *et al.*, 2019).

4.2.2 Coacervation step

Complex coacervation is due to attractive electrostatic interactions which are dependent on the pH. For this, the polyelectrolytes need to carry net opposite electric charges. Furthermore, the phase separation is also largely driven by enthalpic factors (polymer weight ratio and molecular charge density, which is related to the apparent zeta potential), as well as entropic factors (molecular weight and conformation). The geometry of the stirred tank, the agitation speed and duration are other parameters to which some attention should be paid. Coacervation itself is independent of the temperature (Burgess, 1990; de Kruif *et al.*, 2004; Turgeon and Laneuville, 2009).

4.2.2.1 Polymer weight ratio

There is an optimum polymer weight ratio which allows full charge compensation between the two polyelectrolytes and leads to the formation of neutral complexes (de Kruif *et al.*, 2004; Schmitt, 2009).

4.2.2.2 Total biopolymer concentration

The polymer concentration has to remain quite low in order for the phase separation to occur, although a more viscous medium will lead to more stable systems. Indeed, coacervation can be suppressed over a critical concentration. A total biopolymer concentration of 2 to 6 wt% is generally used for complex coacervation (de Kruif *et al.*, 2004; Lemetter *et al.*, 2009; Schmitt, 2009; Turgeon and Laneuville, 2009; Espinosa-Andrews *et al.*, 2010).

4.2.2.3 Optimum pH

Two polysaccharides are oppositely charged between their pKa values (see Table 4.2) (Ghosh and Bandyopadhyay, 2012). In this range, there is a pH where the net charge carried by the two

polyelectrolytes is maximum and equivalent. This is the optimal coacervation pH (pH_{opt}). The behaviour of the complexes is very sensitive to pH changes and even more so close to pH_{opt} (Schmitt, 2009; Yan and Zhang, 2014; Wu and McClements, 2015).

Table 4.2: pKa of the polysaccharides gum arabic and chitosan (Muzzarelli, 2009; Santiago de Alvarenga, 2011; Xiao *et al.*, 2014; Gulão *et al.*, 2016).

Polysaccharides	**pKa**
Gum arabic	2.0
Chitosan	5.5 - 7.0

In order to investigate the pH range, the two polymers should be dissolved at a pH where they are both soluble, and where they carry the same charge so that the coacervation does not initiate upon mixing (Lemetter *et al.*, 2009; Turgeon and Laneuville, 2009). Chitosan is always cationic as it precipitates above its pKa (see **Chapter 3**) and does not exist in solution under its negative form. Gum arabic is predominantly negative as it is only positively charged below pH 2.0. The pH should thus be adjusted by increasing it from acidic medium on the pH range from 2.0 to 5.5 - 7.0 maximum, depending when the precipitation of chitosan occurs.

The complex coacervation can be observed optically with the formation of a visible layer around the emulsion droplets which usually takes a characteristic “eye-shape” (see Figure 4.2). There are three main types of complexes: single core particles (mononucleated complexes), multi-core particles (polynucleated complexes), and aggregated single core particles (“grape” complexes) (Lemetter *et al.*, 2009). The visible formation of a coacervation layer following any of these three configurations should attest of the occurrence of complex coacervation, and enable to identify the optimum pH by optical microscopy.

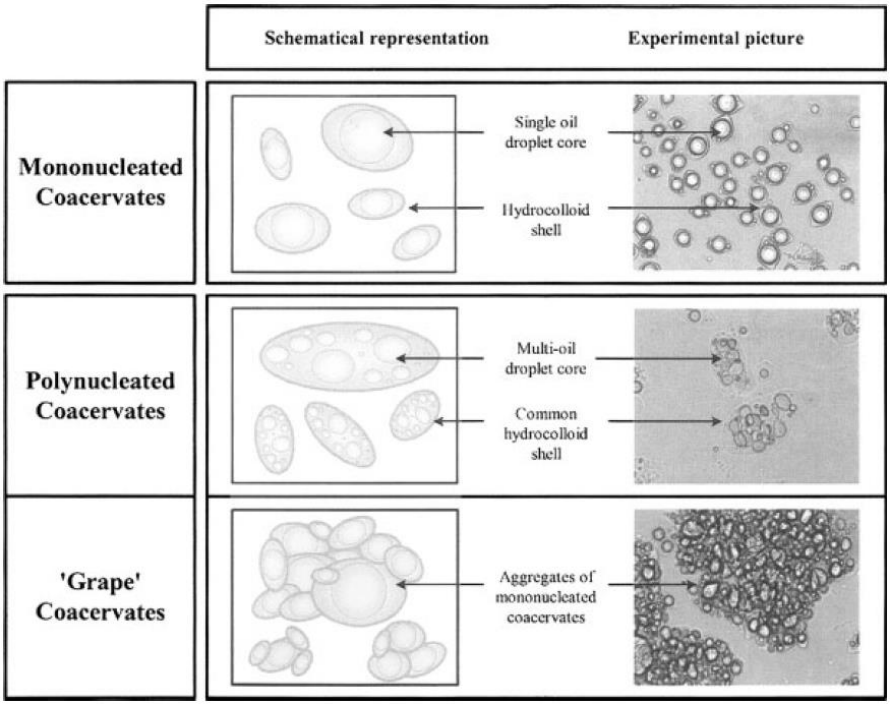


Figure 4.2: Different types of coacervated complexes which can be observed by optical microscopy (Lemetter *et al.*, 2009).

Although it can depend on the needs of the desired application, mononucleated coacervates are generally preferred for their single core and small size (Lemetter *et al.*, 2009). While polynucleation can be controlled by the stirring speed, aggregation is more a matter of the state of the shell and whether it is prone to making the capsules stick together. This latter parameter may therefore be more difficult to overcome.

4.2.2.4 Agitation

The shear rate should be high enough to avoid polynucleation but not too high to avoid foaming which can destabilise the coacervation phenomenon (Turgeon *et al.*, 2007; Lemetter *et al.*, 2009).

4.2.2.5 Coacervation time

It is difficult to predict the ideal time for coacervation as different theories contradict each other. The phenomenon is claimed to be spontaneous according to the Voorn-Overbeek theory (Overbeek and Voorn, 1957; Burgess, 1990) while it could take hours or even days to complete according to the Veis-Aranyi theory (Veis and Aranyi, 1960).

It is unsure which model the gum arabic-chitosan combination would tend to follow given that the gum arabic takes a random coil conformation (Masuelli, 2013) which would favour the Voorn-Overbeek theory, while chitosan exhibits a rod-like conformation (Rinaudo, 2006b) which applies to the Veis-Aranyi theory. As a precautionary measure and unless the coacervation time was further investigated, two hours should be given for the coacervation to happen.

4.2.3 Hardening of the wall

4.2.3.1 Physical hardening

For physical gelation, one of the materials first needs to present some gelling capacity, then its specific gelation mechanism must be identified (e.g. thermal, ionic).

Neither gum arabic nor chitosan can form thermal or ionic gels, a crosslinking step is thus required.

It is possible to use a physical crosslinker, such as pentasodium tripolyphosphate salt (NaTPP), which can interact with chitosan chains by ionic bonding (Anitha *et al.*, 2012).

4.2.3.2 Chemical hardening

For the chemical hardening, an appropriate crosslinker which can create intermolecular covalent bonds with the wall material should be identified (Anitha *et al.*, 2012).

Glutaraldehyde and formaldehyde have been widely and successfully used as crosslinkers in the complex coacervation process. The problem is that those compounds are toxic and therefore not acceptable for food application. A few weaker alternatives have been used to replace those crosslinkers for capsules destined to food products: citric acid, genipin, glyceraldehyde, plant polyphenols, tannins, and enzymes (transglutaminase, laccase) (de Kruif *et al.*, 2004; Dong *et al.*, 2007; Turgeon and Laneuville, 2009; Yan and Zhang, 2014; Wang *et al.*, 2018).

The reactive groups to be crosslinked are carboxyl for gum arabic and primary amine for chitosan (Anitha *et al.*, 2012; Thies, 2012).

The use of enzymatic crosslinkers is specific to proteins (Turgeon and Laneuville, 2009; Yan and Zhang, 2014; Wu and McClements, 2015) so they were not further considered for the gum arabic/chitosan combination.

Genipin reacts with amino acid groups and is therefore suitable for use with chitosan. It is from natural origin (gardenia fruits) and is non-toxic under its crosslinked form. It however presents two main drawbacks: crosslinking with genipin leads to dark blue coloured solutions, and this crosslinker is quite expensive, which is not desirable for chewing gum application (de Kruif *et al.*, 2004; Turgeon and Laneuville, 2009; Wang *et al.*, 2012b; Merck, 2020).

Tannic acid is a plant polyphenol which can be used as an alternative food grade crosslinker. It is relatively cheap but leads to purple solutions (Zhang *et al.*, 2011; Merck, 2020).

4.2.3.3 Crosslinking parameters

Only pentasodium tripolyphosphate (physical crosslinking) and tannic acid (chemical crosslinking) were selected for trials and comparison.

The crosslinking step can be influenced by several parameters: the amount of crosslinker, temperature, pH, and crosslinking time (see Table 4.3) (Zhang *et al.*, 2012).

Table 4.3: Comparison of the crosslinking conditions used for pentasodium tripolyphosphate (NaTPP) and tannic acid (RT: room temperature).

Crosslinker	Amount	Ideal pH	T (°C)	Time	Reference
NaTPP	1 - 20% w/v solution (0.068 g/g of chitosan)	Acidic pH (around 4.0)	RT	1 - 3h	(Jayakumar *et al.*, 2006; Tiwary and Rana, 2010; Wang *et al.*, 2012b; Prata and Grosso, 2015)
Tannic acid	10% w/v solution	4	RT	10 - 12h	(Xing *et al.*, 2004; Xing *et al.*, 2005; Zhang *et al.*, 2011)

4.2.4 Gum arabic/chitosan combination

The different conditions used in the literature for the complex coacervation of gum arabic and chitosan were compared (see Tables 4.4 to 4.8) in order to help determine the initial formulation and parameters required for the process.

Table 4.4: Comparison of the preparation of the chitosan solution from the literature.

Molecular weight	Amount	Acetic acid solution	Temperature	Reference
Medium	2 wt%	1% (v/v)	-	(Espinosa-Andrews *et al.*, 2007; Espinosa-Andrews *et al.*, 2008; Espinosa-Andrews *et al.*, 2010)
-	1 wt%	pH 3.0	-	(Moschakis *et al.*, 2010)
Low	3 wt%	1% (v/v)	-	(Espinosa-Andrews *et al.*, 2013)
Medium	1 wt%	1% (v/v)	50ºC	(Yang *et al.*, 2014)
Low	2 wt%	2% (v/v)	45ºC	(Butstraen and Salaün, 2014)
Low	1 wt%	1% (v/v)	20ºC	(Roldan-Cruz *et al.*, 2016)

Table 4.5: Comparison of the polymer concentrations from the literature.

Total biopolymer concentration	Polymer weight ratio (gum arabic/chitosan)	Reference
6 wt%	5:1	(Espinosa-Andrews *et al.*, 2007; Espinosa-Andrews *et al.*, 2008; Espinosa-Andrews *et al.*, 2010)
0.5 - 3.0 wt%	≥ 5:1	(Moschakis *et al.*, 2010)
5 wt%	5.5:1	(Espinosa-Andrews *et al.*, 2013)
1.5 wt%	2:1	(Yang *et al.*, 2014)
5 wt%	4:1	(Butstraen and Salaün, 2014)
-	5.5:1	(Roldan-Cruz *et al.*, 2016)

Table 4.6: Comparison of the emulsification step from the literature.

Core/ aqueous phase ratio	Emulsifier	Amount	Speed	Time	Reference
-	-	-	-	-	(Espinosa-Andrews *et al.*, 2007; Espinosa-Andrews *et al.*, 2008; Espinosa-Andrews *et al.*, 2010)
15 wt%	Whey protein	1.5 wt%	12000 rpm	2 min	(Moschakis *et al.*, 2010)
-	-	-	-	-	(Espinosa-Andrews *et al.*, 2013)
1%	Span 83	0.3 wt%	5000	5 min	(Yang *et al.*, 2014)
10% (v/v)	-	-	11000	15 min	(Butstraen and Salaün, 2014)
-	-	-	-	-	(Roldan-Cruz *et al.*, 2016)

Table 4.7: Comparison of the coacervation step from the literature.

Optimum pH	Agitation speed	Temperature	Time	Reference
4.5	-	25ºC	-	(Espinosa-Andrews *et al.*, 2007; Espinosa-Andrews *et al.*, 2008; Espinosa-Andrews *et al.*, 2010)
3.0	-	-	-	(Moschakis *et al.*, 2010)
4.0 - 5.5	-	20ºC	-	(Espinosa-Andrews *et al.*, 2013)
3.0 - 6.0	400 rpm	-	30 min	(Yang *et al.*, 2014)
3.6	1000 rpm	-	-	(Butstraen and Salaün, 2014)
3.9	-	20ºC	-	(Roldan-Cruz *et al.*, 2016)

Table 4.8: Comparison of the crosslinking step from the literature.

Crosslinker	Amount	pH	Temperature	Time	Reference
-	-	-	-	-	(Espinosa-Andrews *et al.*, 2007; Espinosa-Andrews *et al.*, 2008; Espinosa-Andrews *et al.*, 2010)
-	-	-	-	-	(Moschakis *et al.*, 2010)
-	-	-	-	-	(Espinosa-Andrews *et al.*, 2013)
25 wt% genipin in ethanol	5 mL	7	0 - 5ºC	-	(Yang *et al.*, 2014)
2% NaTPP	-	3.6	-	2h	(Butstraen and Salaün, 2014)
-	-	-	-	-	(Roldan-Cruz *et al.*, 2016)

The conditions to prepare the chitosan solution as well as the mixing conditions of the two polysaccharides were first compared (see Tables 4.4 and 4.5). Then the different parameters required for the formation of the emulsion were identified (see Table 4.6), followed by the ones necessary for the coacervation step (see Table 4.7). Finally, the different crosslinkers which were used for this polyelectrolyte combinations were listed when possible (see Table 4.8).

From the comparison of all those parameters, it appears that there is no universal set of conditions for carrying out complex coacervation with gum arabic and chitosan.

4.3 Experimental procedures

The protocol used by Butstraen and Salaün (2014) was chosen as a starting point for the investigations, with a higher gum arabic solution concentration of 12 wt% (Huang *et al.*, 2001).

4.3.1 Preparation of polymer solutions

The polyelectrolyte solutions were prepared the day before the experiment. A gum arabic solution (1, 6 or 12 wt%) was made in DI water under mechanical stirring with a Rushton

turbine (see Figure 3.13) at 700 rpm, and equipped with a water bath set at 25ºC. A second solution was made by dissolving low, medium or high molecular weight chitosan (1 or 2 wt%) in a 2 wt% acetic acid aqueous solution at 45ºC. After full dissolution (about 1h), the mixtures were cooled down to 5ºC and left to stir overnight at 500 rpm to ensure full hydration of the polymers (Espinosa-Andrews *et al.*, 2007).

4.3.2 Preparation of emulsions

A desired amount of emulsifier (0 or 1 wt%) was dissolved in the gum arabic solution under magnetic agitation in a 150 mL beaker at room temperature (RT, estimated to be 22 ± 3ºC). L-carvone oil (5, 10, 15 or 20 wt%) was poured into the previous aqueous phase, and the mixture was stirred by mechanical agitation at 500 rpm with a Rushton turbine for pre-emulsification mixing for about 5 min.

The pre-emulsion was then mixed with a high-shear mixer equipped with an emulsor screens head (see Figure 3.14) at 2000 rpm for 15 min to form an O/W emulsion. Following the emulsification, the system was left to rest for two minutes to allow the air bubbles to come to the surface. This foam was scooped off with a spatula.

An O/W emulsion which could be stable for two hours (time of the coacervation process prior to crosslinking) was desired.

4.3.2.1 Emulsifier selection

This investigation was organised in several steps. It was important to first determine the ideal HLB for the emulsion system, then the selection of the chemical type of the surfactant had to be made, and finally this study was completed by interfacial tension measurements.

4.3.2.1.1 Critical HLB determination

The HLB spreadsheet design consists of mixing a lipophilic emulsifier (L) with a hydrophilic one (H) in different proportions. More specifically, the blend of two surfactants of opposite natures but from the same chemical family (Spans and Tweens) should enable to cover most of the HLB range (see Figure 4.3). We can calculate the HLB of the new surfactant combination from the addition of the respective percentage of each emulsifier applied to their individual HLB (ICI Americas Inc., 1976; Macedo *et al.*, 2006).

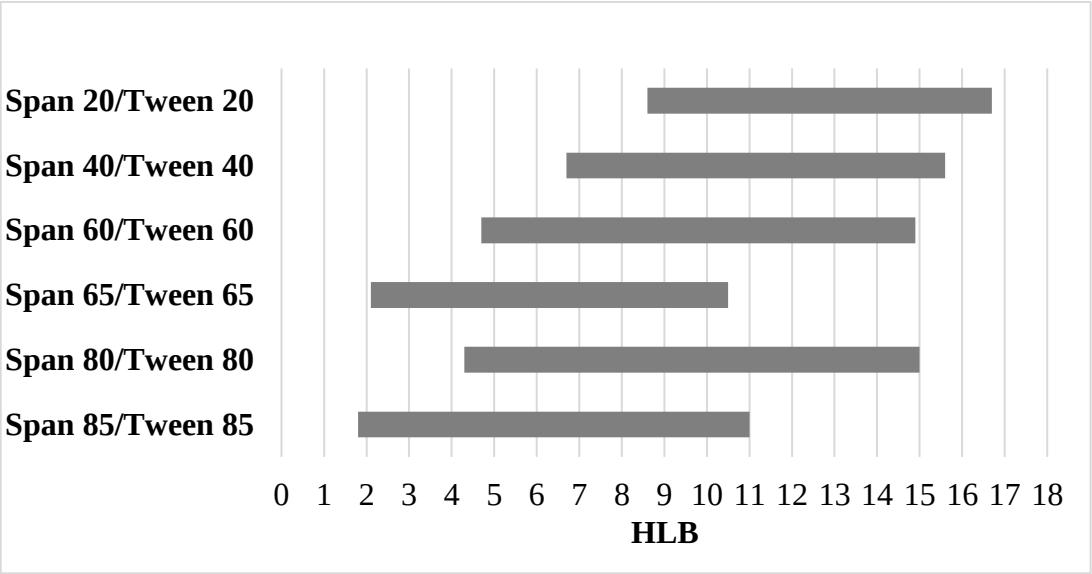


Figure 4.3: HLB range covered by different emulsifier combinations (ICI Americas Inc., 1976; Merck, 2020).

Tween 80 or Span 60/Tween 60 blend are common emulsifying agents for flavour O/W emulsions. The blend of a same family leading to the most stable emulsion gives the indication of HLB_{crit} (ICI Americas Inc., 1976). A series of trial emulsions were made with 1 wt% emulsifier for matched Span and Tween 60 combinations in order to cover the HLB range of interest to obtain an O/W emulsion (8-18) (see Table 4.9). Trials with the combinations leading to a HLB below 8 were also made as a proof of principle.

Table 4.9: Emulsifier combination 60 HLB spreadsheet.

Sample	Span 60 (%)	Tween 60 (%)	Calculated HLB
1	100	-	4.7
2	87	13	6
3	68	32	8
4	48	52	10
5	28	72	12
6	9	91	14
7	-	100	14.9

The stability of the emulsions was evaluated by size distribution measurements (see **Chapter 3**).

4.3.2.1.2 Dynamic interfacial tension (IFT)

Some additional drop tensiometry measurements (see Figure 3.15) were made for L-carvone droplets in water medium containing 0.05 wt% emulsifying agent to understand the effect of the emulsifier on the IFT of this flavour oil dispersed in aqueous phase (the concentration of emulsifier had to be reduced in order for the camera to capture the profile of the drop distinctly enough).

4.3.2.1.3 Surfactant comparison

The next step consisted of identifying the best chemical family of emulsifiers to stabilise the emulsion at HLB_{crit} by trying out different blends (1 wt%): Span 60/Tween 60 (stearates), Span 80/Tween 80 (oleates), Span 85/Tween 85 (trioleates), Span 20 (laurate ester) (ICI Americas Inc., 1976).

For each combination, the proportions of Span and Tween could be easily calculated using the following equations (ICI Americas Inc., 1976):

$$\%\ (\text{Span}) = \frac{100\times(\text{HLB}_{\text{Tween}}-\text{HLB}_{\text{crit}})}{\text{HLB}_{\text{Tween}}-\text{HLB}_{\text{Span}}} \quad \textbf{(Eq. 4.4)}$$

$$\%(\text{Tween}) = 100 - \%\ (\text{Span}) \quad \textbf{(Eq. 4.5)}$$

Similarly to the previous step, the stability of the emulsions was evaluated by size distribution measurements.

4.3.2.2 Mixing speed

Emulsions were prepared at different mixing speeds (500, 700, 900, 1100 and 2000 rpm) and the radius of the droplets was measured by light microscopy using the software (see **Chapter 3**).

4.3.2.3 Formulation optimisation

The optimal formulation of the emulsion system was investigated via a statistical approach: the Design of Experiments (DoE) or experimental design. This technique allows to study the effects of different parameters (involved in the formulation of the emulsion) on a desired response (here the stability of the emulsion) (Catte *et al.*, 2002; Bendjaballah *et al.*, 2010; Dehghan and Kazi, 2014).

A set of different emulsion trials were prepared according to this technique. The stability of the emulsions was evaluated by measuring the size distribution of the fresh emulsions and after 2h (duration of complex coacervation prior to crosslinking).

4.3.2.4 Type of emulsion

A tip of spatula of Nile red fluorescent dye was added to L-carvone, prior to mixing with the gum arabic solution, and dissolved via ultrasonic bath at RT for 10 minutes.

The emulsion was observed by optical microscopy (light and fluorescence) (see **Chapter 3**).

4.3.2.5 Stabilisation of the core

An attempt to stabilise the oil phase was made by mixing L-carvone with three different MCT oils (coconut oil, palm oil and Miglyol 812 N) in the ratio of 1:1 (w/w).

4.3.3 Coacervation step

The emulsion phase was transferred to a 500 mL baffled jacketed beaker with the water bath temperature set at 25ºC. The mixture was put under mechanical stirring with a Rushton turbine at 500 rpm. This agitation was continued until the end of the full process. The pH was adjusted to 2.5 (it was difficult to go as low as 2.0 with a weak acid such as acetic acid) with a 10 wt% acetic acid solution. A desired amount of chitosan solution compared to the quantity of gum arabic (1:2, 1:4 or 1:6 w/w) was added dropwise to the emulsion under agitation.

After the addition was complete, the pH was adjusted (see **Chapter 3**) to the optimal pH (pH_{opt}) using 10 wt% acetic acid and 1M sodium hydroxide (NaOH) solutions. The coacervation was followed visually by optical microscopy (see **Chapter 3**) at different pH (between 2.5 and 6.0) to identify the optimum pH. Once the desired phenomenon had been observed, the batch was left to stir for 2h.

4.3.4 Crosslinking

Finally, a desired amount of crosslinker (tannic acid: 10 g of 10 wt% solution, or NaTPP: 20 g of 3 wt% solution adjusted to pH_{opt}) was added at 25ºC, and the mixture was further left under agitation overnight (16h) to allow time for crosslinking.

The different steps of the process are represented below (see Figure 4.4).

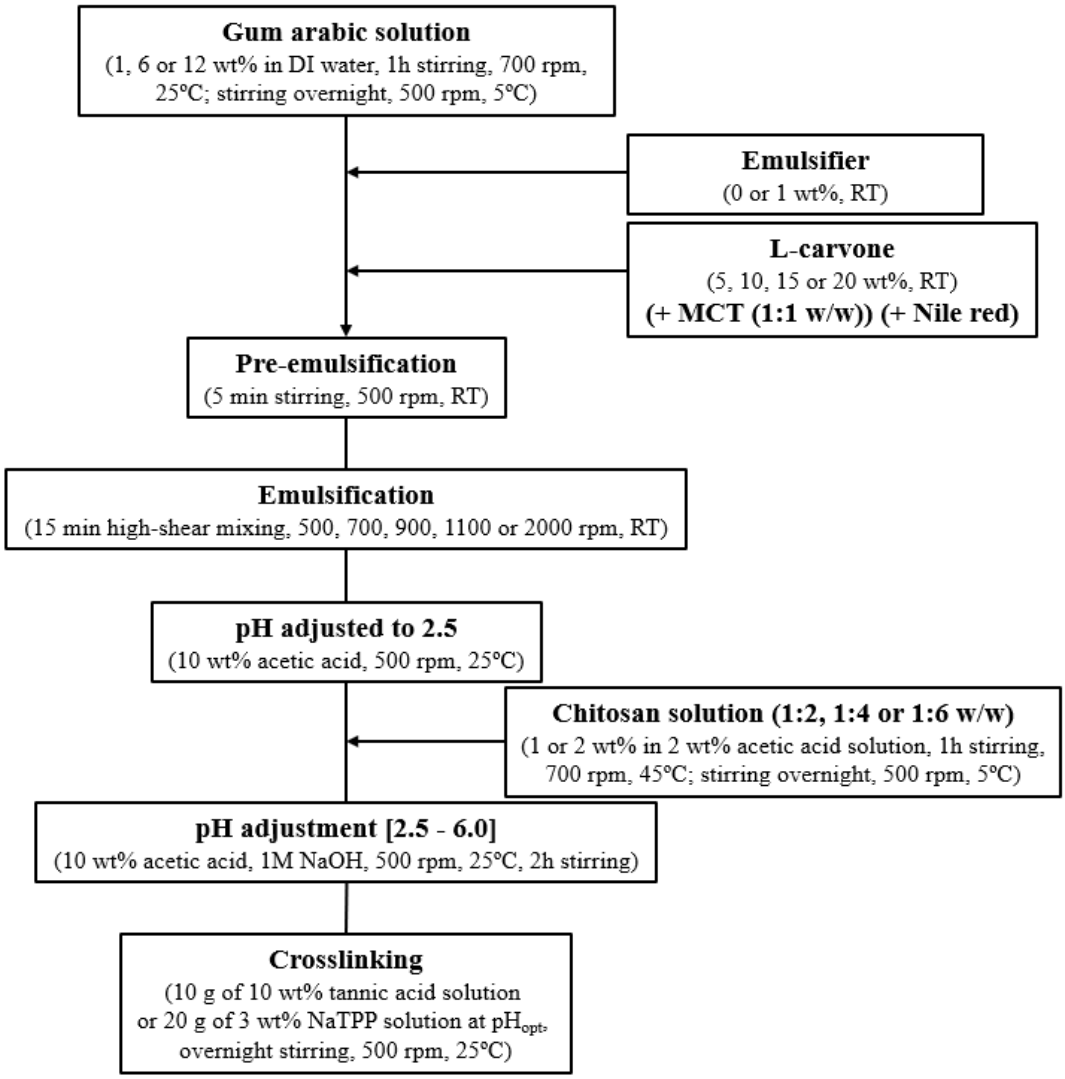


Figure 4.4: Schematic flow chart of the complex coacervation process for the encapsulation of L-carvone within a gum arabic/chitosan shell.

4.3.5 Sensory check of L-carvone in capsules

A drop of the suspension was systematically deposited on a microscope glass slide and left to dry at RT in the open air for 24h. The capsules were then crushed with a spatula and smelling sensory evaluation was used as a preliminary check to confirm whether the encapsulation was successful or not.

This was considered as a quick qualitative way to get an idea of the success or failure of encapsulation, without requiring any further, time consuming characterisation (such as GCMS). Putting in place a sensory panel also requires a lot of resources (people, time and money) as well as training, which was not desired here. Having some experience in olfaction, I subjectively evaluated each sample and characterised the perceived flavour scent using a scale from 0 to 5 (0: no L-carvone smell, 1: very weak, 2: weak, 3: medium, 4: strong, 5: very strong). L-carvone is characterised by a strong, fresh, minty smell which was easily recognisable for those assessments.

4.4 Results and discussion

4.4.1 Stability of the emulsion

4.4.1.1 Selection of an emulsifier

The Sauter diameter (d_{32}) and the span values were collected from the size distribution measurements of emulsions made with different proportions of Span 60 and Tween 60 emulsifiers. Those values were plotted as a function of the HLB on the range allowed by this combination (4.7 – 14.9) (see Figure 4.5).

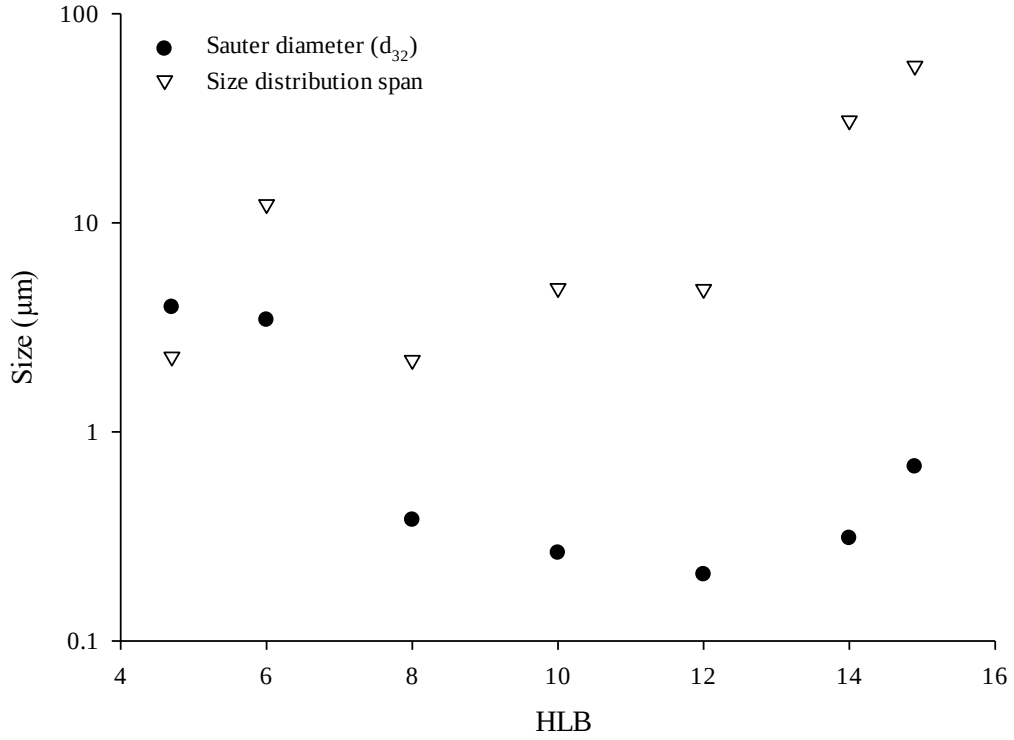


Figure 4.5: Influence of the HLB value of the Span 60/Tween 60 combination (based on mixing samples 1 – 7, see Table 4.9) on the size of emulsion droplets (the values of the plots were calculated by the software using the average size distribution data based on triplicate measurements, the standard deviation resulting from these average values should be negligible for a sample which is non-aggregating, which was the case for those emulsions).

The lower size values on the HLB range 8-15 confirmed that the O/W emulsion was better stabilised with an emulsifying agent displaying an HLB value belonging to this range, as expected.

The variations of the Sauter diameter seemed quite negligible on this range and apart from setting aside the value at HLB = 14.9, it did not permit to conclude on the other four values. The span value however enabled to identify a critical HLB of 8, as a narrower size distribution should attest of a more stable emulsion.

This meant that for the specific emulsion system (L-carvone oil in gum arabic solution) the ideal HLB should be $HLB_{crit} = 8 \pm 2$ (error based on the interval chosen for the measurement points).

Interfacial tension measurements were analysed to understand better the interfacial behaviour of the different emulsifiers and how it could be linked to the HLB. A good emulsifier should rapidly adsorb at the surface of emulsion droplets, to first reduce the interfacial tension and ease the break-up, and secondly to create a protective layer and avoid coalescence (McClements, 2009).

The dynamic interfacial tension of different emulsifiers (Spans and Tweens) was plotted as a function of time, averaged according to a 15 point based moving average due to the very high frequency of the data (see Figures 4.6 and 4.7).

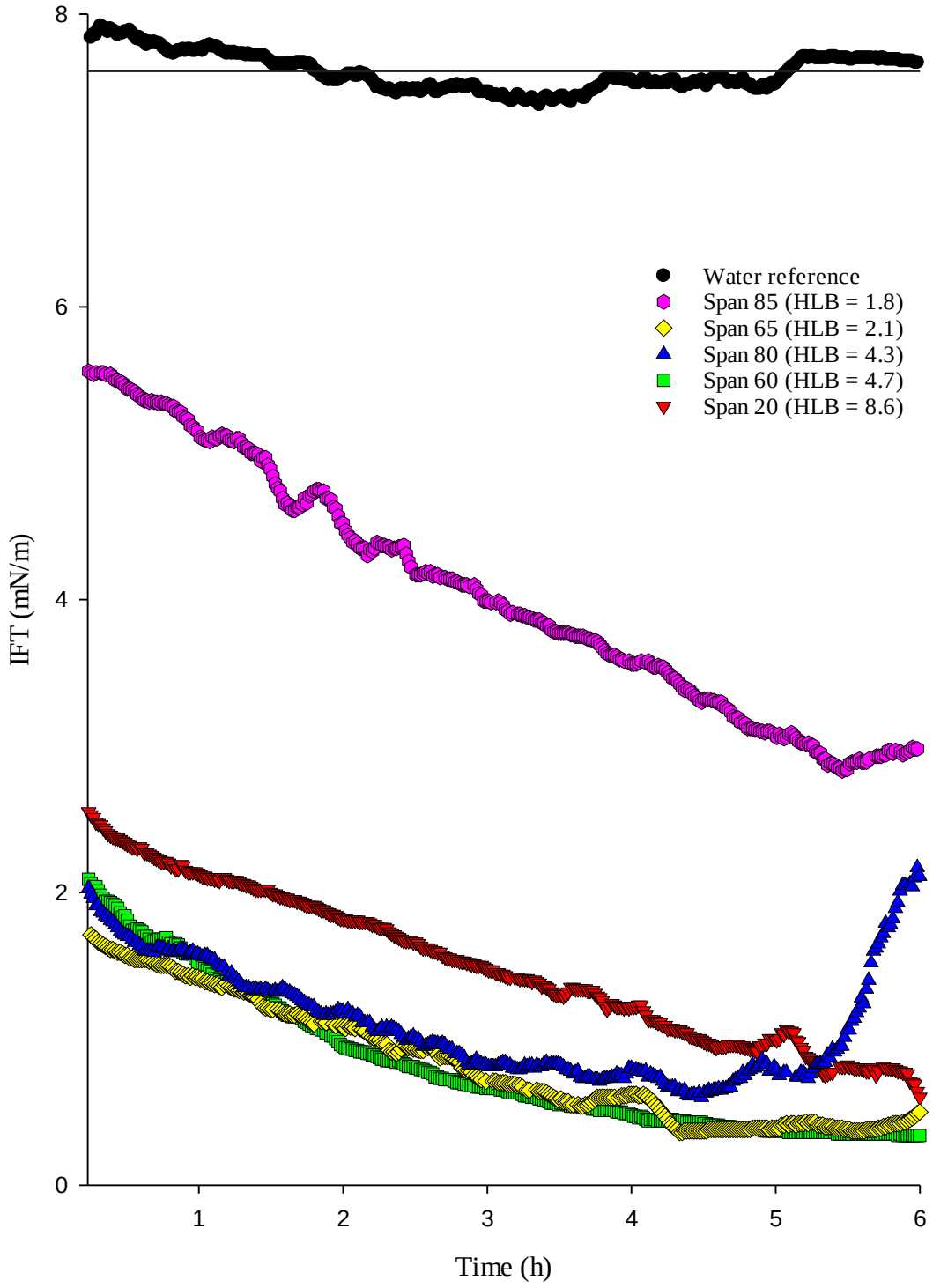


Figure 4.6: Effect of 0.05 wt% of different lipophilic emulsifiers (Span 20, 60, 65, 80 and 85) on the dynamic interfacial tension (IFT) of an L-carvone O/W emulsion (the solid line was only traced to represent the trend of the reference).

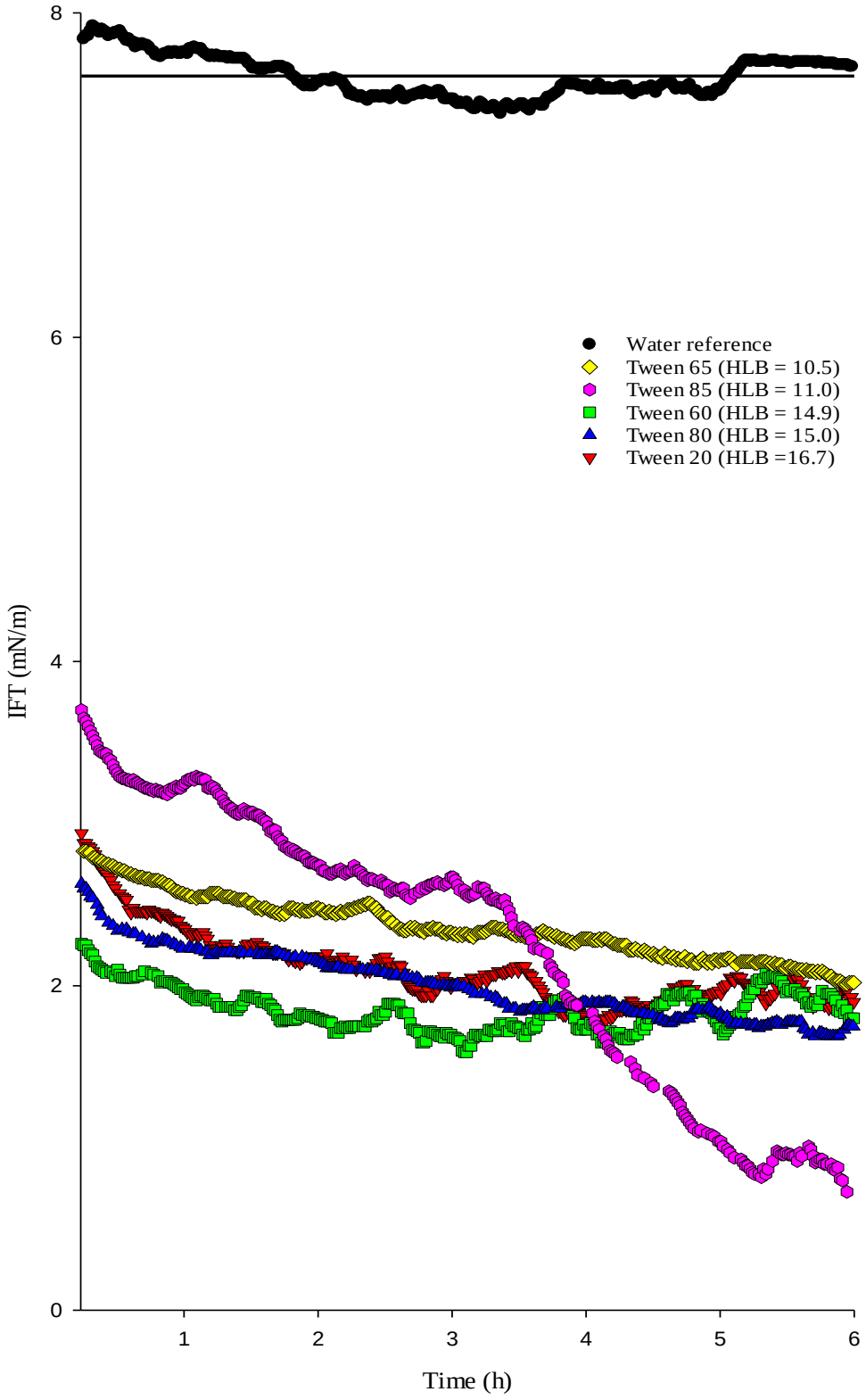


Figure 4.7: Effect of 0.05 wt% of different hydrophilic emulsifiers (Tween 20, 60, 65, 80 and 85) on the dynamic interfacial tension (IFT) of an L-carvone O/W emulsion (the solid line was only traced to represent the trend of the reference).

It could be noticed that all emulsifiers helped to lower the interfacial tension, when comparing to the reference IFT value. However, they were all very slow to adsorb at the surface of L-carvone as none of them reached a clear plateau after 6h. This means the amount of emulsifier would need to be increased in order to adsorb faster at the surface of L-carvone oil droplets.

The effect of those emulsifiers did not seem to be related to their HLB value, when Span 85 (HLB = 1.8) and Tween 85 (HLB = 11.0) showed the least significant initial interfacial tension lowering while Span 65 (HLB = 2.1) and Tween 60 (HLB = 14.9) lowered the interfacial tension the most among the lipophilic and hydrophilic emulsifiers respectively. These observations confirmed the importance of considering additional parameters to the simple HLB value of individual emulsifiers, such as their chemical nature.

It is important to note that in turbulent flow interfacial tension (γ) and Sauter diameter (d_{32}) are linked by the following equation:

$$d_{32} = c \times \left(\frac{\gamma}{\rho_{\Phi}}\right)^{3/5} \times E^{-2/5} \qquad \textbf{(Eq. 4.6)}$$

where c is a dimensionless empirical constant, ρ_{Φ} is the density of the continuous phase, and E is the mean energy dissipation rate per unit mass of fluid (Hall *et al.*, 2013).

This means that if the critical HLB is investigated based on Sauter diameter studies, the HLB and interfacial tension should also be linked. For this reason, the volume of the generated droplet was kept constant from one sample to the other during the interfacial tension measurements, in order to avoid droplet size-dependent variations in the IFT values. Having said that, the HLB still remains the key parameter characterising the effect of an emulsifying agent on a given emulsion system.

An ideal emulsifying agent still had to be identified by comparing several emulsifier systems displaying the critical HLB value previously identified (see Table 4.10) and their effect on the Sauter diameter of the fresh emulsions (Figure 4.8).

Table 4.10: Emulsifier combinations for reaching a HLB of 8.

Chemical family X	Span X (%)	Tween X (%)	Calculated HLB
20	100	0	8.6
60	68	32	8
80	65	35	8
85	33	67	8

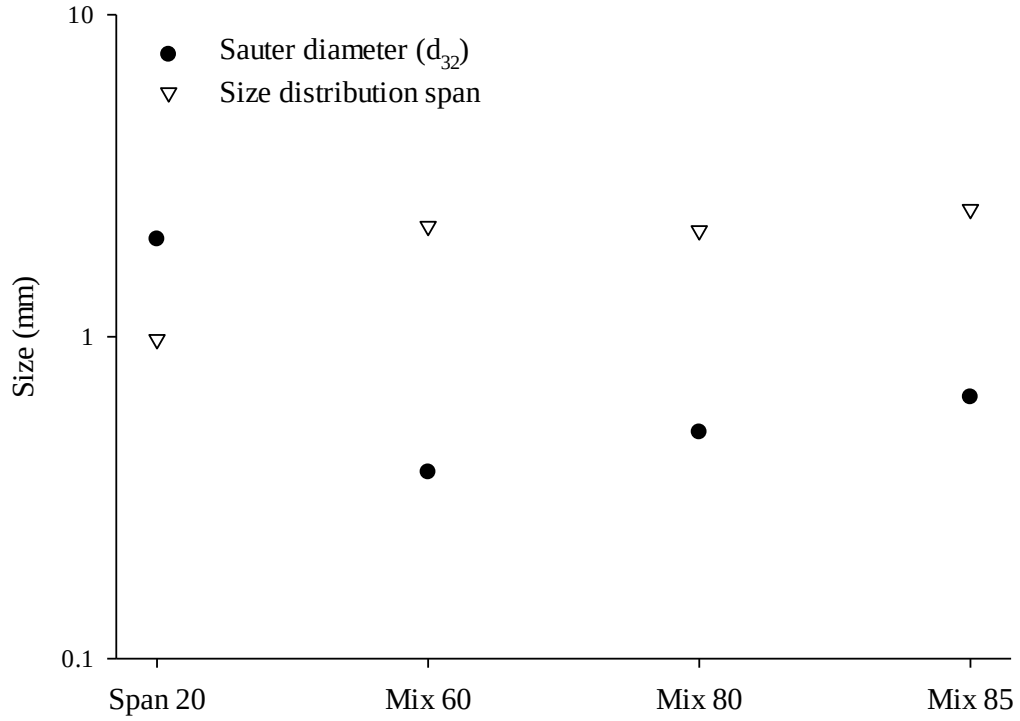


Figure 4.8: Influence of the chemical family of emulsifiers at HLB = 8 (Span 20, Span 60/Tween 60, Span 80/Tween 80 and Span 85/Tween 85 mixes, see Table 4.10) on the droplet size of the fresh emulsions (the values of the plots were calculated by the software using the average size distribution data based on triplicate measurements, the standard deviation resulting from these average values should be negligible for a sample which is non-aggregating, which was the case for those emulsions).

The use of the Span 60/Tween 60 combination at HLB = 8 led to a minimum Sauter diameter value (see Figure 4.8). This meant that among the tested blends, the stearates seemed to be the most adapted chemical family for the early stabilisation of the studied emulsion system.

These observations also explained why the Span 60/Tween 60 blend was attracting a particularly interest for the use in flavour O/W emulsions in food applications, and this combination at HLB = 8 was identified as the best emulsifying agent for stabilising the studied emulsion system.

4.4.1.2 Mixing speed

The influence of the mixing speed used for 15 minutes to form the emulsion on the size of the generated oil droplets was investigated visually by light microscopy (see Figure 4.9).

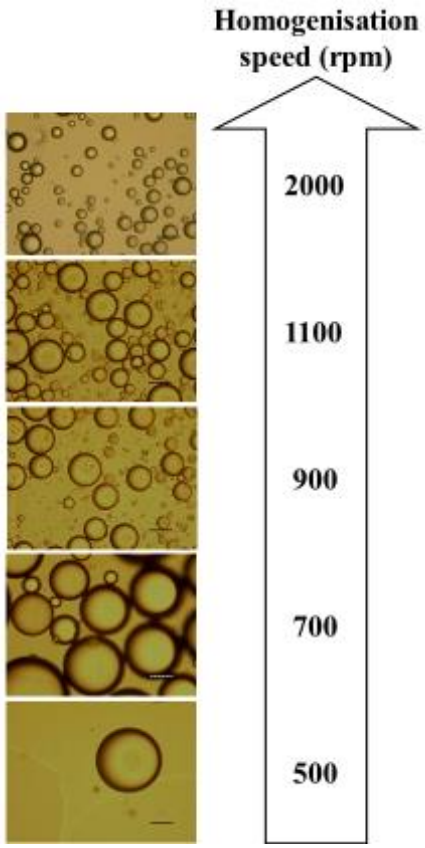


Figure 4.9: Qualitative comparison of the droplet size of emulsions formed at different mixing speeds (500, 700, 900, 1100 and 2000 rpm) for 15 minutes (all scales represent 50 μm).

Based on the targeted size of about 30 μm, the mixing speed of 2000 rpm was selected for further experiments.

4.4.1.3 Optimisation of the emulsion formulation

4.4.1.3.1 Identification of the different parameters of the study system

As previously explained, several parameters can influence the stability of emulsions, requiring a very large number of trials, which can be very time consuming and expensive. Experimental design is an interesting statistical approach which enables to study the effects of different parameters on a given aspect, here the stability of the emulsion, by reducing the number of experiments to a minimum. This method is an efficient way to optimise a formulation.

In order to reduce this to a reasonable number of experiments, some of those parameters were fixed by preliminary investigations as non-varying factors for this study. According to the previous experiments, the nature of the emulsifying agent was chosen to be a Span 60/Tween 60 mix at the HLB value $HLB_{crit} = 8$. As the mixing speed necessarily has an inverse effect on the diameter of the droplets (which is used for the response parameter in this study), this value was also set beforehand to 2000 rpm in agreement with previous investigations. Three variables were identified for this study: the concentration of the gum arabic solution (U_1), the amount of oil (U_2) and the concentration of the emulsifier (U_3).

The experimental domain of each parameter was defined by a minimum and a maximum value. For the concentration of the gum arabic solution, it was noted from the literature (Yang *et al.*, 2014; Roldan-Cruz *et al.*, 2016) that the biopolymer was sometimes used at low concentration, but it was also found that the best emulsification properties were found at a concentration of 12.5 wt%. Different amounts of oil were used depending on the publications (between 1 and 15 wt%). After having fixed the ideal emulsifying system for L-carvone emulsions (Span

60/Tween 60), the question remained whether the addition of an emulsifier was necessary, taking into account that gum arabic already had emulsifying properties. Based on those considerations, the experimental factor domains were defined as follows (see Table 4.11). The variables were then coded (X_i) by levels (-1 for the minimum value and +1 for the maximum value) (Bendjaballah *et al.*, 2010).

Table 4.11: Parameters and domain values of the experimental design.

Parameters	**Lower level (-1)**	**Upper level (+1)**
U_1: GA concentration (wt%)	1	12
U_2: oil in initial emulsion (wt%)	5	20
U_3: emulsifier concentration (wt%)	0	1

4.4.1.3.2 Construction of the experimental design

For studying those parameters by experimental design, a 2^3 factorial design was chosen, which meant 8 experiments. This method enables to study the effect of each factor separately as well as their interactions (Bendjaballah *et al.*, 2010).

A response Y had to be selected in a way that this parameter could be measured and would characterise meaningfully the stability of the emulsion. The Sauter diameter was chosen as the measured parameter leading to the response parameter Y expressed as the relative Sauter diameter:

$$Y = \frac{\left|d_{32}^{2h} - d_{32}^{0}\right|}{d_{32}^{0}} \qquad \textbf{(Eq. 4.7)}$$

where d_{32}^{0} is the Sauter diameter of the fresh emulsion, and d_{32}^{2h} is the Sauter diameter of the emulsion after 2h.

For this method, the response Y was represented by the following second order polynomial model for 3 factors (X_i) (Bendjaballah *et al.*, 2010):

$$Y = b_0 + b_1X_1 + b_2X_2 + b_3X_3 + b_{12}X_1X_2 + b_{13}X_1X_3 + b_{23}X_2X_3 + b_{123}X_1X_2X_3 \quad \textbf{(Eq. 4.8)}$$

where b_i are the coefficients of the model.

A Hadamard matrix was then built according to the construction of Plackett-Burman designs (Plackett and Burman, 1946) (see Table 4.12) in order to determine the experiments to be carried out (see Table 4.13).

Table 4.12: Matrix of the model for 3 factors according to the construction of Plackett-Burman designs.

X_0	X_1	X_2	X_3	X_1X_2	X_1X_3	X_2X_3	$X_1X_2X_3$
1	1	1	-1	1	-1	-1	-1
1	1	-1	1	-1	1	-1	-1
1	-1	1	1	-1	-1	1	-1
1	-1	-1	-1	1	1	1	-1
1	-1	-1	1	1	-1	-1	1
1	-1	1	-1	-1	1	-1	1
1	1	-1	-1	-1	-1	1	1
1	1	1	1	1	1	1	1

Table 4.13: Experimental matrix with experimental response Y (relative d_{32}).

Experiment #	GA concentration (wt%)	Amount of oil (wt%)	Emulsifier concentration (wt%)	Relative d_{32} (Y)
1	12	20	0	0.60
2	12	5	1	0.26
3	1	20	1	0.99
4	1	5	0	1.80
5	1	5	1	0.99
6	1	20	0	0.60
7	12	5	0	0.94
8	12	20	1	0.96

4.4.1.3.3 Study of the effects and interactions

The relative Sauter diameter (Y) was then calculated for each experiment and was processed through NemrodW experimental design software (Bendjaballah *et al.*, 2010).

Some checks were made in order to validate the mathematical model. From the analysis of the variance (Table 4.14) it could be seen that the variance of the regression was higher than the one of the residues, which meant the chosen mathematical model could adequately explain the chosen response for the study.

Table 4.14: Table of the analysis of the variance calculated with NemrodW software.

Source of variation	Sum of the squares	Degrees of freedom	Mean square	Ratio	Significance
Regression	1.4174	6	0.2362	73.820	8.9
Residues	0.0032	1	0.0032		
Total	1.4206	7			

Checking the coefficient of determination (R^2) value (see Table 4.15) gave the information that 99.8% of the behaviour of the response Y could be explained by the variation of the parameters X_i. Furthermore, the adjusted coefficient of determination (R^2a) confirmed the good model fit.

Table 4.15: Estimation of the coefficients calculated with NemrodW software.

Standard deviation of the response	0.057
R2	0.998
R2A	0.984
Number of degrees of freedom	1

All parameters were shown to have significant effects ($b_i > 1/8\ b_{max}$) on the relative Sauter diameter but the concentration of the gum arabic solution was the most important one (see Figure 4.10). The relative Sauter diameter either increased or remained about the same when

going from 12 wt% gum arabic down to 1 wt% (see Table 4.13), which meant a higher concentration would be preferred but that it was not the only influencing parameter.

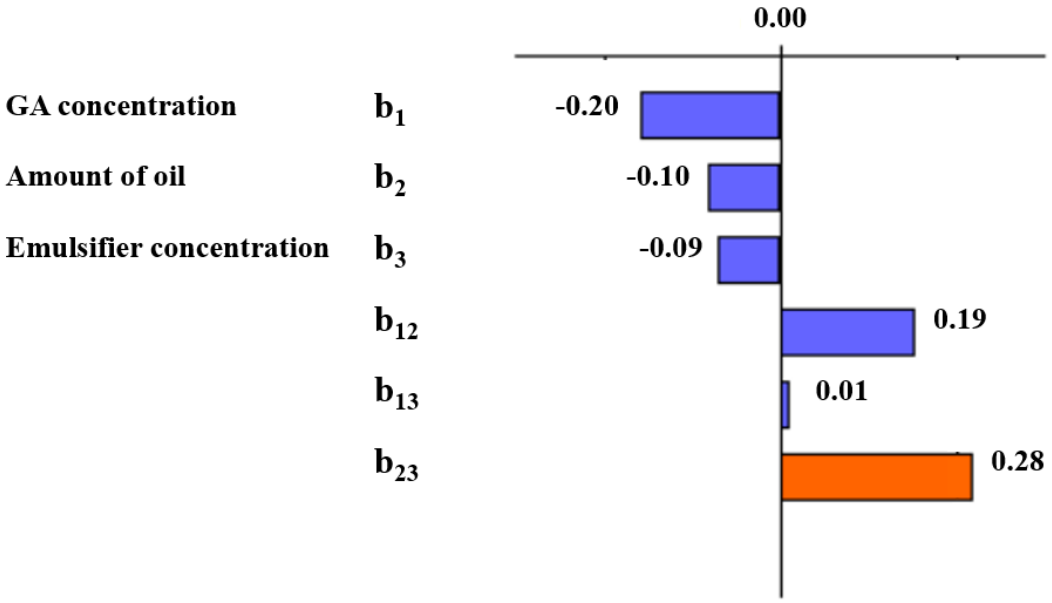


Figure 4.10: Study of the effects given by NemrodW software.

When looking at the interactions, the effect between the amount of L-carvone and the concentration of emulsifier (b_{23}) seemed to have the most importance (see Figure 4.10), which makes sense since the amount of oil influences the surface area to be covered, and thus the required quantity of emulsifier needed. It was however considered that the concentration of the gum arabic solution and the concentration of emulsifier did not interact significantly ($b_{13} < 1/8\ b_{23}$). The polynomial model of the study could therefore be reduced to:

$$\text{Relative } d_{32} = 0.89 - 0.20\ X_1 - 0.10\ X_2 - 0.09\ X_3 + 0.19\ X_1X_2 + 0.28\ X_2X_3 \quad \textbf{(Eq. 4.9)}$$

The effect of the interaction of each parameter U_i with one another was studied graphically with NemrodW software (see Figures 4.11 and 4.12). The value of the answer Y (relative d_{32}) was given for each matrix level configuration (+1/+1, +1/-1, -1/+1 and -1/-1) of the two compared parameters.

When studying the interaction effects diagram between U_2 (amount of oil) and U_3 (emulsifier concentration) (see Figure 4.11) as they were the interacting parameters with the most influence on the model (see Figure 4.10), it could be noticed that although more oil without emulsifier seemed to lead to slightly more stable emulsions (lowest relative d_{32}), the configuration with less oil and emulsifier also seemed to work well as the two values were very close.

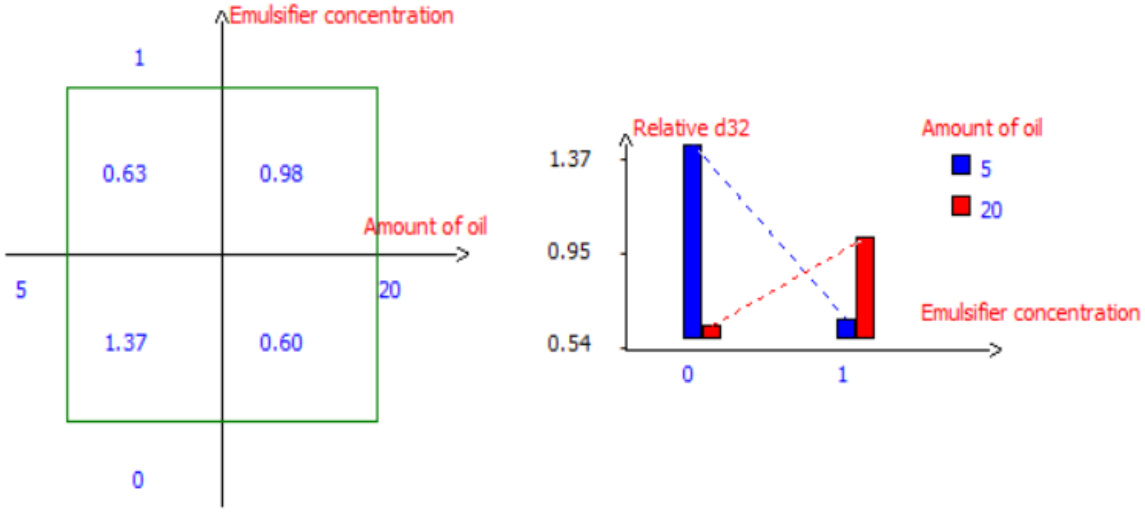


Figure 4.11: Interaction effects diagram between the amount of oil (U_2) and the emulsifier concentration (U_3), given by NemrodW software.

When considering the effects between U_1 (gum arabic concentration) and U_2 (amount of oil) (see Figure 4.12) as their interaction also had a significant influence on the model (see Figure 4.10), it was concluded that less oil in highly concentrated gum arabic solution led to more stable emulsions. The two lowest relative d_{32} values were obtained for 12 wt% gum arabic, which confirmed the choice of using this high concentration for the gum arabic solution to form the emulsion.

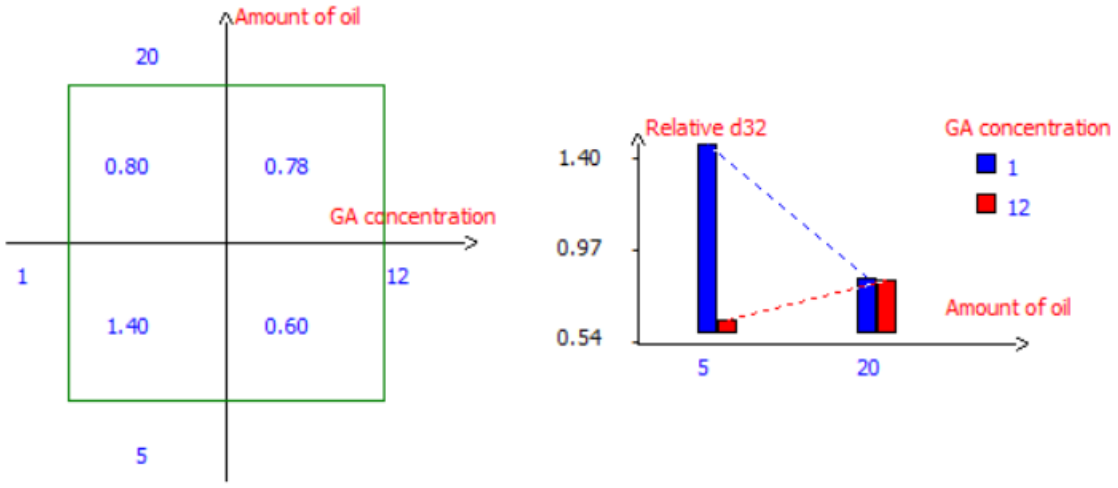


Figure 4.12: Interaction effects diagram between the amount of oil (U_2) and the gum arabic concentration (U_1), given by NemrodW software.

In summary, this experimental design study enabled to identify the influence of the difference parameters on the stability of the emulsions. A minimum amount of L-carvone emulsified in a 12 wt% gum arabic solution with emulsifier seemed to be an ideal formulation, although more oil emulsified in a 12 wt% gum arabic solution with no additional emulsifier also seemed to be an acceptable alternative. This result is understandable as gum arabic also has emulsifying properties due to its protein content, and may be sufficient on its own. It is interesting to note that this result is also in accordance with the critical HLB of 8, previously identified for the L-carvone emulsified in gum arabic system, as the HLB of gum arabic was found to be between 8.0 and 11.9 (Zajic and Panchal, 1976).

If the choice of one formulation over the other did not make a major difference, sparing the addition of two extra ingredients for the emulsifying agent (Span 60/Tween 60) was preferred for the rest of the experiments.

Additional trials were made to verify the results found via the previous methodology by assessing the encapsulation efficiency (data not shown). First, it was confirmed that better

capsules were obtained in the absence of emulsifier (Span 60/Tween 60 mix at HLB = 8). Points at the centre of the domains were also checked: trials were made for gum arabic concentrations of 1, 6 or 12 wt%, as well as for quantities of flavour oil of 5, 10, 15 or 20 wt%. A concentration in gum arabic of 12 wt% with 15 wt% of flavour oil proved to be the formulation which led to the best encapsulation efficiency (see **Chapter 5**).

4.4.1.4 Type of emulsion check

The selective solubility of Nile red in L-carvone was first confirmed by mixing the stained oil with DI water (see Figure 4.13) as we could see the water was not coloured by the fluorescent dye and the mixture appeared as two separate phases after vigorous agitation.



Figure 4.13: L-carvone stained with Nile red fluorescent dye (top) mixed with DI water (bottom).

This preliminary test confirmed that Nile red could successfully be used to check the type of emulsion. Comparing the appearance of the emulsion by light and fluorescence microscopy showed that the formed droplets were stained (see Figure 4.14) and that an O/W emulsion was indeed obtained.

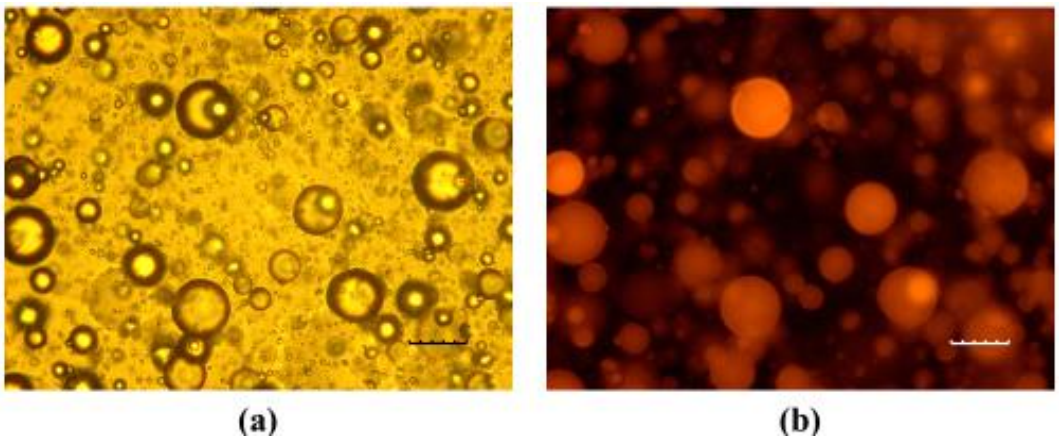


Figure 4.14: Comparison of the emulsion made with L-carvone stained with Nile red by (a) light microscopy and (b) fluorescence microscopy (all scales represent 50 μm).

Furthermore, it was noted that the colour emitted by Nile red in L-carvone was orange (see Figure 4.14), which was in accordance with the expected hue (between orange and red) since ketones are more polar than esters but less polar than alcohols. This also meant that Nile red was a suitable marker to check whether the encapsulation was successful, seeing that the emitted colour was different from red, which is the colour emitted by this solvatochromic dye in contact with air (empty capsule) (Zhang *et al.*, 2019).

4.4.1.5 Core stabilisation

Although various levels of capsule flavour burst were subjectively evaluated, no L-carvone smell at all could be identified when performing the sensory check on the particles obtained by mixing the flavour oil with MCT oils (score of 0 on the scale). This was also confirmed by using Nile red marker as no trace of L-carvone could be observed by fluorescence (see Figure 4.15) when comparing with the expected orange colour (see Figure 4.14).

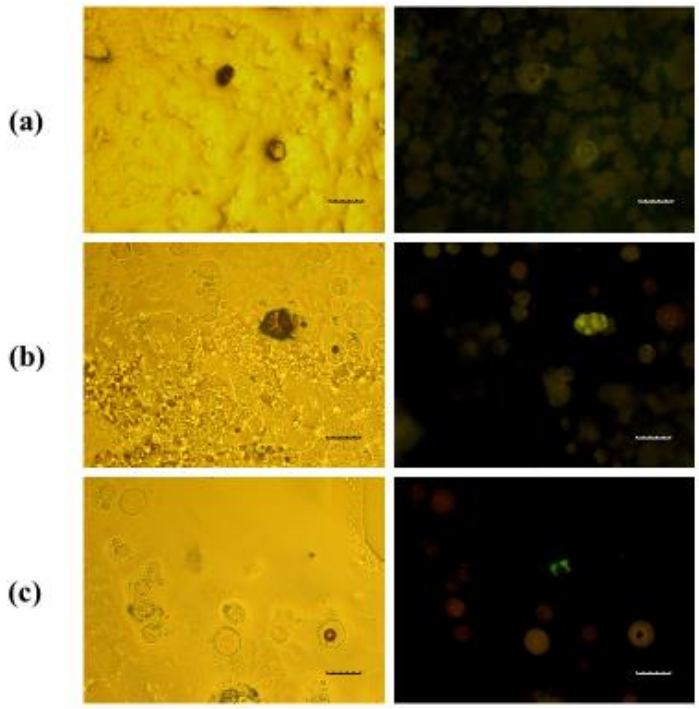


Figure 4.15: Comparison by light microscopy (left) and fluorescence microscopy (right) of dry capsules obtained by mixing L-carvone with different MCT oils: (a) coconut oil (b) palm oil (c) Miglyol 812 N (all scales represent 50 μm).

L-carvone seemed to be better encapsulated under its pure form, which is an advantage as fatty oil-free products are able to deliver a stronger flavour burst (Mao *et al.*, 2014).

4.4.2 Coacervation step

4.4.2.1 Polymer ratio and optimal pH

The optimal pH can vary depending on the selected polymer ratio. Those two parameters were thus studied together. The starting point for this investigation was inspired from the literature (Butstraen and Salaün, 2014; Yang *et al.*, 2014). The gum arabic/chitosan ratios 2:1 (w/w) and 6:1 (w/w) were therefore investigated, as well as a third mid-range ratio (4:1 (w/w)). The adsorption of coacervate droplets at the oil-water interface was observed (see Figure 4.16) and the optimum pH were identified as follows: $pH_{opt}^{2:1} = 4.1$, $pH_{opt}^{4:1} = 3.9$, $pH_{opt}^{6:1} = 3.6$, which was in accordance with the literature.

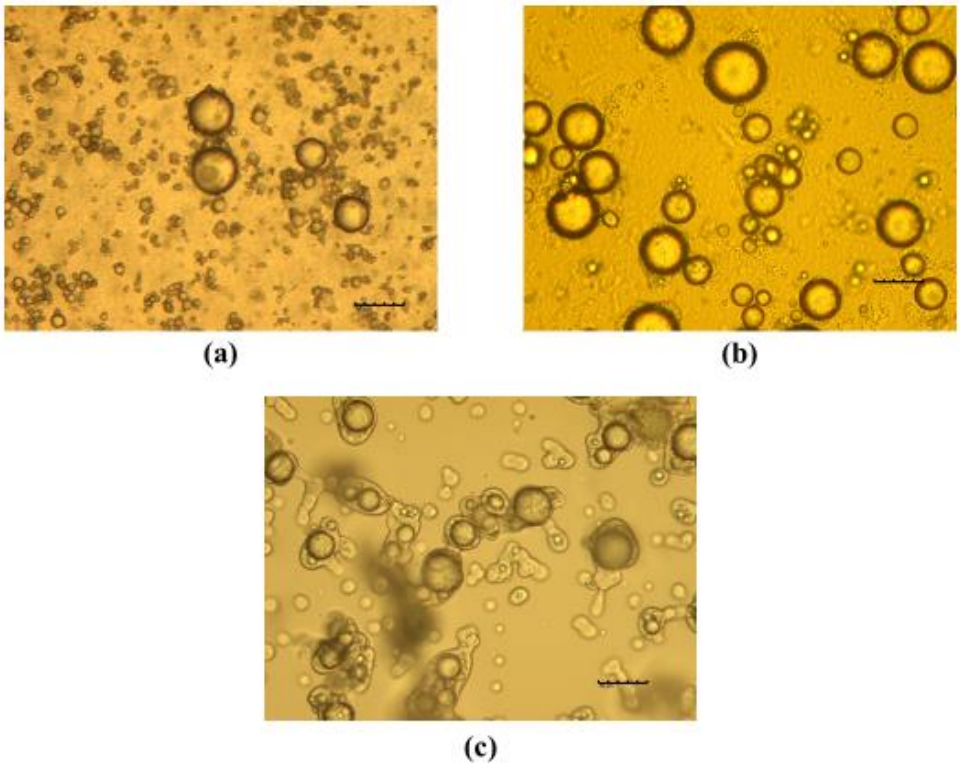


Figure 4.16: Observation of the coacervation step by light microscopy for different gum arabic/chitosan ratios (a) 2:1 (w/w) (pH = 4.1) (b) 4:1 (w/w) (pH = 3.9) (c) 6:1 (w/w) (pH = 3.6) (all scales represent 50 μm).

For the ratio 2:1 (w/w), we could observe small droplets of coacervate phase adsorbing at the oil-water interface (see Figure 4.16) but they did not merge together to form an homogeneous layer, which was not desired. When looking at the ratio 4:1 (w/w), it could be seen that the coacervate droplets merged but did not always cover the full surface of the oil droplets, forming incomplete shells. As for the ratio 6:1 (w/w), homogeneous layers with this characteristic "eye-shape" were formed. This latter ratio was thus identified as the best configuration.

Once the optimal pH for the selected ratio was found by progressive addition of NaOH, all polymer solutions would be prepared at this pH so that the two polyelectrolyte phases would be mixed directly at the optimal pH.

4.4.2.2 Total biopolymer concentration

Following the DoE study of the emulsion formulation, it was found that a higher concentration of gum arabic (12 wt%) was desired. Based on the previously identified gum arabic/chitosan ratio of 6:1 (w/w), this led to a reaction medium containing 7 wt% of total biopolymer, which was not too far from the usual range found in the literature (2 – 6 wt%).

4.4.2.3 Polymer molecular weight

As previously mentioned, it is known that the molecular weight of the biopolymers can also influence the complex coacervation process. There are different grades of chitosan powder (see **Chapter 3**) and some authors suggested medium molecular weight chitosan could lead to better capsules when complexed with gum arabic (Yang *et al.*, 2014).

The use of medium molecular weight chitosan led to an unstable suspension with bursting L-carvone droplets (see Figure 4.17).

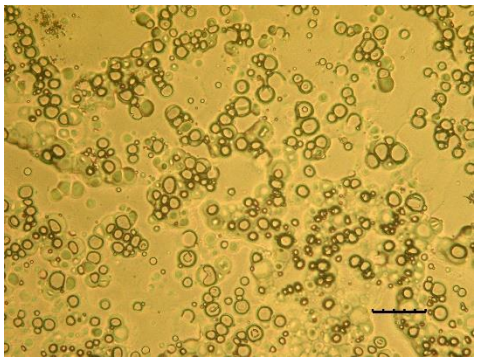


Figure 4.17: Observation of the coacervation phase by light microscopy after the addition of medium molecular weight chitosan (all scales represent 50 µm).

This proved that the use of medium molecular weight chitosan was not suitable in this case and that the suitability of different molecular weights must also be dependent on the nature of the encapsulated oil. The use of high molecular weight chitosan led to highly viscous solutions at

low concentration, which was not desirable for complex coacervation. Low molecular weight chitosan was therefore used in all further experiments.

4.4.2.4 Coacervation time

It was also tried to see if the reduction of the coacervation time impacted the encapsulation efficiency (see **Chapter 5**). It was observed that reducing this time from 2 to 1h did not seem to have any effect on the success of the encapsulation process (data not shown), which led to believe the gum arabic/chitosan coacervation system followed the Voorn-Overbeek theoretical model (Overbeek and Voorn, 1957).

4.4.3 Crosslinking

The idea here was to compare the effect of a chemical crosslinker (tannic acid) with a physical one (NaTPP).

Macroscopically, a dark plum solution with dark purple sedimented particles was obtained for the crosslinking with tannic acid. A colourless solution with white sedimented capsules and surface oil was obtained for the crosslinking with NaTPP. Although the dark purple colour of tannic acid would not be desired for food application, surface oil in the solution also attested of a bad encapsulation in the case of NaTPP. So neither of those two crosslinkers really seemed to give an ideal product at first glance.

After drying in open air for 24h, the capsule morphology was compared at microscopic scale (see Figure 4.18). The capsules crosslinked with tannic acid looked darker, which was in accordance with the purple colouration. However, they seemed to have a somewhat irregular shape and be surrounded by a very thin, soft shell. When comparing with the particles crosslinked with NaTPP, the latter looked more regular in size and seemed to have a stronger wall.

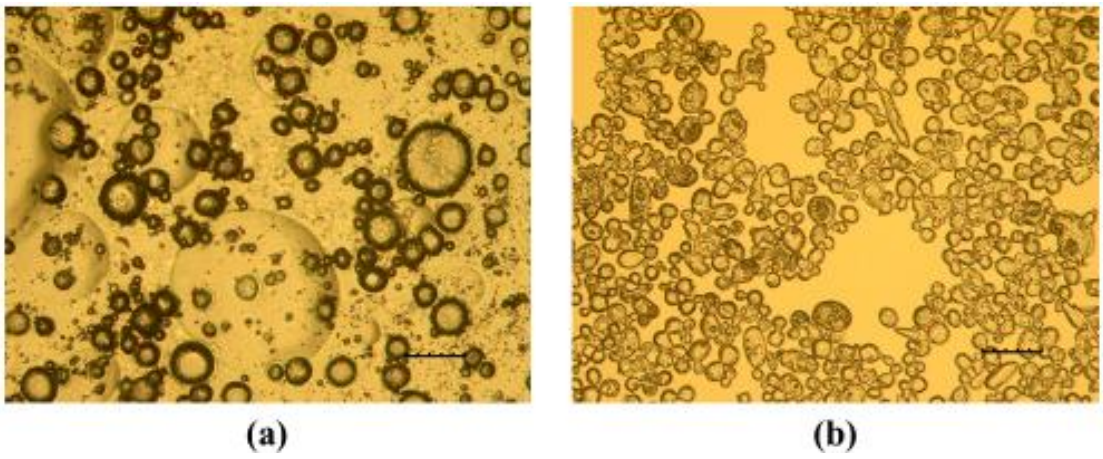


Figure 4.18: Observation of the dried capsules by light microscopy having used different crosslinkers (a) tannic acid (b) NaTPP (all scales represent 50 μm).

Following those observations the encapsulation was qualitatively checked by sensory evaluation. First, it was verified that the particles of the suspension did not evaporate after drying, which confirmed capsules were indeed successfully obtained. Secondly, it was acknowledged that no smell could be perceived prior to crushing the dry particles. After squashing them with the spatula however, a relatively strong L-carvone flavour burst could be smelled. Those two realisations attested that some flavour oil was entrapped in the capsules and that the encapsulation was successful for both batches. The intensity of flavour release was stronger in the case of tannic acid crosslinked particles (score of 4 on the scale compared to 2 for NaTPP), which made sense seeing that if there was surface oil in the batch crosslinked with NaTPP this meant there was probably less oil entrapped in the capsules.

Another trial with NaTPP was attempted using a layer-by-layer crosslinking method (see **Chapter 2**) inspired by the work of Butstraen and Salaün, 2014. A first crosslinking step was operated (15 g of 2 wt% NaTPP solution adjusted to pH 3.6) followed by stirring for 2h at 25°C, then some more 2 wt% chitosan solution (25 g) was added to the mixture and left under agitation

for 1h, finally a second step of crosslinking was carried out by adding 85 g of 2 wt% NaTPP solution adjusted to pH 3.6, and the medium was left to stir overnight.

This time, no surface oil was present in the batch and some particles could clearly be observed macroscopically on the wall of the container, which was not the case for the previous batches. When analysed by optical microscopy, it was noticed that bigger, darker, multicore particles ("grape" complexes) were obtained (see Figure 4.19) and the capsules looked much stronger.

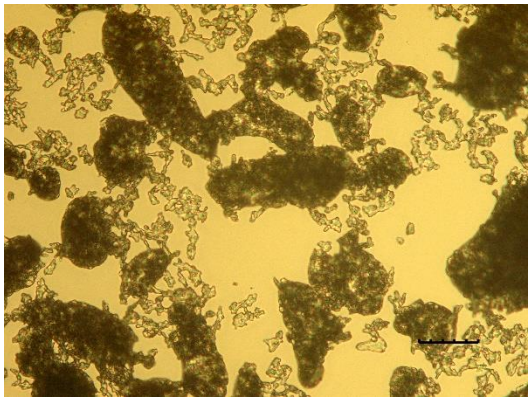


Figure 4.19: Observation of the dried capsules by light microscopy having used the 3-step NaTPP crosslinking modification (all scales represent 50 μm).

When the dry capsules were sensorially assessed, an L-carvone burst similar in intensity to the capsules crosslinked with tannic acid was perceived (score of 4 on the scale).

Following macroscopic, microscopic and sensory checks, the 3-step NaTPP crosslinking seemed to be the best option for hardening the wall of the capsules. This was also an advantage as physical interactions are usually preferred to chemical reactions for food applications.

The capsules were also observed by fluorescence microscopy, with L-carvone stained with Nile red (see Figure 4.20). Some bright orange-yellow colouration could be observed by fluorescence at the periphery of the individual cores of each particle, which was different from the red colour expected in the presence of air. The centre of the core was however dark.

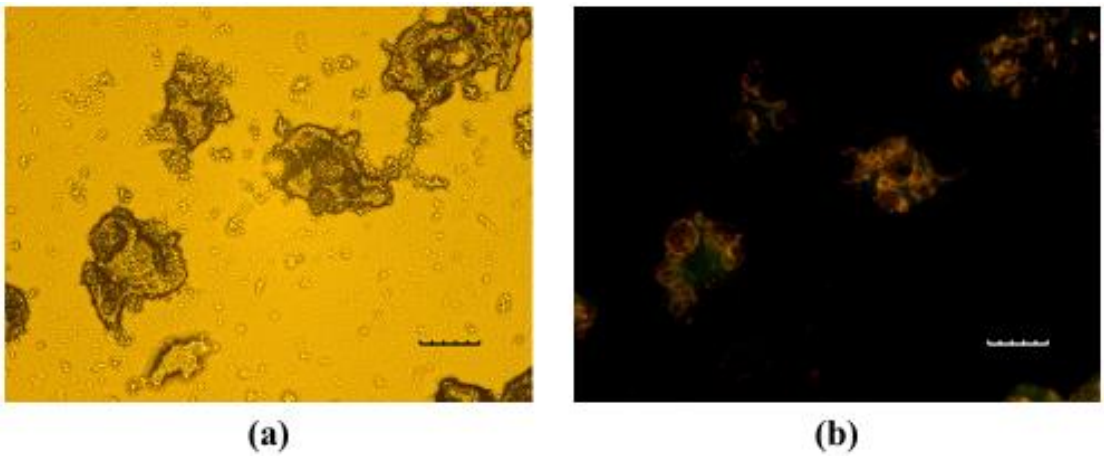


Figure 4.20: Observation of the dried capsules by (a) light microscopy and (b) fluorescence microscopy (all scales represent 50 μm).

It was concluded from those observations that L-carvone was successfully entrapped. Although some of the oil remained in the particles after drying, it was proven that the latter were leaky as attested by the periphery-limited colouration observed by fluorescence.

4.5 Conclusion

In this chapter, some major aspects of the complex coacervation technique were investigated in order to optimise the process for the encapsulation of L-carvone with the gum arabic-chitosan wall material combination.

First and foremost, an ideal formulation was identified for the emulsion step, consisting of 15 wt% of pure L-carvone oil dispersed in a 12 wt% gum arabic solution without emulsifier.

Once this formulation was fixed, the coacervation step was investigated. It was found that low molecular weight chitosan should be added at pH_{opt} = 3.6 in the ratio 1:6 (w/w) compared to the amount of gum arabic to observe optimal coacervation, which was in accordance with the literature.

A 3-step layer-by-layer physical crosslinking with sodium tripolyphosphate was chosen as the best food grade alternative to harden the wall of the capsules.

It was proven that with all those conditions, the encapsulation of L-carvone was successful but led to imperfect, leaky capsules.

In the next chapter (**Chapter 5**) it will be attempted to further process and engineer those particles in order to improve their flavour retention and mechanical properties.

CHAPTER 5 – Engineering and Characterisation of Microcapsules

5.1 Introduction

The complex coacervation process for encapsulating L-carvone with gum arabic and chitosan was optimised by stabilisation of the emulsion and selection of a suitable food grade crosslinker. Although the capsules were quite stable in solution, they were found to collapse and leak upon drying. It was suggested in the literature that particles produced by coacervation might need additional layers to be stable enough (Drusch and Mannino, 2009).

This meant the capsules needed to be further processed while still remaining in solution prior to drying. There are different options for coating particles: spray drying, spray cooling atomisation, spinning disc, layer-by-layer deposition, biopolymer films, hot melt coating, or polymer-polymer incompatibility (see **Chapter 2**).

Spray coating is a simple process which can enable to add an extra shell layer and dry the particles in the same step, which offers the advantage of realising those two achievements in a minimum of time and at low processing costs (see **Chapter 2**).

This chapter will aim at investigating the effect of adding an extra coating layer to the primary capsules formed by complex coacervation, the capsules performance will be characterised, their release profile will be studied, and finally some alternative engineering options will be explored.

5.2 Theoretical considerations for capsules engineering

5.2.1 Spray coating/drying

Spray coating/drying is a physico-mechanical process which converts a liquid with dissolved and/or dispersed material into dry powder. It can either be used for primary encapsulation, which leads to matrix particles, or as a simple coating and drying process (see **Chapter 2**).

For extra coating, the solid particles should be dispersed in an aqueous solution containing the dissolved carrier material. The mixture must not be too viscous, although the wall material should be present at high concentration and exhibit film-forming properties. A wall material concentration of 30 wt% is often used in the literature (Soottitantawat *et al.*, 2005; Madene *et al.*, 2006; Zuidam and Shimoni, 2010).

The suspension medium is pumped and atomised before being uniformly sprayed through a high-pressure nozzle (with an orifice between 0.5 and 4 mm), usually with a co-current flow of gas, at high temperature (150 to 220ºC for flavours) in a hot spraying chamber (see Figure 2.1). The gas flow, inlet temperature and feed rate can be controlled (Madene *et al.*, 2006; Zuidam and Shimoni, 2010; Jacobs, 2014).

The encapsulation is quasi-instantaneous and the core is only exposed to high temperatures for a very short period of time, which makes it suitable for flavour ingredients. The dried particles go through a cyclone separator and are collected in a container at the end. The particles obtained after spray drying are usually water-soluble (Madene *et al.*, 2006; Zuidam and Shimoni, 2010; Gupta *et al.*, 2016).

5.2.2 Chitosan grafting

Polymer grafting consists of adding side chains of monomers covalently bonded to a macromolecule backbone in order to form a block (Anitha *et al.*, 2012; Sherazi, 2016).

A method to produce gum arabic nanoparticles using gallic acid-grafted chitosan with a reaction initiated by ascorbic acid free radical (see Figure 5.1) was reported in the literature (Hu *et al.*, 2016).

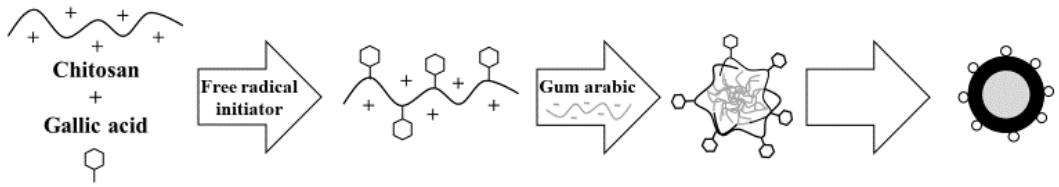


Figure 5.1: Proposed mechanism for nanoparticles formed by chitosan grafting (redrawn from Hu *et al.*, 2016).

The idea here was to use the same technique, but for obtaining capsules with a gum arabic/grafted chitosan shell with an L-carvone core rather than a solid gum arabic core complexed with chitosan. This might work if the gallic acid monomers could be dissolved in L-carvone and grafted to chitosan so it could surround the oil droplets, before it could form a complex with gum arabic on the outside (see Figure 5.2).

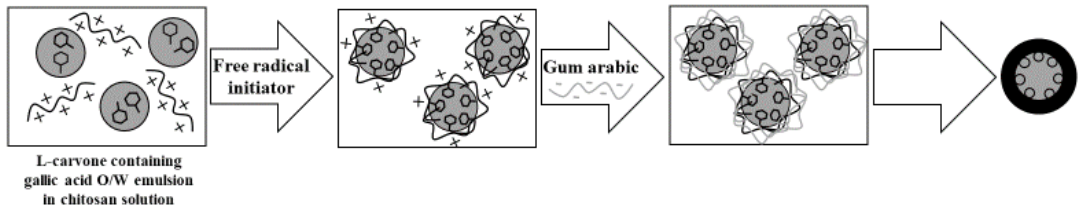


Figure 5.2: Proposed mechanism for microcapsules formed by chitosan grafting (adapted from Hu *et al.*, 2016).

This technique could provide a novel and interesting alternative to spray coating for reinforcing the wall of capsules formed with gum arabic and chitosan.

5.3 Experimental procedures

5.3.1 Encapsulation by complex coacervation

Primary capsules were formed based on the experimental protocol described in **Chapter 4** (see Figure 5.3).

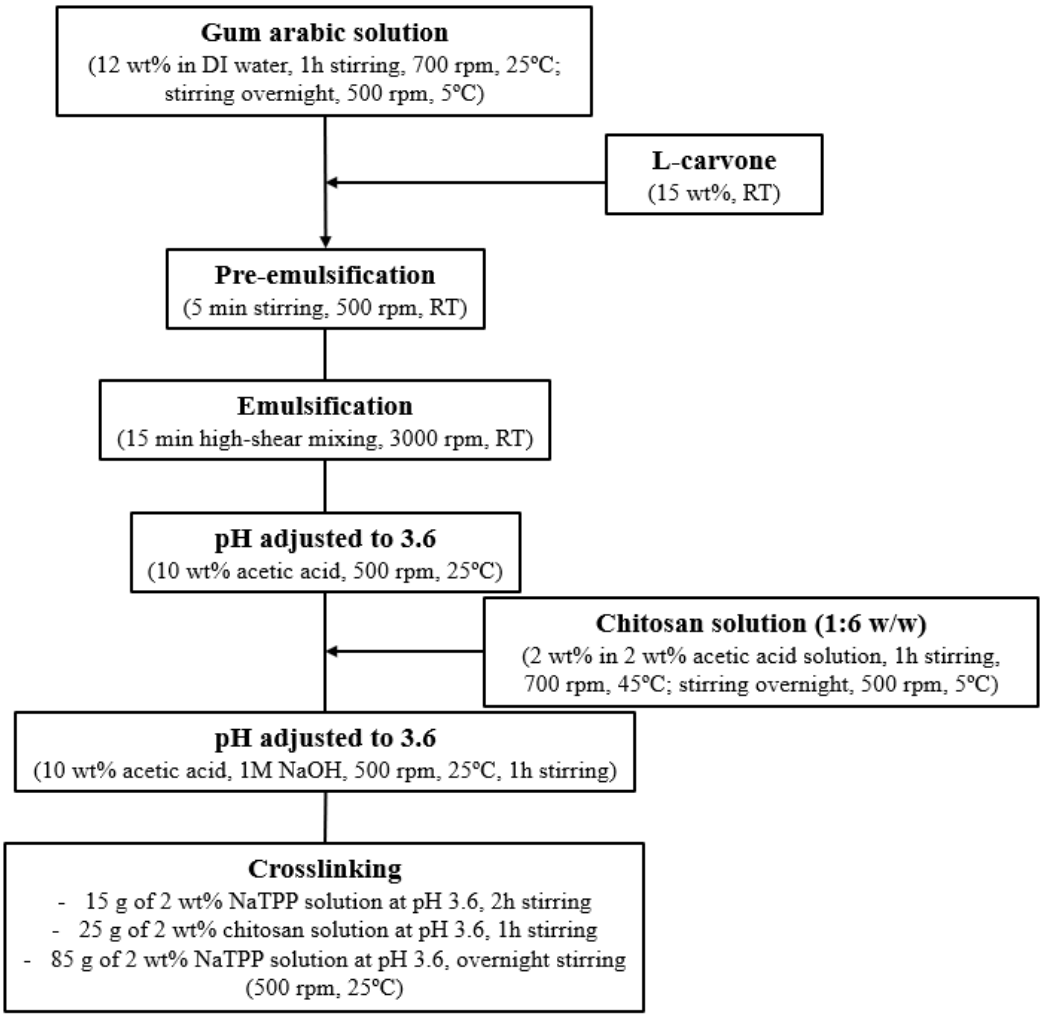


Figure 5.3: Schematic flow chart for the primary encapsulation of L-carvone within a gum arabic/chitosan shell using complex coacervation.

5.3.2 Extra coating by spray drying

5.3.2.1 Encapsulation efficiency (EE) of wet capsules

The encapsulation efficiency (EE) is defined as follows:

$$\mathrm{EE} = \frac{\text{Encapsulated oil}}{\text{Total oil added}} \times 100 \qquad \textbf{(Eq. 5.1)}$$

where Encapsulated oil = Total oil recovered – Free oil (Velasco *et al.*, 2000).

Ethanol was chosen as the extraction solvent since L-carvone is fully miscible with it (see **Chapter 3**).

For the total oil, 1 g of capsule suspension was placed in 40 g of ethanol (EtOH) (see Figure 5.4). The beaker containing the medium was covered with paraffin film to prevent evaporation, and immersed in an ultrasonic bath for 30 minutes to fully disintegrate the capsule wall. After that, it was centrifuged (see **Chapter 3**) with a centrifugal force of 4427 x g (6000 rpm) for 30 minutes and the liquid was immediately transferred to a different vial in order to separate the ethanol phase from the solid shell material residues. The amount of L-carvone was quantified by UV-Vis spectroscopy (see **Chapter 3**).

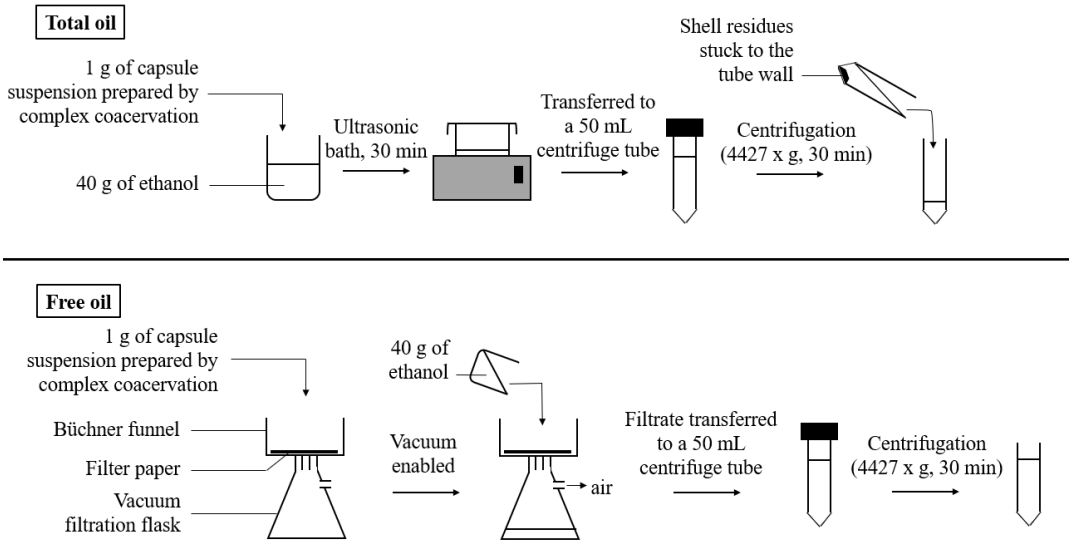


Figure 5.4: Schematic illustration of the sample preparation for the quantification of total oil and free oil by UV-Vis spectroscopy.

For the free oil, 1 g of capsule suspension was briefly washed with 40 g of ethanol using vacuum filtration for 30 seconds with Whatman® grade 1 filter paper on a Büchner funnel, in order to avoid breaking the capsules (see Figure 5.4). The filtrate was collected and centrifuged with a centrifugal force of 4427 x g (6000 rpm) for 30 minutes. The amount of L-carvone was quantified by UV-Vis spectroscopy.

5.3.2.2 Spray coating/drying process

Different secondary coating materials were selected to spray coat the coacervated capsules (see Table 5.1). The initial idea was inspired from the literature and consisted of adding a second layer of the wall materials used for coacervation (gum arabic and chitosan) (Yu *et al.*, 2017). Gum arabic and chitosan have also been used separately for encapsulation by spray drying (Sarkar *et al.*, 2012; Estevinho *et al.*, 2013; Ngan *et al.*, 2014). Chitosan was however too viscous to be used at high solid content. Finally it was found that maltodextrin also was a favoured choice to use with this process, and more specifically in combination with gum arabic

in different proportions (Righetto and Netto, 2005; Carneiro *et al.*, 2013; Janiszewska *et al.*, 2015; Tontul and Topuz, 2015; Watson *et al.*, 2017; Zhang *et al.*, 2018a).

Table 5.1: Coating solution compositions for spray coating/drying.

Materials	Ratio (w/w)	Solid content
Gum arabic/chitosan (GA/Chi)	6:1	7wt%
Gum arabic (GA)	-	24wt%
Chitosan (Chi)	-	1wt%
Gum arabic/ Maltodextrin (GA/MD)	3:1	24wt%
	1:7	30wt%
Maltodextrin (MD)	-	20wt%

The coating solutions were prepared the previous day in acetic acid solutions (pH = 3.6), and stored overnight at 4°C (Mortenson and Reineccius, 2008).

100 mL of the capsule suspension was mixed with 100 mL of coating solution (Yu *et al.*, 2017). This medium was kept under magnetic agitation at room temperature (RT, estimated to be 22 ± 3ºC), and fed into a BÜCHI Mini Spray Dryer B-290 and sprayed through a two-fluid nozzle with a 2.0 mm orifice. The drying gas was compressed air used with the air flow rate set around 473 L/h. The inlet temperature was 160 ± 3°C, with an aspirator rate around 37 m^3/h, and a feed rate of about 2 mL/min regulated by a peristaltic pump. The dry particles were collected and stored at RT until further analysis.

5.3.3 Characterisation

5.3.3.1 Morphology

The capsules with further coating produced by spray coating/drying were observed in two dimensions (2D) by optical microscopy and in three dimensions (3D) by scanning electron microscopy (SEM) (see **Chapter 3**).

5.3.3.2 Size distribution

The size distribution of the dried capsules with double coating was measured using a Mastersizer (see **Chapter 3**).

5.3.3.3 Payload

The particles payload is calculated as follows:

$$\text{Payload} = \frac{\text{Encapsulated oil}}{\text{Mass of the capsules}} \times 100 \qquad \textbf{(Eq. 5.2)}$$

(Xing *et al.*, 2004).

Following the experimental procedure for determining the total amount of oil for the EE, about 300 mg of dry capsules were carefully weighed with a precision scale and placed in 30 g of ethanol (EtOH). The medium was immersed in an ultrasonic bath for 30 minutes to fully disintegrate the capsule wall. After that, it was centrifuged at 6000 rpm for 30 minutes and the liquid was immediately transferred to a different vial in order to separate the ethanol phase from the solid shell material residues.

The amount of L-carvone was quantified by UV-Vis spectroscopy (see **Chapter 3**).

5.3.3.4 Mechanical strength

In order to study their mechanical strength, 30 coacervated capsules further coated by spray coating/drying of each sample were randomly selected and tested by the micromanipulation technique (see **Chapter 3**).

5.3.4 Study of the release profile

This experimental part was done in collaboration with Mondelēz International, whose Food Material Science team kindly invited me to their labs at the RSSL in Reading, UK, supported me and helped me with my experiments.

Unless stated otherwise, all the work in this section was achieved with the help of Dr Beth Green and Dr Barbara Suess from the Food Material Science team.

5.3.4.1 Preparation of the gum samples

In this study, four different samples were used for comparison:

- gum matrix containing primary coacervated capsules with gum arabic/chitosan 6:1 (w/w) double coating prepared by the previously described process (see **Chapter 4**)
- gum matrix containing primary coacervated capsules with gum arabic/gelatine (GA/GE) double coating according to a similar process (complex coacervation followed by spray coating/drying) [This sample was provided by a fellow PhD student from the Microencapsulation group at the University of Birmingham: Fanqianhui Yu. The preparation of those capsules with a different encapsulated oil had already been validated by publication (Yu *et al.*, 2017). Although the use of gelatine was not desired for this project, it was judged interesting to compare the performance of the gum arabic/chitosan double coated capsules with a benchmark.]
- gum matrix containing free L-carvone oil
- blank gum matrix

A target L-carvone level of 0.8 wt% was desired in each chewing gum slab. 2 g pieces of gum matrix (whose composition is a trade secret of Mondelēz International) were weighed with a precision scale and put in the oven for about 30 min at 50°C in order to soften.

The desired amount of capsules to put in the gums in order to achieve the target L-carvone level was calculated from the payload of each sample (see Table 5.2).

Table 5.2: Payloads of the different capsule samples to be incorporated in the gum matrix for the release study.

Samples	Payload
Gum arabic/Chitosan 6:1 (w/w)	2.13%
Gum arabic/Gelatine 1:1 (w/w)	2.90%

The gum matrix was collected from the oven, kneaded with the finger tips (with gloves) for a few seconds, and shaped into a diamond with a curved bottom to receive the capsules. The weighed capsule powder was carefully added in the centre with a spatula, then the gum matrix was folded several times and kneaded until a homogeneous repartition of the particles was achieved. Gum slabs (1.1 x 2.0 cm) were then modelled by hand. Abigail D'Sa, Jessica Dickens and Harriet Turner also kindly helped incorporating capsules into the gum matrix.

Four sets of gums were made with two gums for each different sample (meaning 8 slabs per set).

5.3.4.2 Mastication experiment

A solution aiming at mimicking human saliva was prepared using one phosphate buffered saline tablet (from Sigma-Aldrich) per 200 mL of DI water in order to replicate the mouth environment.

The gum slabs were put in the saliva medium and treated by a mechanical method imitating the mastication process (method not disclosed here for confidentiality reasons).

For each of the four sets, gums were "chewed" for 1, 3, 5 and 10 minutes respectively.

After processing, the saliva samples were collected in 50 mL centrifuge tubes and centrifuged with a centrifugal force of 6130 x g (5300 rpm) for 15 min, with an Avanti J-E centrifuge from Beckman Coulter. The liquid phase was immediately filtered with grade 40 Whatman® filter paper and transferred to a new tube in order to efficiently get rid of the capsules wall material and bolus residues. The samples were immediately frozen until further analysis.

5.3.4.3 Release quantification

Prior to analysis, 1 mL of each defrosted sample was diluted in 9 mL of 95% ethanol and centrifuged with a centrifugal force of 3562 x g (4000 rpm) for 10 min, with a Sorvall Legend T benchtop centrifuge from Marshall Scientific.

The liquid phase was collected and analysed by UV-Vis spectrometry with a Thermo Scientific Evolution 201 spectrometer as single point measurements at 236 nm, according to the analysis method developed by Mondelēz International. At this wavelength, the calibration curve gave the equation: Absorbance = $0.0613 \times$ Concentration $- 0.0125$, with an excellent coefficient of determination $R^2 = 1$.

All UV-Vis measurements were performed by Dr Beth Green, based on a method developed by Jean-François Halbardier.

The flavour cumulative release percentage was calculated as follows:

$$\text{Cumulative release } \% = \frac{m_{\text{carvone detected}}}{m_{\text{capsules}} \times \text{payload}} \times 100 \qquad \textbf{(Eq. 5.3)}$$

where the amount of carvone detected was calculated from the absorbance value using the equation obtained from the calibration.

5.3.5 Alternative engineering methods

5.3.5.1 Extra coating with shellac

Inspired from the experimental protocol of Duque Estrada *et al.* (2017), 25 g of coacervated capsule suspension was added to 75 g of sunflower oil containing 1 wt% Span 85 (see Figure 5.5). The medium was put under mechanical agitation for 10 min at 500 rpm to form a pre-emulsion, based on the system with capsules in suspension in the water phase, and was then mixed for 15 min at 1000 rpm.

10 g of the previously obtained aqueous capsule suspension-in-oil emulsion was poured into 190 g of a 5 wt% shellac solution containing 1 wt% Tween 20 (see Figure 5.5). The mixture was mixed for 15 min at 3000 rpm.

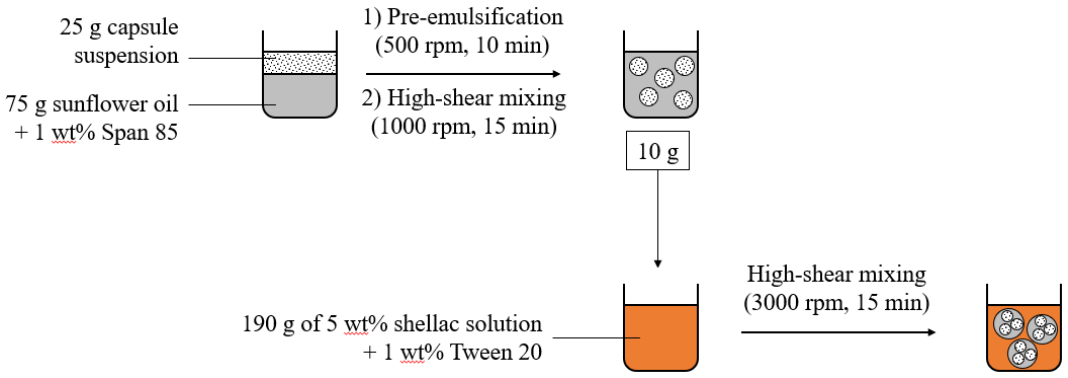


Figure 5.5: Schematic illustration of the double emulsion preparation prior to spray drying.

The double emulsion (aqueous capsule suspension-in-oil-in-water) was fed into a spray dryer with the same setting conditions as previously described.

5.3.5.2 Chitosan grafting

This experimental procedure was inspired from the work of Curcio *et al.* (2009) and Hu *et al.*, (2016).

The day before the experiment, some gallic acid powder was put in pure L-carvone to form a suspension and mixed for 30 minutes in an ultrasonic bath. This suspension was left to rest for 24h to allow the excess of undissolved gallic acid to settle.

A 1 wt% chitosan solution in 2 wt% acetic acid and a 6 wt% gum arabic solution were also prepared according to the same protocol described in **Chapter 4**, and left under agitation overnight at 5°C.

The following day, 108 mg of ascorbic acid were dissolved in 2 g of a 3 wt% hydrogen peroxide (H_2O_2) solution in order to activate the free radical. The ascorbic acid radical solution was then poured into 100 g of the chitosan solution under mechanical agitation at 600 rpm and left to stir for 30 minutes at RT.

After this time, 20 g of L-carvone containing the dissolved gallic acid was added to the medium as a pre-emulsion step. The mixture was further mixed for 10 minutes at 1200 rpm.

The emulsion was transferred into a 500 mL baffled jacketed beaker and the gum arabic solution, previously adjusted to pH 3.6, was added dropwise under mechanical agitation at 600 rpm, in the proportions 6:1 (w/w) (GA/Chi), as previously determined for the complex coacervation. The pH was further adjusted to 3.6, as determined in **Chapter 4**, if needed. The mixture was left to stir for 24h.

5.3.5.3 Nanoparticles

The following protocol was inspired from the work of Long *et al.* (2010).

10 wt% of calcium carbonate ($CaCO_3$) nanoparticles were suspended either in L-carvone oil or in a 12 wt% gum arabic solution.

20 g of L-carvone were poured into 80 g of gum arabic aqueous phase and mixed under mechanical agitation for 10 minutes at 500 rpm as a pre-emulsion step. An O/W emulsion was then formed by mixing for 3 minutes at 2500 rpm.

20 g of 1.5 M $CaCl_2$ and 20 g of 1.5 M Na_2CO_3 solutions were added dropwise in order to ripen the $CaCO_3$ nanoparticles.

The end of the protocol was similar to the complex coacervation process described in **Chapter 4**. A 2 wt% chitosan solution in 2 wt% acetic acid was then added dropwise in the proportions 1:6 (w/w) (Chi/GA) as previously determined for complex coacervation, and the pH was adjusted to 3.6. The mixture was left to stir for 1h, and was crosslinked overnight following the 3-step NaTPP crosslinking previously described.

5.3.6 Statistical analysis

Unless stated otherwise, experiments were made in triplicate. Values were expressed as mean $\pm$ standard error and data were displayed with standard error bars. The results was tested by one-way analysis of variance (ANOVA) with Tukey's post hoc test using SPSS Statistics software. Differences were considered significant at $p \leq 0.05$.

5.4 Results and discussion

5.4.1 Processing of the coacervated capsules in liquid phase

5.4.1.1 Entrapment efficiency

In order to save time and money, a quality control of the coacervated capsules proved to be useful prior to further processing. An assessment of the capsules in liquid phase was desired. The encapsulation efficiency of the capsule suspension was evaluated.

The centrifugation step for the encapsulation efficiency measurement method was adapted in order to fully get rid of the wall material residues which was very prompt to redisperse in the liquid phase and also proved to absorb light at the same wavelength as L-carvone ($\lambda = 320$ nm).

It was therefore judged meaningful to also compare the encapsulation efficiency (EE) with the entrapment efficiency:

$$\text{Entrapment} = \frac{\text{Encapsulated oil}}{\text{Total oil recovered}} \times 100 \qquad \textbf{(Eq. 5.4)}$$

where the total oil recovered is the total amount of oil measured in the final sample, in order to minimise any effect of some possible traces of wall material (Sarkar *et al.*, 2012).

5.4.1.2 Mixing speed for the formation of the emulsion

The choice of the mixing speed during emulsification was further investigated as it had been fixed as a constant value prior to the DoE study (see **Chapter 4**). Reducing the speed was not desired as it would lead to unstable emulsions and big oil droplets.

The influence of the increase of speed was studied by comparing two batches for which the emulsion had been formed over 15 minutes with a mixing speed of 2000 and 3000 rpm. It was noticed that the rise in speed was also leading to a significant increase in the mean EE and

entrapment efficiency ($p < 0.001$) (see Figure 5.6), and the error bars attested of the relevance of the measurement method. This result can be partially explained by the fact that reducing the size of the emulsion droplets by increasing the speed is also responsible for a higher emulsion stability (Carneiro *et al.*, 2013).

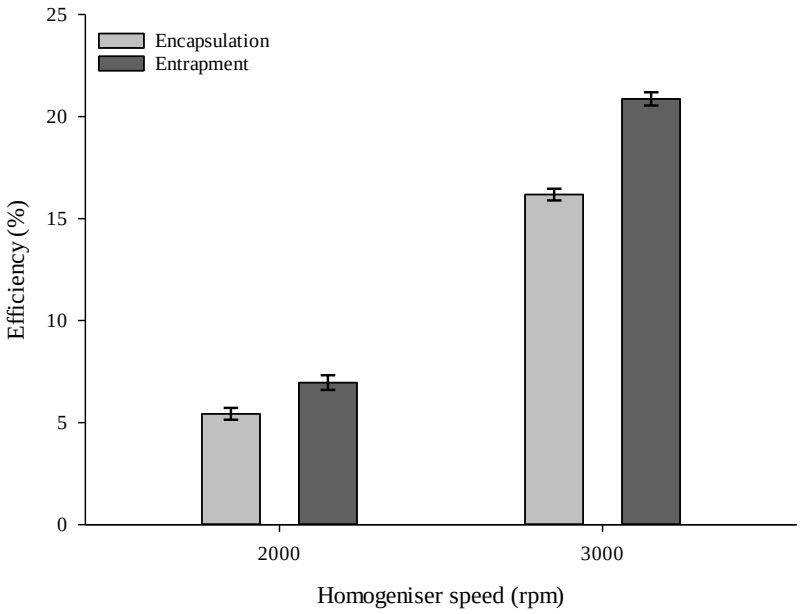


Figure 5.6: Comparison of the mean EE and entrapment efficiency of two batches where the emulsion was formed with different mixing speeds (data are displayed with standard error bars).

Seeing the benefit of increasing the mixing speed during the emulsion formation, a further attempt was made at 4000 rpm. This time, the encapsulation failed and no oil seemed to have been retained in the capsules as the measured encapsulation efficiency had a null value (results not shown). Although "grape" complexes were also formed (see **Chapter 4**), the individual cores were bigger, meaning the emulsion was probably less stable.

The final speed of 3000 rpm for the formation of the emulsion was therefore selected for all further experiments.

5.4.1.3 Reproducibility

The reproducibility of the process was also investigated. The mean EE and entrapment efficiency were calculated for 12 batches prepared in the exact same conditions as previously defined. An average EE of 17 ± 1% and an average entrapment efficiency of 21 ± 1% were obtained for the whole array of samples (see Figure 5.7), which demonstrates the reproducibility of the process.

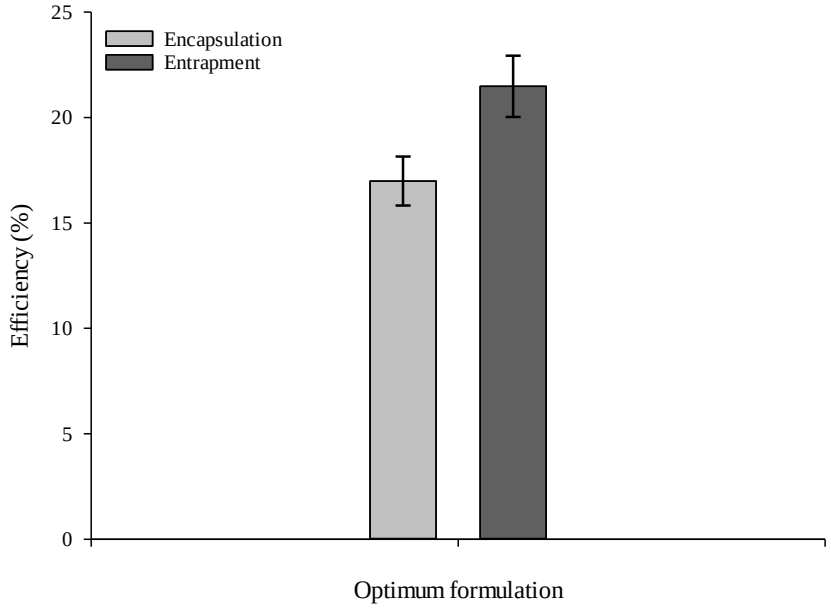


Figure 5.7: Average encapsulation efficiency and entrapment efficiency obtained from 12 batches (data are displayed with standard error bars).

For those batches, it was calculated an average of 21.0 ± 0.8% of L-carvone was lost by evaporation during the process, as the amount of oil lost during the process was deduced by subtracting the amount of oil recovered from the batches from the quantity of oil which was added to form the emulsion.

This result confirmed that the hot melt coating process would not be a recommended coating option here since a significant amount of oil already evaporated at room temperature.

5.4.2 Characterisation

5.4.2.1 Morphology

White cohesive powders were obtained after spray coating/drying for all coating compositions.

These dry powders were first observed by light microscopy (see Figure 5.8) which shows spherical particles seemed to have been obtained. Although there were some isolated capsules, most of them seemed to be aggregating. No major difference in external appearance could be distinguished between the samples using optical microscopy.

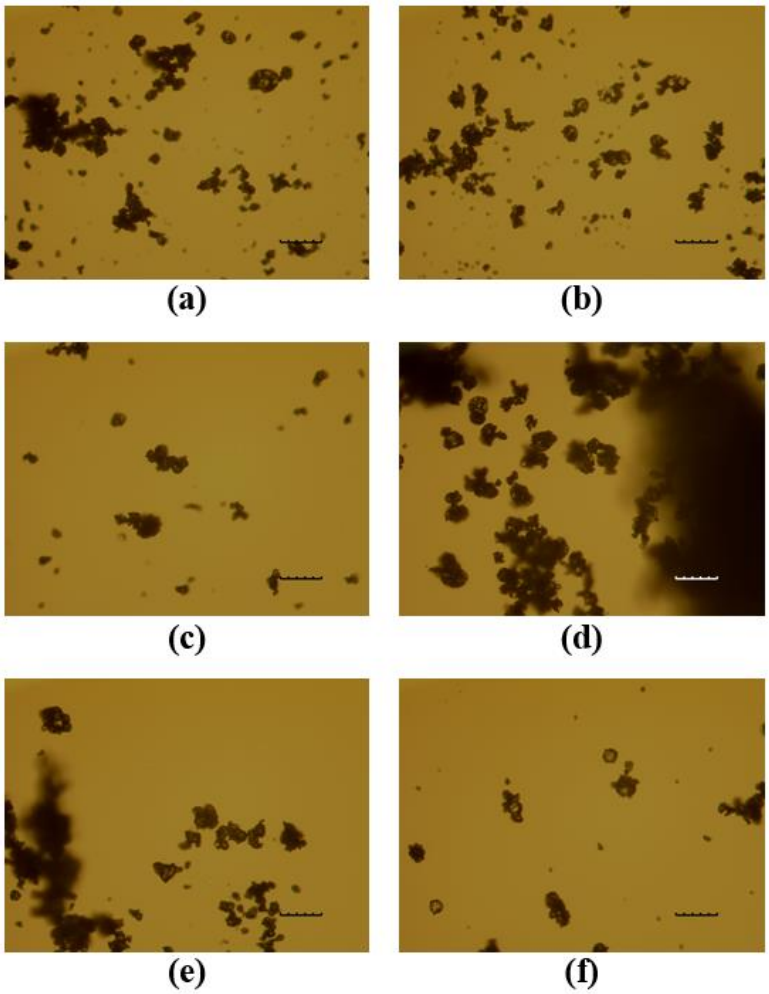
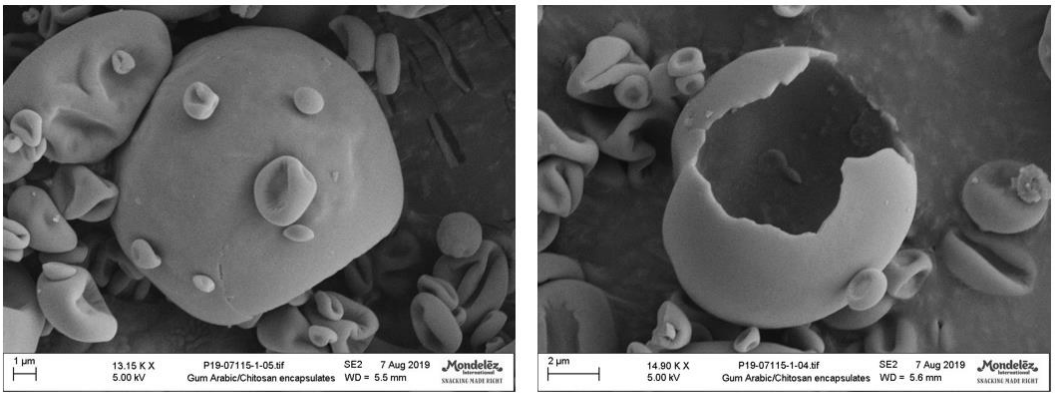


Figure 5.8: Light microscopy observations of dry powder coacervated capsules further coated with (a) gum arabic/chitosan 6:1 (w/w) (b) gum arabic (c) chitosan (d) gum arabic/maltodextrin 3:1 (w/w) (the blurry area corresponds to aggregated particles being in a different focus plan to the observed capsules) (e) gum arabic/maltodextrin 1:7 (w/w) (f) maltodextrin (all scales represent 50 μm).

The external and internal morphologies of coacervated capsules further coated with gum arabic/chitosan 6:1 (w/w) using spray coating/drying were observed with a higher resolution microscopy method (FEG-SEM) (see Figure 5.9).



(a) **(b)**

Figure 5.9: Structure of coacervated capsules further coated by spray coating/drying with gum arabic/chitosan 6:1 (w/w) observed by FEG-SEM imaging, showing (a) the surface morphology and (b) the internal structure of particles.

Although most particles appeared collapsed, several more spherical ones could also be identified (see Figure 5.9). Their surface was smooth and non-porous, which emphasized the high quality of the chosen wall material and encapsulation method. This also meant that the encapsulation was successful in protecting the flavour oil. Some capsules were also found cracked open, which showed the brittleness of the shell. The imaging of the inner capsules confirmed that core-shell particles were obtained since they were hollow, as expected for the complex coacervation encapsulation process.

The observed collapse might have resulted from the high vacuum to which the capsules were exposed in the SEM chamber. This phenomenon could have led to an oil loss although their surface was still smooth and without crack. It could have on the contrary happened to core-shell capsules which did not contain any oil, explaining both why only a few of them were spherical and the low payload value.

However, it was important to note that collapsed particles were not necessarily empty, but would just contain less encapsulated oil, as it was similarly observed by several authors

involved in the encapsulation of peppermint oil and fish oil by coacervation (Yu *et al.*, 2017). Their surface area was however maximised and they would be expected to release the flavour at a higher rate than spherical capsules (Zhang *et al.*, 2012). They would also be supposedly more difficult to rupture by mechanical forces as those collapsed particles appear flatter than whole spherical capsules.

5.4.2.2 Size

The size distribution of the primary capsules further coated with gum arabic/chitosan 6:1 (w/w) was measured (see Figure 5.10). The results were displayed using Mastersizer 2000 software. A polydisperse, mostly monomodal size distribution profile could be observed, with an average mean diameter ($d_{0.5}$) of 21.0 µm, which was in accordance with the scale which could be observed by microscopy techniques. More precisely, 80% of particles had a size between 8.5 µm ($d_{0.1}$) and 49.3 µm ($d_{0.9}$), which was in the targeted order of magnitude and showed the capsules were reasonably homogeneous in size.

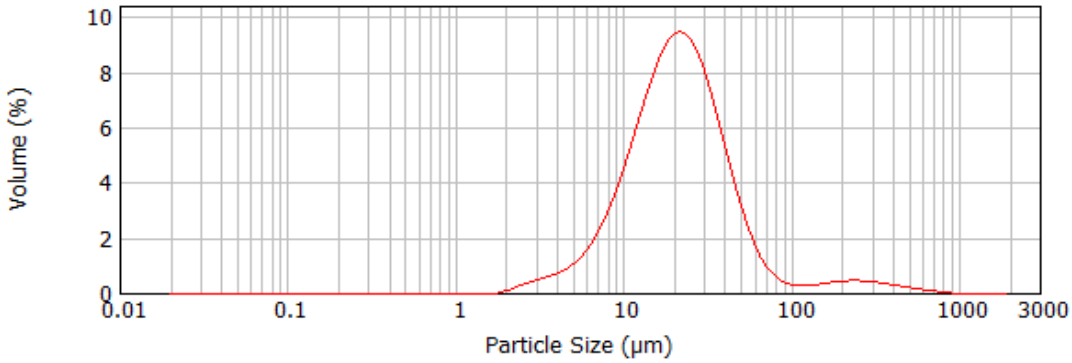


Figure 5.10: Size distribution profile of coacervated capsules further coated with gum arabic/chitosan 6:1 (w/w) obtained with Mastersizer 2000 software.

A small secondary peak could be noticed above 100 µm (see Figure 5.10). It was believed to be due to the aggregation of spray dried particles when suspended in water where the wall tended to soften and lose its brittleness.

As a comparison, the size distribution obtained for the primary coacervated capsules presented a mean diameter (d_{32}) of 54.9 μm (Malvern data not shown). This result was judged as unreliable for making any observation of the size variation before and after secondary coating as the primary coacervates aggregated, were under the form of "grape" complexes (see Figure 5.11) and they seemed to have been dispersed following spray coating/drying (see Figure 5.8).

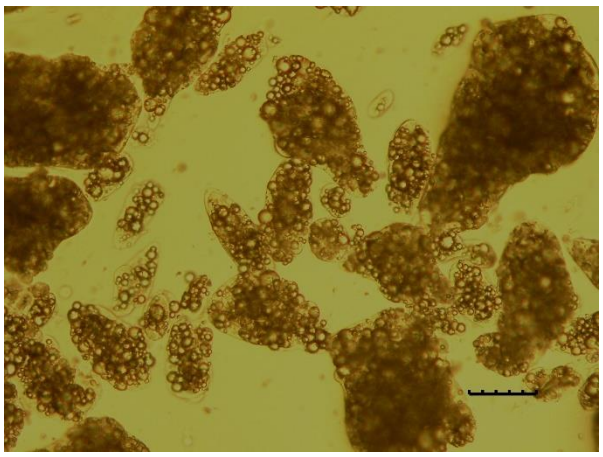


Figure 5.11: Observation of the primary coacervated capsules in liquid phase by light microscopy (all scales represent 50 μm).

The size of the individual primary capsules could be roughly estimated using the microscopy imaging scale (see Figure 5.11). They ranged between 2 and 14 μm, with mean range ones displaying a size around 8 μm. Although quite qualitative, these observations seemed to confirm the addition of an extra coating layer increased the size of the particles when comparing with the Malvern data (see Figure 5.10).

5.4.2.3 Payload

The particles were observed by fluorescence microscopy to compare the capsules directly spray dried or spray coated with an extra layer of gum arabic/chitosan 6:1 (w/w) (see Figure 5.12), and see the effect of double coating. It was clear that while some rare traces of carvone could

be observed in the first case, quite a lot more carvone could be seen (orange colour) in the second case with a higher intensity.

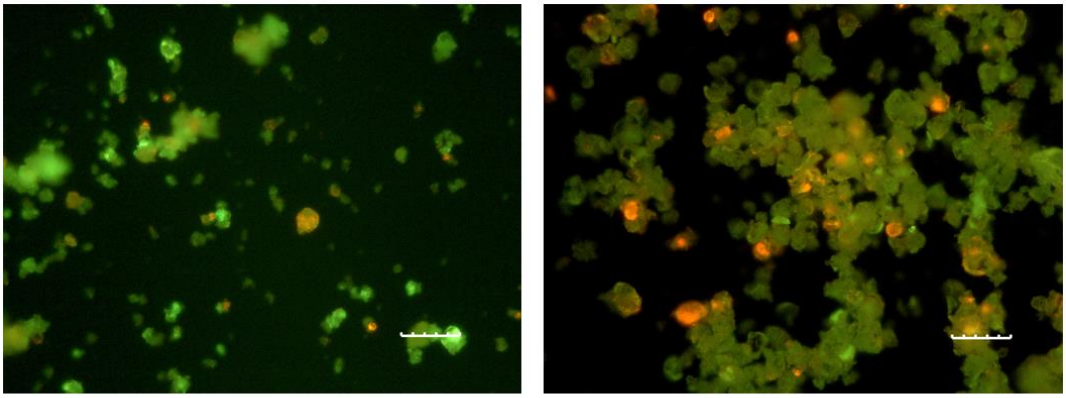


Figure 5.12: Comparison of capsules (a) directly spray dried and (b) spray coated (GA/Chi 6:1 (w/w)) observed by fluorescence microscopy (all scales represent 50 μm).

These results proved the efficacy of adding a second coating layer in solving part of the leaking problems, and also confirmed that some L-carvone remained successfully encapsulated after the drying process.

The amount of oil entrapped in the capsules was quantified by payload measurements. Here the payloads obtained with the different second coating combinations (GA/Chi, GA, Chi, GA/MD, MD) are compared (see Figure 5.13).

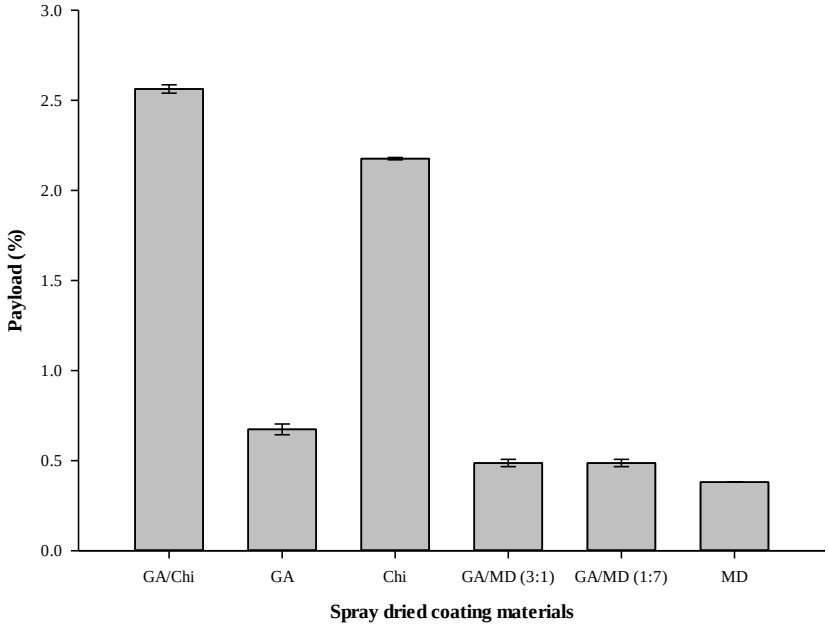


Figure 5.13: Comparison of the payloads of coacervated capsules further coated with different wall material combinations (GA/Chi 6:1 (w/w), GA, Chi, GA/MD 3:1 (w/w) and 1:7 (w/w), MD) by spray coating/drying (data are displayed with standard error bars).

When spray drying was used to encapsulate pure oil, the loading capacity is around 20%, so here the payload was expected to be below this value (Uhlemann *et al.*, 2002). Especially in the case of secondary coatings, the percentage of wall material should be much higher.

The obtained payloads were between 0.3 and 2.6% (see Figure 5.13). All error bars were reasonably negligible, reflecting the accuracy of the measurement method. There was a significant difference in payload between the different types of secondary coating ($p < 0.05$), but the results for the gum arabic/maltodextrin combination with different polymer ratios (3:1 or 1:7) were identical ($p = 1.000$). Therefore the nature of the secondary coating should definitely influence the payload, while the polymer ratio should not have any significant impact.

When comparing the different secondary shell combinations, it was noticed that the best payload result of $2.56 \pm 0.02\%$ was obtained for the gum arabic/chitosan 6:1 (w/w) secondary

coating. Looking at the results with the further coating with either gum arabic or chitosan used separately, it was noticed that the use of chitosan seemed much more effective in protecting the flavour than gum arabic, although it was in much smaller concentration (1 wt% vs 24 wt%). In any case, the use of the combination led to better barrier properties than either polymer used alone, as suggested in the literature (Botrel *et al.*, 2015).

For the secondary coatings involving maltodextrin, the worst payload was obtained for the use of maltodextrin alone, which was expected as it was advised in the literature to use maltodextrin in combination with a second coating material for spray drying (Botrel *et al.*, 2015). When looking at the different combinations with gum arabic, it was observed that the material ratio did not seem to matter as the exact same payload was obtained when using gum arabic in excess or maltodextrin in excess. This blend however displayed a decrease in the retention performance compared to the use of gum arabic alone. So although it was stated in the literature that maltodextrin could offer a good protection when used in combination with another wall material as it was acting as a filler and matrix former (Botrel *et al.*, 2015), it proved here to reduce the capsules capacity to retain the flavour and its use should be avoided in this case.

It was noted that those observations concerning the performance of capsules resulting from the spray drying technique might be linked to the glass transition temperature (T_g) of the materials (see Table 5.3), as suggested by Botrel *et al.* (2015). It was noticed from those results that the payload trend seemed to match the T_g trend of the polysaccharides used for coating. Indeed, the payloads obtained with gum arabic and maltodextrin alone were in the same order of magnitude, although it was a bit higher for gum arabic, but this value was significantly higher when chitosan, which has a much higher T_g than the other two, was used.

Table 5.3: Comparison of the payload data with the glass transition temperature (T_g) of coating materials involved in the spray coating/drying process.

Materials used for secondary coating	Payload (%)	T_g (°C)	Reference
Chitosan	2.18 ± 0.01^a	~ 203	(Sakurai *et al.*, 2000)
Gum arabic	0.67 ± 0.03^b	~ 42 - 62	(Righetto and Netto, 2005)
Maltodextrin	0.38^c	~ 38 – 60	(Righetto and Netto, 2005)

^{a,b,c} Means with different letters are significantly different ($p < 0.05$)

Although L-carvone has a high flavour intensity which could be detected at low loading levels, it would nevertheless be desirable to increase the payload value so as to reduce the number of capsules required in each gum slab, and at least be able to reach this target value of 0.8 wt% of L-carvone incorporated in the gum matrix.

5.4.2.4 Mechanical strength

For this analysis, 30 individual particles were randomly selected for compression to represent the diversity of each sample. The size repartition of the tested population was found to be consistently between 7 and 46 μm (see Table 5.4), and more specifically between 10 and 39 μm for the ones with GA/Chi 6:1 (w/w) double coating, which was in accordance with the measured size distribution of this sample, with a majority of particles being between 8 and 50 μm (see Figure 5.8). It could also be observed from the size range data that both the nature of the secondary coating and the polymer ratio had an influence on the final size of the particles.

Table 5.4: Size range and mean size observed for each sample with secondary coatings for 30 particles randomly selected to be compressed by micromanipulation.

Applied secondary coating	Size range of compressed capsules (μm)	Mean size of compressed capsules (μm)
GA/Chi 6:1 (w/w)	10 - 39	17 ± 1
GA	8 - 34	17 ± 1
Chi	10 - 41	23 ± 1
GA/MD 3:1 (w/w)	13 - 46	29 ± 1
GA/MD 1:7 (w/w)	7 - 26	11 ± 1
MD	10 - 38	18 ± 1

It was noticed during micromanipulation that most particles were actually too hard to be ruptured, leading to a force transducer compliance-like compression profile (see Figure 5.14). The typical compression profile was plotted as the applied force versus the probe displacement (see Figure 5.15). The compression of the capsules was identified by a rise in the applied force due to the contact with the particle, followed by a sudden drop (1) as a result of the bursting of the shell, and finally another steep increase (2) corresponding to the compression of the capsule debris and glass slide.

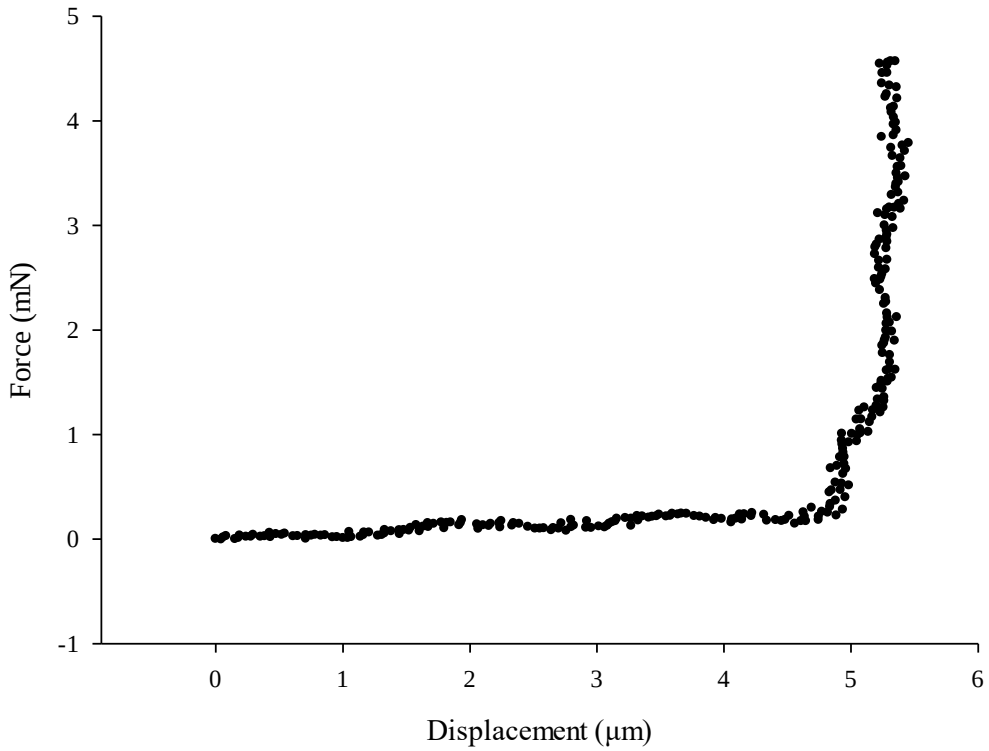


Figure 5.14: Example of a force transducer compliance-like compression profile obtained for capsules which were too hard to rupture.

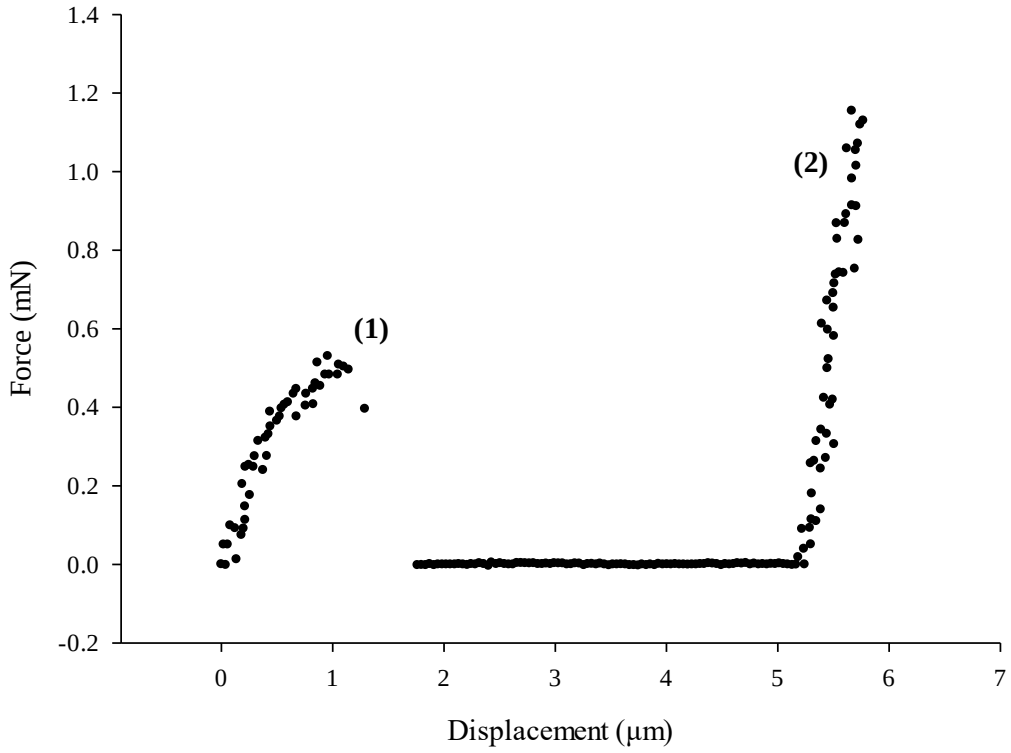


Figure 5.15: Compression profile of a 9 μm capsule with GA/Chi 6:1 (w/w) double coating showing a single rupture event, obtained by micromanipulation (1) rupture event (2) compression of the capsule debris and glass slide.

The amount of particles which were successfully ruptured by micromanipulation was reported (see Table 5.5). It was noted that only a small proportion of them showed clear rupture under compression.

Table 5.5: Percentage of capsules ruptured by micromanipulation among a sample of 30 randomly selected particles.

Coatings used for spray coating/drying	Ruptured capsules
MD	16.7%
GA/MD 1:7 (w/w)	20%
GA/MD 3:1 (w/w)	23.3%
GA	26.7%
Chi	30%
GA/Chi 6:1 (w/w)	36.7%

Interestingly, it was noticed that the percentage of ruptured capsules seemed to follow a similar trend compared to the payload values of each sample (see Figure 5.16). It was thus suspected that there should be a relationship between the payload (and therefore the nature of the secondary coating) and the percentage of capsules which could be ruptured by micromanipulation. This correlation was not further investigated due to time limitations.

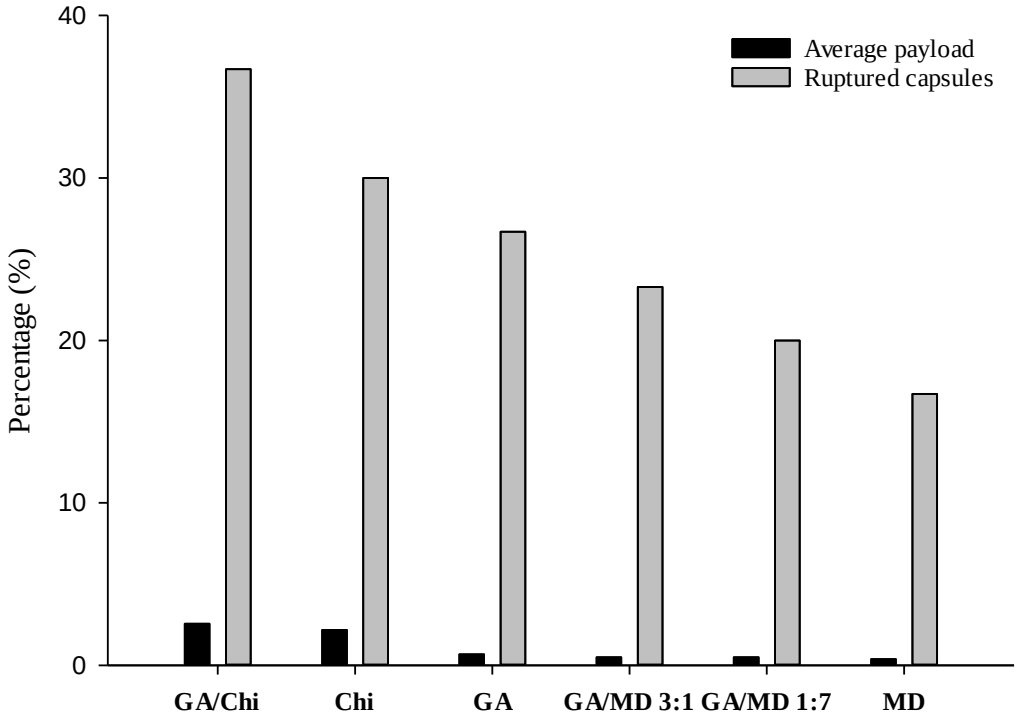


Figure 5.16: Comparison of the trends in average payload value and percentage of particles successfully ruptured by micromanipulation for coacervated capsules further coated with GA/Chi 6:1 (w/w), Chi, GA, GA/MD 3:1 (w/w), GA/MD 1:7 (w/w), or MD.

It was indeed judged highly probable that the particles which could not be ruptured had a matrix structure made of wall material only, rather than a core-shell capsule. These particles could easily be formed with an excess of coating material during the spray coating/drying process, which would explain the low payload values obtained. Taking this into consideration, the

payload value would not be an accurate reflection of the actual loading of the capsules, but would rather attest of the small amount of capsules actually containing flavour oil among the full powder sample. It would therefore be reasonable to suspect the actual payload of the individual capsules should be higher than the quantified amount.

Among the successfully ruptured capsules, 2/3 displayed the previously described bursting behaviour (see Figure 5.15), while the other 1/3 exhibited a two rupture-event profile (see Figure 5.17).

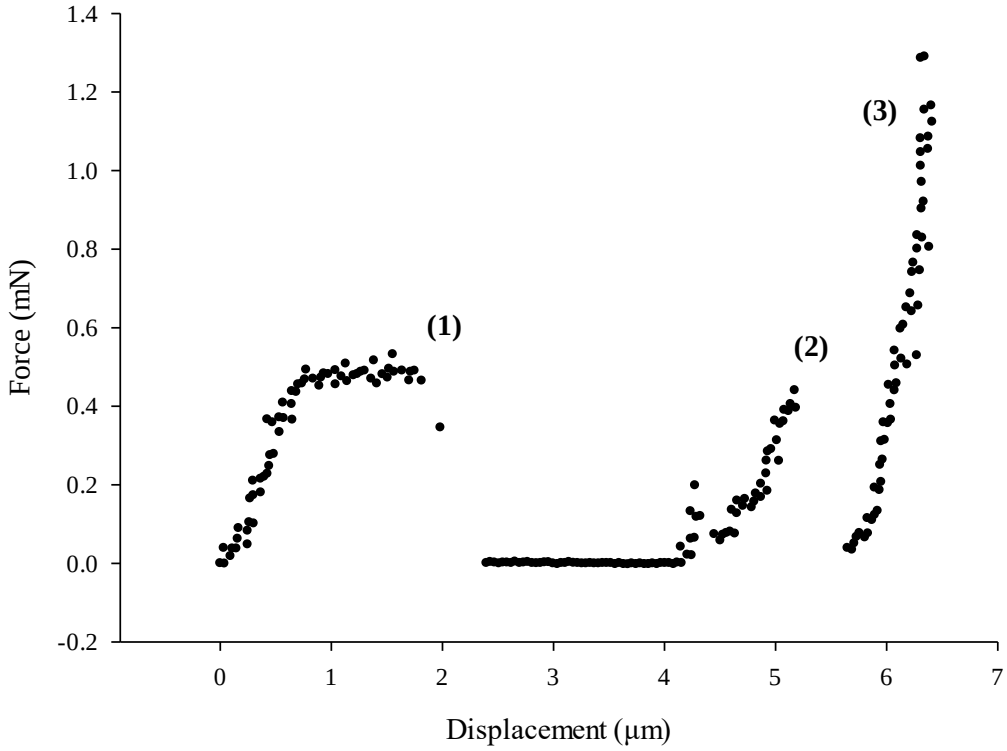


Figure 5.17: Compression profile of a 9 µm capsule with GA/Chi 6:1 (w/w) double coating showing two rupture events, obtained by micromanipulation (1) first rupture event (2) second rupture event (3) compression of the capsule debris and glass slide.

The single rupture profile was useful as it confirmed the capsules could successfully be ruptured and was likely to help to determine the number of core-shell particles within the sample. The

two-rupture-event profile was particularly interesting as it should prove that not one shell but two layers were successfully compressed, attesting of the success of the double coating applied by complex coacervation process followed by spray coating/drying.

The rupture force was identified as the compression force preceding the sudden drop characterising the bursting of the shell. The rupture force was expected to increase with the capsules diameter, which was in accordance with what was reported in the literature (Zhang *et al.*, 1999; Hu *et al.*, 2009). The large scatter of the rupture force data for given diameters (see Figure 5.18) could imply that the wall composition and the shell thickness which affect the rupture force were not homogeneous among the capsules (Zhang *et al.*, 1999).

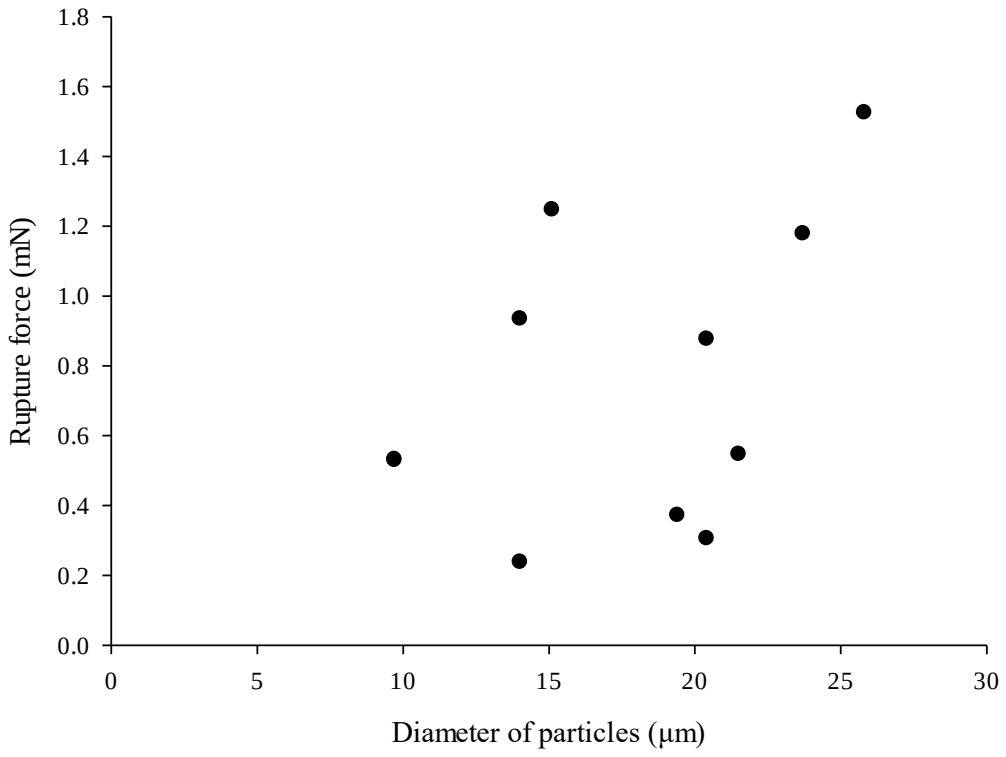


Figure 5.18: Rupture force versus particle diameter for coacervated capsules with GA/Chi 6:1 (w/w) double coating.

The rupture force required for breaking particles of a given size was of the same order as reported in the literature for melamine formaldehyde microcapsules (Hu *et al.*, 2009). The results obtained here were only slightly lower (in the order of 0.5 mN), which confirmed the secondary coating layer was efficient in strengthening the capsules so as to compensate for the weakness of food grade crosslinkers.

When comparing those results with data obtained for calcium-shellac microspheres (Xue and Zhang, 2009), however, the rupture force was found to be lower for the coacervated capsules, which also made sense as core-shell particles are a lot less dense than microspheres, and therefore expected to be a lot easier to break.

The nominal rupture stress versus particle diameter was also plotted (see Figure 5.19), and was expected to decrease with the diameter of the capsules on average. Indeed, at equivalent wall thickness smaller capsules should therefore be denser, meaning smaller capsules were more difficult to break than larger ones. The large scatter obtained from the micromanipulation data can be explained by the variety of morphologies which could be observed throughout the sample (see Figure 5.5), and seemed to attest of a stochastic process.

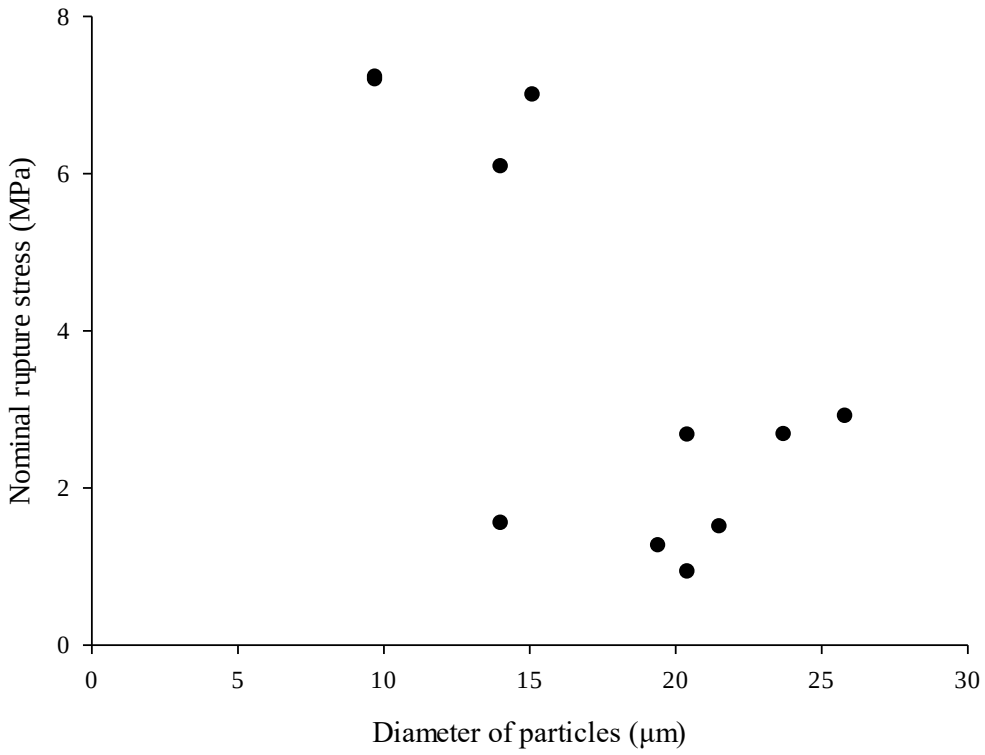


Figure 5.19: Nominal rupture stress versus particle diameter for coacervated capsules with GA/Chi 6:1 (w/w) double coating.

The order of magnitude of the results was in line with what was reported in the literature (Hu *et al.*, 2009; Xue and Zhang, 2009), although the capsules were a bit weaker when comparing with the data obtained for other microcapsules (Hu *et al.*, 2009). This could possibly be explained by the nature of the flavour oil used in this project as the L-carvone molecule is composed of several reactive unsaturated functional groups (see **Chapter 3**), and was suspected to interact with the wall material and therefore affect the quality of the capsules.

Finally the deformation at rupture versus particle diameter was plotted (see Figure 5.20). This parameter did not seem to be size dependent, which was in accordance with other observations in the literature (Xue and Zhang, 2009).

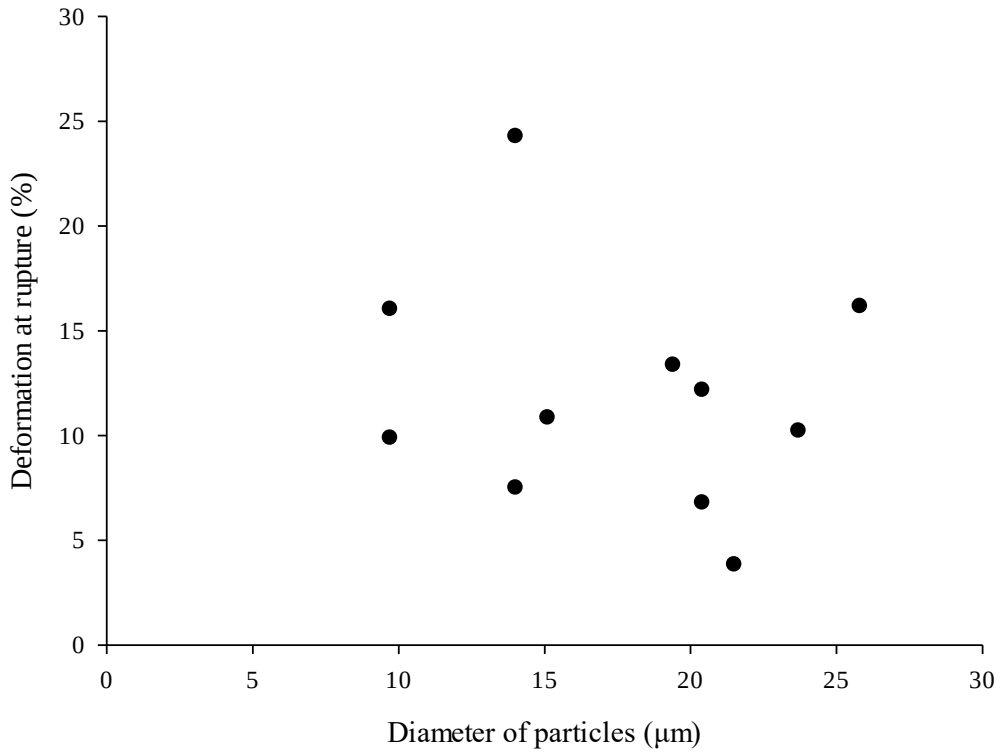


Figure 5.20: Deformation at rupture versus particle diameter for coacervated capsules with GA/Chi 6:1 (w/w) double coating.

An average deformation of 11.9 ± 1.7% was obtained for the sample. This meant that the capsules were quite brittle rather than elastic, which was a good sign for the expected burst delivery.

5.4.3 Release profile

The initial L-carvone level to be incorporated in each gum slab was 0.8 wt% of the gum matrix mass, based on commercial product insight. Due to the low payload of the capsules (2.13%), however, this meant a high volume of particles had to be added to the gum matrix. Early mixing trials revealed the amount of capsule powder was too high to be successfully added to 2 g of gum matrix, as the latter was falling apart and losing its elasticity. Therefore the amount of L-

carvone in each gum slab had to be adapted to 0.25 wt% for all samples in order to reach an acceptable amount of solid added to the gum matrix.

The L-carvone release percentage was calculated from the absorbance values and the average cumulative release was plotted as a function of time (see Figure 5.21). Release points at 1, 3, 5 and 10 minutes were selected based on the release study protocol previously established by Mondelēz. This amount of time should be enough to get a good idea of the release profile of capsules from the gum matrix. Based on those results, extended investigations on longer periods of time could be carried out in the future, only with the most promising capsule batches as those measurements are very time consuming. The baseline was adapted by subtracting the results of the release obtained from the blank slabs.

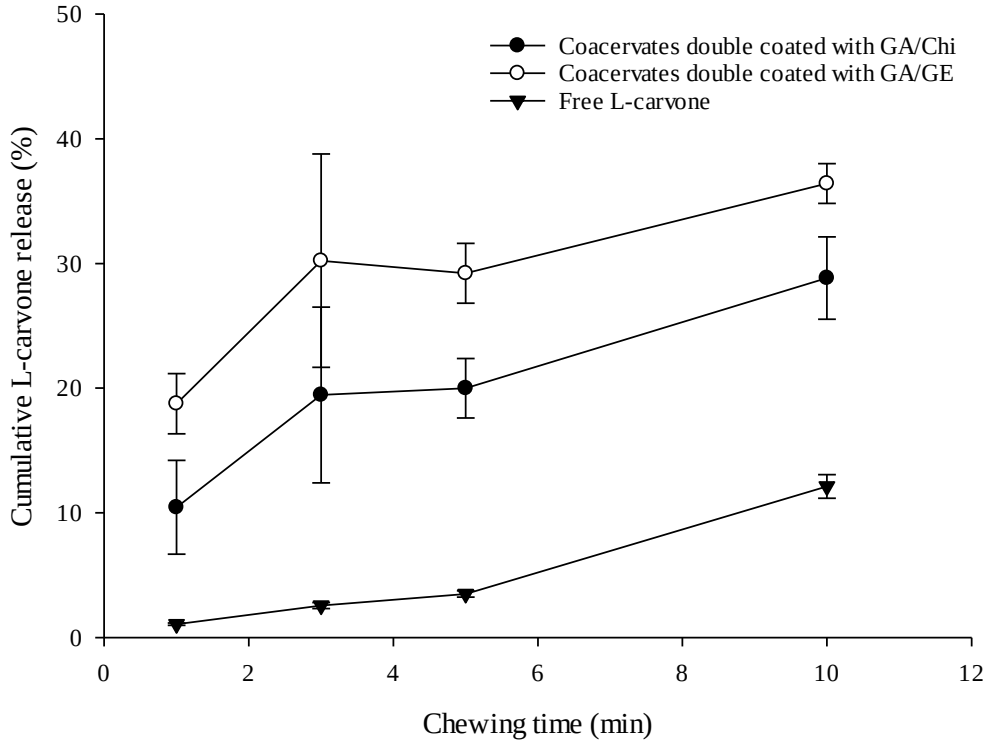


Figure 5.21: Average L-carvone cumulative release from the gum matrix with a 0.25 wt% load for two samples of coacervated capsules with different wall materials (GA/Chi or GA/GE) double coating compared with the release profile of free flavour oil in gum (displayed with standard error bars).

A maximum error of 2.4% was additionally measured for gums "chewed" for 10 minutes with blank capsules with GA/Chi double coating. This error was due to a small absorption of the wall materials at 236 nm. A similar phenomenon was suspected to happen with the other particle samples but the error was not measured.

It was noted that the release observed for the free oil reference was almost linear (no burst), starting from zero and reaching a maximum of 12.1% after 10 minutes of "chewing". This slow release was expected as the flavour oil is hydrophobic and would have a better affinity for the gum base than the saliva and would therefore remain embedded in its matrix, diffusing slowly and in limited quantities. The advantage of encapsulation here was precisely to counter this affinity by isolating the flavour from the gum base to make it more available for release upon rupture. It is possible that encapsulation could also protect the flavour from evaporation, as a significant amount of L-carvone (21.0 $\pm$ 0.8%) was previously found to have evaporated during the process at RT. It was indeed found by Mondelēz, following gas chromatography with flame ionisation detector (GC-FID) characterisation of the reference gum samples performed by Orlando Herrera Gomez, had a significantly lower L-carvone content compared to the 0.8 wt% target, which was therefore expected due to the evaporation of L-carvone during the chewing gum processing at 50°C.

When looking at the release from the gum samples containing capsules, it was noticed that they both exhibited a similar profile with no significant difference ($p > 0.05$) and a characteristic burst effect around 3 minutes of "chewing". The profile of the flavour release was however clearly different for the two capsule sets when compared to what was observed for the free oil released from the gum matrix ($p < 0.001$). The flavour was made more available from the start with a release of 10.4 and 18.7% for the capsules made with GA/Chi and GA/GE double coatings respectively, which was of the same order or higher than the maximum release

obtained at 10 minutes for the sample containing the free oil. To confirm this benefit, it would be necessary to demonstrate that these capsules do prevent evaporation of flavour during the normal gum preparation process, although this has not been possible in the current work as it would require a large volume of capsules to be produced.

At 10 minutes, a maximum release of respectively 28.8 and 36.4% for the GA/Chi and GA/GE particles was achieved, which was equivalent to two to three times the amount made available by the release of the flavour oil incorporated directly in the gum. Although this value was quite high, there was still space for prolonging the release over a longer period of time, as it would be desirable to extend the flavour perception.

It was reassuring to verify the two capsule samples had a similar release profile as it enabled to validate the success of encapsulation with GA/Chi when comparing to an already tested and published encapsulation method with GA/GE (Yu *et al.*, 2017). Although the latter showed a slightly higher release than the former, which may be due to the difference in shell composition (Soottitantawat *et al.*, 2005), this combination was however not investigated further as the use of gelatine was not desired by Mondelēz International for this chewing gum application.

5.4.4 Alternative engineering of the coacervated capsules

5.4.4.1 Shellac coating

The preparation method which was previously used with GA/Chi for adding an extra coating layer by spray coating/drying did not work here. The problem was that the coacervated capsules needed to remain in acidic medium prior to the second coating so as to not destabilise the complex formation which was reversible, and because chitosan would precipitate around pH 6, while shellac was only soluble in alkali conditions (pH > 7) (see **Chapter 3**). So precipitation would immediately occur upon mixing of the suspension with the shellac solution.

Since the two phases could not be in direct contact, the idea of forming a double emulsion was thought as a way to bypass this precipitation issue (see **Chapter 2**). In this way, an oil phase would separate the inner acidic aqueous suspension containing the coacervated capsules from the alkali shellac coating solution. A double emulsion was indeed successfully formed without any precipitation occurring.

Following the spray coating/drying step, brown crystallised solids were obtained rather than a spherical particle powder. Furthermore, no L-carvone flavour release could be perceived upon crushing the dry crystals with a spatula. On a more practical point, shellac created a horribly sticky layer on the wall of the full spray drying device, whose removal was particularly difficult to handle and would not be recommended to be used at industrial scale.

It was then thought to use the precipitation issue as an advantage instead, in order to create the coating layer. Inspired from the gelation process by extrusion (Xue and Zhang, 2008; Martins *et al.*, 2015), some trials were made using acidic precipitation dropping. Instead of using ionic crosslinking to harden the shellac layer, the pH-induced precipitation was used in that way.

As a trial, droplets of the capsule suspension were dropped with a plastic pipette into the shellac solution under magnetic agitation. The precipitation was instantaneous, and very circular particles of a few mm were obtained. The capsules further needed to be filtered, washed, and stored in a $CaCl_2$ solution prior to drying.

The problem here was that the size was way above the target (about 30 μm). This process could be adapted to reduce the size by using microfluidics for example, an electrospray extrusion device (Martins *et al.*, 2015), or an Encapsulator (from BÜCHI).

This could potentially be an interesting lead as the advantage of the hydrophobicity of shellac could truly bring a high value to the mechanical strength of the capsules compared to most of

the other spray dried materials which would lead to particles soluble in water. It would however have involved a significant new effort, which is beyond the scope of this PhD project due to the limited time.

5.4.4.2 Chitosan grafting

The colouration of L-carvone went from pale yellow to light orange after mixing with the gallic acid powder. Although a fair amount of powder was deposited at the bottom of the vial after 24h, it was thought that at least a part of the acid was successfully dissolved in the flavour oil.

Some capsules seemed to have been obtained (see Figure 5.22). In the wet sample, most particles were very circular, with a few more irregular ones. Following drying in open air for 24h, some circular particles with a rigid wall could still be observed. However, it was noticed that they all seemed to be leaking as some liquid oil appeared to be getting out from the capsules (see Figure 5.22 (b)).

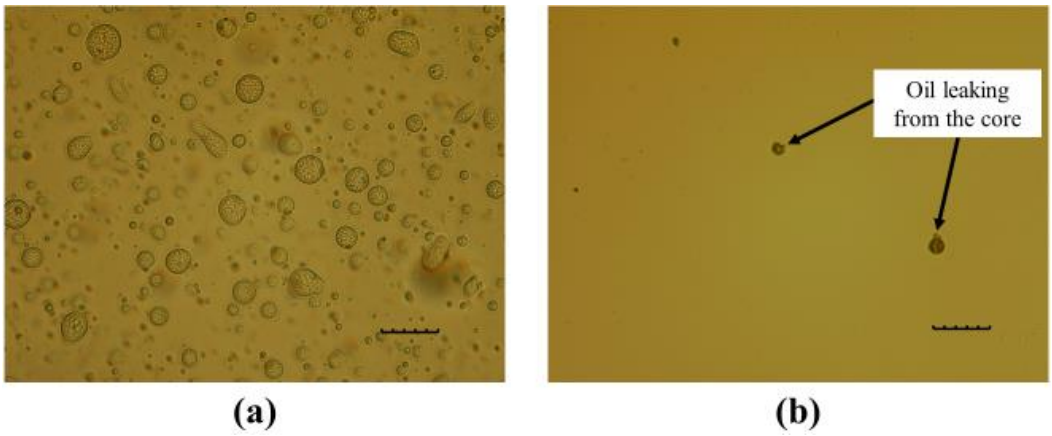


Figure 5.22: (a) Wet and (b) dry particles obtained from the chitosan grafting inspired protocol, observed by light microscopy (all scales represent 50 μm).

Unfortunately, no L-carvone flavour could be perceived when crushing dry particles for the sensory check (score of 0 on the scale, see **Chapter 4**).

It might be that this technique did not work because the gallic acid was denatured in the oil phase, or that it was not dissolved in sufficient quantity, so that there would just be the normal complexed shell surrounding the core. It might also be that, similarly to the primary coacervated capsules, an extra coating layer would be required to prevent the leaking.

In any case, this technique might or might not work but would require further investigating and processing, and therefore did not provide a more advantageous alternative to the coacervated capsules further coated by spray coating/drying as presented above.

5.4.4.3 Nanoparticles

The use of nanoparticles was thought as a potential alternative to harden the coacervated capsule wall without requiring the extra coating step.

Some particles were successfully obtained, as observed by microscopy (see Figure 5.23).

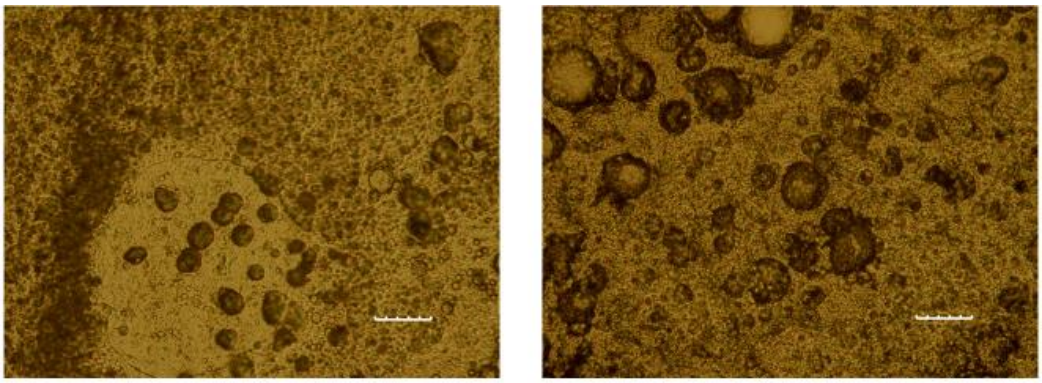


Figure 5.23: Dry particles observed by light microscopy obtained with $CaCO_3$ nanoparticles suspended (a) in the aqueous phase and (b) in the oil phase (all scales represent 50 μm).

Unfortunately, no L-carvone flavour could be perceived for either of the two batches when crushing dry particles for the sensory check (score of 0 on the scale).

During the acidification step, a lot of bubbles were observed in the medium. This phenomenon could be explained by the following reaction:

$$CaCO_3 + 2\ CH_3COOH \rightarrow CO_2 + H_2O + Ca(CH_3COO)_2$$

Indeed, a possible decomposition of $CaCO_3$, in the presence of acetic acid, into water and gas could explain the observed bubbles and why the method was not successful.

The use of nanoparticles could not work in the case of gum arabic/chitosan combination where acidification was required. However, it could still be an interesting method for other combinations where acidification is not required or in alkali medium.

5.5 Conclusion

An extra coating layer was successfully added by spray coating/drying to the previously obtained gum arabic/chitosan coacervated capsules, using the same wall material combination, and the particles were characterised.

Some more or less spherical core-shell capsules in the desired size range were obtained. The measured payload was around 2% and would need to be further increased to be able to reach the targeted flavour level required in the gum matrix. It was concluded from micromanipulation measurements that it could potentially be improved by separating actual capsules from wall material beads, although this could be quite difficult and would moreover add an extra processing step. The samples also exhibited a good release profile with a burst under compression, showing the advantage of encapsulation compared to free oil directly incorporated into the gum matrix.

Some additional trials were made using different techniques to attempt to harden the primary coacervated capsule wall in a more advantageous way, and would require less post-processing steps. An extra coating layer using a resin (shellac) was considered. This was proven to be a possibly promising option but required a much more thorough investigation, which was unfortunately out of the scope of this project. A method using grafted chitosan could be a potential alternative, but there was not enough evidence to show this technique could work, and it was definitely not more advantageous as it would still require an extra coating step. Finally, the use of nanoparticles to harden the wall could have been a good idea, however it did not work in the case of gum arabic/chitosan combination where acidification was required.

All those results confirmed the produced sample could be a possible option for the desired application. It was also desired to obtain different sets of capsules with different mechanical properties in order to get a delayed burst.

In the next chapter (**Chapter 6**), alternative wall material combinations will be considered for the complex coacervation process.

CHAPTER 6 – Development of a Technique to Investigate New Wall Material Combinations

6.1 Introduction

In the previous chapter, capsules obtained by complex coacervation with the gum arabic/chitosan 6:1 (w/w) combination were further coated by spray coating/drying, using the same wall material layer, and fully characterised. Although a characteristic burst and sustained release were successfully obtained for at least 10 minutes when those capsules in the gum matrix were compressed, the payload was still below the target value for commercial application and a delayed burst was desired to extend the flavour perception over time. The use of wall materials of different natures could offer the possibility to obtain capsules with different properties in the hope of getting a higher flavour load. Furthermore, the mix of capsules presenting various mechanical properties in the gum matrix could enable to obtain burst releases at different times.

New polymer combinations were thus considered for use in the complex coacervation process. When looking at the most commonly used wall material combination for complex coacervation, gelatine/gum arabic, it can be noted that the gelling power of gelatine plays a great role in the solidification of the capsules wall.

Neither gum arabic nor chitosan presented any gelling properties at low concentration, and the sole option for hardening the wall was by crosslinking. The main disadvantage of food grade

crosslinkers is that they are quite weak compared to the commonly used toxic crosslinkers such as glutaraldehyde and formaldehyde (see **Chapter 4**).

The idea here was to systematically select one material displaying gelling capacities for complex coacervation, so that the association of hardening by gelation in addition to the use of a crosslinker could overcome the weakness of food grade binders, and produce capsules with better mechanical properties.

6.2 Theoretical considerations

For a polysaccharide/polysaccharide combination, it was previously mentioned that chitosan was one of the only rare cationic polymers available (see **Chapter 2**).

A handful of anionic gelling polysaccharides were selected from the available materials identified in **Chapter 2** (see Table 6.1), regardless of their gelling mechanism. It was important to check the pKa of each material for investigating their combination with chitosan using the complex coacervation process in order to have an idea of the coacervation pH range.

Table 6.1: pKa values for different anionic gelling polysaccharides.

Polysaccharides	pKa	References
Alginates	3.0 - 4.4	(Rinaudo, 2006a; Draget, 2009; Shinde and Nagarsenker, 2009)
Carrageenans	4.9	(Sadeghi, 2012)
Gellan gum	3.0 - 3.6	(Fasolin *et al.*, 2013; Yang *et al.*, 2013; Würstenberg, 2015)
Xanthan gum	3.1	(Oprea *et al.*, 2013)
Pectin	3.5 - 4.0	(Chen *et al.*, 2012; Xiao *et al.*, 2014)
Karaya gum	Anionic	(Pegg, 2012)

It was noted that all of those anionic gelling polysaccharides also presented emulsifying capacities (see **Chapter 2**). Similarly to what was observed with gum arabic, the use of an emulsifier may not be needed (see **Chapter 4**).

The key parameters (polymer ratio and optimum pH) for complex coacervation between chitosan and the previously mentioned anionic polysaccharides as reported in the literature are listed (see Table 6.2).

Table 6.2: Key parameters for the complex interaction of chitosan with selected anionic polysaccharides (alginate, carrageenan, gellan gum, xanthan gum, pectin, karaya gum), based on the literature (v/v: volume ratio, w/w: weight ratio, w/v: weight per volume ratio).

Anionic polymer	Cationic polymer	Polymer ratio (-/+)	Optimum pH	References
Alginate	Chitosan	4:5 - 1:1 (v/v)	3.9	(Kulig *et al.*, 2016)
		1:1 (v/v)	4.5	(Phoeung *et al.*, 2017)
		12:5 (molar)	3.25	(Rabelo *et al.*, 2019)
κ-Carrageenan	Chitosan	3:1 (w/w)	4.5	(Dima *et al.*, 2014)
		1:1 (w/w)	4.6	(Deka *et al.*, 2016)
		9:5 (molar)	4	(Rabelo *et al.*, 2019)
Gellan gum	Chitosan	5:3 (w/v)	3.5	(Dixit *et al.*, 2012)
		7:3 (w/v)	4.5	(Picone and Cunha, 2013)
Xanthan gum	Chitosan	1:1 (w/v)	3.6 - 8.0	(Dadou *et al.*, 2018)
Pectin	Chitosan	1:1 (w/w)	6.1	(Wang *et al.*, 2017)
Karaya gum	Chitosan	15:1 (w/w)	4.5	(Lankalapalli and Kolapalli, 2012)

Although numerous articles dealt with the polyelectrolyte complex formation between chitosan and some natural polysaccharides (alginate, carrageenan, gellan gum, xanthan gum, pectin), only a few of those publications were specific about the polymer ratio and the optimum pH, and this information was not always presented explicitly. Furthermore, those values were rarely in accordance from one article to the other.

This means that those parameters have not been clearly nor universally defined for the previously listed combinations. This could partly be explained by the fact that the ideal condition may slightly vary due to natural variability of the raw materials used.

6.3 Experimental procedures

6.3.1 Zeta potential measurements

Stock solutions were made by dissolving 0.05 wt% of polymer (gum arabic, chitosan, sodium alginate, ι-carrageenan, gellan gum, xanthan gum, pectin, karaya gum, guar gum, corn starch, and whey protein), carefully weighed with a precision scale (0.0001 g), in DI water (Espinosa-Andrews *et al.*, 2013; Liu *et al.*, 2015a). The mixtures were stirred at 500 rpm in a beaker under mechanic agitation with a Rushton turbine at room temperature (RT, estimated to be 22 $\pm$ 3ºC) for 2h.

The pH of aliquots of each stock solution was then adjusted under magnetic agitation, using acetic acid and 1M sodium hydroxide solutions, in order to cover the pH range between 2.0 and 8.0 with values incremented every 0.5 pH units (resulting in 13 samples per material). A small amount of potassium chloride (KCl, 10^{-3} M) was further added to each specimen.

The apparent zeta potential of each sample was evaluated by zeta potential measurements (see **Chapter 3**).

6.3.2 Preparation of polymer solutions

Gum arabic 12 wt% solution and chitosan 2 wt% solution were prepared in the same conditions as specified in **Chapter 4**. A 1 wt% chitosan solution was also made for combining with the other anionic polysaccharides.

The other polymer solutions were prepared so as to meet their gelling conditions (see **Chapter 3**). They were all placed in a 500 mL jacketed beaker under mechanical agitation with a Rushton turbine at 500 rpm.

Sodium alginate 0.5 wt% solution was prepared in DI water at 25ºC.

ι-Carrageenan 0.5 wt% solution was prepared in DI water at 80ºC.

Gellan gum 0.5 wt% solution was prepared in DI water at 90ºC.

Xanthan gum 0.5 wt% solution was prepared in DI water at 50ºC.

Citrus pectin 1 wt% solution was prepared in 2 wt% acetic acid aqueous solution containing 65 wt% of white granulated sugar, at 95ºC.

Corn starch 10 wt% solution was prepared in DI water at 80ºC.

Whey protein isolate (WPI) 1 wt% solution was prepared in DI water at 25ºC.

6.3.3 Turbidity measurements

The different polymer solutions were mixed in proportions matching up with the optimal ratios identified from the zeta potential measurements.

The pH of smaller portions of each stock solution was then adjusted under magnetic agitation, using acetic acid and 1M sodium hydroxide solutions, in order to cover the pH range between 2.0 and 7.0, with values incremented every 0.5 pH units, and every 0.2 pH units in the range of the identified $pH_{opt} \pm 0.5$.

The turbidity of the different mixtures was measured at each pH point (see **Chapter 3**). Each material sample was diluted in the same proportion at the different pH points, based on the

required dilution imposed by the most turbid sample, seeing that the equipment could only detect a maximum turbidity of 1000 FTU.

6.3.4 Complex coacervation with different wall material combinations

6.3.4.1 Combinations with chitosan

Complex coacervation between karaya gum and chitosan, and corn starch and chitosan was undertaken. The process followed the same steps as previously described in **Chapter 4**.

L-carvone oil was poured into the gelling polysaccharide aqueous phase, maintained at 50°C in a 500 mL jacketed beaker, and the mixture was stirred by mechanical agitation at 500 rpm with a Rushton turbine for pre-emulsification mixing for about 5 min.

The pre-emulsion was then mixed at 3000 rpm for 10 min to form an O/W emulsion (see **Chapter 3**). Following the emulsification, the system was left to rest for a couple of minutes, at 50°C, to allow the air bubbles to come to the surface. This foam was scooped off with a spatula.

The mixture was put under mechanical stirring with a Rushton turbine at 500 rpm. This agitation was continued until the end of the full process. A desired amount of chitosan solution was added dropwise to the emulsion under agitation.

After the addition was complete, the pH was adjusted (see **Chapter 3**) to the optimum pH (pH_{opt}) using a 1M sodium hydroxide (NaOH) solution. The batch was left to stir for 1h before cooling the medium down to 25°C.

Finally, the 3-step NaTPP crosslinking (see **Chapter 4**) was carried out at 25°C, and the mixture was further left under agitation overnight to allow time for crosslinking.

6.3.4.2 Combinations with whey protein

The complex coacervation process was almost identical as the previously described protocol, replacing the chitosan phase by the desired amount of whey protein.

The main difference was in the crosslinking step as sodium tripolyphosphate was specifically used to crosslink chitosan. In this case, 10 g of a 10 wt% calcium chloride ($CaCl_2$) solution was added at RT to crosslink the whey protein. The mixture was further left under agitation overnight to allow time for crosslinking.

6.3.5 Spray drying

The entrapment efficiency of the capsules in liquid phase was evaluated by UV measurements (see **Chapters 3 and 5**).

The corn starch/chitosan and corn starch/WPI capsule suspensions were turned into powder by direct spray drying (no extra polymer coating added) using the same spraying settings as previously described (see **Chapter 5**).

6.3.6 Characterisation

The 2D morphology of the particles was observed by optical microscopy (see **Chapter 3**).

The payload was quantified by UV measurements (see **Chapters 3 and 5**).

The mechanical strength of the capsules was studied using the micromanipulation technique (see **Chapter 3**).

6.3.7 Statistical analysis

Experiments were made in triplicate. Values were expressed as mean $\pm$ standard error and data were displayed with standard error bars. The results was tested by one-way analysis of variance

(ANOVA) with Tukey's post hoc test using SPSS Statistics software. Differences were considered significant at $p \leq 0.05$.

6.4 Results and discussion

6.4.1 Polymer mixing ratio

6.4.1.1 Gum arabic/chitosan combination checks

Some checks against the proposed method were first made with gum arabic and chitosan. The apparent zeta potential of these two materials was plotted as a function of pH (see Figure 6.1).

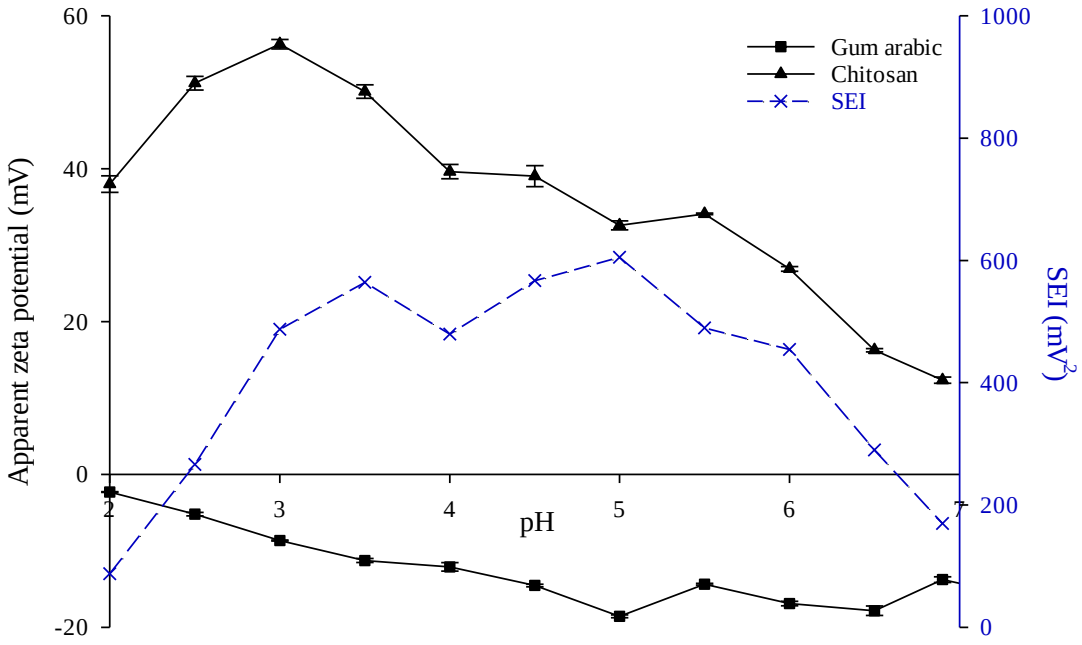


Figure 6.1: Apparent zeta potential of gum arabic and chitosan plotted as a function of pH, displayed with the strength of their electrostatic interaction (SEI) at each pH value (apparent zeta potential data are displayed with standard error bars).

The strength of the electrostatic interaction (SEI) curve between the two polysaccharides was also added to the graph (see Figure 6.1). The ideal polymer ratio could then be estimated according to the method explained in **Chapter 3**.

The apparent zeta potential profiles of the individual materials (see Figure 6.1) were in the same range as what was reported in the literature, with chitosan having values between 10 and 60 mV on the pH range [2.0-7.0], and values between 0 and -20 mV for gum arabic (Espinosa-Andrews *et al.*, 2013; Huang *et al.*, 2015; Barbosa *et al.*, 2019; Rabelo *et al.*, 2019). This also proved that gum arabic and chitosan were indeed oppositely charged and could interact successfully.

It appeared in this graph (see Figure 6.1) that the SEI plot had an M shape with two distinct peaks, which was in accordance with the literature (Espinosa-Andrews *et al.*, 2013). The maximum SEI was observed at pH = 5.0 $\pm$ 0.5 (error based on the interval chosen for the measurement points) and corresponded to a gum arabic/chitosan ratio of 7:4 (w/w). It was also interesting to consider the second peak in this case as it was further away from the precipitation pH of chitosan, and it coincided with the peak which was showing a maximum at pH 4.0 in the literature (Espinosa-Andrews *et al.*, 2013). It was found that the SEI peak at pH 3.5 $\pm$ 0.5 corresponded to a gum arabic/chitosan ratio of 4.5:1 (w/w).

This second pH matched up better with what was observed experimentally in **Chapter 4**, although the ratio was not completely accurate. It was noticed from the literature, however, that a gum arabic/chitosan ratio of 6:1 (w/v) could also be estimated at pH 3.5 from zeta potential measurements, which corresponded to the experimental conditions of **Chapter 4** (Huang *et al.*, 2015). But it was also stated in the literature that there was an acceptable high interaction region between ratios 4.5:1 and 6:1 (w/w) which was in accordance with both ratios found at pH 3.5

(zeta potential measurements: 4.5:1 (w/w), and experimentally: 6:1 (w/w)) (Espinosa-Andrews *et al.*, 2013).

From this experiment, it was concluded that zeta potential measurements were an interesting exploration tool for studying the interaction of polymers, although it would not give the precise conditions for complex coacervation upfront. It would therefore require a complementary characterisation method, such as turbidity for example, in order to confirm the exact optimum pH at a given polymer ratio. The observed variations between the obtained results, the example in the literature and the experimental conditions previously identified (see **Chapter 4**) could be explained by several causes. Being from natural origin, the different batches of raw material might have had slightly varied properties.

6.4.1.2 Ionic vs non-ionic polysaccharides

The apparent zeta potential of different polysaccharides was plotted as a function of pH (see Figures 6.2 and 6.3). Guar gum was investigated as a reference since this polymer was supposed to be non-ionic (see **Chapter 2**).

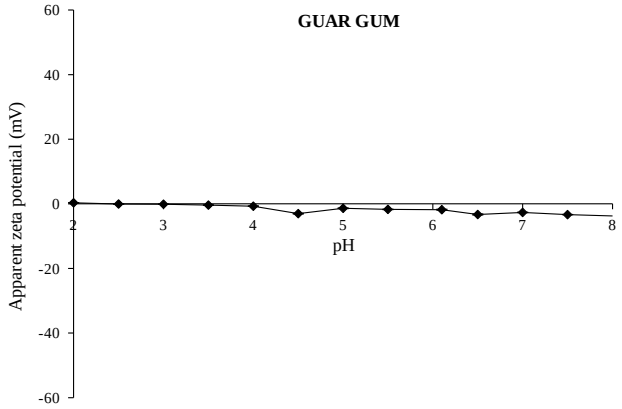


Figure 6.2: Apparent zeta potential of guar gum (data are displayed with standard error bars).

As expected, the apparent zeta potential of guar gum was close to zero on the whole pH range (see Figure 6.2).

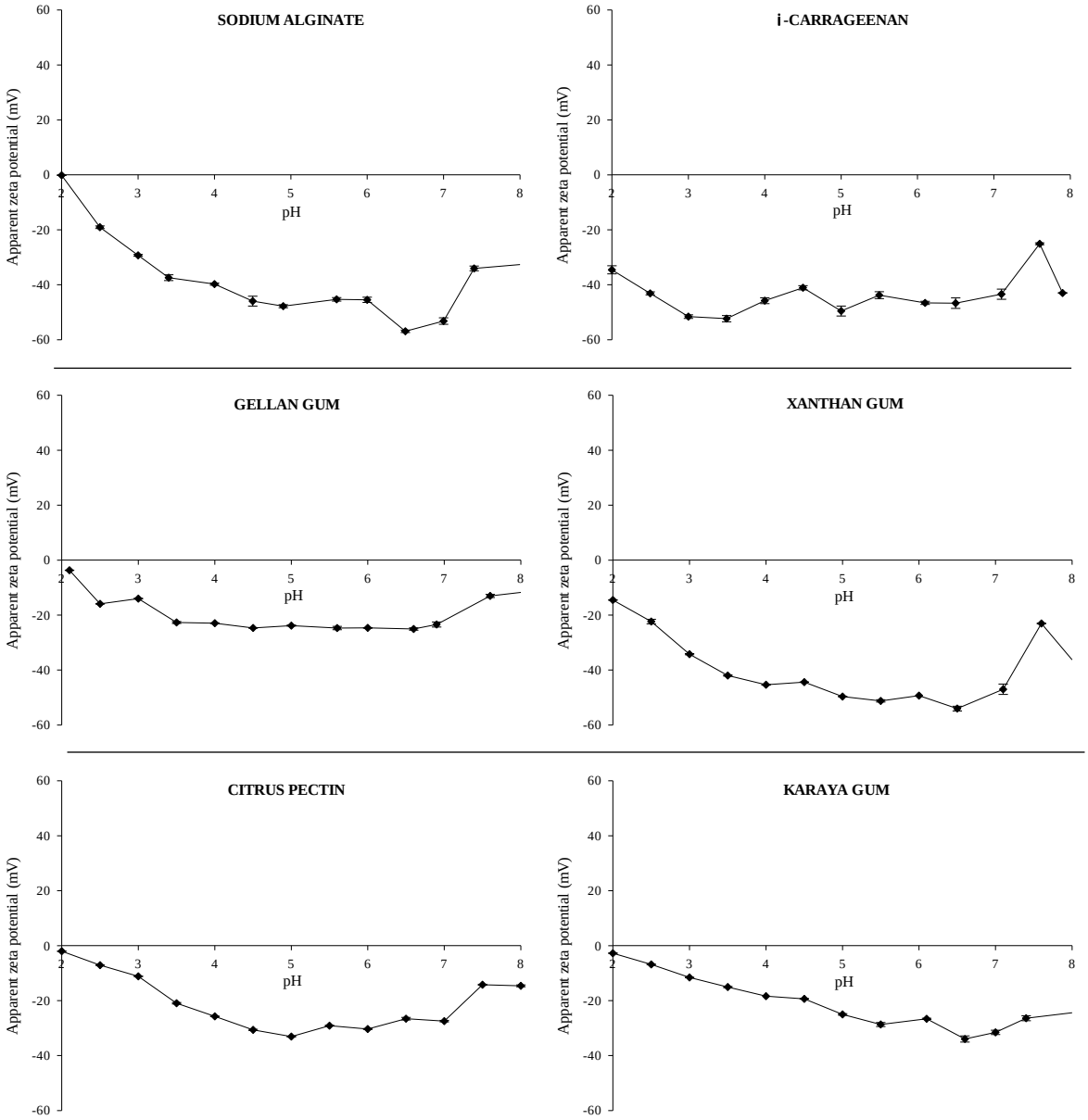


Figure 6.3: Apparent zeta potential of anionic polysaccharides: sodium alginate, ι-carrageenan, gellan gum, xanthan gum, citrus pectin, karaya gum (data are displayed with standard error bars).

The apparent zeta potential profiles of the selected gelling polysaccharides clearly confirmed that they were all anionic and could successfully interact with chitosan (see Figure 6.3). The small error bars attested of the precision of the zeta potential measurements.

Furthermore, the values and apparent zeta potential profiles of sodium alginate, carrageenan, gellan gum, xanthan gum and citrus pectin were in accordance with what was reported in the literature (Picone and Cunha, 2013; Joshi *et al.*, 2018; Barbosa *et al.*, 2019; Rabelo *et al.*, 2019). Karaya gum was not studied with this method in the literature.

6.4.1.3 New anionic polysaccharide/chitosan combinations

Similarly to the investigation of the gum arabic and chitosan combination, the apparent zeta potential of the two oppositely charged polyelectrolytes was plotted as a function of pH for each combination of gelling anionic polysaccharide with chitosan, as well as their SEI (see Figures 6.4 to 6.9). From those results, the optimal pH for complex coacervation was forecast and the ideal polymer ratio was estimated at this pH.

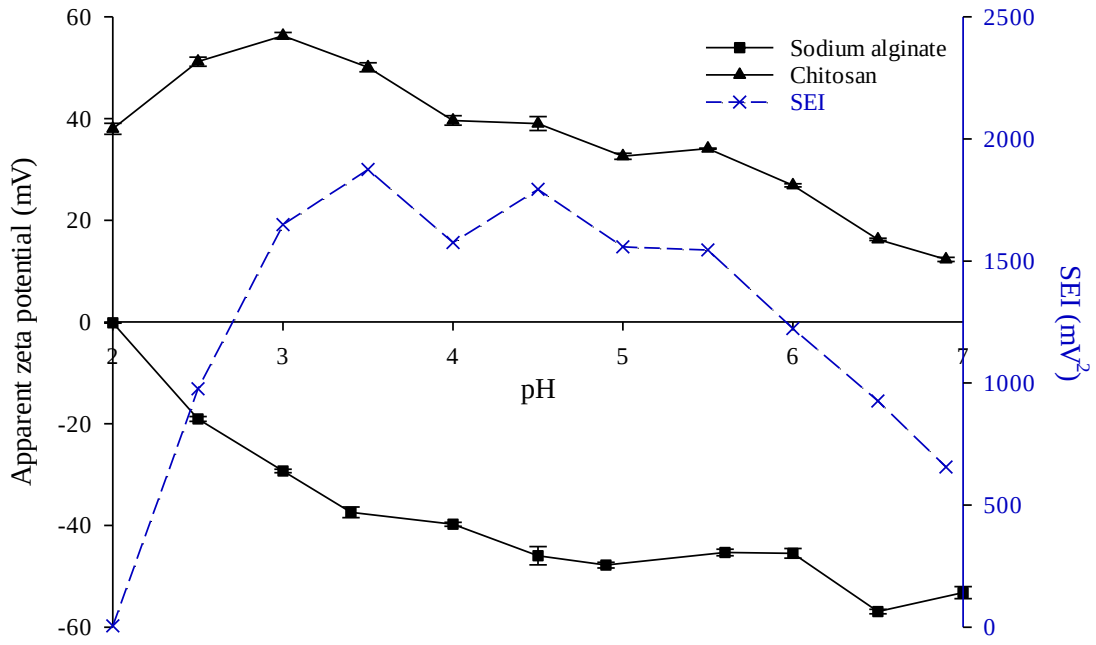


Figure 6.4: Apparent zeta potential of sodium alginate and chitosan plotted as a function of pH, displayed with the strength of their electrostatic interaction (SEI) at each pH value (apparent zeta potential data are displayed with standard error bars).

For the sodium alginate/chitosan combination, a ratio of 4:3 (w/w) was estimated at pH_{opt} = 3.5 ± 0.5 (see Figure 6.4). This result was close to the 1:1 (v/v) ratio which was mentioned in the literature (Kulig *et al.*, 2016; Phoeung *et al.*, 2017). An optimum pH between 3.0 and 4.0 was also reported (Kulig *et al.*, 2016; Rabelo *et al.*, 2019).

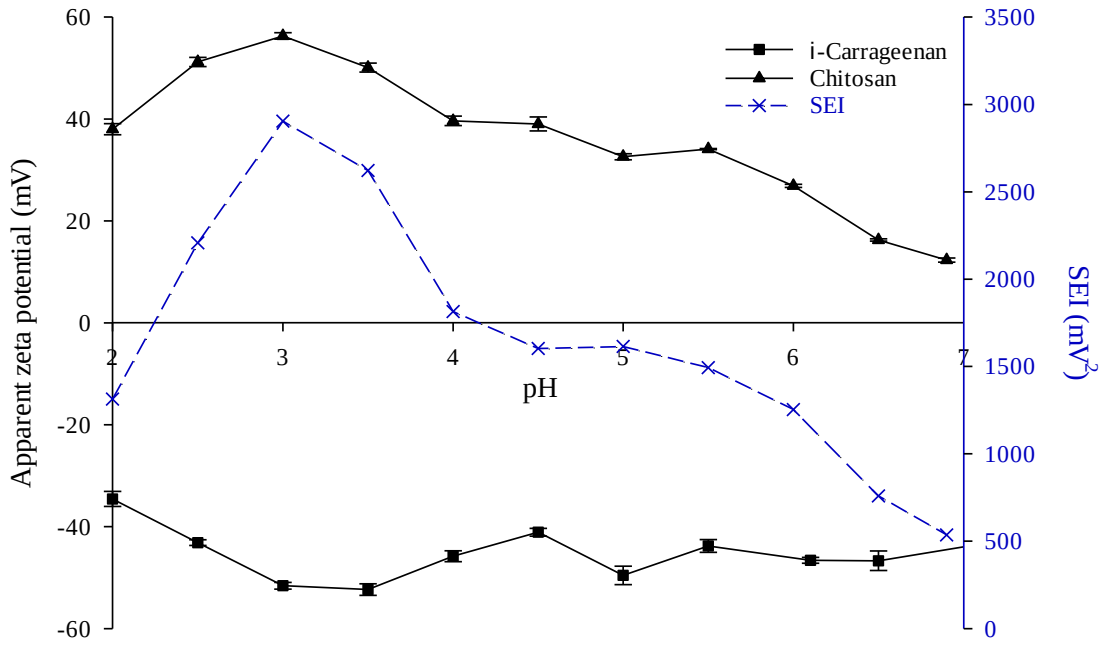


Figure 6.5: Apparent zeta potential of ι-carrageenan and chitosan plotted as a function of pH, displayed with the strength of their electrostatic interaction (SEI) at each pH value (apparent zeta potential data are displayed with standard error bars).

For the ι-carrageenan/chitosan combination, a ratio of 1:1 (w/w) was estimated at pH_{opt} = 3.0 ± 0.5 (see Figure 6.5). A polymer ratio of 1:1 (w/w) was also mentioned in the literature (Deka *et al.*, 2016). However, an optimum pH between 4.0 and 5.0 was rather reported (Dima *et al.*, 2014; Deka *et al.*, 2016; Rabelo *et al.*, 2019). This small difference could possibly come from the fact that ι-carrageenan was used in those experiments compared to κ-carrageenan in all the examples from the literature.

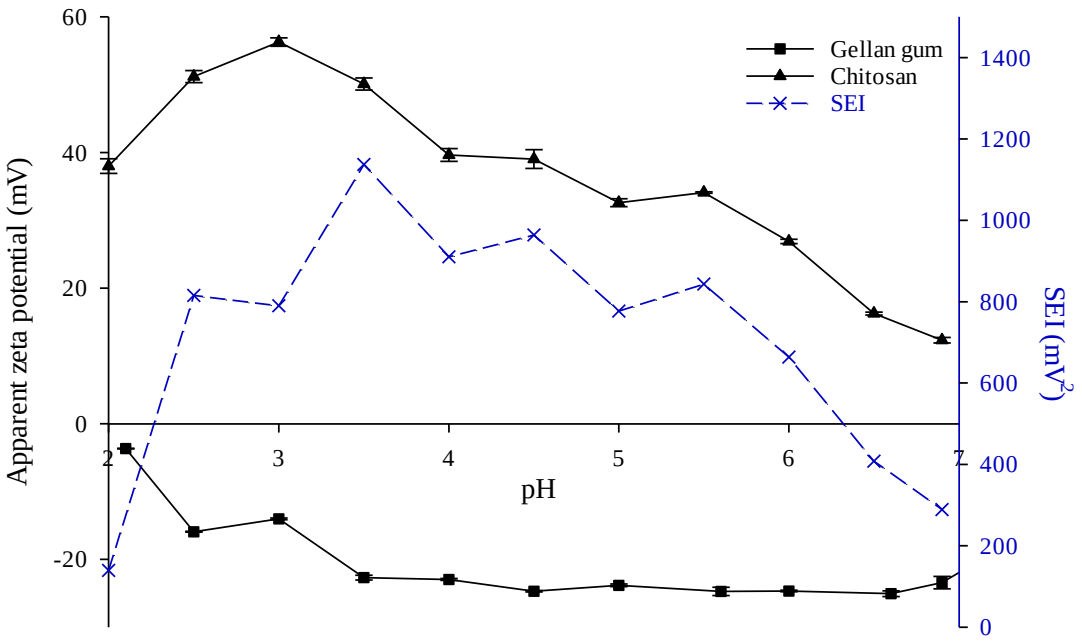


Figure 6.6: Apparent zeta potential of gellan gum and chitosan plotted as a function of pH, displayed with the strength of their electrostatic interaction (SEI) at each pH value (apparent zeta potential data are displayed with standard error bars).

For the gellan gum/chitosan combination, a ratio of 9:4 (w/w) was estimated at $pH_{opt} = 3.5 \pm 0.5$ (see Figure 6.6). This result was close to the 7:3 (w/v) ratio which was mentioned in the literature, but with a different optimum pH of 4.5 (Picone and Cunha, 2013). An optimum pH of 3.5 was also reported, but with a ratio of 5:3 (w/v) (Dixit *et al.*, 2012), which shows coacervation was observed at the identified pH as well. This variety of values for the optimum pH and polymer ratio proves that there are discrepancies from one experiment to the other, possibly due to the differences among the distinct natural material batches.

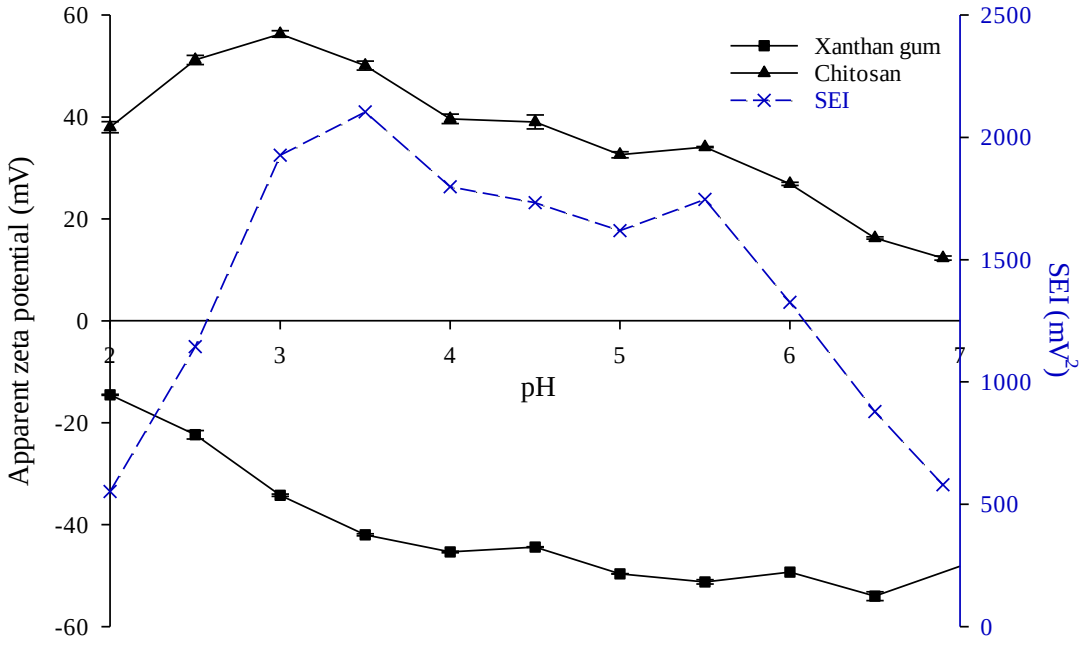


Figure 6.7: Apparent zeta potential of xanthan gum and chitosan plotted as a function of pH, displayed with the strength of their electrostatic interaction (SEI) at each pH value (apparent zeta potential data are displayed with standard error bars).

For the xanthan gum/chitosan combination, a ratio of 6:5 (w/w) was estimated at $pH_{opt} = 3.5 \pm 0.5$ (see Figure 6.7). This result was close to the 1:1 (w/v) ratio which was mentioned in the literature (Dadou *et al.*, 2018). An optimum pH between 3.0 and 4.0 was also reported (Dadou *et al.*, 2018).

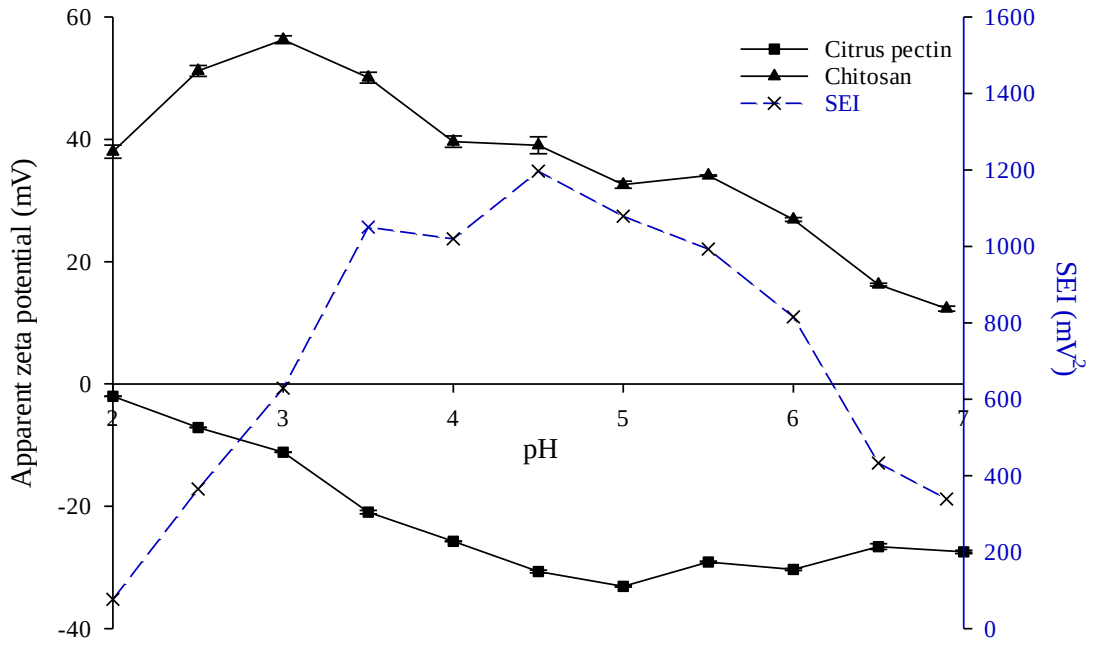


Figure 6.8: Apparent zeta potential of citrus pectin and chitosan plotted as a function of pH, displayed with the strength of their electrostatic interaction (SEI) at each pH value (apparent zeta potential data are displayed with standard error bars).

For the citrus pectin/chitosan combination, a ratio of 5:4 (w/w) was estimated at $pH_{opt} = 4.5 \pm 0.5$ (see Figure 6.8). This result was close to the 1:1 (w/w) ratio which was mentioned in the literature (Wang *et al.*, 2017). A much higher optimum pH of 6.1 was however reported, which was not very desirable as it was close to the precipitation pH of chitosan (Wang *et al.*, 2017). Although HM pectin was used in the work reported in this article, no information on the origin of the material was provided. If it came from a different fruit origin such as apple or orange for example, this could possibly have explained such a variation in optimum pH.

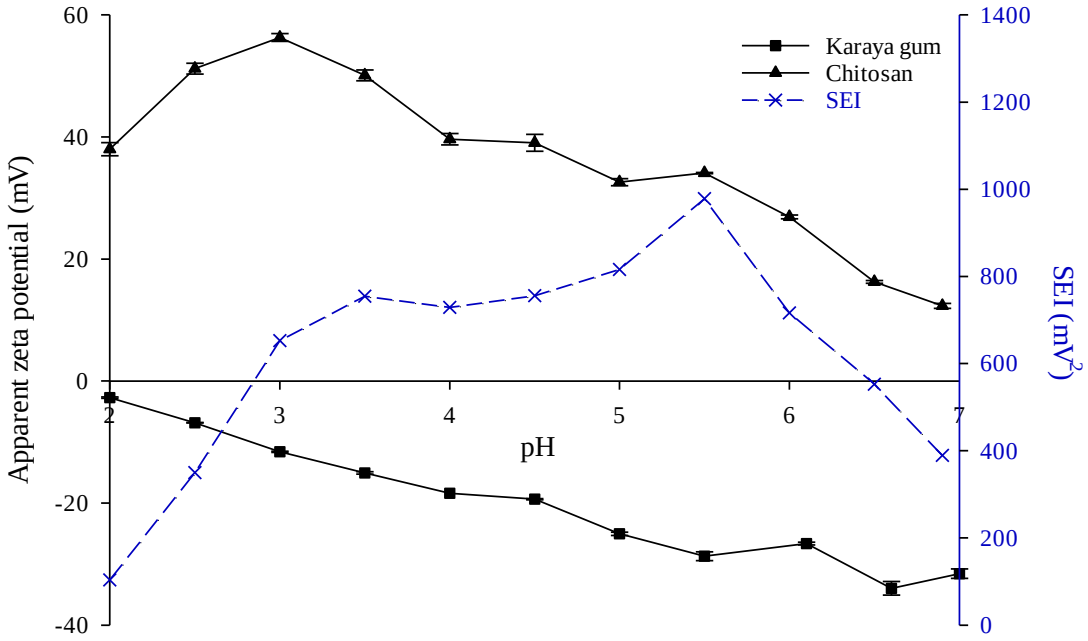


Figure 6.9: Apparent zeta potential of karaya gum and chitosan plotted as a function of pH, displayed with the strength of their electrostatic interaction (SEI) at each pH value (apparent zeta potential data are displayed with standard error bars).

For the karaya gum/chitosan combination, a ratio of 6:5 (w/w) was estimated at $pH_{opt} = 5.5 \pm 0.5$ (see Figure 6.9). The use of karaya gum was very rare in the literature and was investigated here as a fairly novel material.

All those results confirmed that various raw material batches could lead to experimental conditions which were different from what was reported in the literature, especially so when dealing with natural materials. It would therefore be strongly advised to systematically operate those checks with the used materials rather than reproduce the experimental conditions reported in other publications.

6.4.1.4 Corn starch behaviour

The apparent zeta potential of corn starch was plotted alongside with guar gum (see Figure 6.10) in order to display the profile of non-ionic polysaccharides (see **Chapter 2**). However, the graph which was obtained from this material was quite different from what was expected. Instead of the linear plot very close to zero which was observed for guar gum, a more pronounced signal was obtained with corn starch.

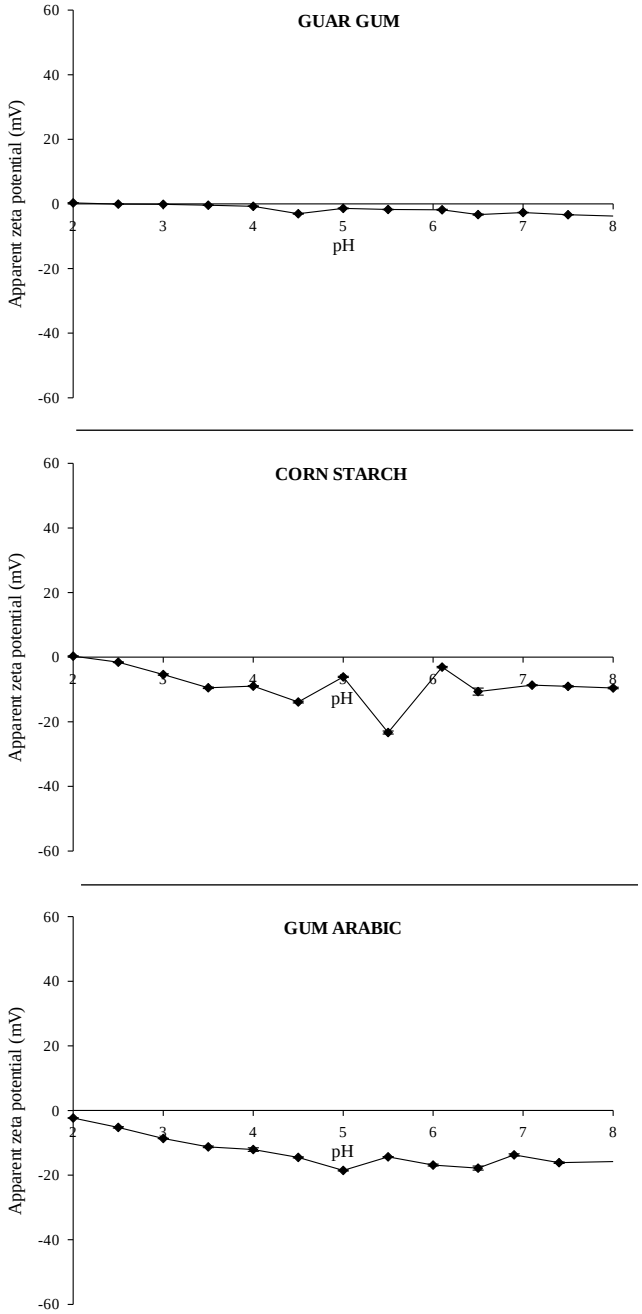


Figure 6.10: Comparison of the apparent zeta potentials measured for guar gum, corn starch and gum arabic (data are displayed with standard error bars).

It was pointed out that the strength of the signal was somewhat similar to the one obtained for gum arabic (see Figure 6.10), which is a clearly charged polysaccharide and was proven to interact successfully with chitosan (see **Chapter 4**). Although amylose and amylopectin, which

are the main components of starch, are non-ionic, the presence of traces of proteins (see **Chapter 3**) could possibly explain the charge which was observed for corn starch. Therefore, the apparent zeta potential of corn starch and chitosan was also plotted as a function of pH along with their SEI (see Figure 6.11).

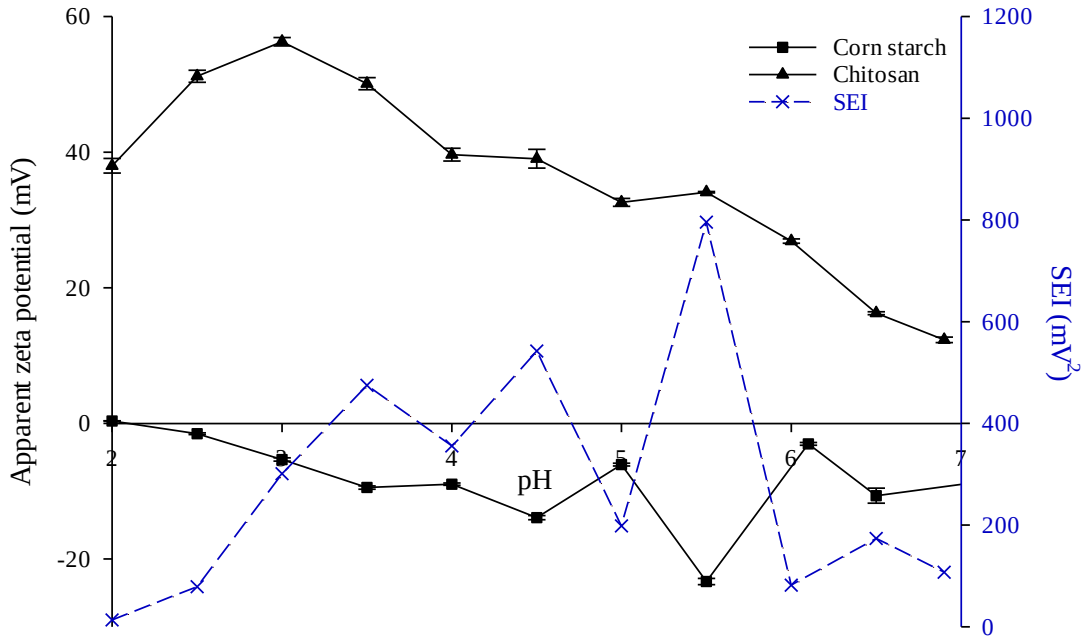


Figure 6.11: Measured apparent zeta potential of corn starch and chitosan plotted as a function of pH, displayed with the strength of their electrostatic interaction (SEI) at each pH value (apparent zeta potential data are displayed with standard error bars).

For the corn starch/chitosan combination, a ratio of 3:2 (w/w) was estimated at $pH_{opt} = 5.5 \pm 0.5$ (see Figure 6.11).

6.4.2 Optimum pH

In order to confirm the precipitation pH of chitosan, the turbidity of this pure raw material was first investigated as a function of pH (see Figure 6.12). The turbidity of the solution could also be followed visually.

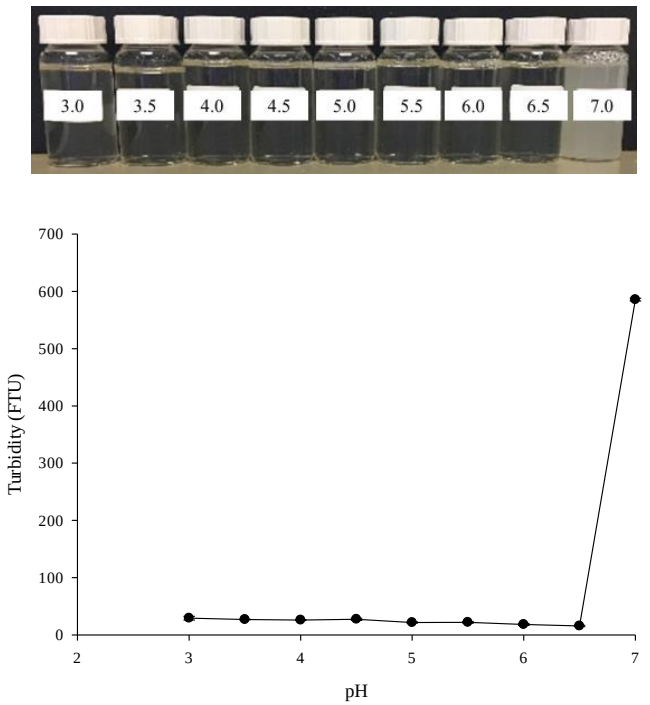


Figure 6.12: Macroscopic appearance of pure chitosan solution and its turbidity plotted as a function of pH (data are displayed with standard error bars).

It was observed that the turbidity of chitosan solution was rather low on most of the pH range and a sudden steep increase was recorded between pH 6.5 and 7.0 (see Figure 6.12). This phenomenon should be due to the precipitation of chitosan above pH 6.0 (see **Chapter 3**). From these results, it could be concluded that the turbidity of chitosan would not interfere with the measurements of the turbidity of the different combinations in the pH range below 6.5.

When sodium alginate, ι-carrageenan, xanthan gum, and citrus pectin solutions were each mixed with chitosan solution, instant gelation happened, no matter what the mixing pH was. For gellan gum, a precipitate was formed at all pH values (see Figure 6.13), although the denser precipitate seemed to be observed between pH 3.0 and 4.0, as predicted by the apparent zeta potential data. Due to these reasons, the listed combinations were not further investigated.

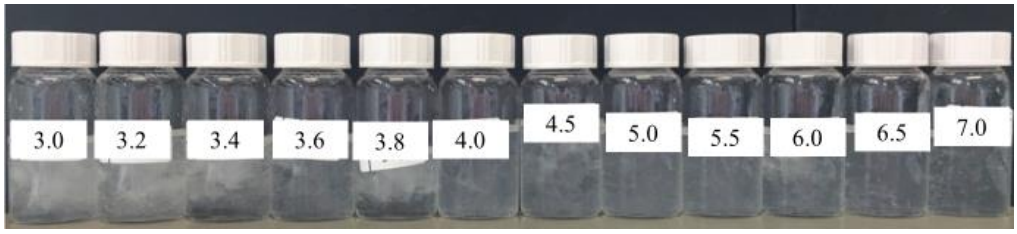


Figure 6.13: Macroscopic appearance of gellan gum/chitosan mixture (9:4) as a function of pH.

The turbidity of the gum arabic/chitosan 4.5:1 (w/w) combination was plotted as a function of pH (see Figure 6.14), as a means of checking the apparent zeta potential data and the previously identified optimum pH (see **Chapter 4**).

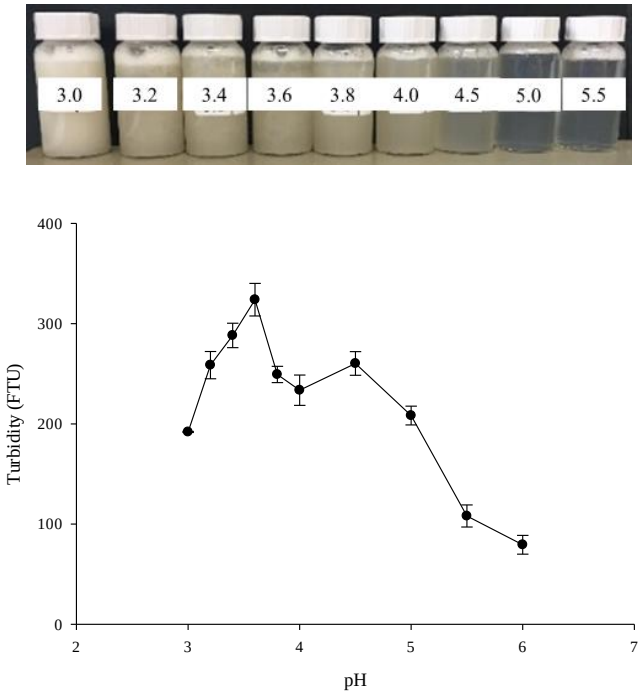


Figure 6.14: Macroscopic appearance of the gum arabic/chitosan mixture 4.5:1 (w/w) and its turbidity plotted as a function of pH (data are displayed with standard error bars).

A maximum in the turbidity profile of gum arabic/chitosan 4.5:1 (w/w) combination was observed at pH 3.6 (see Figure 6.14). This result was both in accordance with the optimum pH identified experimentally in **Chapter 4** and with the previous apparent zeta potential data. This

control study enabled to confirm that zeta potential and turbidity measurements data were well correlated. The use of those two methods as systematic investigation of complex coacervation combinations was therefore judged efficient in identifying an estimated ideal polymer ratio and the optimum coacervation pH.

The turbidity of the remaining possible combinations (karaya gum/chitosan and corn starch/chitosan) was thus plotted as a function of pH (see Figure 6.15 and 6.16) to help confirm their optimum coacervation pH.

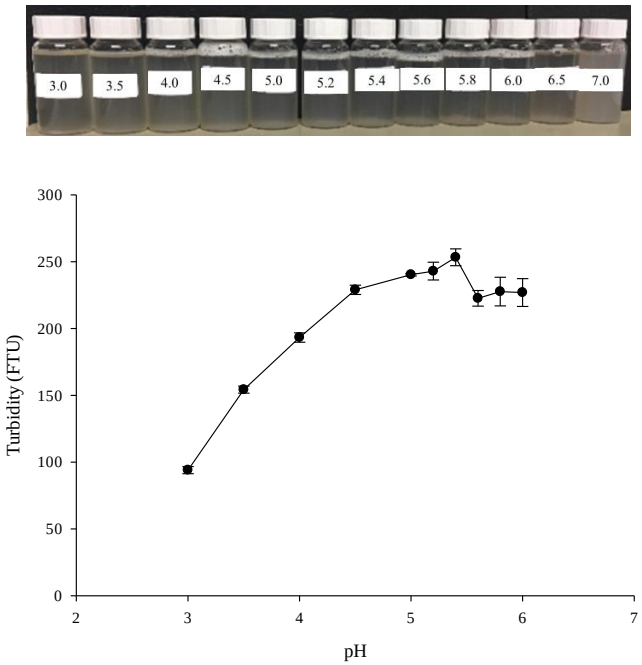


Figure 6.15: Macroscopic appearance of the karaya gum/chitosan mixture 6:5 (w/w) and its turbidity plotted as a function of pH (data are displayed with standard error bars).

A maximum in the turbidity profile of karaya gum/chitosan 6:5 (w/w) combination was observed at pH 5.4 (see Figure 6.15). This was, as suspected, in accordance with the apparent zeta potential data and helped confirm the exact pH at which complex coacervation should happen.

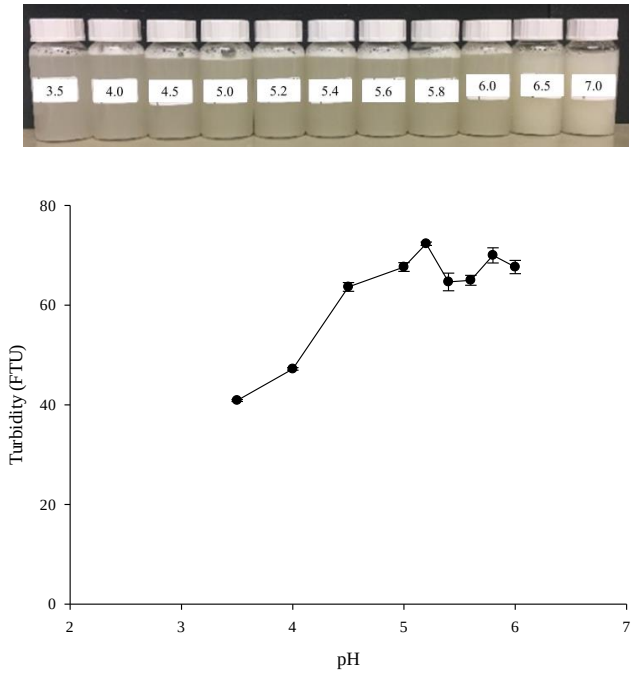


Figure 6.16: Macroscopic appearance of the corn starch/chitosan mixture 3:2 (w/w) and its turbidity plotted as a function of pH (data are displayed with standard error bars).

A maximum in the turbidity profile of corn starch/chitosan 3:2 (w/w) combination was observed at pH 5.2 (see Figure 6.16). This was also in accordance with the apparent zeta potential data and helped specify the exact pH at which the maximum electrostatic interaction should occur.

6.4.3 Promising combinations

6.4.3.1 Entrapment efficiency

As previously explained (see **Chapter 5**), the entrapment efficiency of the particles in liquid phase was quantified prior to spray drying (see Figure 6.17) in order to make sure the encapsulation using the new combinations was successful, and thus save time and money.

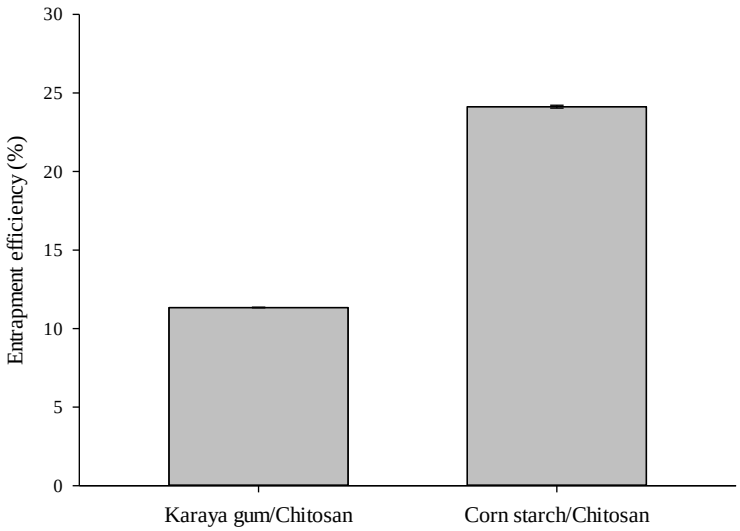


Figure 6.17: Average entrapment efficiency of the wet capsules obtained by complex coacervation with karaya gum/chitosan and corn starch/chitosan combinations (data are displayed with standard error bars).

An average entrapment efficiency of 11.34% ± 0.02% was obtained for the batch made with karaya gum and chitosan (see Figure 6.17), and 24.13 ± 0.09% for corn starch interacting with chitosan. The tiny error bars attested of the precision of the measurements.

These results confirmed that, in both cases, the encapsulation was successful in entrapping L-carvone with the experimental conditions established thanks to zeta potential and turbidity measurements. Although the entrapment efficiency was quite a lot lower for the karaya gum/chitosan 6:5 (w/w) combination compared to gum arabic/chitosan 6:1 (w/w), it was slightly higher for the corn starch/chitosan combination. Quite surprisingly, the latter seemed to be the most promising combination for this process, which could be due to its higher gelation capacities or the structure of starch granules (Qi and Tester, 2019).

6.4.3.2 Morphology

The 2D morphology of wet and dry capsules was also checked by light microscopy (see Figures 6.18 and 6.19) in order to make sure that proper capsules were obtained.

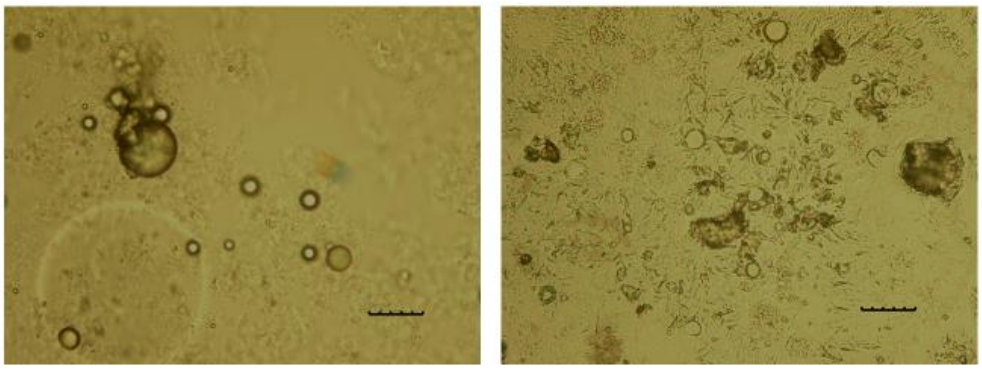


Figure 6.18: (a) Wet and (b) dry particles obtained with the karaya gum/chitosan 6:5 (w/w) combination, observed by light microscopy (all scales represent 50 μm).

For the karaya gum/chitosan combination, it seemed that some coacervate phase was successfully formed (see Figure 6.18 (a)) but that it neither surrounded the oil droplets properly nor in a homogeneous way. The resulting dry capsules were mostly burst with a few darker, irregular particles (see Figure 6.18 (b)), which could explain the lower entrapment efficiency.

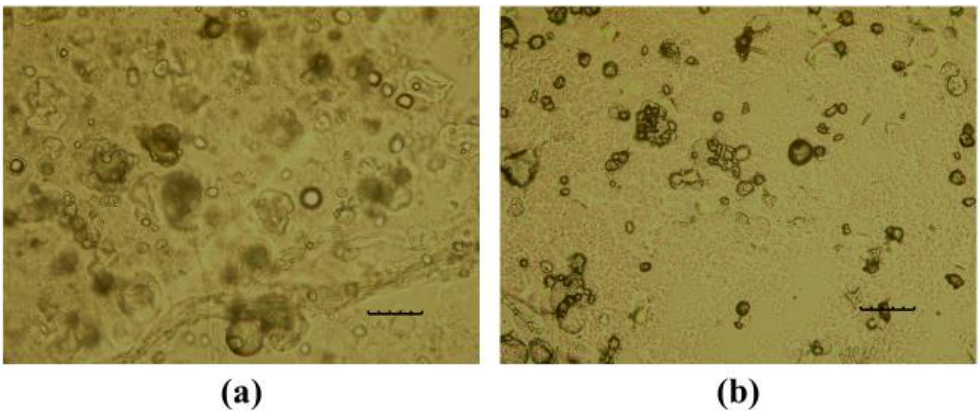


Figure 6.19: (a) Wet and (b) dry particles obtained with the corn starch/chitosan 3:2 (w/w) combination, observed by light microscopy (all scales represent 50 μm).

For the corn starch/chitosan combination, a much better coacervation shell was obtained (see Figure 6.19 (a)), sometimes even with the characteristic "eye shape". The resulting dry capsules also had a much more spherical shape (see Figure 6.19 (b)).

As a result, only the corn starch/chitosan coacervated capsules were further processed by spray drying. The dry powder obtained after this extra processing step also had a spherical morphology (see Figure 6.20), similar to what was obtained with gum arabic and chitosan (see **Chapter 5**).

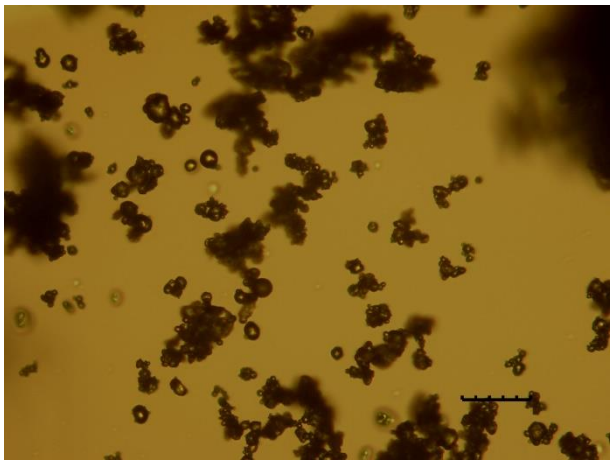


Figure 6.20: Light microscopy observations of dry powder corn starch/chitosan coacervated capsules directly spray dried (all scales represent 50 μm).

6.4.3.3 Payload

The entrapment efficiency and payload of the newly obtained corn starch/chitosan 3:2 (w/w) capsules were compared with the ones measured for the double coated gum arabic/chitosan 6:1 (w/w) capsules (see **Chapter 5**).

While the entrapment efficiency was only slightly higher following the coacervation process for corn starch/chitosan 3:2 (w/w), the final payload after spray drying was significantly higher ($p < 0.001$) with an average of $3.39\% \pm 0.10\%$ compared to $2.56\% \pm 0.02\%$ for the gum

arabic/chitosan double coated particles. It is also important to note that the capsules obtained with the new combination seemed to have better physical and mechanical properties since they did not require an extra coating layer to maintain their mechanical integrity after drying, which would also save both time and money.

6.4.3.4 Mechanical strength

30 individual particles were randomly selected for compression to represent the diversity of the sample. The size of the compressed particles ranged between 9 and 31 μm, which was in the same order as the size of those compressed in **Chapter 5**.

For this batch (corn starch/chitosan) most of the capsules (66.7%) showed clear rupture under compression, which was a higher percentage than any of the previous batches obtained for the gum arabic/chitosan coacervated capsules further coated by spray coating/drying (see **Chapter 5**). This may possibly be due to the hollow structure of starch granules.

Furthermore, no double rupture event profile was observed throughout the sample, which made sense since those particles did not have any extra coating layer.

The typical compression profile was plotted as the applied force versus the probe displacement (see Figure 6.21). The compression of the capsules was identified by a rise in the applied force due to the deformation of the particle, followed by a sudden drop (1) as a result of the bursting of the shell, and finally another steep increase (2) corresponding to the compression of the glass slide.

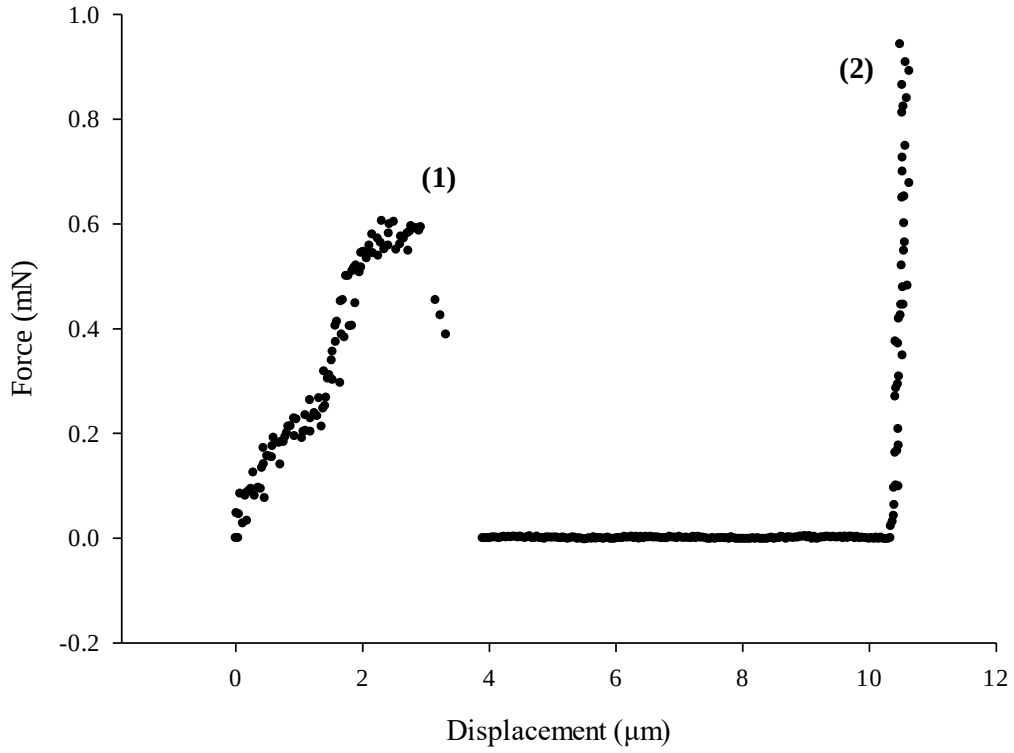


Figure 6.21: Compression profile of a 13 μm coacervated capsule obtained with the corn starch/chitosan 3:2 (w/w) combination, showing a single rupture event when compressed by micromanipulation (1) rupture event (2) compression of the capsule debris and glass slide.

Among the ruptured particles, a minority of those (15%) displayed a multiple rupture event compression profile (see Figure 6.22). This profile is typical of spray dried microspheres (Zhang and Adams, 2014) as several droplets of oil are embedded in the wall material matrix. This phenomenon could possibly result from a small amount of non-coacervated wall material encapsulating some free L-carvone oil, remaining in the liquid phase, by direct spray drying.

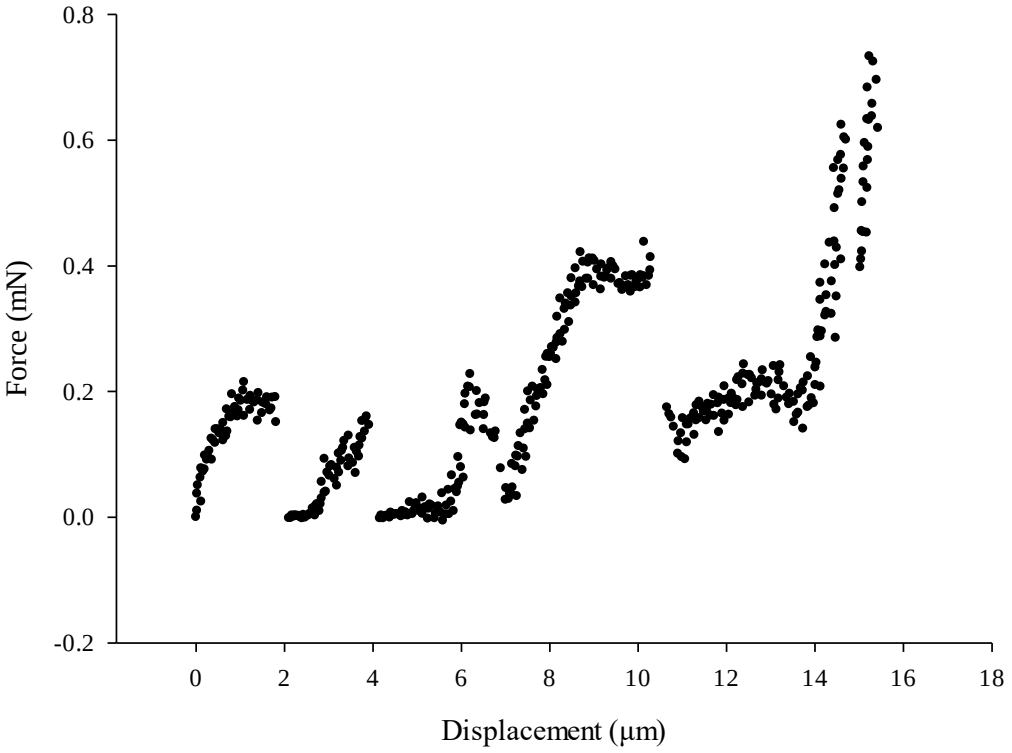


Figure 6.22: Compression profile of a 31 μm coacervated capsule obtained with the corn starch/chitosan 3:2 (w/w) combination showing several rupture events, obtained when compressed by micromanipulation.

The rupture force versus the diameter of the particles was plotted (see Figure 6.23), and gave a scattered plot due to the polydispersity and natural variation of the capsules.

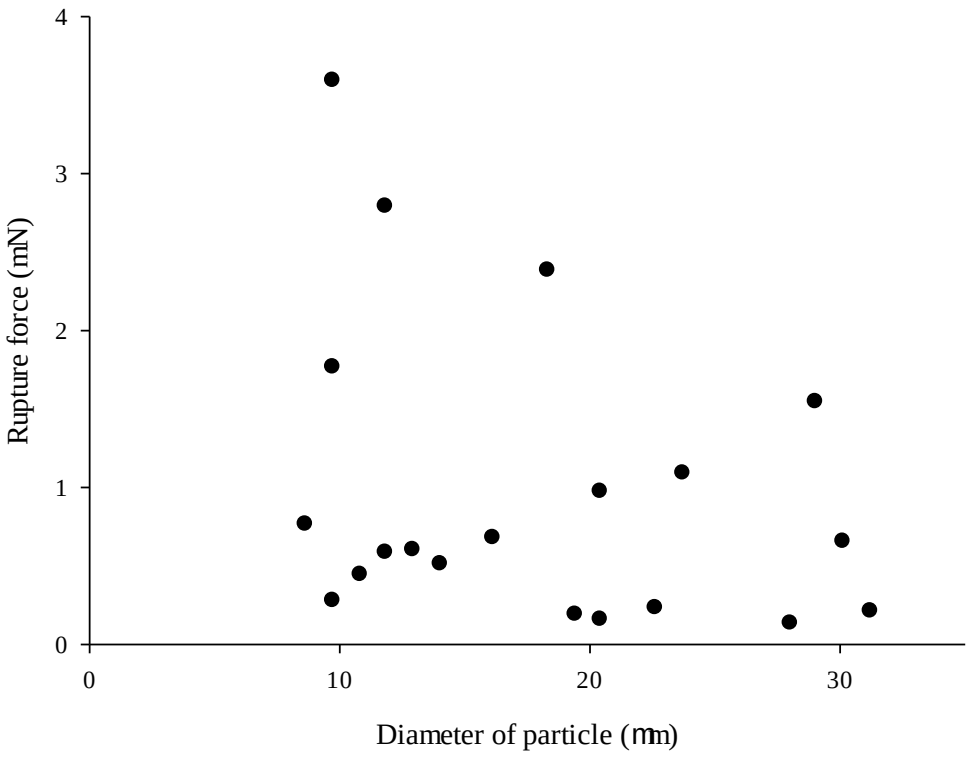


Figure 6.23: Rupture force versus particle diameter for coacervated capsules obtained with the corn starch/chitosan 3:2 (w/w) combination.

The nominal rupture stress versus particle diameter was also plotted (see Figure 6.24), which seemed to decrease with the diameter in general, confirming the expected conclusion that smaller capsules are harder to break than bigger ones.

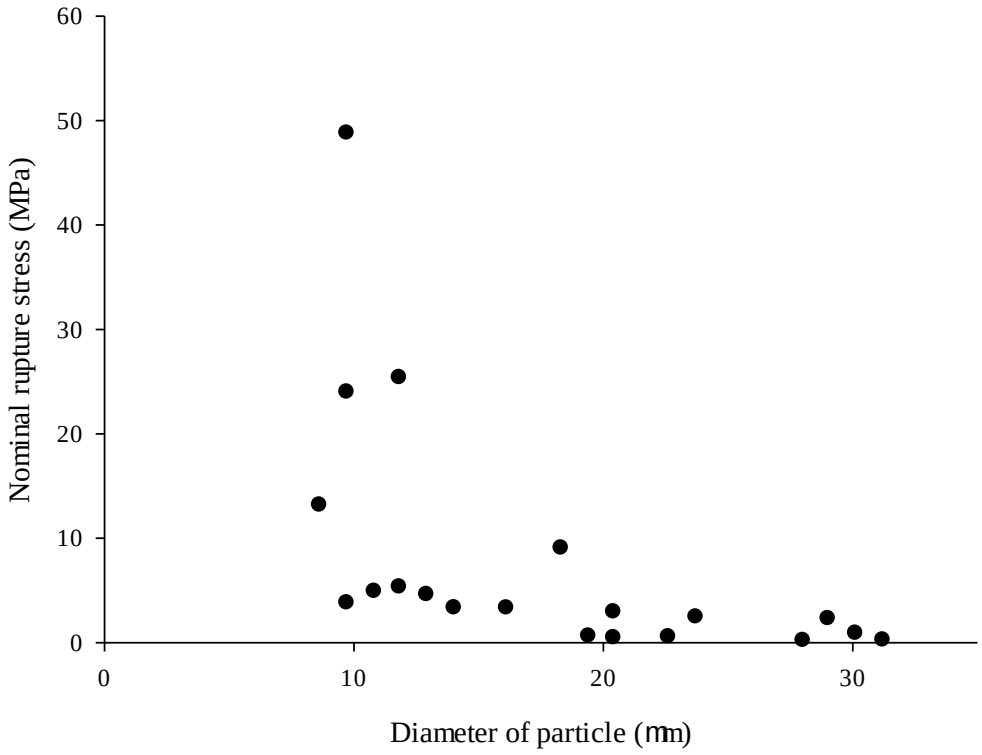


Figure 6.24: Nominal rupture stress versus particle diameter for coacervated capsules obtained with the corn starch/chitosan 3:2 (w/w) combination.

When plotting the deformation at rupture versus the particle diameter (see Figure 6.25), it was noticed that this parameter did not seemed to be size dependent, as observed for the previous capsules with GA/Chi double coating (see **Chapter 5**).

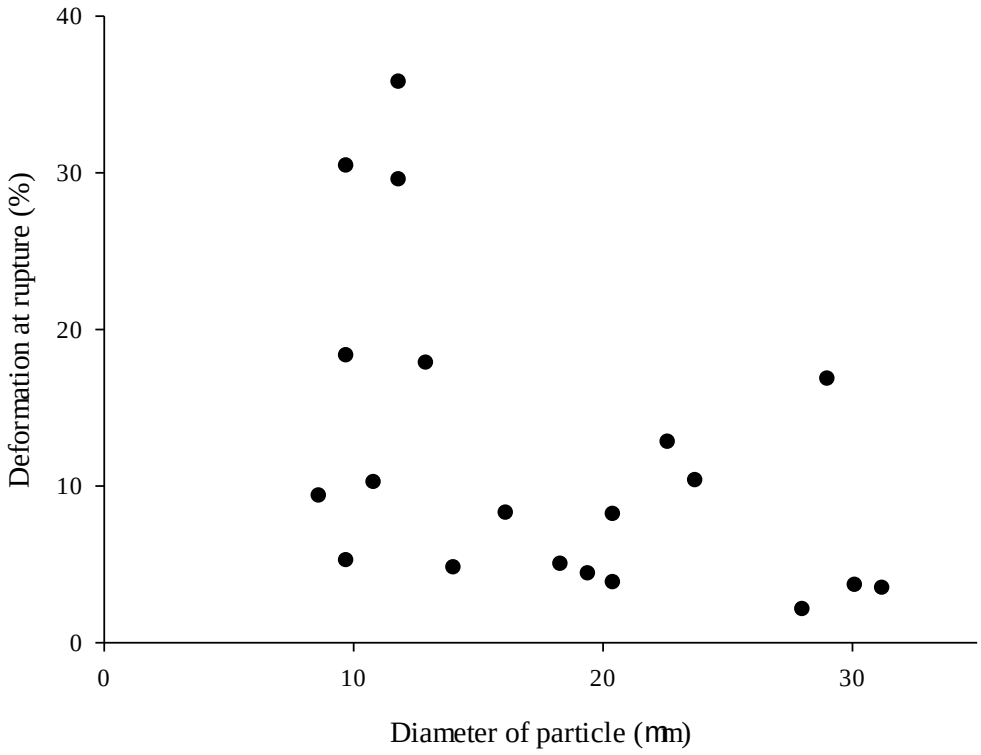


Figure 6.25: Deformation at rupture versus particle diameter for coacervated capsules obtained with the corn starch/chitosan 3:2 (w/w) combination.

This could mean that the behaviour of the corn starch/chitosan capsules was non-homogeneous among the batch and smaller capsules could be less brittle than bigger ones, which could again be due to the layered structure of starch granules. Another assumption would be that due to the limited charge of corn starch, only part of this material interacted with chitosan through complex coacervation, and that the remaining amount of chitosan underwent simple coacervation in alkali conditions and in the presence of sodium tripolyphosphate crosslinker. In this way, the simple layering by chitosan only could explain the more brittle particles, while the complex association with corn starch would have led to the less brittle ones, which is also in accordance with the gelling ability of this material.

Although this phenomenon did not seem advantageous at first, since it led to a non-homogeneous batch and the capsules properties would be difficult to control here, it could also prove to actually turn into a promising asset for chewing gum application. Indeed, if capsules with different mechanical properties could be obtained in one batch, this could provide a flavour release in gum which would vary according to different compression conditions and could possibly be triggered at different times.

6.4.4 Trials with proteins (WPI)

Although the use of proteins was not particularly desired for this project, the previous combinations with gelling polysaccharides were also investigated, out of scientific curiosity, by replacing chitosan with whey protein. A lot of gelling problems were encountered for the previous combinations when adding the chitosan solution, and the use of less viscous protein solutions was thought to help limit this issue as well as offer a wider range of possibilities for the use of complex coacervation in the food industry.

6.4.4.1 Polymer mixing ratio

The apparent zeta potential as well as the strength of the electrostatic interaction (SEI) of whey protein with different gelling polysaccharides (sodium alginate, ι-carrageenan, gellan gum, xanthan gum, citrus pectin, karaya gum, and corn starch) were plotted as a function of pH (see Figures 6.26 to 6.32).

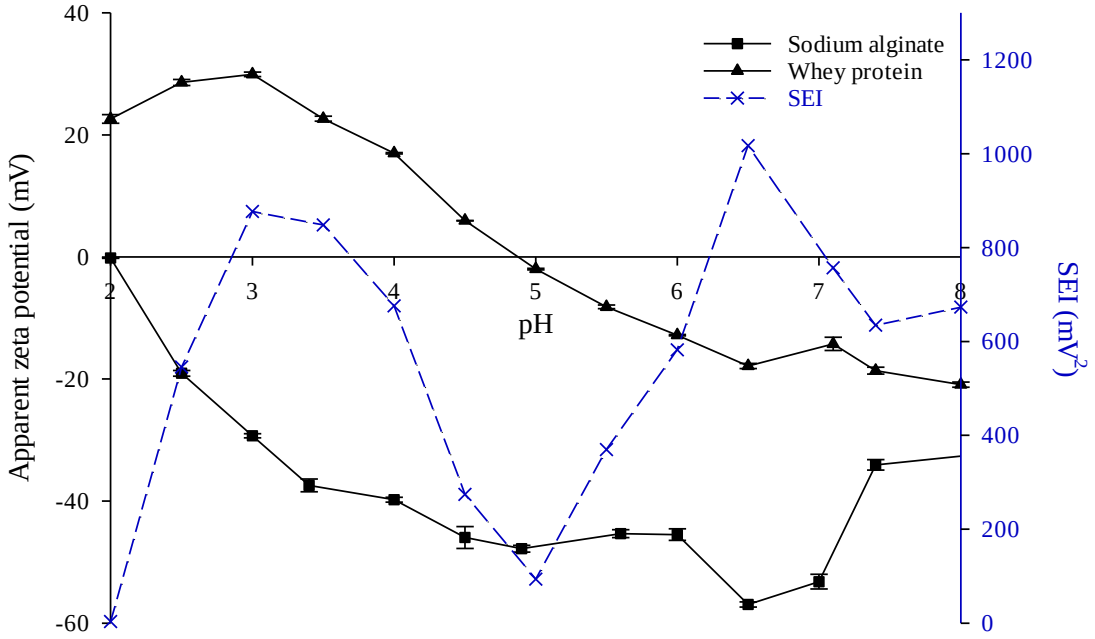


Figure 6.26: Apparent zeta potential of sodium alginate and whey protein plotted as a function of pH, displayed with the strength of their electrostatic interaction (SEI) at each pH value (apparent zeta potential data are displayed with standard error bars).

For the sodium alginate/whey protein combination, a ratio of 1:1 (w/w) was estimated at pH_{opt} = 3.0 $\pm$ 0.5 (see Figure 6.26).

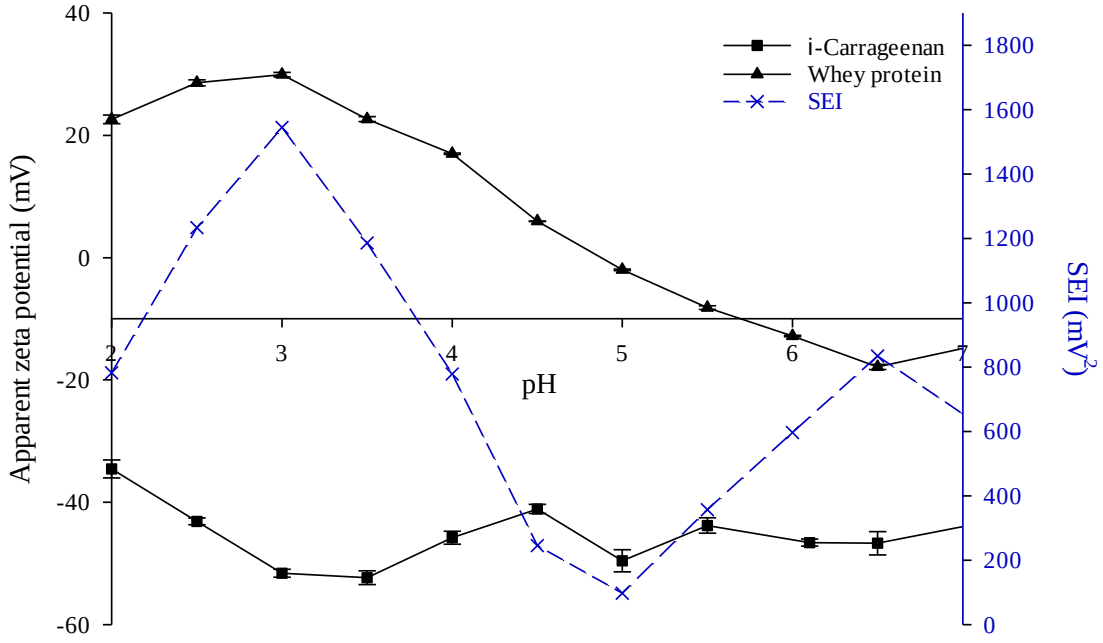


Figure 6.27: Apparent zeta potential of ι-carrageenan and whey protein plotted as a function of pH, displayed with the strength of their electrostatic interaction (SEI) at each pH value (apparent zeta potential data are displayed with standard error bars).

For the ι-carrageenan/whey protein combination, a ratio of 4:7 (w/w) was estimated at pH_{opt} = 3.0 $\pm$ 0.5 (see Figure 6.27).

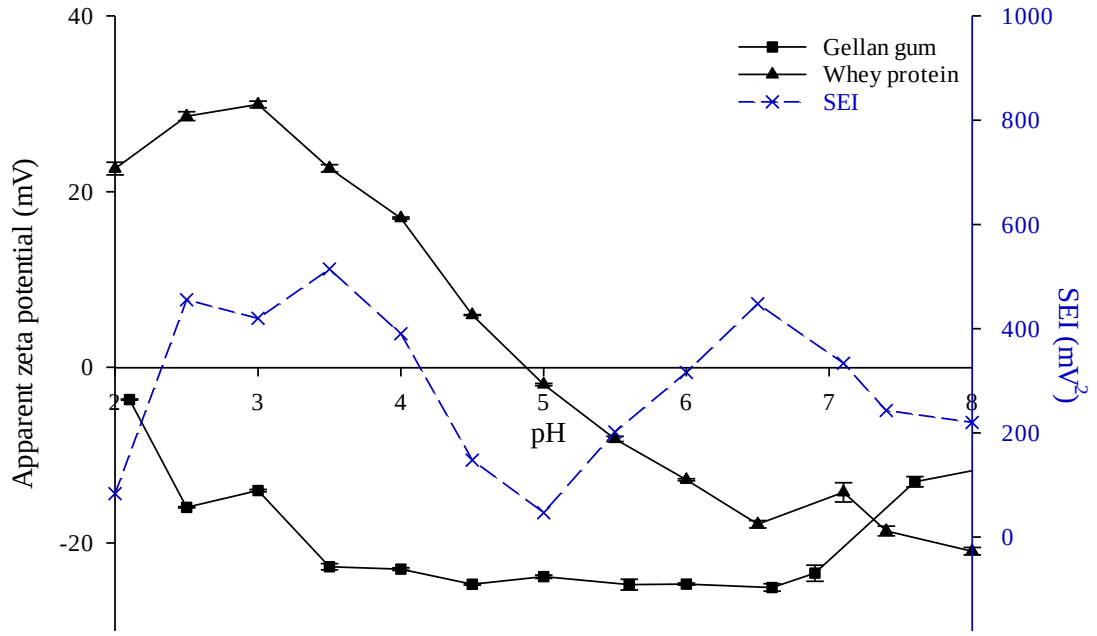


Figure 6.28: Apparent zeta potential of gellan gum and whey protein plotted as a function of pH, displayed with the strength of their electrostatic interaction (SEI) at each pH value (apparent zeta potential data are displayed with standard error bars).

For the gellan gum/whey protein combination, a ratio of 1:1 (w/w) was estimated at pH_{opt} = 3.5 $\pm$ 0.5 (see Figure 6.28).

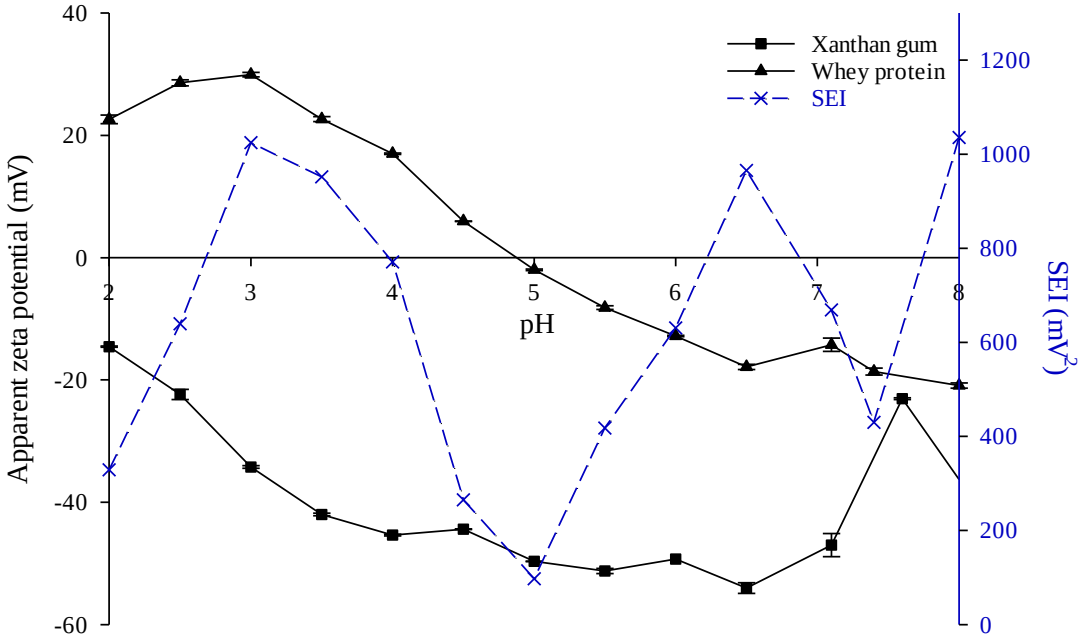


Figure 6.29: Apparent zeta potential of xanthan gum and whey protein plotted as a function of pH, displayed with the strength of their electrostatic interaction (SEI) at each pH value (apparent zeta potential data are displayed with standard error bars).

For the xanthan gum/whey protein combination, a ratio of 7:8 (w/w) was estimated at pH_{opt} = 3.0 $\pm$ 0.5 (see Figure 6.29).

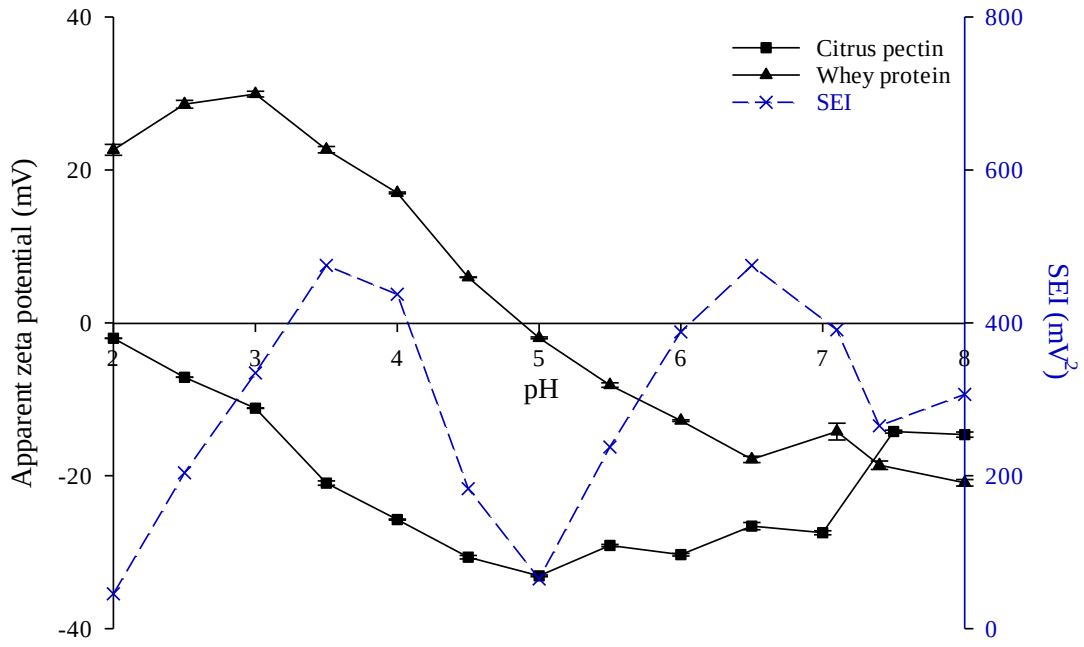


Figure 6.30: Apparent zeta potential of citrus pectin and whey protein plotted as a function of pH, displayed with the strength of their electrostatic interaction (SEI) at each pH value (apparent zeta potential data are displayed with standard error bars).

For the citrus pectin/whey protein combination, a ratio of 1:1 (w/w) was estimated at pH_{opt} = 3.5 $\pm$ 0.5 (see Figure 6.30).

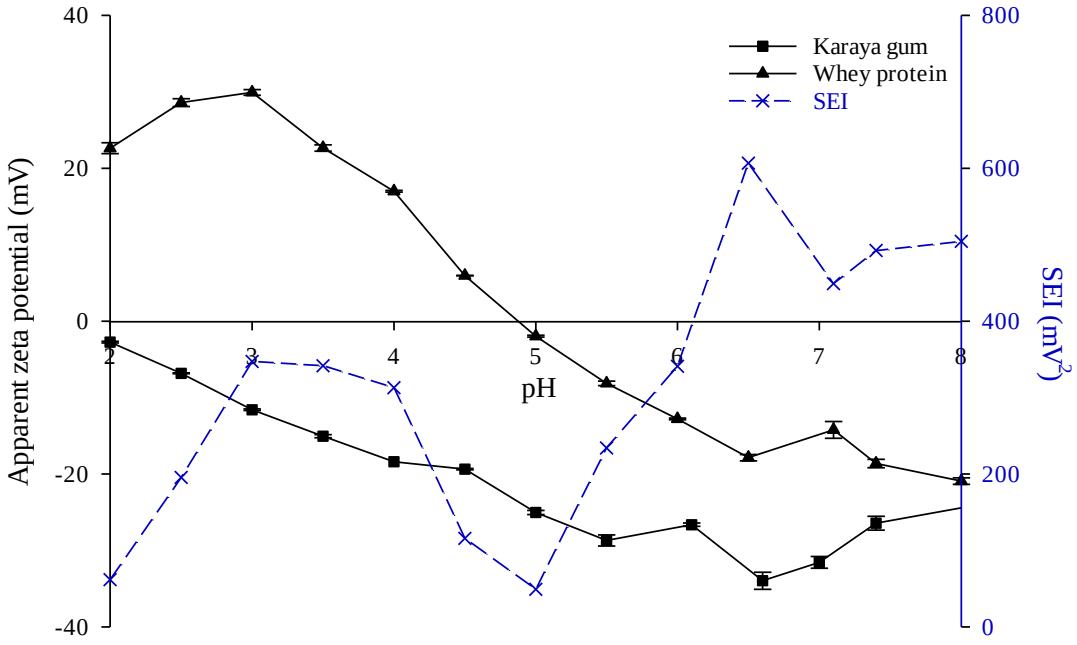


Figure 6.31: Apparent zeta potential of karaya gum and whey protein plotted as a function of pH, displayed with the strength of their electrostatic interaction (SEI) at each pH value (apparent zeta potential data are displayed with standard error bars).

For the karaya gum/whey protein combination, a ratio of 18:7 (w/w) was estimated at pH_{opt} = 3.0 $\pm$ 0.5 (see Figure 6.31).

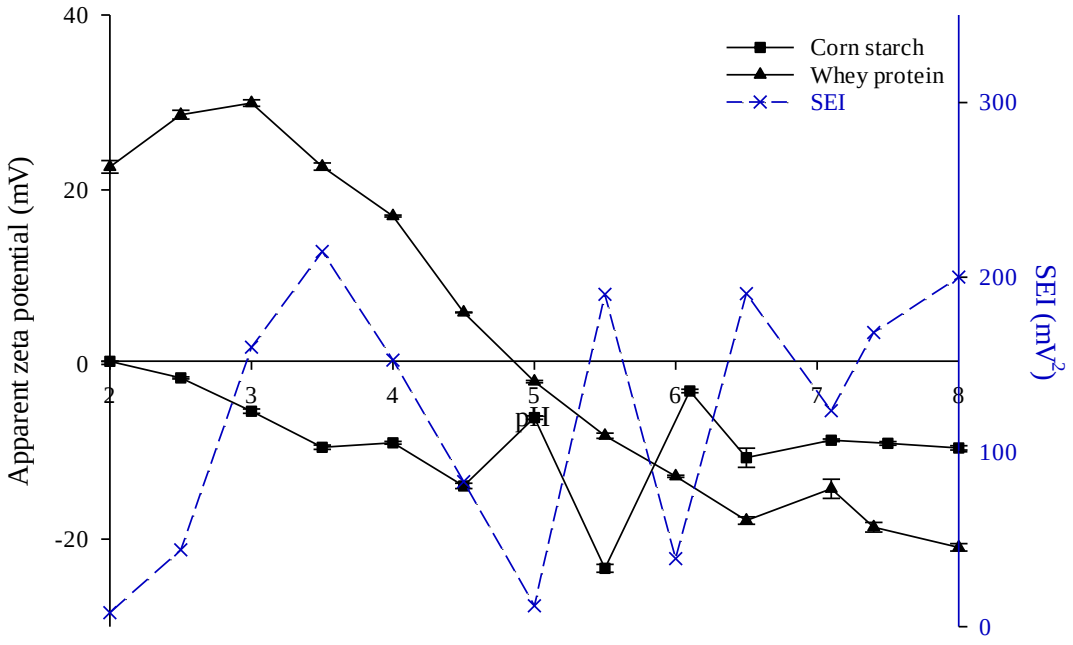


Figure 6.32: Measured apparent zeta potential of corn starch and whey protein plotted as a function of pH, displayed with the strength of their electrostatic interaction (SEI) at each pH value (apparent zeta potential data are displayed with standard error bars).

For the corn starch/whey protein combination, a ratio of 12:5 (w/w) was estimated at pH_{opt} = 3.5 $\pm$ 0.5 (see Figure 6.32).

6.4.4.2 Optimum pH

Following the mixing ratios determined by zeta potential measurements, the turbidity of pure WPI as well as the different polymer combinations was plotted as a function of pH (see Figures 6.33 to 6.38). The combinations of whey protein with xanthan gum and karaya gum were not further investigated as they respectively led to irreversible gelation and precipitation upon mixing, and this phenomenon was found to be independent of the pH.

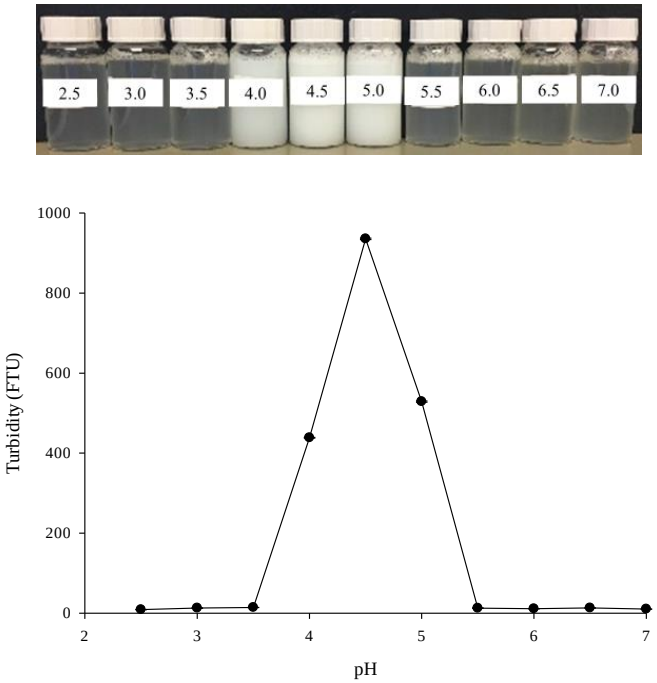


Figure 6.33: Macroscopic appearance of pure whey protein solution and its turbidity plotted as a function of pH (data are displayed with standard error bars).

It was noticed that whey protein was mostly leading to clear solutions except between pH 4.0 and 5.0, with a peak in turbidity around pH 4.5 (see Figure 6.33). This phenomenon can be explained by the formation of a precipitate as whey protein is insoluble in water close to its isoelectric point (pI), which should indeed be between pH 4.4 and 5.2 (see **Chapter 3**).

This behaviour should be taken into account when interpreting the turbidity results.

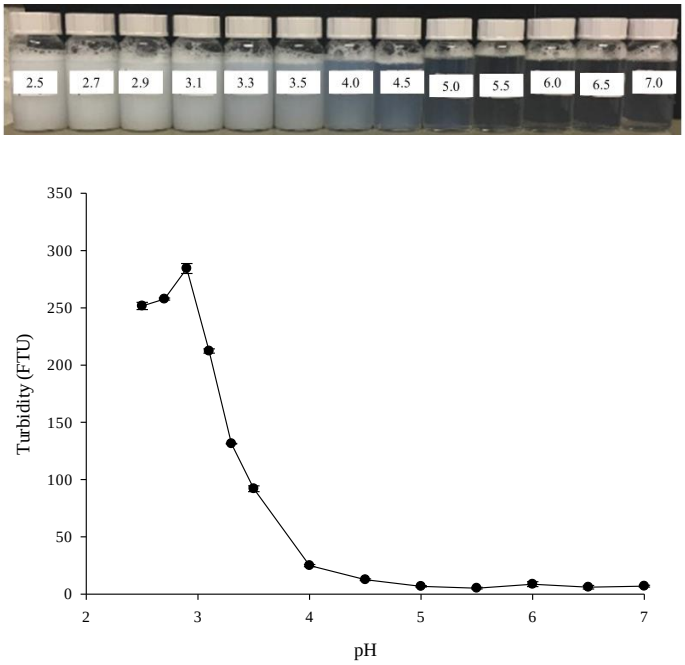


Figure 6.34: Macroscopic appearance of the sodium alginate/whey protein mixture 1:1 (w/w) and its turbidity plotted as a function of pH (data are displayed with standard error bars).

A maximum in the turbidity profile of sodium alginate/whey protein 1:1 (w/w) combination was observed at pH 2.9 (see Figure 6.34), which was in accordance with the zeta potential measurements. There was a good confidence that this result was representative of the formation of complexes as it was far from the pI of whey protein.

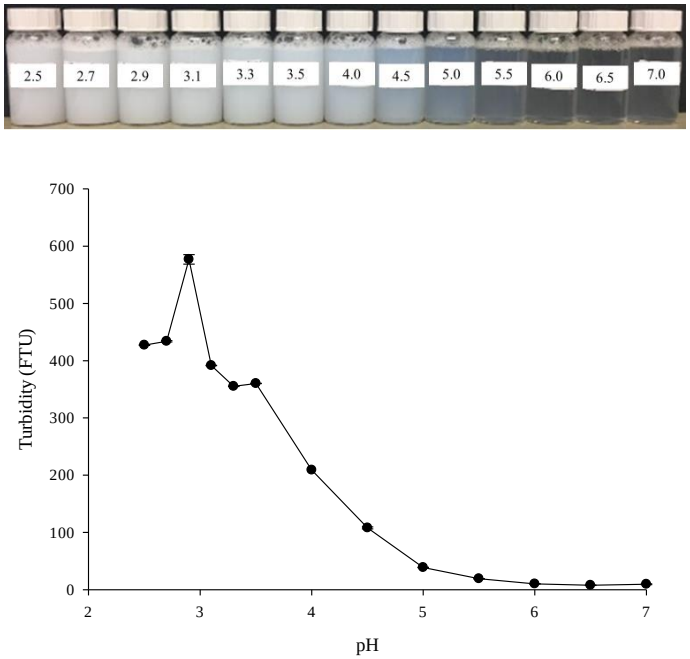


Figure 6.35: Macroscopic appearance of the ι-carrageenan/whey protein mixture 4:7 (w/w) and its turbidity plotted as a function of pH (data are displayed with standard error bars).

A maximum in the turbidity profile of ι-carrageenan/whey protein 4:7 (w/w) combination was observed at pH 2.9 (see Figure 6.35), which was in accordance with the zeta potential measurements. There was a good confidence that this result was representative of the formation of complexes as it was far from the pI of whey protein.

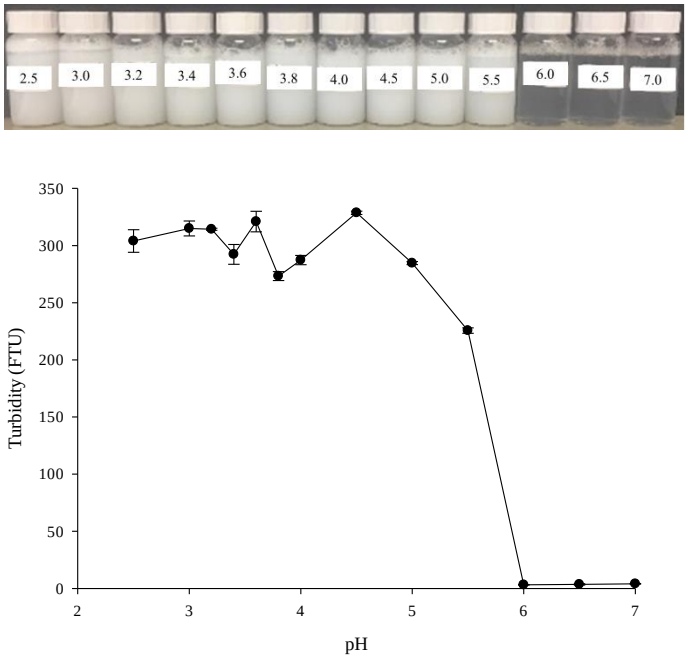


Figure 6.36: Macroscopic appearance of the gellan gum/whey protein mixture 1:1 (w/w) and its turbidity plotted as a function of pH (data are displayed with standard error bars).

A maximum in the turbidity profile of gellan gum/whey protein 1:1 (w/w) combination was observed at pH 4.5 (see Figure 6.36), which corresponded to the pI of whey protein. A secondary peak was also observed at pH 3.6, which would be more in accordance with zeta potential measurements.

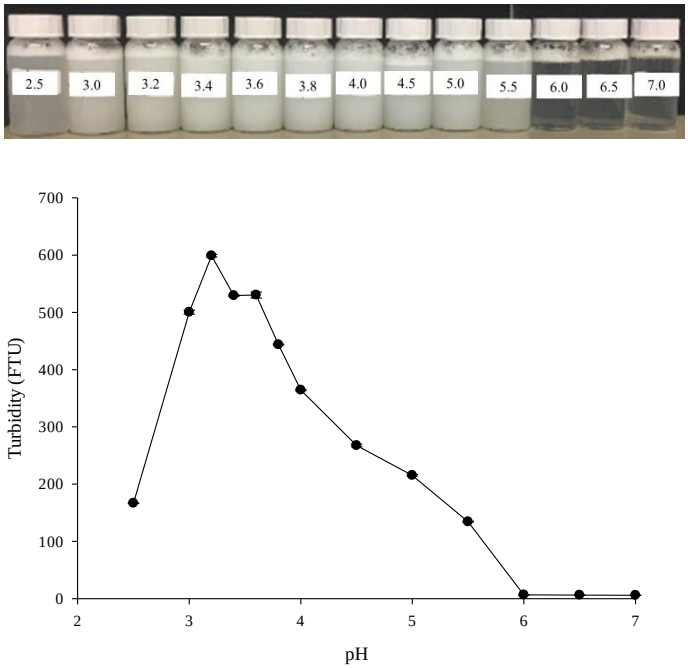


Figure 6.37: Macroscopic appearance of the citrus pectin/whey protein mixture 1:1 (w/w) and its turbidity plotted as a function of pH (data are displayed with standard error bars).

A maximum in the turbidity profile of citrus pectin/whey protein 1:1 (w/w) combination was observed at pH 3.2 (see Figure 6.37), which was in accordance with the zeta potential measurements. There was a good confidence that this result was representative of the formation of complexes as it was far from the pI of whey protein.

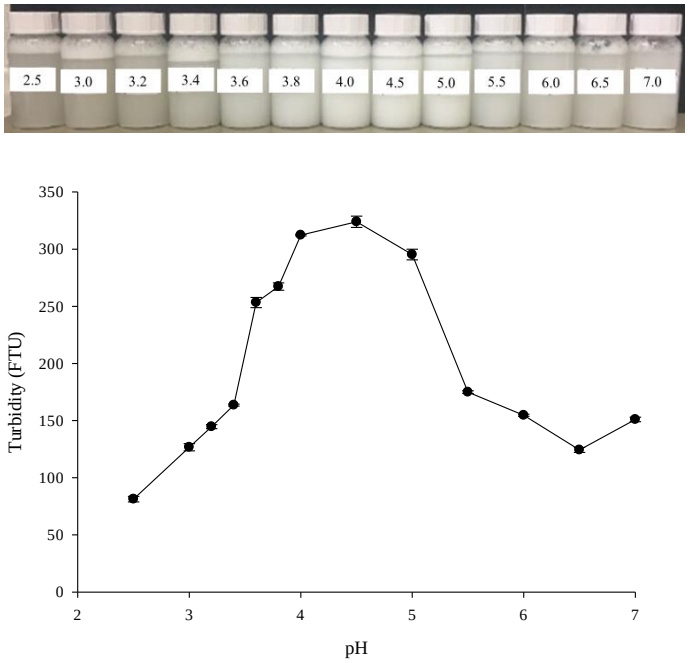


Figure 6.38: Macroscopic appearance of the corn starch/whey protein mixture 12:5 (w/w) and its turbidity plotted as a function of pH (data are displayed with standard error bars).

A maximum in the turbidity profile of corn starch/whey protein 12:5 (w/w) combination was observed at pH 4.5 (see Figure 6.38), which corresponded to the pI of whey protein. This value was slightly out of the pH range determined by zeta potential measurements, although no clear secondary peak could be observed.

The complex coacervation batches were made based on the values determined by the previous method.

6.4.4.3 Entrapment efficiency and morphology

The entrapment efficiency was measured according to the method previously detailed in **Chapter 5**, and plotted for the different batches made by the complex coacervation method based on the results obtained from the zeta potential and turbidity measurements (see Table 6.3 and Figure 6.39). The entrapment efficiency obtained for the sodium alginate/WPI combination was not plotted as it was zero.

Table 6.3: Complex coacervation conditions for the combination of whey protein with different gelling polysaccharides (sodium alginate, ι-carrageenan, gellan gum, citrus pectin, corn starch), based on zeta potential and turbidity measurements.

Combinations	Polymer mixing ratio (w/w)	Coacervation pH
Sodium alginate/WPI	1:1	2.9
ι-Carrageenan/WPI	4:7	2.9
Gellan gum/WPI	1:1	4.5
Citrus pectin/WPI	1:1	3.0
Corn starch/WPI	12:5	4.5

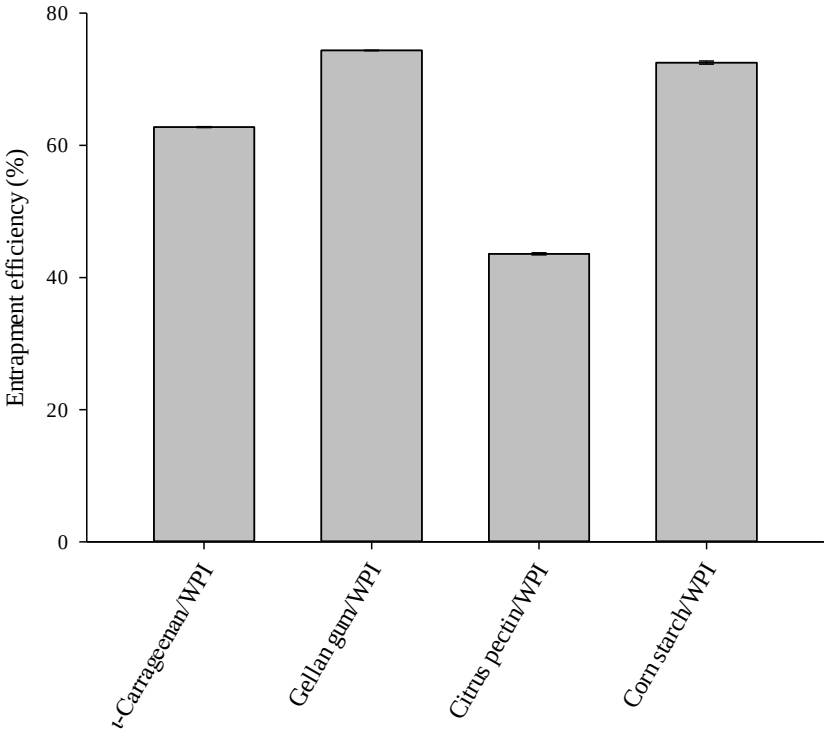


Figure 6.39: Average entrapment efficiency of the wet capsules obtained by complex coacervation between whey protein isolate (WPI) and different gelling polysaccharides (ι-carrageenan, gellan gum, citrus pectin, corn starch) (data are displayed with standard error bars).

The measured entrapment efficiencies were very high, but were not reflective of the actual values due to limitations in the measurement method. It was indeed observed that when WPI

was used as wall material, the shell debris were particularly prompt to redisperse in ethanol following the centrifugation step, and absorbed light at the same wavelength as L-carvone. This meant there should be a baseline to subtract from these values, which was not measured here due to time limitation, resulting from the wall material traces. Although the measurement method should be adapted in the case of whey protein particles, it was still judged as a useful way to compare the difference in flavour retention between the different batches; with the lowest value obtained for the citrus pectin/WPI combination, and gellan gum/WPI and corn starch/WPI displaying the highest values.

The 2D morphology of each capsule suspension was also observed by light microscopy (see Figures 6.40 to 6.44). For all batches but the citrus pectin/WPI combination (see Figure 6.43), the formation of a coacervate phase could be seen from the observation of particles in liquid phase (see Figures 6.40 (a) to 6.42 (a), and 6.44 (a)), which proved the effectiveness of the zeta potential measurements associated with turbidity measurements method in identifying the conditions for complex coacervation. The citrus pectin batch was the only sample which did not coacervate as expected, possibly because the pectin solution had a high sugar content to promote the gelation, which could have affected the interactions between pectin and the protein.

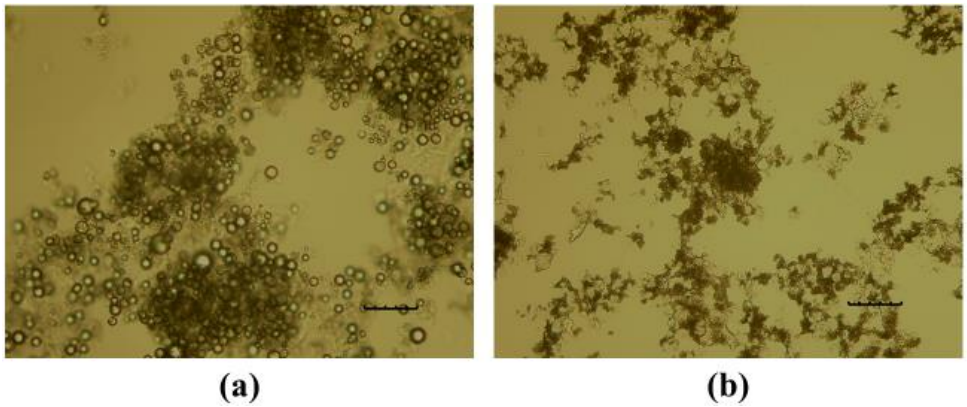


Figure 6.40: (a) Wet and (b) dry particles obtained with the sodium alginate/whey protein 1:1 (w/w) combination, observed by light microscopy (all scales represent 50 μm).

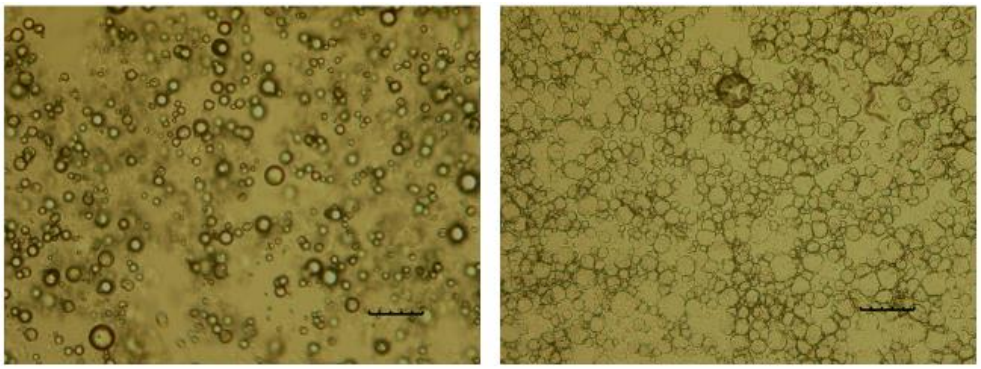


Figure 6.41: (a) Wet and (b) dry particles obtained with the ι-carrageenan/whey protein 4:7 (w/w) combination, observed by light microscopy (all scales represent 50 μm).

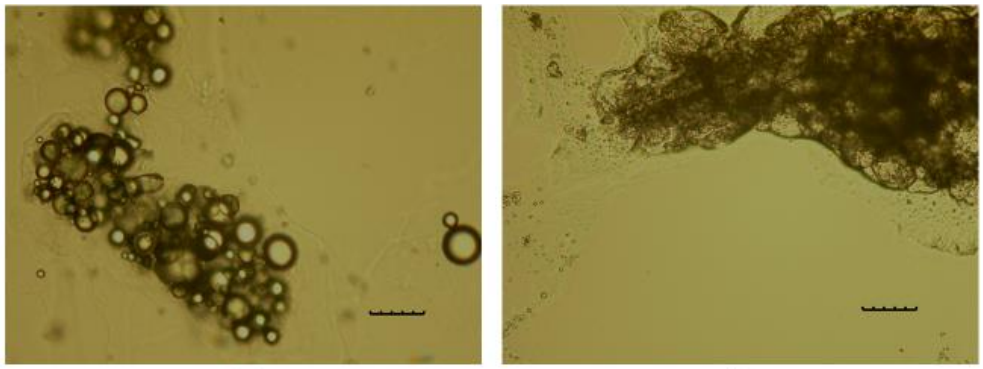


Figure 6.42: (a) Wet and (b) dry particles obtained with the gellan gum/whey protein 1:1 (w/w) combination, observed by light microscopy (all scales represent 50 μm).

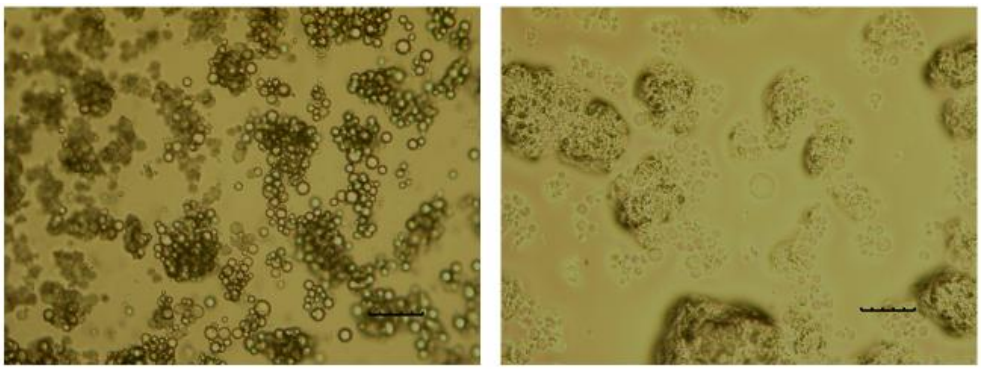


Figure 6.43: (a) Wet and (b) dry particles obtained with the citrus pectin/whey protein 1:1 (w/w) combination, observed by light microscopy (all scales represent 50 μm).

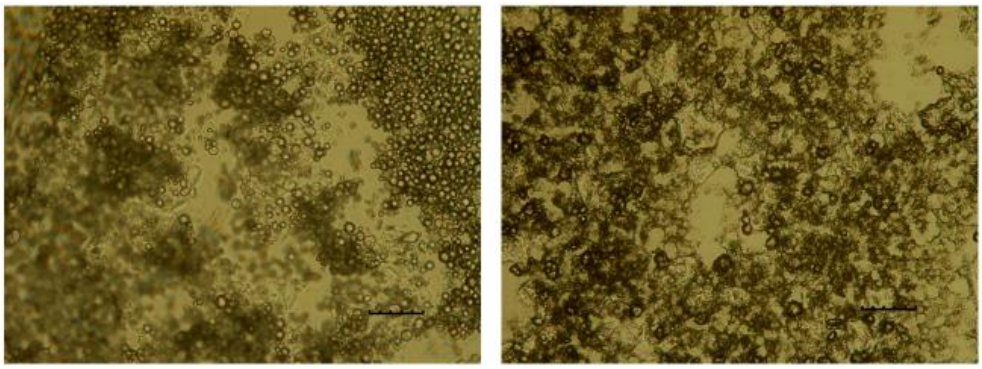


Figure 6.44: (a) Wet and (b) dry particles obtained with the corn starch/whey protein 12:5 (w/w) combination, observed by light microscopy (all scales represent 50 μm).

Further observations could be made from the imaging of the dry particles (see Figures 6.40 (b) to 6.44 (b)). The sodium alginate/WPI batch (see Figure 6.40) proved that morphology characterisations were not enough to confirm the success of the complex coacervation combinations, as small aggregated spherical capsules seemed to have been obtained after drying, but no oil was retained as the entrapment efficiency was zero. The particles obtained from the ι-carrageenan/WPI combination were not stable as they burst when dried in open air (see Figure 6.41). The capsules obtained from the gellan gum/WPI and corn starch/WPI combinations appeared to resist the drying step (see Figures 6.42 (b) and 6.44 (b)), which was in agreement with the entrapment efficiency data.

However, no flavour could be detected by sensory check from the capsules made with gellan gum and WPI (score of 0 on the scale). The aggregated “grape” complex aspect appeared similar to what was observed for the gum arabic/chitosan combination. It was thought that the gellan gum/WPI combination could still work but required further coating processing, and was therefore not further investigated.

The corn starch/WPI capsule suspension was dried by direct spray drying and further characterised.

6.4.4.4 Promising combination (corn starch/whey protein)

A payload of 5.83 ± 0.02% was measured according to the method previously detailed in **Chapter 5**. Similarly to what was observed for the entrapment efficiency measurements, the actual payload value may be a bit lower than the measured value. It is believed a baseline value should be subtracted from this result due to the light absorption of suspended shell debris, which showed the limitations of the method when whey protein was used as the wall material, as commented above.

30 individual particles were randomly selected for compression to represent the diversity of the sample. Capsules between 11 and 30 μm were thus characterised by the micromanipulation technique. For this batch (corn starch/WPI 12:5 (w/w)), 43.3% of particles showed clear rupture under compression.

The compression profile was plotted as the applied force versus the probe displacement (see Figure 6.45).

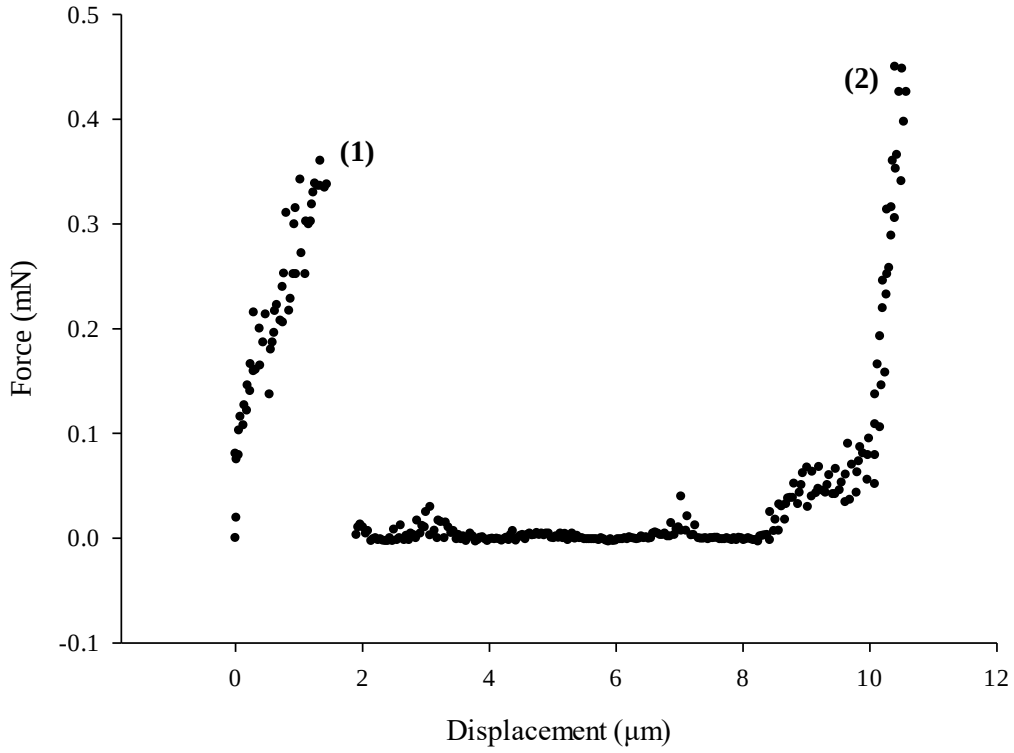


Figure 6.45: Compression profile of a 12 μm coacervated corn starch/whey protein 12:5 (w/w) capsule showing a single rupture event, obtained by micromanipulation (1) rupture event (2) compression of the capsule debris and glass slide.

Some of the ruptured particles (23%) showed a two rupture event compression profile (see Figure 6.46), although they were not further coated by a secondary layer. None exhibited a multiple rupture event profile like the corn starch/chitosan capsules did.

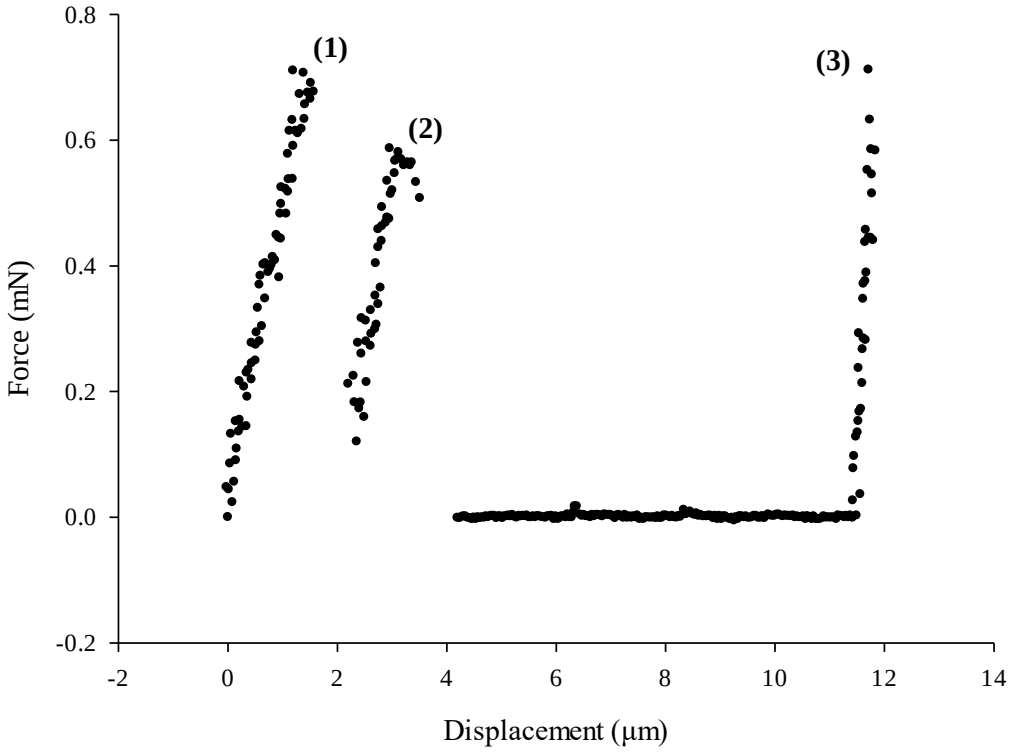


Figure 6.46: Compression profile of a 12 μm coacervated corn starch/whey protein 12:5 (w/w) showing two rupture events, obtained by micromanipulation (1) first rupture event (2) second rupture event (3) compression of the capsule debris and glass slide.

The compression profile with two rupture events suggested those capsules presented two coating layers, contrary to expectations. This phenomenon was thought to possibly result from the fact that complex coacervation was carried out at a pH close to the pI of the protein, and part of the WPI was under precipitate form at this pH. Therefore, there may have been an excess of dissolved corn starch which did not interact with the protein precipitate, and could have added a secondary layer to the coacervated capsules when the suspension was spray dried.

This batch displayed mechanical properties which appeared similar to what could be observed for the capsules with gum arabic/chitosan double coating (see Figures 6.47 to 6.49 and **Chapter 5**).

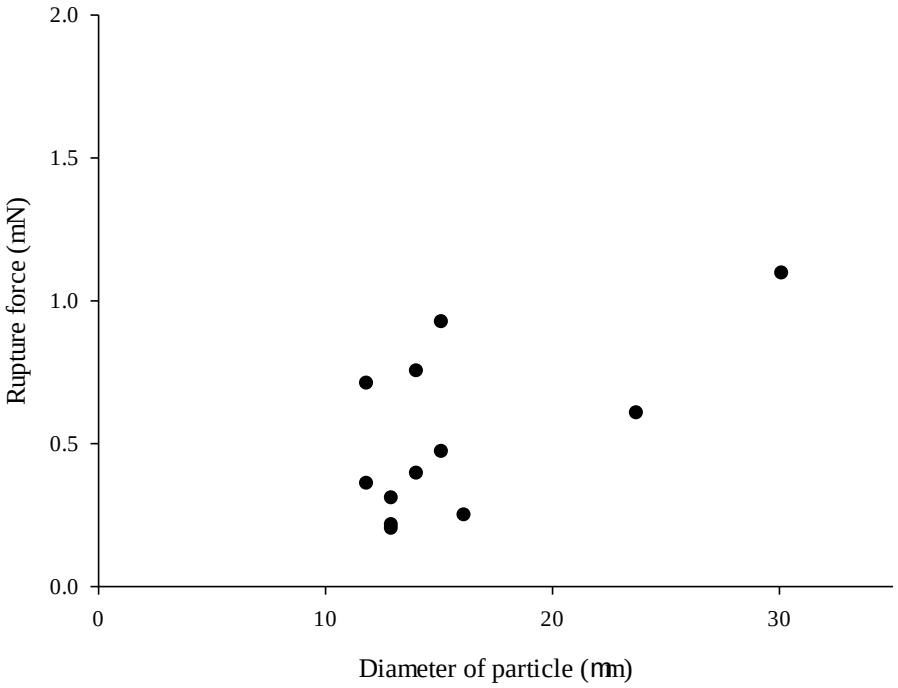


Figure 6.47: Rupture force versus particle diameter for coacervated particles obtained with the corn starch/whey protein 12:5 (w/w) combination.

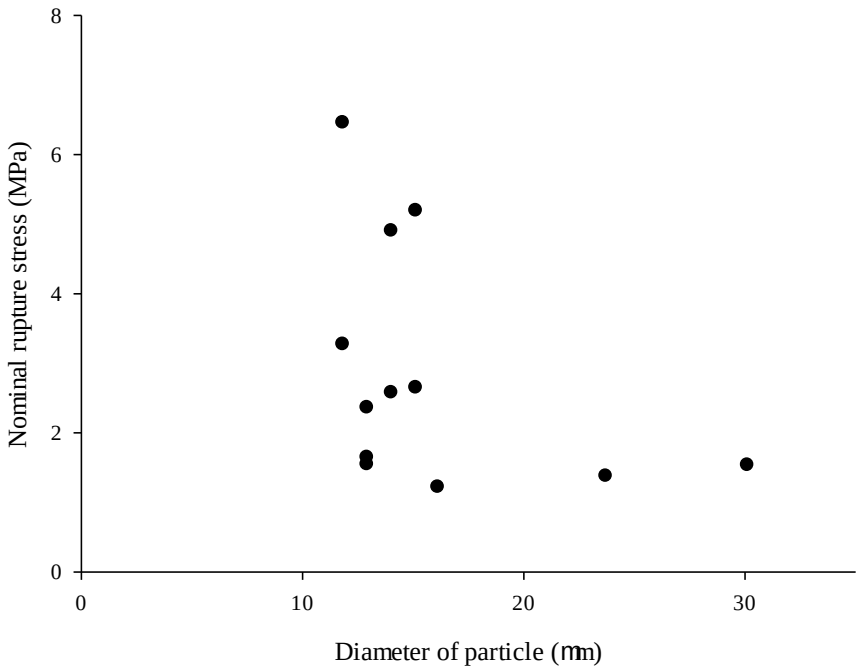


Figure 6.48: Nominal rupture stress versus particle diameter for coacervated capsules obtained with the corn starch/whey protein 12:5 (w/w) combination.

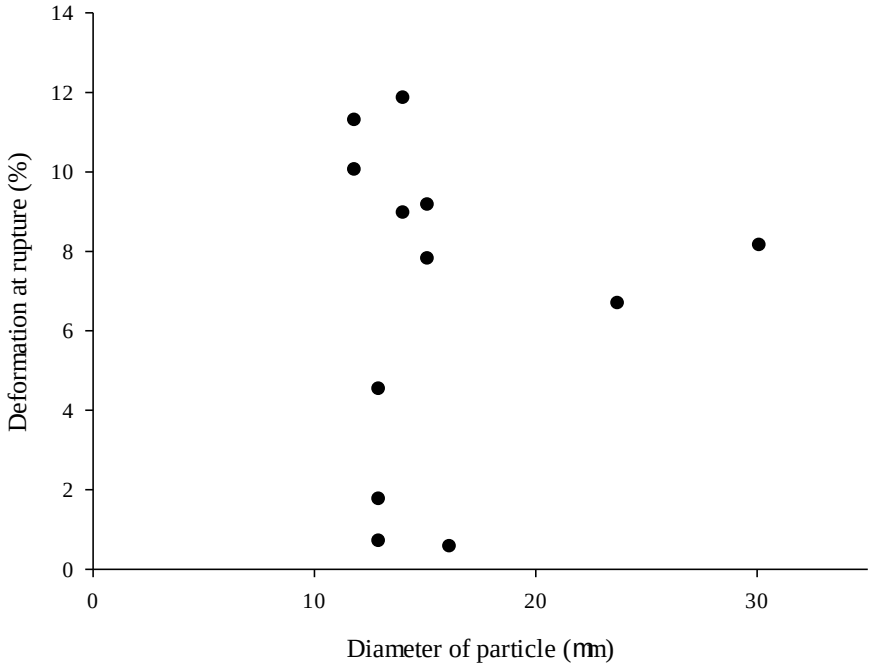


Figure 6.49: Deformation at rupture versus particle diameter for coacervated capsules obtained with the corn starch/whey protein 12:5 (w/w) combination.

The mean value of each mechanical parameter (rupture force, nominal rupture stress and deformation at rupture) was calculated for each characterised batch (gum arabic/chitosan 6:1 (w/w), corn starch/chitosan 3:2 (w/w), and corn starch/whey protein 12:5 (w/w)) (see Table 6.4), in order to compare the mechanical properties of the different capsules.

Table 6.4: Comparison of the different mechanical properties (rupture force, nominal rupture stress, deformation at rupture) obtained for the most promising batches (GA/Chi double coating, corn starch/chitosan single coating, and corn starch/WPI single coating).

Wall material	Diameter (µm)	Rupture force (mN)	Nominal rupture stress (MPa)	Deformation at rupture (%)
GA/Chi 6:1 double coating (w/w)	17.6 ± 1.6	0.8 ± 0.1	3.7 ± 0.8	11.9 ± 1.7
Corn starch/Chi 3:2 (w/w)	17.9 ± 1.7	1.0 ± 0.2	7.8 ± 2.7	12.0 ± 2.2
Corn starch/WPI 12:5 (w/w)	15.9 ± 1.6	0.5 ± 0.1	2.9 ± 0.5	6.8 ± 1.2

It was found that all batches displayed a similar size range ($p > 0.05$), which could be imposed by the processing steps rather than the nature of the capsule shell, or possibly the starch granules could have swollen due to oil absorption and compensate for the difference in size due to the extra layer for the gum arabic/chitosan capsules. The mechanical properties of the capsules did not display any significant difference either from one batch to the other ($p > 0.05$). This means the use of corn starch seemed more advantageous as only a single coating was used for both batches containing this material, compared to the gum arabic/chitosan capsules which had a double coating. This could confirm the previously suspected strengthening advantage of working with gelling materials in order to counter the weakness of food grade crosslinkers. Finally, the deformation at rupture was low for all batches, which reflected the sought brittleness which was obtained by this encapsulation method. It was noticed that the capsules produced with whey protein seemed more brittle in general than the capsules of the other two batches. This phenomenon could be due to the presence of precipitated whey protein particles in the shell due to carrying out the process close to the pI of the protein, but this assumption would need to be further checked, possibly by scanning electron microscopy (SEM) and/or transmission electron microscopy (TEM).

6.5 Conclusion

In this chapter, it was emphasized that experimental conditions for complex coacervation reported in the literature should be taken with extra care, especially when using polymers from natural origin, whose quality and properties can vary slightly from one batch to another.

The use of zeta potential measurements in combination with turbidity measurements was proven to be a useful and efficient tool for predicting the complex coacervation key parameters

(polymer ratio and optimum pH) for existing and novel polymer combinations, without having prior knowledge of their conditions of interaction. The limitations of this method were also emphasised when working with materials already displaying a turbid behaviour in solution.

Several new polysaccharide/polysaccharide combinations were successfully investigated using this exploratory methodology, although the possible options remained scarce due to the gelation between the different anionic polysaccharides and chitosan, which was one of the only cationic polysaccharide options.

Although corn starch was not expected to be charged in theory, it did show some negative charges at different pH, which could be due to its protein content, and its combination with chitosan and whey protein led to capsules with promising properties.

The investigation of combinations involving whey protein isolate instead of chitosan proved the further options offered by proteins for the use of complex coacervation encapsulation technique in food applications. The use of corn starch was once again confirmed to be a promising investigation lead.

CHAPTER 7 – Overall Conclusions and Future Prospects

Providing a technology for flavour delivery in the food industry is a challenging task as every type of food is different and the number of available materials is limited by food regulations. Food grade crosslinkers, such as tannic acid or transglutaminase for example, do not perform as well as the more commonly used glutaraldehyde, which is toxic.

This project aimed at providing a burst delivery of spearmint flavour (L-carvone) in chewing gum application by the means of microencapsulation, in a way that could extend the flavour perception in time.

In this chapter, the work which was done to meet this objective is summarised and recommendations for future investigations are given.

7.1 Overall conclusions

The literature was reviewed in order to develop a good understanding of the different microencapsulation processes available for application in the food industry. The techniques were compared in regards to the end particle morphology they offered, the nature of the core material that could be encapsulated, the size of particles which could be obtained, the trigger mechanisms employed to release the active, the available food grade wall materials for each method, and the cost involved. Complex coacervation was selected as a technique leading to core-shell microcapsules with a lipophilic core, in the desired size range (30-100 μm), allowing to provide a burst delivery using mechanical trigger, with a good amount of possible shell

materials, and medium cost when comparing with other processes. Among the panel of acceptable food grade materials, the choice was limited to polysaccharides in order to avoid regulatory issues posed by allergens. A good wall material for complex coacervation destined to food application needed to be soluble in water, ionic, have film-forming properties, optionally present emulsifying and/or gelling properties, be tasteless and be a food additive with E number (Europe) or have a GRAS status granted by the FDA (USA). It was found that chitosan was the main cationic polysaccharide used for polysaccharide/polysaccharide combinations. It also presented good barrier and mechanical properties, and the availability of a vegetable chitosan alternative made it an interesting option. Gum arabic was selected as the anionic polyelectrolyte based on its low pKa value, as well as its unique emulsifying and film-forming properties.

It was found that it was difficult to obtain satisfying results based on experimental protocols reported in the literature for the use of the gum arabic/chitosan combination for complex coacervation to encapsulate L-carvone, as it appeared each flavour/wall material system seemed to be unique. The complex coacervation was broken down into different investigations so as to get a better understanding of the multiple parameters which can influence the resulting capsules, and optimise the process. More specifically the stabilisation of the initial O/W emulsion was believed to be crucial for ensuring the stability of the coacervated capsules. For the emulsion step, an experimental design study was carried out to optimise the formulation. It was desired to reduce the number of influencing parameters for this statistics approach so the nature of emulsifier was previously determined through a separate investigation based on HLB considerations; the emulsification speed and time were also set as non-varying parameters and studied separately. This helped to limit the experimental design to three influencing parameters (concentration of gum arabic, amount of flavour oil, presence or absence of an emulsifying

agent). It was concluded that the emulsifying capacity of gum arabic at high concentrations was sufficient to avoid using an additional emulsifier. The geometry of the stirred tank was standardised, and the behaviour of the polymer mix was carefully monitored by optical microscopy over the pH range 3.0-6.0. Finally, several food grade crosslinkers were also tested. A better understanding of the different steps involved in the complex coacervation process and of their importance was developed. As a result of this work, it was identified that the best conditions for complex coacervation to encapsulate L-carvone with gum arabic/chitosan were achieved for a ratio of 6:1 (w/w), using highly concentrated gum arabic (12 wt%), without any additional emulsifying agent, at a coacervation pH of 3.6, and by crosslinking with sodium tripolyphosphate applied as a layer-by-layer deposition alternating with chitosan.

Due to an instability upon drying (leakage and collapsing), the capsules had to be further coated to strengthen them. This phenomenon was indeed expected due to the weakness of food grade crosslinkers. A second gum arabic/chitosan 6:1 (w/w) layer was successfully applied by spray coating/drying. This further processing led to more or less spherical capsules which could be observed by light and SEM microscopy techniques, and which were within the desired size range with a mean diameter of 21.0 μm. The characterisation of the capsules by UV-Vis measurements confirmed that L-carvone was successfully retained within the double coated capsules, although the obtained payload was only about 2%, which did not allow to reach the targeted flavour amount to be incorporated in chewing gum matrix. The mechanical properties of the capsules (rupture force, nominal rupture stress and deformation at rupture) were characterised by micromanipulation, and they proved to have a similar strength to other microcapsules made with melamine formaldehyde (Hu *et al.*, 2009), which confirmed the efficacy of the secondary coating in strengthening the wall when crosslinked with weak food grade materials. It was observed from the study of the release profile of L-carvone from

capsules within the gum matrix when mechanically ruptured, that it however displayed a desired peak corresponding to burst and sustained delivery for 10 minutes of chewing. This work showed that it was possible to obtain capsules with good mechanical properties using only food grade materials, although it remained challenging and further processing was required. The capsules performance in matter of oil retention however needed improving.

It was interesting to consider using different wall materials to provide capsules with improved flavour load and different mechanical properties so they could provide burst release at different times and lead to a prolonged flavour perception. Taking the oldest, most studied combination for complex coacervation (gelatine/gum arabic) as an example, it was thought that it would be advantageous to use at least one gelling polysaccharide (sodium alginate, ι-carrageenan, gellan gum, xanthan gum, citrus pectin or karaya gum) in order to overcome the weakness of food grade crosslinkers. The use of zeta potential measurements associated with turbidity measurements helped to determine the polymer mixing ratio for new combinations and the optimum coacervation pH for this ratio respectively. This method was successfully employed to investigate the ability of different polysaccharides to interact with each other and be a possible new interesting combination to use in complex coacervation. Unfortunately, most candidate polymers underwent instant gelation upon mixing with chitosan, which was the main cationic polymer option for polysaccharide/polysaccharide combinations, and could not be further investigated. Contrarily to the initial assumption that corn starch should be a non-ionic gelling polysaccharide, this polymer appeared to be charged as it displayed a negative apparent zeta potential, which could be due to the protein content of the material. Therefore the corn starch/chitosan 3:2 (w/w) combination was investigated at pH 5.2 and actually led to particles with better payload and mechanical properties than the capsules obtained with gum arabic/chitosan, and without requiring a second coating. This result seemed to confirm the

advantage of using a polysaccharide with mechanical strengthening capacities in addition to crosslinking with food grade materials. Indeed, the interesting structure of starch granules enables to have gelling benefits due to swelling, as well as brittleness and good mechanical properties resulting from their layer arrangement. Further investigations were made by replacing chitosan with whey protein, which showed the amount of alternative options offered by the use of protein/polysaccharide combinations. The use of corn starch with whey protein 12:5 (w/w) at pH 4.5 also led here to the most promising results among the different combinations tried with whey protein. The systematic use of zeta potential and turbidity measurements was defined as a powerful exploratory tool. This method can be used as starting point for the investigation of new polymer combinations, rather than following experimental conditions reported in the literature. There are a lot of discrepancies among the published work between the parameters used for complex coacervation, which can possibly originate from the use of natural raw materials whose properties can vary slightly from one batch to the other.

7.2 Recommendations and future work

Due to the limited time available for this project, several other research leads were considered but still remain yet to be investigated.

7.2.1 Recommendations for the gum arabic/chitosan combination

7.2.1.1 Formulation

It was noted from the literature that the crosslinking step may play a crucial role in determining the mechanical strength of the capsules (Zhang *et al.*, 2012; Yu *et al.*, 2017). Although the

crosslinking time was quite extended (16h), it would be interesting to study the effect of the amount of crosslinker on the capsules morphology and mechanical integrity.

Alternative foodgrade crosslinkers could be investigated. Glyceraldehyde is a sugar which can react with the amino groups of chitosan (de Kruif *et al.*, 2004; Turgeon and Laneuville, 2009). Dextran sulphate is a food grade anionic polymer which can be used to crosslink chitosan as its sulphate groups can interact with protonated amino groups (Anitha *et al.*, 2012; Merck, 2020). Dehydroascorbic acid was found to form covalent bonds with primary amines and it could therefore also be worth testing its ability to crosslink chitosan capsules (Turgeon and Laneuville, 2009).

7.2.1.2 Strengthening of the capsules wall

Regarding the relationship which could be observed in **Chapter 5** between the glass transition temperature (T_g) of materials used for the second coating by spray drying and the measured payload, it would be interesting to see if polysaccharides having a higher T_g than chitosan could be used as a secondary coating for the coacervated gum arabic/chitosan capsules, and investigate the effect on the payload.

It was also highlighted in **Chapter 5** that adding an extra layer of shellac coating by acidic precipitation could have a good potential, but would require some investigations on microfluidics in order to generate a drop, containing the primary coacervated capsules in suspension, with a size which would be small enough to generate final capsules of less than 100 µm with the secondary layer. The shellac coating would provide a hydrophobic brittle shell which could have different mechanical properties from the outer water soluble coating produced by spray coating/drying. If successful, those capsules could be incorporated together with the

spray coated capsules in the gum matrix so as to provide flavour bursts at different chewing times.

Another option would be to apply layer-by-layer deposition using in turn gum arabic and chitosan as an alternative to the double coating by spray drying. The charge of the intermediate particles can be checked thanks to zeta potential measurements to determine which of the anionic or cationic polysaccharide should be added at each stage, which is however time consuming.

It was also found that the use of protein fibrils (ovalbumin or lysozyme) could be an interesting way to strengthen the shell of microcapsules (Sagis, 2015). If the use of proteins poses any issue, cellulose could be considered as an alternative for this method since it also has a fibrillar composition (Klemm *et al.*, 2005).

7.2.1.3 Extend the release study to the gas phase

For the release of L-carvone from the gum matrix, the amount of flavour present in the saliva phase was quantified (see **Chapter 5**). Although this technique gave an insight into the release profile obtained from the produced capsules, measuring the aroma compound concentration in the nasal cavity would give a better reflection of the aroma perception of the consumer.

During mastication, the flavour is perceived both by aroma receptors in the nasal cavity resulting from the volatile molecules which are carried in the breath, and by the activation of taste receptors on the tongue by non-volatile flavour molecules in the saliva (McClements, 2009). Considering the high hydrophobicity of L-carvone it would seem interesting to also quantify the amount of flavour released in the gas phase, using gas chromatography – mass spectrometry (GC-MS) or proton transfer reaction – mass spectrometry (PTR-MS) analyses for example.

Some analytical methods allow to characterise both the exhaled breath and saliva during mastication (Potineni and Peterson, 2008a). The use of an artificial mouth device, for example, would be very desirable to carry out such a characterisation (Peyron and Woda, 2016).

7.2.1.4 Storage stability studies

If time had permitted it would have also been helpful to carry out storage stability studies on both the dry powder before incorporation inside the gum matrix, and after. The characterisations of the morphology, payload and mechanical strength of the capsules could have been undertaken in time to define the stability of particles before being mixed in the product matrix. For the capsules in the gum matrix, the evolution of the flavour release profile in time could have been monitored in order to determine the product shelf life when stored at RT.

7.2.2 Recommendations for the investigation of new shell material combinations

7.2.2.1 Recommendations for investigating new shell material combinations

It would have been interesting to dissolve both polymers already premixed in order to see if the gelation upon addition of chitosan could be avoided in that way.

7.2.2.2 Composition characterisation of corn starch powder

It would be useful to investigate further the use of starch, seeing the promising results obtained when combined with chitosan (see **Chapter 6**). Starch was also found to be advantageous for the release in mouth as it is sensitive to the amylase contained in the saliva (Sobel *et al.*, 2014a).

In order to elucidate which element or impurity of the corn starch powder is responsible for the electric charge, it would be interesting to analyse its composition, using SEM with Energy Dispersive X-Ray (EDX) analysis for example.

7.2.2.3 Future work on the corn starch/chitosan and corn starch/whey protein combinations

It would be interesting to study the flavour release profile obtained from the capsules made by complex coacervation with the corn starch/chitosan 3:2 (w/w) combination when incorporated in the gum matrix, in order to confirm if several release peaks can be obtained, as suspected from the mechanical properties data (rupture force and deformation at rupture) obtained by micromanipulation (see **Chapter 6**).

For the corn starch/whey protein 12:5 (w/w) combination, the influence of the decrease of the amount of corn starch on the compression profile of the capsules could be studied. This would help to determine whether the polymer ratio can be adapted so that all of the corn starch would react with the non-precipitated whey protein and avoid obtaining capsules with two layers (compression profiles with a double rupture event).

7.2.2.4 Extend investigation to other polysaccharide materials

Some attractive polysaccharides could not be tested during this project but would be worth investigating using the technique explained in **Chapter 6**.

Cationic guar gum would be an interesting alternative to chitosan to investigate since the choice of positively charged polyelectrolyte was very limited in the case of polysaccharide/polysaccharide combinations (Kaur and Kaur, 2018).

Seeing the promising results obtained with starch, it may also be interesting to investigate further some charged modified starch alternatives, such as carboxymethyl starch, or starch sodium octenyl succinate, which has been used to replace gum arabic in flavour encapsulation (Taggart and Mitchell, 2009).

Finally, the method used in **Chapter 6** would be most advantageous to study novel materials which could find an application in food, such as fucoidan, acetan, emulsan, welan gum, flaxseed gum, gum ghatti, gum tragacanth or psyllium, which are all ionic polysaccharides (see **Chapter 2**).

7.2.2.5 Extend the combinations to the use of proteins

Although they were not desired ingredients for this project, the introduction of animal- or dairy-derived proteins to form protein/polysaccharide combinations would offer a much wider range of possibilities to use in food application, as it was shown with whey protein in **Chapter 6**, using the same investigation method. In order to still avoid materials from animal origin, focus should be put on vegetable proteins such as soy and wheat proteins for example.

7.2.3 Other recommendations

7.2.3.1 Reactivity of L-carvone

It was suspected that L-carvone may react with the wall material due to its reactive unsaturated functional groups (see **Chapter 3**). This could partially explain the weakness of the primary gum arabic/chitosan shell, prior to applying the secondary layer by spray coating/drying.

Due to the lack of information about the reactivity of L-carvone in the literature, it would be useful to develop a better understanding of the possible interactions between this flavour oil and the wall materials. This reactivity could be investigated by Fourier Transform Infrared (FTIR) Spectroscopy and Raman Spectroscopy for example (Shukla *et al.*, 2017).

It would also be interesting to study the effect of the nature of the encapsulated flavour oil on the mechanical properties of the capsules.

7.2.3.2 Non-ionic gelling polysaccharide

Some other GRAS polysaccharides (agar, oat gum, dextran, scleroglucan, guar gum, locust bean gum and konjac mannan) presented interesting gelling properties but were not investigated for complex coacervation as they are non-ionic. It could be interesting to consider the use of those materials for simple coacervation as they may lead to capsules with enhanced mechanical properties resulting from gelation.

References

Abson, R.; Gaddipati, S. R.; Hort, J.; Mitchell, J. R.; Wolf, B.; Hill, S. E. (2014) **A comparison of the sensory and rheological properties of molecular and particulate forms of xanthan gum**, *Food Hydrocolloids*, Vol. 35: 85-90

Ach, D.; Briançon, S.; Broze, G.; Puel, F.; Rivoire, A.; Galvan, J.-M.; Chevalier, Y. (2015) **Formation of microcapsules by complex coacervation**, *The Canadian Journal of Chemical Engineering*, Vol. 93: 183-191

Adeyibi, A. P.; Aluko, R. E. (2011) **Functional properties of protein fractions obtained from commercial yellow field pea (*Pisum sativum* L.) seed protein isolate**, *Food Chemistry*, Vol. 128: 902-908

Aider, M.; Barbana, C. (2011) **Canola proteins: composition, extraction, functional properties, bioactivity, applications as a food ingredient and allergenicity – A practical and critical review**, *Trends in Food Science & Technology*, Vol. 22: 21-39

Al-Assaf, S.; Phillips, G. O.; Amar, V. (2009) **Gum ghatti**, *Handbook of Hydrocolloids*, Chapter 17: 477-494

Ale, M. T.; Meyer, A. S. (2013) **Fucoidans from brown seaweeds: an update on structures, extraction techniques and use of enzymes as tools for structural elucidation**, *RSC Advances*, Vol. 3: 8131-8141

Ale, M. T.; Mikkelsen, J. D.; Meyer, A. S. (2011) **Important Determinants for Fucoidan Bioactivity: A Critical Review of Structure-Function Relations and Extraction Methods for Fucose-Containing Sulfated Polysaccharides from Brown Seaweeds**, *Marine Drugs*, Vol. 9: 2106-2130

Alexander, E.; Yach, D.; Mensah, G. A. (2011) **Major multinational food and beverage companies and informal sector contributions to global food consumption: implications for nutrition policy**, *Globalization and Health*, Vol. 7: 26

Althubiani, A. S.; Al-Ghamdi, S. B.; Samreen; Qais, F. A.; Khan, M. S.; Ahmad, I.; Malak, H. A. (2019) **Plant-Derived Prebiotics and Its Health Benefits**, *New Look to Phytomedicine*, Chapter 4: 63-88

Alting, A. C.; Pouvreau, L.; Giuseppin, M. L. F.; van Nieuwenhuijzen, N. H. (2011) **Potato proteins**, *Handbook of Food Proteins*, Chapter 12: 316-334

Amidon, G. E.; Meyer, P. J.; Mudie, D. M. (2017) **Particle, Powder, and Compact Characterization**, *Developing Solid Oral Dosage Forms*, Chapter 10: 271-293

Anitha, A.; Rejinold, N. S.; Bumgardner, J. D.; Nair, S. V.; Jayakumar, R. (2012) **Approaches for Functional Modification or Cross-linking of Chitosan**, *Chitosan-Based Systems for Biopharmaceuticals: Delivery, Targeting and Polymer Therapeutics*, Chapter 7: 107-124

Anton, M.; Nau, F.; Guérin-Dubiard, C. (2011) **Bioactive fractions of eggs for human and animal health**, *Improving the Safety and Quality of Eggs and Egg Products*, Chapter 16: 321-345

Anton, M.; Nau, F.; Lechevalier, V. (2009) **Egg proteins**, *Handbook of Hydrocolloids*, Chapter 14: 359-382

Antoniou, J.; Liu, F.; Majeed, H.; Zhong, F. (2015) **Characterization of tara gum edible films incorporated with bulk chitosan and chitosan nanoparticles: A comparative study**, *Food Hydrocolloids*, Vol. 44: 309-319

Arendt, E. K.; Zannini, E. (2013) **Barley**, *Cereal Grains for the Food and Beverage Industries*, Chapter 4: 155-200

Ariyarathna, I. R.; Karunaratne, D. N. (2015) **Use of chickpea protein for encapsulation of folate to enhance nutritional potency and stability**, *Food and Bioproducts Processing*, Vol. 95: 76-82

Armisén, R.; Galatas, F. (2009) **Agar**, *Handbook of Hydrocolloids*, Chapter 4: 82-107

Arntfield, S. D.; Maskus, H. D. (2011) **Peas and other legume proteins**, *Handbook of Food Proteins*, Chapter 9: 233-266

Augustin, M. A.; Oliver, C. M. (2014) **Use of Milk Proteins for Encapsulation of Food Ingredients**, *Microencapsulation in the Food Industry*, Chapter

Auvray, M.; Spence, C. (2008) **The multisensory perception of flavor**, *Consciousness and Cognition*, Vol. 17: 1016-1031

Aveling, E. M.; Heron, C. (1999) **Chewing tar in the early Holocene: an archaeological and ethnographic evaluation**, *Antiquity*, Vol. 73: 579-584

Avramenko, N. A.; Chang, C.; Low, N. H.; Nickerson, M. T. (2016) **Encapsulation of flaxseed oil within native and modified lentil protein-based microcapsules**, *Food Research International*, Vol. 81: 17-24

Babault, N.; Païzis, C.; Deley, G.; Guérin-Deremaux, L.; Saniez, M.-H.; Lefranc-Millot, C.; Allaert, F. A. (2015) **Pea proteins oral supplementation promotes muscle thickness gains during resistance training: a double-blind, randomized, Placebo-controlled clinical trial vs. Whey protein**, *Journal of the International Society of Sports Nutrition*, Vol. 12 (3): 1-9

Balcão, V. M.; Glasser, C. A.; Chaud, M. V.; Vila, M. M. D. C. (2015) **Water-in-Oil-in-Water Nanoencapsulation Systems**, *Microencapsulation and Microspheres for Food Applications*, Chapter 6: 95-129

Barać, M. B.; Cabrilo, S.; Pešić, M. B.; Stanojević, S. P.; Zilic, S.; Macej, O.; Ristic, N. (2010) **Profile and functional properties of seed proteins from six pea (*Pisum sativum*) genotypes**, *International Journal of Molecular Science*, Vol. 11 (12): 4973-4990

Barać, M. B.; Pešić, M. B.; Stanojević, S. P.; Kostić, A. Ž.; Čabrilo, S. B. (2015) **Techno-functional properties of pea (Pisum sativum) protein isolates - A review**, *APTEFF*, Vol. 46: 1-18

Barbosa, J. A. C.; Abdelsadig, M. S. E.; Conway, B. R.; Merchant, H. A. (2019) **Using zeta potential to study the ionisation behaviour of polymers employed in modified-release dosage forms and estimating their pKa**, *International Journal of Pharmaceutics: X*, Vol. 1: 100024

Barrow, C. J.; Nolan, C.; Jin, Y. (2007) **Stabilization of highly unsaturated fatty acids and delivery into foods**, *Lipid Technology*, Vol. 19 (5): 108-111

Baumgartner, S.; Pavli, M.; Kristl, J. (2008) **Effect of calcium ions on the gelling and drug release characteristics of xanthan matrix tablets**, *European Journal of Pharmaceutics and Biopharmaceutics*, Vol. 69: 698-707

Bello Perez, L. A.; Agama-Acevedo, E. (2017) **Starch**, *Starch-Based Materials in Food Packaging*, Chapter 1: 1-18

Belyadi, H.; Fathi, E.; Belyadi, F. (2019) **Multiscale Fluid Flow and Transport in Organic-Rich Shale**, *Hydraulic Fracturing in Unconventional Reservoirs*, Chapter Four: 35-45

BeMiller, J. N. (2008) **Hydrocolloids**, *Gluten-Free Cereal Products and Beverages*, Chapter 9: 203-215

BeMiller, J. N. (2019a) **Guar, Locust Bean, Tara, and Cassia Gums**, *Carbohydrate Chemistry for Food Scientists*, Chapter 9: 241-252

BeMiller, J. N. (2019b) **Inulin and Konjac Glucomannan**, *Carbohydrate Chemistry for Food Scientists*, Chapter 10: 253-259

BeMiller, J. N. (2019c) **Pectins**, *Carbohydrate Chemistry for Food Scientists*, Chapter 15: 303-312

BeMiller, J. N. (2019d) **Polysaccharides: Occurrence, Structures, and Chemistry**, *Carbohydrate Chemistry for Food Scientists*, Chapter 4: 75-101

Bendjaballah, M.; Canselier, J.-P.; Oumeddour, R. (2010) **Optimization of Oil-in-Water Emulsion Stability: Experimental Design, Multiple Light Scattering, and Acoustic Attenuation Spectroscopy**, *Journal of Dispersion Science and Technology*, Vol. 31 (9): 1260-1272

Boland, M. (2011) **Whey proteins**, *Handbook of Food Proteins*, Chapter 2: 30-55

Botrel, D. A.; de Barros Fernandes, R. V.; Borges, S. V. (2015) **Microencapsulation of Essential Oils Using Spray Drying Technology**, *Microencapsulation and Microspheres for Food Applications*, Chapter 12: 235-251

Bouquerand, P.-E.; Dardelle, G.; Erni, P.; Normand, V. (2012) **An industry perspective on the advantages and disadvantages of different flavor delivery systems**, *Encapsulation Technologies and Delivery Systems for Food Ingredients and Nutraceuticals*, Chapter 15: 453-487

Brandau, T. (2014) **Annular Jet-Based Processes**, *Microencapsulation in the Food Industry*, Chapter 10: 99-110

Brummer, Y.; Cui, W.; Wang, Q. (2003) **Extraction, purification and physicochemical characterization of fenugreek gum**, *Food Hydrocolloids*, Vol. 17: 229-236

Budavari, S. (1996) *The Merck Index – An Encyclopedia of Chemicals, Drugs, and Biologicals*

Bulgarelli, E.; Forni, F.; Bernabei, M. T. (1999) **Casein/gelatin beads: I. Cross-linker solution composition effect on cross-linking degree**, *International Journal of Pharmaceutics*, Vol. 190: 175-182

Burdock, G. A. (2005) **Carvone**, *Fenaroli's Handbook of Flavor Ingredients*, Fifth Edition: 265-267

Burgain, J.; Corgneau, M.; Scher, J.; Gaiani, C. (2015) **Encapsulation of Probiotics in Milk Protein Microcapsules**, *Microencapsulation and Microspheres for Food Applications*, Chapter 20: 391-406

Burgess, D. J. (1990) **Practical Analysis of Complex Coacervate Systems**, *Journal of Colloid and Interface Science*, Vol. 140 (1): 227-238

Burgess, D. J.; Carless, J. E. (1984) **Microelectrophoretic Studies of Gelatin and Acacia for the Prediction of Complex Coacervation**, *Journal of Colloid and Interface Science*, Vol. 98 (1): 1-8

Burnside, E. (2014) **Hydrocolloids and Gums as Encapsulating Agents**, *Microencapsulation in the Food Industry*, Chapter 21: 241-252

Burseg, K. M. M.; Brattinga, C.; de Kok, P. M. T.; Bult, J. H. F. (2010) **Sweet taste enhancement through pulsatile stimulation depends on pulsation period not on conscious pulse perception**, *Physiology & Behavior*, Vol. 100: 327-331

Butstraen, C.; Salaün, F. (2014) **Preparation of microcapsules by complex coacervation of gum Arabic and chitosan**, *Carbohydrate Polymers*, Vol. 99: 608-616

Campana, S.; Andrade, C.; Milas, M.; Rinaudo, M. (1990) **Polyelectrolyte and rheological studies on the polysaccharide welan**, *International Journal of Biological Macromolecules*, Vol. 12: 379-384

Cao, L.; Liu, W.; Wang, L. (2018) **Developing a green and edible film from Cassia gum: The effects of glycerol and sorbitol**, *Journal of Cleaner Production*, Vol. 175: 276-282

Carlsson, A.; Lindman, B.; Nilsson, P.-G.; Karlsson, G. (1986) **Hydration of ethyl hydroxyethyl cellulose**, *Polymer*, Vol. 27 (3): 431-436

Carneiro, H. C. F.; Tonon, R. V.; Grosso, C. R. F.; Hubinger, M. D. (2013) **Encapsulation efficiency and oxidative stability of flaxseed oil microencapsulated by spray drying using different combinations of wall materials**, *Journal of Food Engineering*, Vol. 115: 443-451

Casana Giner, V.; Gimeno Sierra, M.; Gimeno Sierra, B.; Moser, M. (2006) **Continuous multi-microencapsulation process for improving the stability and storage life of biologically active ingredients**, Patent EP1702675

Castro, G. R.; Panilaitis, B.; Kaplan, D. L. (2008) **Emulsan, a tailorable biopolymer for controlled release**, *Bioresource Technology*, Vol. 99: 4566-4571

Catte, M.; Poprawski, J.; Aubry, J. M.; van Hecke, E. (2002) **Analysis of an Emulsification Process Using Fractional Experimental Design**, *Journal of Dispersion Science and Technology*, Vol. 23 (1-3): 323-331

Cekinski, E.; Giulietti, M.; Seckler, M. M. (2010) **A New Approach to Characterize Suspensions in Stirred Vessels Based on Computational Fluid Dynamics**, *Brazilian Journal of Chemical Engineering*, Vol. 27 (2): 265-273

Chakraborty, J. N. (2014) **Colouring materials**, *Fundamentals and Practices in Colouration of Textiles*, Chapter 2: 12-21

Chang, P. G.; Gupta, R.; Timilsena, Y. P.; Adhikari, B. (2016) **Optimisation of the complex coacervation between canola protein isolate and chitosan**, *Journal of Food Engineering*, Vol. 191: 58-66

Chang, Q. (2016) **Emulsion, Foam, and Gel**, *Colloid and Interface Chemistry for Water Quality Control*, Chapter 11: 227-245

Chang, Y. W.; Alli, I.; Konishi, Y.; Ziomek, E. (2011) **Characterization of protein fractions from chickpea (*Cicer arietinum* L.) and oat (*Avena sativa* L.) seeds using proteomic techniques**, *Food Research International*, Vol. 44: 3094-3104

Chay Pak Ting, B. P.; Pouliot, Y.; Gauthier, S. F.; Mine, Y. (2010) **Fractionation of egg proteins and peptides for nutraceutical applications**, *Separation, Extraction and Concentration Processes in the Food, Beverage and Nutraceutical Industries*, Chapter 19: 595-618

Chen, B.; Li, H.; Ding, Y.; Suo, H. (2012) **Formation and microstructural characterization of whey protein isolate/beet pectin coacervations by laccase catalyzed cross-linking**, *LWT - Food Science and Technology*, Vol. 47: 31-38

Chen, H.; Ouyang, W.; Lawuyi, B.; Prakash, S. (2006) **Genipin Cross-Linked Alginate-Chitosan Microcapsules: Membrane Characterization and Optimization of Cross-Linking Reaction**, *Biomacromolecules*, Vol. 7: 2091-2098

Chen, L. (2015) **Emulsifiers as food texture modifiers**, *Modifying Food Texture*, Vol. 1, Chapter 2: 27-49

Chivero, P.; Gohtani, S.; Ikeda, S.; Nakamura, A. (2014) **The structure of soy soluble polysaccharide in aqueous solution**, *Food Hydrocolloids*, Vol. 35: 279-286

Choi, S. J.; Decker, E. A.; Henson, L.; Popplewell, L. M.; McClements, D. J. (2009) **Stability of Citral in Oil-in-Water Emulsions Prepared with Medium-Chain Triacylglycerols and Triacetin**, *Journal of Agricultural and Food Chemistry*, Vol. 57 (23): 11349-11353

Chove, B. E.; Grandison, A. S.; Lewis, M. J. (2001) **Emulsifying properties of soy protein isolate fractions obtained by isoelectric precipitation**, *Journal of the Science of Food and Agriculture*, Vol. 81 (8): 759-763

Cilurzo, F.; Cupone, I. E.; Minghetti, P.; Selmin, F.; Montanari, L. (2008) **Fast dissolving films made of maltodextrins**, *European Journal of Pharmaceutics and Biopharmaceutics*, Vol. 70 (3): 895-900

Citkowska, A.; Szekalska, M.; Winnicka, K. (2019) **Possibilities of Fucoidan Utilization in the Development of Pharmaceutical Dosage Forms**, *Marine Drugs*, Vol. 17: 458

Comert, F.; Malanowski, A. J.; Azarikia, F.; Dubin, P. L. (2016) **Coacervation and precipitation in polysaccharide-protein systems**, *Soft Matter*, Vol. 12: 4154-4161

Copeland, L.; Blazek, J.; Salman, H.; Tang, M. C. (2009) **Form and functionality of starch**, *Food Hydrocolloids*, Vol. 23: 1527-1534

Cui, S. W.; Roberts, K. T. (2009) **Dietary Fiber: Fulfilling the Promise of Added-Value Formulations**, *Modern Biopolymer Science*, Chapter 13: 399-448

Cui, S. W.; Wu, Y.; Ding, H. (2013) **The range of dietary fibre ingredients and a comparison of their technical functionality**, *Fibre-Rich and Wholegrain Foods*, Chapter 5: 96-119

Curcio, M.; Puoci, F.; Iemma, F.; Parisi, O. I.; Cirillo, G.; Spizzirri, U. G.; Picci, N. (2009) **Covalent Insertion of Antioxidant Molecules on Chitosan by a Free Radical Grafting Procedure**, *Journal of Agricultural and Food Chemistry*, Vol. 57: 5933-5938

Dadou, S. M.; Antonijevic, M. D.; Chowdhry, B. Z.; Badwan, A. A. (2018) **An Overview of Chitosan-Xanthan Gum Matrices as Controlled Release Drug Carriers**, *Chitin-Chitosan – Myriad Functionalities in Science and Technology*, Chapter 11: 219-243

Dário, A. F.; Hortêncio, L. M. A.; Sierakowski, M. R.; Queiroz Neto, J. C.; Petri, D. F. S. (2011) **The effect of calcium salts on the viscosity and adsorption behavior of xanthan**, *Carbohydrate Polymers*, Vol. 84: 669-676

Das, S. K.; David, S. R. N.; Rajabalaya, R.; Mukhopadhyay, H. K.; Halder, T.; Palanisamy, M.; Khanam, J.; Nanda, A. (2011) **Microencapsulation techniques and its practice**, *International Journal of Pharmaceuticle Science and Technology*, Vol. 6 (2)

Davidson, J. M.; Linforth, R. S. T.; Hollowood, T. A.; Taylor, A. J. (1999) **Effect of Sucrose on the Perceived Flavor Intensity of Chewing Gum**, *Journal of Agricultural and Food Chemistry*, Vol. 47 (10): 4336-4340

Dawkins, N. L.; Nnanna, I. A. (1993) **Oat Gum and β-Glucan Extraction from Oat Bran and Rolled Oats: Temperature and pH Effects**, *Journal of Food Science*, Vol. 58 (3): 562-566

Dawkins, N. L.; Nnanna, I. A. (1995) **Studies on oat gum [(1→3, 1→4)-β-D-glucan]: composition, molecular weight estimation and rheological properties**, *Food Hydrocolloids*, Vol. 9 (1): 1-7

Day, L. (2011) **Wheat gluten: production, properties and application**, *Handbook of Food Proteins*, Chapter 11: 267-288

de Kruif, C. G.; Weinbreck, F.; de Vries, R. (2004) **Complex coacervation of proteins and anionic polysaccharides**, *Current Opinion in Colloid & Interface Science*, Vol. 9: 340-349

Deeth, H.; Bansal, N. (2019) **Whey Proteins: An Overview**, *Whey Proteins*, Chapter 1: 1-50

Dehghan, M. H. G.; Kazi, M. (2014) **Lyophilized Chitosan/xanthan Polyelectrolyte Complex Based Mucoadhesive Inserts for Nasal Delivery of Promethazine Hydrochloride**, *Iranian Journal of Pharmaceutical Research*, Vol. 13 (3): 769-784

Deka, C.; Dutta, M.; Deka, D.; Jha, D. K.; Kakati, D. K. (2016) **Study of olive oil-loaded chitosan/carrageenan coacervate and its antibacterial property**, *International Journal of Pharma Sciences*, Vol. 6 (3): 1524-1533

Delafosse, A.; Line, A.; Morchain, J.; Guiraud, P. (2008) **LES and URANS simulations of hydrodynamics in mixing tank: Comparison to PIV experiments**, *Chemical Engineering Research and Design*, Vol. 86: 1322-1330

Delwiche, J. (2004) **The impact of perceptual interactions on perceived flavor**, *Food Quality and Preference*, Vol. 15: 137-146

Desai, K. G. H.; Park, H. J. (2005) **Recent Developments in Microencapsulation of Food Ingredients**, *Drying Technology*, Vol. 23: 1361-1394

Deshmukh, A. S.; Setty, C. M.; Badiger, A. M.; Muralikrishna, K. S. (2012) **Gum ghatti: A promising polysaccharide for pharmaceutical applications**, *Carbohydrate Polymers*, Vol. 87: 980-986

Dey, S.; Nandy, B. C.; De, J. N.; Hasnain, M. S.; Nayak, A. K. (2019) **Tamarind gum in drug delivery applications**, *Natural Polysaccharides in Drug Delivery and Biomedical Applications*, Chapter 12: 285-306

Dhillon, G. S.; Kaur, S.; Oberoi, H. S.; Spier, M. R.; Brar, S. K. (2016) **Agricultural-Based Protein By-Products: Characterization and Applications**, *Protein Byproducts*, Chapter 2: 21-36

Dickinson, E. (2009) **Hydrocolloids and emulsion stability**, *Handbook of Hydrocolloids*, Chapter 2: 23-49

Dima, C.; Cotârlet, M.; Alexe, P.; Dima, S. (2014) **Microencapsulation of essential oil of pimento [*Pimenta dioica* (L) Merr.] by chitosan/k-carrageenan complex coacervation method**, *Innovative Food Science and Emerging Technologies*, Vol. 22: 203-2011

Dixit, R.; Verma, A.; Mishra, A. K.; Verma, N.; Pandit, J. K. (2012) **Floating Gellan-Chitosan Polyelectrolyte Complex Beads: Effect of Gelucires Incorporation on Encapsulation Efficiency and Drug Release**, *Latin American Journal of Pharmacy*, Vol. 31 (1): 37-42

Dong, Z.; Ma, Y.; Hayat, K.; Jia, C.; Xia, S.; Zhang, X. (2011) **Morphology and release profile of microcapsules encapsulating peppermint oil by complex coacervation**, *Journal of Food Engineering*, Vol. 104: 455-460

Dong, Z. J.; Touré, A.; Jia, C. S.; Zhang, X. M.; Xu, S. Y. (2007) **Effect of processing parameters on the formation of spherical multinuclear microcapsules encapsulating peppermint oil by coacervation**, *Journal of Microencapsulation*, Vol. 24 (7): 634-646

dos Santos Araújo, P.; Belini, G. B.; Mambrini, G. P.; Yamaji, F. M.; Waldman, W. R. (2019) **Thermal degradation of calcium and sodium alginate: A greener synthesis towards calcium oxide micro/nanoparticles**, *International Journal of Biological Macromolecules*, Vol. 140: 749-760

Draget, K. I. (2009) **Alginates**, *Handbook of Hydrocolloids*, Chapter 29: 807-828

Drusch, S.; Mannino, S. (2009) **Patent-based review on industrial approaches for the microencapsulation of oils rich in polyunsaturated fatty acids**, *Trends in Food Science & Technology*, Vol. 20: 237-244

Du, L.; Brenner, T.; Xie, J.; Liu, Z.; Wang, S.; Matsukawa, S. (2016) **Gelation of Iota/Kappa Carrageenan Mixtures**, *Gums and Stabilisers for the Food Industry 18: Hydrocolloid Functionality for Affordable and Sustainable Global Food Solutions*: 47-55

Ducel, V.; Richard, J.; Popineau, Y.; Boury, F. (2004a) **Adsorption Kinetics and Rheological Interfacial Properties of Plant Proteins at the Oil-Water Interface**, *Biomacromolecules*, Vol. 5: 2088-2093

Ducel, V.; Richard, J.; Popineau, Y.; Boury, F. (2005) **Rheological Interfacial Properties of Plant Protein-Arabic Gum Coacervates at the Oil-Water Interface**, *Biomacromolecules*, Vol. 6: 790-796

Ducel, V.; Richard, J.; Saulnier, P.; Popineau, Y.; Boury, F. (2004b) **Evidence and characterization of complex coacervates containing plant proteins: application to the microencapsulation of oil droplets**, *Colloids and Surfaces A: Physicochemical Engineering Aspects*, Vol. 232: 239-247

Duque Estrada, P.; Berton-Carabin, C. C.; van der Goot, A. J. (2017) **Stability of double emulsions for iron encapsulation**, *25th International Conference on Bioencapsulation*, O4-6: 74-75

Dziuba, M.; Nałęcz, D.; Szerszunowicz, I.; Waga, J. (2014) **Proteomic analysis of wheat α/A- and β-gliadins**, *Czech Journal of Food Sciences*, Vol. 32 (5): 437-442

Edwards, W. P. (2003) **SWEETS AND CANDIES/Sugar confectionery**, *Encyclopedia of Food Sciences and Nutrition*, Second Edition: 5703-5710

Elabbadi, A.; Erni, P. (2019) **Gum Arabic/chitosan coacervate system**, Patent WO2019020646

Elmer, C.; Can Karaca, A.; Low, N. H.; Nickerson, M. T. (2011) **Complex coacervation in pea protein isolate-chitosan mixtures**, *Food Research International*, Vol. 44: 1441-1446

Elzoghby, A. O.; Elgohary, M. M.; Kamel, N. M. (2015) **Implications of Protein- and Peptide-Based Nanoparticles as Potential Vehicles for Anticancer Drugs**, *Advances in Protein Chemistry and Structural Biology*, Vol. 98, Chapter 6: 169-221

Endreß, H.-U.; Christensen, S. H. (2009) **Pectins**, *Handbook of Hydrocolloids*, Chapter 12: 274-297

Enescu, D.; Olteanu, C. E. (2008) **Functionalized Chitosan and Its Use in Pharmaceutical, Biomedical, and Biotechnological Research**, *Chemical Engineering Communications*, Vol. 195: 1269-1291

Espinosa-Andrews, H.; Báez-González, J. G.; Cruz-Sosa, F.; Vernon-Carter, E. J. (2007) **Gum Arabic-Chitosan Complex Coacervation**, *Biomacromolecules*, Vol. 8: 1313-1318

Espinosa-Andrews, H.; Enríquez-Ramírez, K. E.; García-Márquez, E.; Ramírez-Santiago, C.; Lobato-Calleros, C.; Vernon-Carter, J. (2013) **Interrelashionship between the zeta potential and viscoelastic properties in coacervates complexes**, *Carbohydrate Polymers*, Vol. 95: 161-166

Espinosa-Andrews, H.; Lobato-Calleros, C.; Loeza-Corte, J. M.; Beristain, C. I.; Rodríguez-Huezo, M. E.; Vernon-Carter, E. J. (2008) **Quantification of the Composition of Gum Arabic-Chitosan Coacervates by HPLC**, *Revista Mexicana de Ingeniería Química*, Vol. 7 (3): 293-298

Espinosa-Andrews, H.; Sandoval-Castilla, O.; Vázquez-Torres, H.; Vernon-Carter, E. J.; Lobato-Calleros, C. (2010) **Determination of the gum Arabic-chitosan interactions by Fourier Transform Infrared Spectroscopy and characterization of the microstructure and rheological features of their coacervates**, *Carbohydrate Polymers*, Vol. 79: 541-546

Estevinho, B. N.; Rocha, F.; Santos, L.; Alves, A. (2013) **Microencapsulation with chitosan by spray drying for industry applications – A review**, *Trends in Food Science & Technology*, Vol. 31: 138-155

Euromonitor (2020) https://www.portal.euromonitor.com/portal/, accessed 6 January 2020

Fallourd, M. J.; Viscione, L. (2009) **Ingredient selection for stabilisation and texture optimisation of functional beverages and the inclusion of dietary fibres**, *Functional and Speciality Beverage Technology*, Chapter 1: 3-38

Fang, Z. (2012) **Spray drying, freeze drying and related processes for food ingredient and nutraceutical encapsulation**, *Encapsulation Technologies and Delivery Systems for Food Ingredients and Nutraceuticals*, Chapter 4: 73-109

Farag, Y.; Leopold, C. S. (2009) **Physicochemical Properties of Various Shellac Types**, *Dissolution Technologies*, Vol. 16 (2): 33-39

Fasolin, L. H.; Picone, C. F. S.; Santana, R. C.; Cunha, R. L. (2013) **Production of hybrid gels from polysorbate and gellan gum**, *Food Research International*, Vol. 54 (1): 501-507

Featherstone, S. (2015) **Ingredients used in the preparation of canned foods**, *A Complete Course in Canning and Related Processes*, Chapter 8: 147-211

Featherstone, S. (2016) **Jams, jellies, and related products**, *A Complete Course in Canning and Related Processes*, Chapter 9: 313-349

Fee, C. J.; Billakanti, J. M.; Saufi, S. M. (2010) **Methods for purification of dairy nutraceuticals**, *Separation, Extraction and Concentration Processes in the Food, Beverage and Nutraceutical Industries*, Chapter 16: 450-482

Feng, T.; Xiao, Z.; Tian, H. (2009) **Recent patents in flavor microencapsulation**, *Recent patents on Food, Nutrition, & Agriculture*, Vol. 1: 193-202

Fett, W. F.; Wells, J. M.; Cescutti, P.; Wijey, C. (1995) **Identification of Exopolysaccharides Produced by Fluorescent Pseudomonads Associated with Commercial Mushroom (*Agaricus bisporus*) Production**, *Applied and Environmental Microbiology*, Vol. 61 (2): 513-517

Food and Drug Administration (2004) **Food Allergen Labeling and Consumer Protection Act of 2004 (FALCPA)**, *Public Law 108-282*, Title II

Food and Drug Administration (2018) https://www.fda.gov/food/ingredientspackaginglabeling/gras/

Food and Drug Administration (2020) https://www.fda.gov/

Frey, C. (2014) **Fluid Bed Coating-Based Microencapsulation**, *Microencapsulation in the Food Industry*, Chapter 7: 65-79

Fukushima, D. (2011) **Soy proteins**, *Handbook of Food Proteins*, Chapter 8: 210-232

Furuta, H.; Tobe, J.; Kiwata, R.; Maeda, H. (1999) **Rheological Properties of a Heat-reversible Gel of Water-soluble Soybean Polysaccharide Extracted under Acidic Conditions**, *Bioscience, Biotechnology, and Biochemistry*, Vol. 63 (12): 2075-2081

Gadkari, P. V.; Tu, S.; Chiyarda, K.; Reaney, M. J. T.; Ghosh, S. (2018) **Rheological characterization of fenugreek gum and comparison with other galactomannans**, *International Journal of Biological Macromolecules*, Vol. 119: 486-495

Gaidamauskas, E.; Norkus, E.; Butkus, E.; Crans, D. C.; Grincienė, G. (2009) **Deprotonation of β-cyclodextrin in alkaline solutions**, *Carbohydrate Research*, Vol. 344: 250-254

García-Ochoa, F.; Santos, V. E.; Casas, J. A.; Gómez, E. (2000) **Xanthan gum: production, recovery, and properties**, *Biotechnology Advances*, Vol. 18: 549-579

Garti, N.; Aserin, A. (2012) **Micelles and microemulsions as food ingredient and nutraceutical delivery systems**, *Encapsulation Technologies and Delivery Systems*, Chapter 9: 211-251

Garti, N.; Madar, Z.; Aserin, A.; Sternheim, B. (1997) **Fenugreek Galactomannans as Food Emulsifiers**, *Lebensmittel-Wissenschaft und -Technologie*, Vol. 30: 305-311

Gawai, K. M.; Mudgal, S. P.; Prajapati, J. B. (2017) **Stabilizers, Colorants, and Exopolysaccharides in Yogurt**, *Yogurt in Health and Disease Prevention*, Chapter 3: 49-68

Gelinsky, M. (2018) **Biopolymer hydrogel bioinks**, *3D Bioprinting for Reconstructive Surgery*, Chapter 6: 125-136

Gharsallaoui, A.; Roudaut, G.; Chambin, O.; Voilley, A.; Saurel, R. (2007) **Applications of spray-drying in microencapsulation of food ingredients: An overview**, *Food Research International*, Vol. 40: 1107-1121

Gholami, R.; Fakhari, N. (2017) **Support Vector Machine: Principles, Parameters, and Applications**, *Handbook of Neural Computation*, Chapter 27: 515-535

Ghosh, A. K.; Bandyopadhyay, P. (2012) **Polysaccharide-Protein Interactions and Their Relevance in Food Colloids**, *The Complex World of Polysaccharides*, Chapter 14: 395-408

Giavasis, I. (2013) **Production of microbial polysaccharides for use in food**, *Microbial Production of Food Ingredients, Enzymes and Nutraceuticals*, Chapter 16: 413-468

Gidley, M. J.; Nishinari, K. (2009) **Physico-chemistry of (1,3)-β-Glucans**, *Chemistry, Biochemistry, and Biology of 1-3 Beta Glucans and Related Polysaccharides*, Chapter 2.2: 47-118

González-Pérez, S. (2015) **Sunflower Proteins**, *Sunflower*, Chapter 12: 331-393

González-Pérez, S.; Arellano, J. B. (2009) **Vegetable protein isolates**, *Handbook of Hydrocolloids*, Chapter 15: 383-419

Grandtner, G.; Joly, N.; Cavrot, J.-P.; Granet, R.; Bandur, G.; Rusnac, L.; Martin, P.; Krausz, P. (2005) **Synthesis of fructooligosaccharide-based plastic films starting from inulin**, *e-Polymers*, Vol. 5 (1)

Gray, A.; Egan, S.; Bakalis, S.; Zhang, Z. (2016) **Determination of microcapsule physicochemical, structural, and mechanical properties**, *Particuology*, Vol. 24: 32-43

Guignard, J.-P. (2017) **Postnatal Development of Glomerular Filtration Rate in Neonates**, *Fetal and Neonatal Physiology*, Chapter 103: 993-1002

Guimarães, D. H. P.; Gasparetto, C. A. (2005) **Whey proteins solubility as function of temperature an pH**, *LWT - Food Science and Technology*, Vol. 38 (1): 77-80

Gulão, E. D. S.; de Souza, C. J. F.; Andrade, C. T.; Garcia-Rojas, E. E. (2016) **Complex coacervates obtained from peptide leucine and gum arabic: Formation and characterization**, *Food Chemistry*, Vol. 194: 680-686

Gupta, S.; Khan, S.; Muzafar, M.; Kushwaha, M.; Yadav, A. K.; Gupta, A. P. (2016) **Encapsulation: entrapping essential oil/flavors/aromas in food**, *Encapsulations*, Chapter 6: 229-268

Gupta, S.; Sharma, P.; Soni, P. L. (2005) **Chemical modification of *Cassia occidentalis* seed gum: carbamoylethylation**, *Carbohydrate Polymers*, Vol. 59: 501-506

Gupta, S.; Variyar, P. S. (2018) **Guar Gum: A Versatile Polymer for the Food Industry**, *Biopolymers for Food Design*, Chapter 12: 383-407

Gustaitis, J. (1998) **The sticky history of chewing gum**, *American History*, Vol. 33 (4): 30-34 and 69-71

Gutnick, D. L. (1987) **The Emulsan Polymer: Perspectives on a Microbial Capsule as an Industrial Product**, *Biopolymers*, Vol. 26: S223-S240

Gutnick, D. L.; Zosim, Z.; Rosenberg, E. (1982) **The Interaction of Emulsan with Hydrocarbons**, *Microbial Enhancement of Oil Recovery*, Section 1: 6-11

Haack, D.; Koeberle, M. (2014) **Hot Melt Coating for Controlling the Stability, Release Properties and Taste of Solid Oral Dosage Forms**, *TechnoPharm*, Vol. 4 (5): 258-263

Haahr, A.-M.; Bardow, A.; Thomsen, C. E.; Jensen, S. B.; Nauntofte, B.; Bakke, M.; Adler-Nissen, J.; Bredie, W. L. P. (2004) **Release of peppermint flavour compounds from chewing gum : effect of oral functions**, *Physiology & Behavior*, Vol. 82: 531-540

Hall, S.; Pacek, A. W.; Kowalski, A. J.; Cooke, M.; Rothman, D. (2013) **The effect of scale and interfacial tension on liquid-liquid dispersion in in-line Silverson rotor-stator mixers**, *Chemical Engineering Research and Design*, Vol. 91: 2156-2168

Hallagan, J. B.; La Du, B. N.; Pariza, M. W.; Putnam, J. M.; Borzelleca, J. F. (1997) **Assessment of Cassia Gum**, *Food and Chemical Toxicology*, Vol. 35: 625-632

Hamman, J. H. (2010) **Chitosan Based Polyelectrolyte Complexes as Potential Carrier Materials in Drug Delivery Systems**, *Marine Drugs*, Vol. 8: 1305-1322

Harrington, J.; Schaefer, M. (2014) **Extrusion-Based Microencapsulation for the Food Industry**, *Microencapsulation in the Food Industry*, Chapter 8: 81-84

Haug, I. J.; Draget, K. I. (2009) **Gelatin**, *Handbook of Hydrocolloids*, Chapter 6: 142-163

Haug, A.; Høstmark, A. T.; Harstad, O. M. (2007) **Bovine milk in human nutrition – A review**, *Lipids in Health and Disease*, Vol. 6 (25)

Hawley, G. G. (1977) *The Condensed Chemical Dictionary*

Haynes, W. M. (2010) **Solvents for ultraviolet spectrophotometry**, *CRC Handbook of Chemistry and Physics*, 91st Edition: 8-127

Heidebach, T.; Först, P.; Kulozik, U. (2009a) **Microencapsulation of probiotic cells by means of rennet-gelation of milk proteins**, *Food Hydrocolloids*, Vol. 23: 1670-1677

Heidebach, T.; Först, P.; Kulozik, U. (2009b) **Transglutaminase-induced caseinate gelation for the microencapsulation of probiotic cells**, *International Dairy Journal*, Vol. 19: 77-84

Hember, M. W. N.; Richardson, R. K.; Morris, E. R. (1994) **Native ordered structure of welan polysaccharide: conformational transitions and gel formation in aqueous dimethyl sulphoxide**, *Carbohydrate Research*, Vol. 252: 209-221

Hermida, L. G.; Gallardo, G. (2015) **Food Applications of Microencapsulated Omega-3 Oils**, *Microencapsulation and Microspheres for Food Applications*, Chapter 14: 271-299

Herrero, A. M.; Carmona, P.; Pintado, T.; Jiménez-Colmenero, F.; Ruíz-Capillas, C. (2011) **Infrared spectroscopic analysis of structural features and interactions in olive oil-in-water emulsions stabilized with soy protein**, *Food Research International*, Vol. 44: 360-366

Hifney, A. F.; Fawzy, M. A.; Abdel-Gawad, K. M.; Gomaa, M. (2016) **Industrial optimization of fucoidan extraction from *Sargassum* sp. and its potential antioxidant and emulsifying activities**, *Food Hydrocolloids*, Vol. 54: 77-88

Highberger, J. H. (1939) **The isoelectric point of collagen**, *Journal of the American Chemical Society*, Vol. 61 (9): 2302-2303

Ho, T. T. M. (2015) **Formation and characterisation of fucoidan-based polyelectrolyte multilayers for applications in biomaterials**, BSc. Thesis, University of South Australia

Hoffmann, J. (2014) **Regulatory Considerations of Encapsulation Used in the Food Industry**, *Microencapsulation in the Food Industy*, Chapter 29: 385-390

Hu, J.; Chen, H.-Q.; Zhang, Z. (2009) **Mechanical properties of melamine formaldehyde microcapsules for self-healing materials**, *Materials Chemistry and Physics*, Vol. 118: 63-70

Hu, Q.; Wang, T.; Zhou, M.; Xue, J.; Luo, Y. (2016) **Formation of redispersible polyelectrolyte complex nanoparticles from gallic acid-chitosan conjugate and gum arabic**, *International Journal of Biological Macromolecules*, Vol. 92: 812-819

Hu, Y.; Shen, J.; Shim, Y. Y.; Reaney, M. J. T. (2017) **Functional properties of flaxseed gum solutions**, *Journal of Experimental Food Chemistry*, Vol. 3 (2): 71

Huang, G.-Q.; Xiao, J.-X.; Jia, L.; Yang, J. (2015) **Complex Coacervation of O-Carboxymethylated Chitosan and Gum Arabic**, *International Journal of Polymeric Materials and Polymeric Biomaterials*, Vol. 64: 198-204

Huang, X.; Kakuda, Y.; Cui, W. (2001) **Hydrocolloids in emulsions: particle size distribution and interfacial activity**, *Food Hydrocolloids*, Vol. 15: 533-542

Ibrahim, S. B. (2007) **Mixing in the Mechanically Agitated Bioreactor: "A Matter of Being Stirred, not Shaken"**, *Journal of the Institution of Engineers, Malaysia*, Vol. 68 (3): 43-47

ICI Americas Inc. (1976) *The HLB SYSTEM a time-saving guide to emulsifier selection*

Imeson, A. P. (2009) **Carrageenan and furcellaran**, *Handbook of Hydrocolloids*, Chapter 7: 164-185

Ishida, T.; Mitarai, M.; Sugano, Y.; Shoda, M. (2003) **Role of Water-Soluble Polysaccharides in Bacterial Cellulose Production**, *Biotechnology and Bioenginnering*, Vol. 83 (4): 474-478

Islam, S.; Ma, W.; Yan, G.; Bekes, F.; Appels, R. (2012) **Novel approaches to modifying wheat flour processing characteristics and health attributes: from genetics to food technology**, *Breadmaking*, Chapter 11: 259-295

Izydorczyk, M. S. (2009) **Arabinoxylans**, *Handbook of Hydrocolloids*, Chapter 23: 653-692

Izydorczyk, M. S.; Cui, S. W.; Wang, Q. (2005) **Polysaccharide Gums: Structures, Functional Properties, and Applications**, *Food Carbohydrates*, Chapter 6

Jacobs, I. C. (2014) **Atomization and Spray-Drying Processes**, *Microencapsulation in the Food Industry*, Chapter 5: 47-56

Janiszewska, E.; Jedlińska, A.; Witrowa-Rajchert, D. (2015) **Effect of homogenization parameters on selected physical properties of lemon aroma powder**, *Food and Bioproducts Processing*, Vol. 94: 405-413

Jayakumar, R.; Reis, R. L.; Mano, J. F. (2006) **Phosphorous Containing Chitosan Beads for Controlled Oral Drug Delivery**, *Journal of Bioactive and Compatible Polymers*, Vol. 21: 327-340

Jégat, C.; Taverdet, J. L. (2000) **Stirring speed influence study on the microencapsulation process and on the drug release from microcapsules**, *Polymer Bulletin*, Vol. 44: 345-351

Jindal, N.; Khattar, J. S. (2018) **Microbial Polysaccharides in Food Industry**, *Biopolymers for Food Design*, Chapter 4: 95-123

Johnston, S. P.; Nickerson, M. T.; Low, N. H. (2015) **The physicochemical properties of legume protein isolates and their ability to stabilize oil-in-water emulsions with and without genipin**, *Journal of Food Science and Technology*, Vol. 52 (7): 4135-4145

Joiner, A. (2007) **The Cleaning of Teeth**, *Handbook for Cleaning/Decontamination of Surfaces*, Vol. 1: 371-405

Joshi, M.; Adhikari, B.; Aldred, P.; Panozzo, J. F.; Kasapis, S. (2011) **Physicochemical and functional properties of lentil protein isolates prepared by different drying methods**, *Food Chemistry*, Vol. 129: 1513-1522

Joshi, N.; Rawat, K.; Bohidar, H. B. (2018) **pH and ionic strength induced complex coacervation of Pectin and Gelatin A**, *Food Hydrocolloids*, Vol. 74: 132-138

Ju, Z. Y.; Kilara, A. (1998) **Gelation of pH-aggregated whey protein isolate solution induced by heat, protease, calcium salt, and acidulant**, *Journal of Agricultural and Food Chemistry*, Vol. 46 (5): 1830-1835

Juturu, V.; Gormley, J. J. (2013) **Bioactive Nutrients and Cardiovascular Disease**, *Bioactive Food as Dietary Interventions for Cardiovascular Disease*, Chapter 4: 73-88

Jyothi, N. V. N.; Prasanna, P. M.; Sakarkar, S. N.; Prabha, K. S.; Ramaiah, P. S.; Srawan, G. Y. (2010) **Microencapsulation techniques, factors influencing encapsulation efficiency**, *Journal of Microencapsulation*, Vol. 27 (3): 187-197

Kamble, R.; Maheshwari, M.; Paradkar, A.; Kadam, S. (2004) **Melt Solidification Technique: Incorporation of Higher Wax Content in Ibuprofen Beads**, *AAPS PharmSciTech*, Vol. 5 (4), Article 61

Kang, J.; Cui, S. W.; Chen, J.; Phillips, G. O.; Wu, Y.; Wang, Q. (2011) **New studies on gum ghatti (*Anogeissus latifolia*) part I. Fractionation, chemical and physical characterization of the gum**, *Food Hydrocolloids*, Vol. 25: 1984-1990

Karandikar, S.; Mirani, A.; Waybhase, V.; Patravale, V. B.; Patankar, S. (2017) **Nanovaccines for Oral Delivery-Formulation Strategies and Challenges**, *Nanostructures for Oral Medicine*, Chapter 10: 263-293

Karastogianni, S.; Girousi, S.; Sotiropoulos, S. (2016) **pH: Principles and Measurement**, *The Encyclopedia of Food and Health*, Vol. 4: 333-338

Kasala, D.; Yun, C.-O. (2016) **Polymer-Anchored Adenovirus as a Therapeutic Agent for Cancer Gene Therapy**, *Adenoviral Vectors for Gene Therapy*, Chapter 29: 707-737

Kaur, J.; Kaur, G. (2018) **Optimization of pH conditions and characterization of polyelectrolyte complexes between gellan gum and cationic guar gum**, *Polymers Advanced Technologies*, Vol. 29: 3035-3048

Kaur, L.; Singh, J.; Singh, H.; McCarthy, O. J. (2008) **Starch-cassia gum interactions: A microstructure – Rheology study**, *Food Chemistry*, Vol. 111: 1-10

Kaur, V.; Bera, M. B.; Panesar, P. S.; Kumar, H.; Kennedy, J. F. (2014) **Welan gum: Microbial production, characterization, and applications**, *International Journal of Biological Macromolecules*, Vol. 65: 454-461

Kayitmazer, A. B.; Strand, S. P.; Tribet, C.; Jaeger, W.; Dubin, P. L. (2007) **Effect of polyelectrolyte structure on protein-polyelectrolyte coacervates: coacervates of bovine serum albumin with poly(diallyldimethylammonium chloride) versus chitosan**, *Biomacromolecules*, Vol. 8: 3568-3577

Keller, M. W.; Sottos, N. R. (2006) **Mechanical properties of Microcapsules Used in a Self-Healing Polymer**, *Experimental Mechanics*, Vol. 46: 725-733

Khan, H.; Marya (2019) **Konjac (*Amorphophallus konjac*)**, *Nonvitamin and Nonmineral Nutritional Supplements*, Chapter 3.28: 307-312

Khounvilay, K.; Sittikijyothin, W. (2012) **Rheological behaviour of tamarind seed gum in aqueous solutions**, *Food Hydrocolloids*, Vol. 26: 334-338

Kilara, A.; Vaghela, M. N. (2018) **Whey proteins**, *Proteins in Food Processing*, Chapter 4: 93-126

Klassen, D. R.; Nickerson, M. T. (2012) **Effect of pH on the formation of electrostatic complexes within admixtures of partially purified pea proteins (legumin and vicilin) and gum Arabic polysaccharides**, *Food Research International*, Vol. 46: 167-176

Klemm, D.; Heublein, B.; Fink, H.-P.; Bohn, A. (2005) **Cellulose: Fascinating Biopolymer and Sustainable Raw Material**, *Angewandte Chemie International Edition*, Vol. 44: 3358-3393

Klinjapo, R.; Krasaekoopt, W. (2018) **Microencapsulation of Color and Flavor in Confectionery Products**, *Natural and Artificial Flavoring Agents and Food Dyes*, Chapter 14: 457-494

Klose, R. E. (1973) **Gums**, *CRC Handbook of Food Additives*, Chapter 7: 295-360

Klymchenko, A. S. (2017) **Solvatochromic and Fluorogenic Dyes as Environment-Sensitive Probes: Design and Biological Applications**, *Accounts of Chemical Research*, Vol. 50: 366-375

Komaiko, J. S.; McClements, D. J. (2016) **Formation of Food-Grade Nanoemulsions Using Low-Energy Preparation Methods: A Review of Available Methods**, *Comprehensive Reviews in Food Science and Food Safety*, Vol. 15: 331-352

Kooiman, P. (1968) **The chemical structure of kefiran, the water-soluble polysaccharide of the kefir grain**, *Carbohydrate Research*, Vol. 7: 200-211

Krawczyk, G.; Venables, A.; Tuason, D. (2009) **Microcrystalline cellulose**, *Handbook of Hydrocolloids*, Chapter 27: 740-759

KRÜSS GmbH (2010) **Determining the surface tension of liquids by measurements on pendant drops**, *Technical Note*

Kulig, D.; Zimoch-Korzycka, A.; Jarmoluk, A.; Marycz, K. (2016) **Study on Alginate-Chitosan Complex Formed with Different Polymers Ratio**, *Polymers*, Vol. 8: 167

Kupongsak, S.; Sathitvorapojjana, S. (2017) **Properties and Storage Stability of O/W Emulsion Replaced with Medium-Chain Fatty Acid Oil**, *Polish Journal of Food and Nutrition Sciences*, Vol. 67 (2): 107-115

Kurita, K. (2006) **Chitin and Chitosan: Functional Biopolymers from Marine Crustaceans**, *Marine Biotechnology*, Vol. 8: 203-226

Lacroix, M.; Le Tien, C. (2005) **Edible films and coatings from nonstarch polysaccharides**, *Innovations in Food Packaging*, Chapter 20: 338-361

Ladjal-Ettoumi, Y.; Boudries, H.; Chibane, M.; Romero, A. (2016) **Pea, chickpea and lentil protein isolates: physicochemical characterization and emulsifying properties**, *Food Biophysics*, Vol. 11 (1): 43-51

Lahaye, M.; Rochas, C. (1991) **Chemical structure and physico-chemical properties of agar**, *Hydrobiologia*, Vol. 221: 137-148

Laing, D. G.; Jinks, A. (1996) **Flavour perception mechanisms**, *Trends in Food Science & Technology*, Vol. 7: 387-389

Lam, R. S. H.; Nickerson, M. T. (2013) **Food proteins: A review on their emulsifying properties using a structure-function approach**, *Food Chemistry*, Vol. 141: 975-984

Lankalapalli, S.; Kolapalli, R. M. (2012) **Biopharmaceutical evaluation of diclofenac sodium controlled release tablets prepared from gum karaya – chitosan polyelectrolyte complexes**, *Drug Development and Industrial Pharmacy*, Vol. 38 (7): 815-824

Lazou, A.; Krokida, M. K. (2017) **Extrusion for Microencapsulation**, *Thermal and Nonthermal Encapsulation Methods*, Chapter 5

Lemetter, C. Y. G.; Meeuse, F. M.; Zuidam, N. J. (2009) **Control of the Morphology and the Size of Complex Coacervate Microcapsules During Scale-Up**, *AIChE Journal*, Vol. 55 (6): 1487-1496

Lewis, R. J. Sr. (1997) *Hawley's Condensed Chemical Dictionary*, 13th Edition

Li, J.; Liu, X.; Liang, X.; Zhang, M.; Han, L.; Song, J. (2019) **Simultaneous detection of five flavoring agents in chewing gum by ultrasound-microwave synergistic extraction coupled with gas chromatography**, *Scientific Reports*, Vol. 9

Li, J. Z. (2014) **The Use of Starch-Based Materials for Microencapsulation**, *Microencapsulation in the Food Industry*, Chapter 18: 195-210

Lim, L.-T.; Mendes, A. C.; Chronakis, I. S. (2019) **Electrospinning and electrospraying technologies for food applications**, *Advances in Food and Nutrition Research*, Vol. 88, Chapter 5: 167-234

Liu, F.; Chang, W.; Chen, M.; Xu, F.; Ma, J.; Zhong, F. (2020) **Film-forming properties of guar gum, tara gum and locust bean gum**, *Food Hydrocolloids*, Vol. 98: 105007

Liu, J.; Luo, D.; Li, X.; Xu, B.; Zhang, X.; Liu, J. (2016) **Effects of inulin on the structure and emulsifying properties of protein components in dough**, *Food Chemistry,* Vol. 210: 235-241

Liu, J.; Shim, Y. Y.; Wang, Y.; Reaney, M. J. T. (2015a) **Intermolecular interaction and complex coacervation between bovine serum albumin and gum from whole flaxseed (*Linum usitatissimum* L.)**, *Food Hydrocolloids*, Vol. 49: 95-103

Liu, S.; Cao, Y.-L.; Ghosh, S.; Rousseau, D.; Low, N. H.; Nickerson, M. T. (2010a) **Intermolecular Interactions during Complex Coacervation of Pea Protein Isolate and Gum Arabic**, *Journal of Agricultural and Food Chemistry*, Vol. 58: 552-556

Liu, S.; Elmer, C.; Low, N. H.; Nickerson, M. T. (2010b) **Effect of pH on the functional behaviour of pea protein isolate-gum Arabic complexes**, *Food Research International*, Vol. 43: 489-495

Liu, W.; Ye, A.; Singh, H. (2015b) **Progress in Applications of Liposomes in Food Systems**, *Microencapsulation and Microspheres for Food Applications*, Chapter 8: 151-170

Long, Y.; Song, K.; York, D.; Zhang, Z.; Preece, J. A. (2015) **Composite microcapsules with enhanced mechanical stability and reduced active ingredient leakage**, *Particuology,* Vol. 26: 40-46

Long, Y.; Vinvent, B.; York, D.; Zhang, Z.; Preece, J. A. (2010) **Organic-inorganic double shell composite microcapsules**, *Chemical Communications*, Vol. 46: 1718-1720

López-Franco, Y.; Higuera-Ciapara, I.; Goycoolea, F. M.; Wang, W. (2009) **Other exudates: tragacanth, karaya, mesquite gum and larchwood arabinogalactan**, *Handbook of Hydrocolloids*, Chapter 18: 495-534

Loret, C.; Meunier, V.; Frith, W. J.; Fryer, P. J. (2004) **Rheological characterisation of the gelation behaviour of maltodextrin aqueous solution**, *Carbohydrate Polymers*, Vol. 57: 153-163

Ma, Q.; Hu, D.; Wang, H.; Wang, L. (2016a) **Tara gum edible film incorporated with oleic acid**, *Food Hydrocolloids*, Vol. 56: 127-133

Ma, Q.; Hu, D.; Wang, L. (2016b) **Preparation and physical properties of tara gum film reinforced with cellulose nanocrystals**, *International Journal of Biological Macromolecules*, Vol. 86: 606-612

Macedo, J. P. F.; Fernandes, L. L.; Formiga, F. R.; Reis, M. F.; Júnior, T. N.; Soares, L. A. L.; Egito, E. S. T. (2006) **Micro-emultocrit Technique: A Valuable Tool for Determination of Critical HLB Value of Emulsions**, *AAPS PharmSciTech*, Vol. 7 (1): Article 21

Machiulskiene, V.; Nyvad, B.; Baelum, V. (2001) **Caries preventive effect of sugar-substituted chewing gum**, *Community Dentistry and Oral Epidemiology,* Vol. 29: 278-288

Madene, A.; Jacquot, M.; Scher, J.; Desobry, S. (2006) **Flavour encapsulation and controlled release - a review**, *International Journal of Food Science and Technology*, Vol. 41 (1): 1-21

Maeda, H.; Nakamura, A. (2009) **Soluble soybean polysaccharide**, *Handbook of Hydrocolloids*, Chapter 24: 693-709

Mäkinen, K. K. (2014) **Authorised EU health claims for xylitol and sugar-free chewing gum (SFCG)**, *Foods, Nutrients and Food Ingredients with Authorised EU Health Claims*, Chapter 3: 46-72

Mali, K. K.; Dhawale, S. C.; Dias, R. J. (2017) **Synthesis and characterization of hydrogel films of carboxymethyl tamarind gum using citric acid**, *International Journal of Biological Macromolecules*, Vol. 105: 463-470

Malvern Instruments Ltd. (2005) *Mastersizer 2000 – Integrated systems for particle sizing*

Malvern Instruments Ltd. (2007) **Understanding the views**, *Mastersizer 2000 User Manual*, Chapter 6: 6-1-6-16

Malvern Intruments Ltd. (2013) *Zetasizer Nano User Manual*, MAN0485, Issue 1.1

Mao, L.; Roos, Y. H.; Biliaderis, C. G.; Miao, S. (2017) **Food emulsions as delivery systems for flavor compounds: A review**, *Critical Reviews in Food Science and Nutrition*, Vol. 57 (15): 3173-3187

Mao, L.; Roos, Y. H.; Miao, S. (2014) **Flavour Release from Monoglyceride Structured Oil-in-Water Emulsions through Static Headspace Analysis**, *Food Biophysics*, Vol. 9: 359-367

Mariod, A. A. (2018) **Enhancement of Color Stability in Foods by Gum Arabic**, *Gum Arabic*, Chapter 12: 143-150

Mark, H. F. (2007) **Microencapsulation**, *Encyclopedia of Polymer Science and Technology*, Concise Third Edition: 691-694

Martins, E.; Renard, D.; Davy, J.; Marquis, M.; Poncelet, D. (2015) **Oil core microcapsules by inverse gelation technique**, *Journal of Microencapsulation*, Vol. 32 (1): 86-95

Martins, I. M.; Barreiro, M. F.; Coelho, M.; Rodrigues, A. E. (2014) **Microencapsulation of essential oils with biodegradable polymeric carriers for cosmetic applications**, *Chemical Engineering Journal*, Vol. 245: 191-200

Masuelli, M. A. (2013) **Hydrodynamic Properties of Whole Arabic Gum**, *American Journal of Food Science and Technology*, Vol. 1 (3): 60-66

Masumoto, N.; Yamaguchi, K.; Fujimoto, S. (2009) **Daily chewing gum exercise for stabilizing the vertical occlusion**, *Journal of Oral Rehabilitation*, Vol. 36: 857-863

McArdle, R.; Hamill, R.; Kerry, J. P. (2011) **Utilisation of hydrocolloids in processed meat systems**, *Processed Meats*, Chapter 10: 243-269

McClements, D. J. (2009) **Biopolymers in Food Emulsions**, *Modern Biopolymer Science*, Chapter 4: 129-166

Meiners, J. A. (2012) **Fluid bed microencapsulation and other coating methods for food ingredient and nutraceutical bioactive compounds**, *Encapsulation Technologies and Delivery Systems for Food Ingredients and Nutraceuticals*, Chapter 7: 151-176

Meng, Y.; Cloutier, S. (2014) **Gelatin and Other Proteins for Microencapsulation**, *Microencapsulation in the Food Industry*, Chapter 20: 227-239

Mentink, L. (1999) **β-Cyclodextrin Emulsion: Mecanism of Emulsification and Application to the Preparation of Green Metalworking Fluids**, *Proceedings of the Ninth International Symposium on Cyclodextrins*: 693-696

Merck (2020) https://www.sigmaaldrich.com/united-kingdom.html

MeSH database (2020) https://www.ncbi.nlm.nih.gov/

Meyer, D.; Blaauwhoed, J.-P. (2009) **Inulin**, *Handbook of Hydrocolloids*, Chapter 30: 829-848

Meyers, M. A. (2014) **Flavor release and application in chewing gum and confections**, *Microencapsulation in the Food Industry*, Chapter 34: 443-453

Migliori, M.; Gabriele, D.; Checchetti, A.; Battipede, B. (2010) **Compatibility analysis of pectin at different esterification degree from intrinsic viscosity data of diluted ternary solutions**, *Reactive & Functional Polymers*, Vol. 70: 863-867

Milanovic, J.; Manojlovic, V.; Levic, S.; Rajic, N.; Nedovic, V.; Bugarski, B. (2010) **Microencapsulation of Flavors in Carnauba Wax**, *Sensors*, Vol. 10: 901-912

Milov, D. E.; Andres, J. M.; Erhart, N. A.; Bailey, D. J. (1998) **Chewing Gum Bezoars of the Gastrointestinal Tract**, *Pediatrics*, Vol. 102 (2)

Mine, Y.; Yang, M. (2011) **Egg allergy**, *Improving the Safety and Quality of Eggs and Egg Products*, Chapter 13: 254-271

Mirafzali, Z.; Thompson, C. S.; Tallua, K. (2014) **Application of Liposomes in the Food Industry**, *Microencapsulation in the Food Industry*, Chapter 13: 139-150

Mishra, M. K. (2015) **Overview of Encapsulation and Controlled Release**, *Handbook of Encapsulation and Controlled Release*, Chapter 1: 3-19

Mishra, N.; Rai, V. K.; Yadav, K. S.; Sinha, P.; Kanaujia, A.; Chanda, D.; Jakhmola, A.; Saikia, D.; Yadav, N. P. (2016) **Encapsulation of Mentha Oil in Chitosan Polymer Matrix Alleviates Skin Irritation**, *AAPS PharmSciTech*, Vol. 17 (2): 482-492

Moradi, Z.; Kalanpour, N. (2019) **Kefiran, a branched polysaccharide: Preparation, properties and applications: A review**, *Carbohydrate Polymers*, Vol. 223: 115100

Morales, E.; Rubilar, M.; Burgos-Díaz, C.; Acevedo, F.; Penning, M.; Shene, C. (2017) **Alginate/Shellac beads developed by external gelation as a highly efficient model system for oil encapsulation with intestinal delivery**, *Food Hydrocolloids*, Vol. 70: 321-328

Moreno, F. J.; Clemente, A. (2008) **2S albumin storage proteins: What makes them food allergens?**, *The Open Biochemistry Journal*, Vol. 2: 16-28

Mortenson, M. A.; Reineccius, G. A. (2008) **Encapsulation and release of menthol. Part 1: the influence of OSAn modification of carriers on the encapsulation of L-menthol by spray drying**, *Flavour and Fragrance Journal*, Vol. 23: 392-397

Moschakis, T.; Murray, B. S.; Biliaderis, C. G. (2010) **Modifications in stability and structure of whey protein-coated o/w emulsions by interacting chitosan and gum arabic mixed dispersions**, *Food Hydrocolloids*, Vol. 24: 8-17

Mostafa, D. M.; Abd El-Alim, S. H.; Kassem, A. A. (2017) **Nanoemulsions: A New Approach for Enhancing Phytonutrient Efficacy**, *Nanotechnology Applications in Food*, Chapter 6: 107-127

Mostafavi, S. F.; Kadkhodaee, R.; Emadzadeh, B.; Koocheki, A. (2016) **Preparation and characterization of tragacanth-locust bean gum edible blend films**, *Carbohydrate Polymers*, Vol. 139: 20-27

Mourya, V. K.; Inamdar, N. N. (2008) **Chitosan-modifications and applications: Opportunities galore**, *Reactive & Functional Polymers*, Vol. 68: 1013-1051

Murray, J. C. F. (2009) **Cellulosics**, *Handbook of Hydrocolloids*, Chapter 25: 710-723

Muzzarelli, R. A. A. (1996) **Chitosan-based dietary foods**, *Carbohydrate Polymers*, Vol. 29: 309-316

Muzzarelli, R. A. A. (2009) **Chitin and chitosan hydrogels**, *Handbook of Hydrocolloids*, Chapter 31: 849-888

Nakamura, A.; Furuta, H.; Maeda, H.; Nagamatsu, Y.; Yoshimoto, A. (2000) **The structure of soluble soybean polysaccharide**, *Hydrocolloids*, Part 1: 235-241

Nakamura, A.; Takahashi, T.; Yoshida, R.; Maeda, H.; Corredig, M. (2004) **Emulsifying properties of soluble soybean polysaccharide**, *Food Hydrocolloids*, Vol. 18: 795-803

Nakamura, A.; Yoshida, R.; Maeda, H.; Corredig, M. (2006) **Soy soluble polysaccharide stabilization at oil-water interface**, *Food Hydrocolloids*, Vol. 20: 277-283

Nandi, L. G.; Guerra, J. P. T. A.; Bellettini, I. C.; Machado, V. G.; Minatti, E. (2013) **Properties of aqueous solutions of lentinan in the absence and presence of zwitterionic surfactants**, *Carbohydrate Polymers*, Vol. 98: 1-7

National Institute for Occupational Safety and Health (NIOSH) (2007) *NIOSH Pocket Guide to Chemical Hazards*

Nedovic, V.; Kalusevic, A.; Manojlovic, V.; Levic, S.; Bugarski, B. (2011) **An overview of encapsulation technologies for food applications**, *Procedia Food Science*, Vol. 1: 1806-1815

Nehete, J. Y.; Bhambar, R. S.; Narkhede, M. R.; Gawali, S. R. (2013) **Natural proteins: Sources, isolation, characterization and applications**, *Pharmacognosy Reviews*, Vol. 7 (14): 107-116

Nesterenko, A.; Alric, I.; Silvestre, F.; Durrieu, V. (2013a) **Vegetable proteins in microencapsulation: a review of recent interventions and their effectiveness**, *Industrial Crops and Products*, Vol. 42: 469-479

Nesterenko, A.; Alric, I.; Violleau, F.; Silvestre, F.; Durrieu, V. (2013b) **A new way of valorizing biomaterials: The use of sunflower protein for α-tocopherol microencapsulation**, *Food Research International*, Vol. 53 (1): 115-124

Ngan, L. T. K.; Wang, S.-L.; Hiep, Đ. M.; Luong, P. M.; Vui, N. T.; Đinh, T. M.; Dzung, N. A. (2014) **Preparation of chitosan nanoparticles by spray drying, and their antibacterial activity**, *Research on Chemical Intermediates*, Vol. 40: 2165-2175

Nie, S.; Cui, S. W.; Xie, M. (2018) **Psyllium Polysaccharide**, *Bioactive Polysaccharides*, Chapter 8 : 395-443

Nishinari, K.; Takemasa, M.; Yamatoya, K.; Shirakawa, M. (2009a) **Xyloglucan**, *Handbook of Hydrocolloids*, Chapter 19: 535-566

Nishinari, K.; Zhang, H.; Funami, T. (2009b) **Curdlan**, *Handbook of Hydrocolloids*, Chapter 20: 567-591

Nogourani, M. K.; Janghorbani, M.; Isfahan, R. K.; Beheshti, M. H. (2012) **Effects of Chewing Different Flavored Gums on Salivary Flow Rate and pH**, *International Journal of Dentistry*, Vol. 2012

O'Callaghan, K. A. M.; Kerry, J. P. (2016) **Preparation of low- and medium-molecular weight chitosan nanoparticles and their antimicrobial evaluation against a panel of microorganisms, including cheese-derived cultures**, *Food Control*, Vol. 69: 256-261

O'Kennedy, B. T. (2011) **Caseins**, *Handbook of Food Proteins*, Chapter 2: 13-29

O'Neil, M. J. (2013) *The Merck Index – An Encyclopedia of Chemicals, Drugs, and Biologicals*

O'Regan, J.; Ennis, M. P.; Mulvihill, D. M. (2009) **Milk proteins**, *Handbook of Hydrocolloids*, Chapter 13: 298-358

Ochirkhuyag, B.; Chobert, J.-M.; Dalgalarrondo, M.; Haertlé, T. (2000) **Characterization of mare caseins. Identification of αS1- and αS2-caseins**, *Lait*, Vol. 80: 223-235

Ojinnaka, C.; Jay, A. J.; Colquhoun, I. J.; Brownsey, G. J.; Morris, E. R.; Morris, V. J. (1996) **Structure and conformation of acetan polysaccharide**, *International Journal of Biological Macromolecules*, Vol. 19: 149-156

Ololade, O. (2018) **Processing and Modification of Gum Arabic in Specific Applications**, *Gum Arabic*, Chapter 11: 127-142

Oprea, A.-M.; Nistor, M.-T.; Profire, L.; Popa, M. I.; Lupusoru, C. E.; Vasile, C. (2013) **Evaluation of the controlled release ability of theophylline from xanthan/chondroitin sulfate hydrogels**, *Journal of Biomaterials and Nanobiotechnology*, Vol. 4: 123-131

Ouwehand, A. C.; Tiihonen, K.; Mäkeläinen, H.; Rautonen, N.; Hasselwander, O.; Sworn, G. (2009) **Non-starch polysaccharides in the gastrointestinal tract**, *Designing Functional Foods*, Chapter 5: 126-147

Overbeek, J. T. G.; Voorn, M. J. (1957) **Phase separation in polyelectrolyte solutions. Theory of complex coacervation**, *Journal of Cellular and Comparative Physiology*, Vol. 49 (S1): 7-26

Overduin, J.; Guérin-Deremaux, L.; Wils, D.; Lambers, T. T. (2015) **NUTRALYS® pea protein: characterization of in vitro gastric digestion and in vivo gastrointestinal peptide responses relevant to satiety**, *Food & Nutrition Research*, Vol. 59 (1): 1-9

Oxley, J. D. (2012a) **Coextrusion for food ingredients and nutraceutical encapsulation: principles and technology**, *Encapsulation Technologies and Delivery Systems for Food Ingredients and Nutraceuticals*, Chapter 6: 131-150

Oxley, J. D. (2012b) **Spray cooloing and spray chilling for food ingredient and nutraceutical encapsulation**, *Encapsulation Technologies and Delivery Systems for Food Ingredients and Nutraceuticals*, Chapter 5: 110-130

Oxley, J. (2014) **Overview of Microencapsulation Process Technologies**, *Microencapsulation in the Food Industry*, Chapter 4: 35-46

Padua, G. W.; Guardiola, L. V. (2015) **Microcapsules Produced from Zein**, *Microencapsulation and Microspheres for Food Applications*, Chapter 1: 3-20

Pal, R. (1996) **Multiple O/W/O Emulsion Rheology**, *Langmuir*, Vol. 12: 2220-2225

Paques, J. P. (2015) **Alginate Nanospheres Prepared by Internal or External Gelation with Nanoparticles**, *Microencapsulation and Microspheres for Food Applications*, Chapter 3: 39-55

Parida, K. R.; Panda, S. K.; Ravanan, P.; Roy, H.; Manickam, M.; Talwar, P. (2013) **Microparticles based drug delivery systems: Preparation and application in cancer therapeutics**, *International Archives of Applied Sciences and Technology*, Vol. 4 (3): 68-75

Park, J. K.; Jung, J. Y.; Khan, T. (2009) **Bacterial cellulose**, *Handbook of Hydrocolloids*, Chapter 26: 724-739

Park, J. K.; Khan, T. (2009) **Other microbial polysaccharides: pullulan, scleroglucan, elsinan, levan, alternant, dextran**, *Handbook of Hydrocolloids*, Chapter 21: 592-614

Parker, R.; Ring, S. G. (2001) **Aspects of the Physical Chemistry of Starch**, *Journal of Cereal Science*, Vol. 34: 1-17

Pedroche, J. (2015) **Utilization of Sunflower Proteins**, *Sunflower*, Chapter 13: 395-439

Pegg, A. M. (2012) **The application of natural hydrocolloids to foods and beverages**, *Natural Food Additives, Ingredients and Flavourings*, Chapter 8: 175-196

Pérez-Gago, M. B.; Rhim, J.-W. (2014) **Edible Coating and Film Materials: Lipid Bilayers and Lipid Emulsions**, *Innovations in Food Packaging*, Chapter 13: 325-350

Peyron, M.-A.; Woda, A. (2016) **An update about artificial mastication**, *Current Opinion in Food Science*, Vol. 9: 21-28

Pfeiffer, J. C.; Hollowood, T. A.; Hort, J.; Taylor, A. J. (2005) **Temporal Synchrony and Integration of Sub-threshold Taste and Smell Signals**, *Chemical Senses*, Vol. 30: 539-545

Phoeung, T.; Spanedda, M. V.; Roger, E.; Heurtault, B.; Fournel, S.; Reisch, A.; Mutschler, A.; Perrin-Schmitt, F.; Hemmerlé, J.; Collin, D.; Rawiso, M.; Boulmedais, F.; Schaaf, P.; Lavalle, P.; Frisch, B. (2017) **Alginate/Chitosan Compact Polyelectrolyte Complexes: A Cell and Bacterial Repellent Material**, *Chemistry of Materials*, Vol. 29: 10418-10425

Picone, C. S. F.; Cunha, R. L. (2013) **Chitosan-gellan electrostatic complexes: Influence of preparation conditions and surfactant presence**, *Carbohydrate Polymers*, Vol. 94: 695-703

Piermaria, J.; Diosma, G.; Aquino, C.; Garrote, G.; Abraham, A. (2015) **Edible kefiran films as vehicle for prebiotic microorganisms**, *Innovative Food Science and Emerging Technologies*, Vol. 32: 193-199

Piermaria, J. A.; de la Canal, M. L.; Abraham, A. G. (2008) **Gelling properties of kefiran, a food-grade polysaccharide obtained from kefir grain**, *Food Hydrocolloids*, Vol. 22: 1520-1527

Piermaria, J. A.; Pinotti, A.; Garcia, M. A.; Abraham, A. G. (2009) **Films based on kefiran, an exopolysaccharide obtained from kefir grain: Development and characterization**, *Food Hydrocolloids*, Vol. 23: 684-690

Plackett, R. L.; Burman, J. P. (1946) **The design of optimum multifactorial experiments**, *Biometrika*, Vol. 33 (4): 305-325

Polifka, J. E.; Habermann, J. (2015) **Anticoagulants, thrombocyte aggregation inhibitors, fibrinolytics and volume replacement agents**, *Drugs During Pregnancy and Lactation*, Chapter 2.9: 225-249

Post, A. E.; Arnold, B.; Weiss, J.; Hinrichs, J. (2012) **Effect of temperature and pH on the solubility of caseins: Environmental influences on the dissociation of α_S- and β-casein**, *Journal of Dairy Science*, Vol. 95: 1603-1616

Potineni, R. V.; Peterson, D. G. (2008a) **Influence of Flavor Solvent on Flavor Release and Perception in Sugar-Free Chewing Gum**, *Journal of Agricultural and Food Chemistry*, Vol. 56 (9): 3254-3259

Potineni, R. V.; Peterson, D. G. (2008b) **Mechanisms of Flavor Release in Chewing Gum: Cinnamaldehyde**, *Journal of Agricultural and Food Chemistry*, Vol. 56 (9): 3260-3267

Prata, A. S.; Grosso, C. R. F. (2015) **Production of microparticles with gelatin and chitosan**, *Carbohydrate Polymers*, Vol. 116: 292-299

PubChem Compound database (2020) https://www.ncbi.nlm.nih.gov/

Qi, X.; Tester, R. F. (2019) **Starch granules as active guest molecules or microorganism delivery systems**, *Food Chemistry*, Vol. 271: 182-186

Rabelo, R. S.; Tavares, G. M.; Prata, A. S.; Hubinger, M. D. (2019) **Complexation of chitosan with gum Arabic, sodium alginate and κ-carrageenan: Effects of pH, polymer ratio and salt concentration**, *Carbohydrate Polymers*, Vol. 223: 115120

Rabišková, M.; Valášková, J. (1998) **The influence of HLB on the encapsulation of oils by complex coacervation**, *Journal of Microencapsulation*, Vol. 15 (6): 747-751

Rahaiee, S.; Zare, M.; Jafari, S. M. (2019) **Nanostructures of silk fibroin for encapsulation of food ingredients**, *Biopolymer Nanostructures for Food Encapsulation Purposes*, Chapter 12: 305-331

Rahma, E. H. (1988) **Functional and electrophoretic characteristics of faba bean (Vicia faba) flour proteins as affected by germination**, *Die Nahrung*, Vol. 32 (6): 577-583

Rakhee; Mishra, J.; Sharma, R. K.; Misra, K. (2018) **Characterization Techniques for Herbal Products**, *Management of High Altitude Pathophysiology*, Chapter 9: 171-202

Ramos, P. E.; Silva, P.; Alario, M. M.; Pastrana, L. M.; Teixeira, J. A.; Cerqueira, M. A.; Vicente, A. A. (2018) **Effect of alginate molecular weight and M/G ratio in beads properties foreseeing the protection of probiotics**, *Food Hydrocolloids*, Vol. 77: 8-16

Ray, S. S. (2013) **Structure and Morphology Characterization Techniques**, *Clay-Containing Polymer Nanocomposites*, Chapter 3: 39-66

Rayment, P.; Ellis, P. R. (2003) **GUMS/Nutritional Role of Guar Gum**, *Encyclopedia of Food Sciences and Nutrition*: 3012-3021

Rennie, M. Y.; Whiteley, K. J.; Sled, J. G.; Adamson, S. L. (2014) **Scanning Electron Microscopy and Micro-Computed Tomography Imaging of the Utero- and Fetoplacental Circulations**, *The Guide to Investigation of Mouse Pregnancy*, Chapter 55: 637-648

Rezaei, L.; Safavi, M. S.; Shojaosadati, S. A. (2019) **Protein Nanocarriers for Targeted Drug Delivery**, *Characterization and Biology of Nanomaterials for Drug Delivery*, Chapter 8: 199-218

Righetto, A. M.; Netto, F. M. (2005) **Effect of Encapsulating Materials on Water Sorption, Glass Transition and Stability of Juice From Immature Acerola**, *International Journal of Food Properties*, Vol. 8: 337-346

Rijavec, T.; Bračko, S. (2007) **Smart dyes for medical and other textiles**, *Smart Textiles for Medicine and Healthcare*, Chapter 7: 123-149

Rinaudo, M. (2006a) **Characterization and Properties of Some Polysaccharides used as Biomaterials**, *Macromolecular Symposia*, Vol.245-246 (1): 549-557

Rinaudo, M. (2006b) **Chitin and chitosan: Properties and applications**, *Progress in Polymer Science*, Vol. 31: 603-632

Rochas, C. (1989) **Average Molecular Weight and Molecular Weight Distribution of Agarose and Agarose-Type Polysaccharides**, *Carbohydrate Polymers*, Vol. 10: 289-298

Roldan-Cruz, C.; Carmona-Ascencio, J.; Vernon-Carter, E. J.; Alvarez-Ramirez, J. (2016) **Electrical impedance spectroscopy for monitoring the gum Arabic-chitosan complexation process in bulk solution**, *Colloids and Surfaces A: Physicochemical and Engineering Aspects*, Vol. 495: 125-135

Rosa, D. (2006) **Making flavors do tricks**, *The Manufacturing Confectioner*, Vol. 86 (5): 81-86

Sabbah, M.; Giosafatto, C. V. L.; Esposito, M.; Di Pierro, P.; Mariniello, L.; Porta, R. (2019) **Transglutaminase Cross-Linked Edible Films and Coatings for Food Applications**, *Enzymes in Food Biotechnology*, Chapter 21: 369-388

Sakurai, K.; Maegawa, T.; Takahashi, T. (2000) **Glass transition temperature of chitosan and miscibility of chitosan/poly(N-vinyl pyrrolidone) blends**, *Polymer*, Vol. 41 (19): 7051-7056

Sadeghi, M. (2012) **Synthesis of a biocopolymer carrageenan-g-poly(Aam-co-IA)/montmorilonite superabsorbent hydrogel composite**, *Brazilian Journal of Chemical Engineering*, Vol. 29, No. 2: 295-305

Sagis, L. M. C. (2015) **Microcapsules with Protein Fibril-Reinforced Shells**, *Microencapsulation and Microspheres for Food Applications*, Chapter 2: 21-37

Salarbashi, D.; Bazeli, J.; Fahmideh-Rad, E. (2019) **Fenugreek seed gum: Biological properties, chemical modifications, and structural analysis – A review**, *International Journal of Biological Macromolecules*, Vol. 138: 386-393

Salgado, P. R.; Molina Ortiz, S. E.; Petruccelli, S.; Mauri, A. N. (2010) **Biodegradable sunflower protein films naturally activated with antioxidant compounds**, *Food Hydrocolloids*, Vol. 24: 525-533

Salles, C.; Chagnon, M.-C.; Feron, G.; Guichard, E.; Laboure, H.; Morzel, M.; Semon, E.; Tarrega, A.; Yven, C. (2011) **In-Mouth Mechanisms Leading to Flavor Release and Perception**, *Critical Reviews in Food Science and Nutrition*, Vol. 51: 67-90

Samimi, S.; Maghsoudnia, N.; Eftekhari, R. B.; Dorkoosh, F. (2019) **Lipid-Based Nanoparticles for Drug Delivery Systems**, *Characterization and Biology of Nanomaterials for Drug Delivery*, Chapter 3: 47-76

Sánchez, M. C.; Berjano, M.; Guerrero, A.; Brito, E.; Gallegos, C. (1998) **Evolution of the Microstructure and Rheology of O/W Emulsions During the Emulsification Process**, *The Canadian Journal of Chemical Engineering*, Vol. 76: 479-485

Sánchez-Vioque, R.; Clemente, A.; Vioque, J.; Bautista Palomas, J. D.; Et Millan, F. (1999) **Protein isolates from chickpea (Cicer arietinum L.): Chemical composition, functional properties and protein characterization**, *Food Chemistry*, Vol. 64 (2): 237-243

Sandberg, A.-S. (2011) **Developing functional ingredients: a case study of pea protein**, *Functional Foods*, Chapter 15: 358-382

Santiago de Alvarenga, E. (2011) **Characterization and Properties of Chitosan**, *Biotechnology of Biopolymers*, Chapter 5: 91-108

Santos, M. B.; dos Santos, C. H. C.; de Carvalho, M. G.; de Carvalho, C. W. P.; Garcia-Rojas, E. E. (2019) **Physicochemical, thermal and rheological properties of synthesized carboxymethyl tara gum (*Caesalpinia spinosa*)**, *International Journal of Biological Macromolecules*, Vol. 134: 595-603

Sarkar, S.; Gupta, S.; Variyar, P. S.; Sharma, A.; Singhal, R. S. (2012) **Irradiation depolymerized guar gum as partial replacement of gum Arabic for microencapsulation of mint oil**, *Carbohydrate Polymers*, Vol. 90: 1685-1694

Sax, N. I.; Bracken, S. C. (1979) **An Industrial Response to Chronic Health Hazards**, *Dangerous Properties of Industrial Materials*, Section 10B: 303-1106

Schmitt, C. (2009) **Protein-polysaccharide complexes and coacervates**, *Handbook of Hydrocolloids*, Chapter 16: 420-476

Semeijn, C.; Buwalda, P. L. (2018) **Potato Starch**, *Starch in Food*, Chapter 9: 353-372

Senoo, S.; White, A. J. (2017) **Analysis and design of wet-steam stages**, *Advances in Steam Turbines for Modern Power Plants*, Chapter 9: 165-218

Senuma, Y.; Franceschin, S.; Hilborn, J. G.; Tissières, P.; Bisson, I.; Frey, P. (2000) **Bioresorbable microspheres by spinning disk atomization as injectable cell carrier: from preparation to in vitro evaluation**, *Biomaterials*, Vol. 21: 1135-1144

Sessa, M.; Donsì, F. (2015) **Nanoemulsion-Based Delivery Systems**, *Microencapsulation and Microspheres for Food Applications*, Chapter 5: 79-94

Shanmugan, H.; Sathasivam, R.; Rathinam, R.; Arunkumar, K.; Carvalho, I. S. (2018) **Algal Biotechnology: An Update From Industrial and Medical Point of View**, *Omics Technologies and Bio-Engineering: Towards Improving Quality of Life*, Chapter 3: 31-52

Sharma, M.; Mondal, D.; Mukesh, C.; Prasad, K. (2014) **Preparation of tamarind gum based soft ion gels having thixotropic properties**, *Carbohydrate Polymers*, Vol. 102: 467-471

Sharma, R. (2019) **Whey Proteins in Functional Foods**, *Whey Proteins*, Chapter 17: 637-663

Sherazi, T. A. (2016) **Graft Polymerization**, *Encyclopedia of Membranes*

Shi, W.; Dumont, M.-J. (2014) **Processing and physical properties of canola protein isolate-based films**, *Industrial Crops and Products*, Vol. 52: 269-277

Shinde, U. A.; Nagarsenker, M. S. (2009) **Characterization of gelatin-sodium alginate complex coacervation system**, *Indian Journal of Pharmaceutical Sciences*, Vol. 71 (3): 313-317

Shit, S. C.; Shah, P. M. (2014) **Edible Polymers: Challenges and Opportunities**, *Journal of Polymers*: Vol. 2014:1-13

Shnoudeh, A. J.; Hamad, I.; Abdo, R. W.; Qadumii, L.; Jaber, A. Y.; Surchi, H. S.; Alkelany, S. Z. (2019) **Synthesis, Characterization, and Applications of Metal Nanoparticles**, *Biomaterials and Bionanotechnology*, Chapter 15: 527-612

Shukla, A.; Khan, E.; Srivastava, K.; Sinha, K.; Tandon, P.; Vangala, V. R. (2017) **Study of molecular interactions and chemical reactivity of the nitrofurantoin-3-aminobenzoic acid cocrystal using quantum chemical and spectroscopic (IR, Raman, ^{13}C SS-NMR) approaches**, *CrystEngComm*, Vol. 19: 3921-3930

Shukla, R.; Cheryan, M. (2001) **Zein: the industrial protein from corn**, *Industrial Crops and Products*, Vol. 13: 171-192

Silverson (2020) https://www.silverson.com/us/products/laboratory-mixers/

Singh, H.; Thompson, A.; Corredig, M. (2012) **Liposomes as food ingredients and nutraceutical delivery systems**, *Encapsulation Technologies and Delivery Systems for Food Ingredients and Nutraceuticals*, Chapter 11: 287-318

Singh, R.; Malviya, R.; Sharma, P. K. (2011) **Extraction and Characterization of Tamarind Seed Polysaccharide as a Pharmaceutical Excipient**, *Pharmacognosy Journal*, Vol. 3 (20): 17-19

Sobel, R.; Versic, R.; Gaonkar, A. G. (2014a) **Introduction to Microencapsulation and Controlled Delivery in Foods**, *Microencapsulation in the Food Industry*, Chapter 1: 3-12

Sobel, R.; Gundlach, M.; Su, C.-P. (2014b) **Novel concepts and challenges of flavor microencapsulation and taste modification**, *Microencapsulation in the Food Industry*, Chapter 33: 421-442

Soni, S. R.; Ghosh, A. (2018) **Grafting Onto Biopolymers: Application in Targeted Drug Delivery**, *Biopolymer Grafting*, Chapter 9: 335-389

Soottitantawat, A.; Takayama, K.; Okamura, K.; Muranaka, D.; Yoshii, H.; Furuta, T.; Ohkawara, M.; Linko, P. (2005) **Microencapsulation of l-menthol by spray drying and its release characteristics**, *Innovative Food Science and Emerging Technologies*, Vol. 6: 163-170

Southwest Research Institute (2015) **Micro-nano-encapsulation** [Brochure], San Antonio, Texas

Spence, C. (2015) **Multisensory Flavor Perception**, *Cell*, Vol. 161: 24-35

Sri, S. J.; Seethadevi, A.; Prabha, K. S.; Muthuprasanna, P.; Pavitra, P. (2012) **Microencapsulation: A review**, *International Journal of Pharma and Bio Sciences*, Vol. 3 (1): 509-531

Stevenson, D. G. (2009) **Cereal β-glucans**, *Handbook of Food Hydrocolloids*, Chapter 22: 615-652

Stone, B. A. (2009) **Chemistry of β-Glucans**, *Chemistry, Biochemistry, and Biology of 1-3 Beta Glucans and Related Polysaccharides*, Chapter 2.1: 5-46

Strixner, T.; Kulozik, U. (2011) **Egg proteins**, *Handbook of Food Proteins*, Chapter 7: 150-209

Sulieman, A. M. E.-H. (2018) **Gum Arabic as Thickener and Stabilizing Agents in Dairy Products**, *Gum Arabic*, Chapter 13: 151-165

Swaroop, A.; Bagchi, M.; Moriyama, H.; Bagchi, D. (2017) **Salient Features for Designing a Functional Beverage Formulation to Boost Energy**, *Sustained Energy for Enhanced Human Functions and Activity*, Chapter 25: 411-419

Sworn, G. (2009a) **Gellan gum**, *Handbook of Hydrocolloids*, Second Edition, Chapter 9: 204-227

Sworn, G. (2009b) **Xanthan gum**, *Handbook of Hydrocolloids*, Second Edition, Chapter 8: 186-203

Taggart, P.; Mitchell, J. R. (2009) **Starch**, *Handbook of Hydrocolloids*, Second Edition, Chapter 5: 108-141

Tajik, S.; Maghsoudlou, Y.; Khodaiyan, F.; Jafari, S. M.; Ghasemlou, M.; Aalami, M. (2013) **Soluble soybean polysaccharide: A new carbohydrate to make a biodegradable film for sustainable green packaging**, *Carbohydrate Polymers*, Vol. 97: 817-824

Takigami, S. (2009) **Konjac mannan**, *Handbook of Hydrocolloids*, Chapter 32: 889-901

Tan, S. H.; Mailer, R. J.; Blanchard, C. L.; Agboola, S. O. (2011) **Canola proteins for human consumption: Extraction, profile, and functional properties**, *Journal of Food Science*, Vol. 76 (1): R16-R28

Taulbee, D. N.; Maroto-Valer, M. M. (2000) **Centrifugation**, *Encyclopedia of Separation Science*: 17-40

Tarté, R. (2011) **Meat protein ingredients**, *Handbook of Food Proteins*, Chapter 4: 56-91

Thakur, S.; Thakur, V. K.; Arotiba, O. (2018) **History, Classification, Properties and Application of Hydrogels: An Overview**, *Hydrogels*, Chapter 2: 29-50

Thies, C. (2012) **Microencapsulation methods based on biopolymer phase separation and gelation phenomena in aqueous media**, *Encapsulation Technologies and Delivery Systems for Food Ingredients and Nutraceuticals*, Chapter 8: 177-207

Tiefenbacher, K. F. (2017a) **Technology of Main Ingredients – Sweeteners and Lipids**, *The Technology of Wafers and Waffles*, Chapter 3: 123-225

Tiefenbacher, K. F. (2017b) **Technology of Main Ingredients – Water and Flours**, *The Technology of Wafers and Waffles*, Chapter 2: 15-121

Tiwary, A. K.; Rana, V. (2010) **Cross-linked chitosan films: Effect of cross-linking density on swelling parameters**, *Pakistan Journal of Pharmaceutical Sciences*, Vol. 23 (4): 443-448

Tolve, R.; Galgano, F.; Caruso, M. C.; Tchuenbou-Magaia, F. L.; Condelli, N.; Favati, F.; Zhang, Z. (2016) **Encapsulation of health-promoting ingredients: applications in foodstuffs**, *International Journal of Food Sciences and Nutrition*, Vol. 67 (8): 888-918

Tontul, I.; Topuz, A. (2015) **Microencapsulation of Plant Oils Rich in Alpha-Linolenic Acid: Effect of Processing Parameters**, *Microencapsulation and Microspheres for Food Applications*, Chapter 13: 253-269

Trinetta, V.; Cutter, C. N. (2016) **Pullulan: A Suitable Biopolymer for Antimicrobial Food Packaging Applications**, *Antimicrobial Food Packaging*, Chapter 30: 385-397

Turgeon, S. L.; Laneuville, S. I. (2009) **Protein + Polysaccharide Coacervates and Complexes : From Scientific Background to their Application as Functional Ingredients in Food Products**, *Modern Biopolymer Science*, Chapter 11: 327-363

Turgeon, S. L.; Schmitt, C.; Sanchez, C. (2007) **Protein-polysaccharide complexes and coacervates**, *Current Opinion in Colloid & Interface Science*, Vol. 12: 166-178

Tyler, A. H. (1869) **Improved Chewing-Gum Compound**, Patent US93141

Uhlemann, J.; Schleifenbaum, B.; Bertram, H.-J. (2002) **Flavor Encapsulation technologies: An overview including recent developments**, *Perfumer & Flavorist*, Vol. 27 (September/October): 52-61

Uthayakumaran, S.; Wrigley, C. (2017) **Wheat: Grain-Quality Characteristics and Management of Quality Requirements**, *Cereal Grains*, Chapter 5: 91-134

van Ruth, S. M.; Roozen, J. P. (2000) **Influence of mastication and saliva on aroma release in a model mouth system**, *Food Chemistry*, Vol. 71: 339-345

Vasisht, N. (2014) **Selection of Materials for Microencapsulation**, *Microencapsulation in the Food Industry*, Chapter 16: 173-180

Veis, A.; Aranyi, C. (1960) **Phase separation in polyelectrolyte systems. I. Complex coacervates of gelatin**, *The Journal of Physical Chemistry*, Vol. 64 (9): 1203-1210

Velasco, J.; Dobarganes, M. C.; Márquez-Ruiz, G. (2000) **Oxidation of free and encapsulated oil fractions in dried microencapsulated fish oils**, *Grasas y Aceites*, Vol. 51 (6): 439-446

Vicente, A. A.; Cerqueira, M. A.; Hilliou, L.; Rocha, C. M. R. (2011) **Protein-based resins for food packaging**, *Multifunctional and Nanoreinforced Polymers for Food Packaging*, Chapter 22: 610-648

Villanueva, A.; Vioque, J.; Sánchez-Vioque, R.; Clemente, A.; Bautista, J.; Millán, F. (1999) **Production of an extensive sunflower protein hydrolysate by sequential hydrolysis with endo- and exo-proteases**, *Grasas y Aceites*, Vol. 50 (6): 472-476

Viscione, L. (2013) **Fibre-enriched beverages**, *Fibre-Rich and Wholegrain Foods*, Chapter 18: 369-388

Waglay, A.; Karboune, S.; Alli, I. (2014) **Potato protein isolates: Recovery and characterization of their properties**, *Food Chemistry*, Vol. 142: 373-382

Wallick, D. (2014) **Cellulose Polymers in Microencapsulation of Food Additives**, *Microencapsulation in the Food Industry*, Chapter 17: 181-193

Wandrey, C.; Bartkowiak, A.; Harding, S. E. (2010) **Materials for encapsulation**, *Encapsulation Technologies for Active Food Ingredients and Food Processing*, Chapter 3: 31-100

Wang, B.; Akanbi, T. O.; Agyei, D.; Holland, B. J.; Barrow, C. J. (2018) **Coacervation Technique as an Encapsulation and Delivery Tool for Hydrophobic Biofunctional Compounds**, *Role of Materials Science in Food Bioengineering*, Chapter 7: 235-261

Wang, C.; Chang, T.; Zhang, D.; Ma, C.; Chen, S.; Li, H. (2020) **Preparation and characterization of potato protein-based microcapsules with an emphasis on the mechanism of interaction among the main components**, *Journal of the Science of Food and Agriculture*, Vol. 100: 2866-2872

Wang, F.; Wang, D.; Wang, Q.; Yu, J.; Shi, J. (2019) **Impact of Welan Gum on Cement Paste Containing PCE Superplasticizers with Different Charge Densities**, *ChemistrySelect*, Vol. 4 (5): 1722-1726

Wang, H.; Gurau, G.; Rogers, R. D. (2012a) **Ionic liquid processing of cellulose**, *Chemical Society Reviews*, Vol. 41: 1519-1537

Wang, H.; Yang, B.; Sun, H. (2017) **Pectin-Chitosan Polyelectrolyte Complex Nanoparticles for Encapsulation and Controlled Release of Nisin**, *American Journal of Polymer Science and Technology*, Vol. 3 (5): 82-88

Wang, R.; Tian, Z.; Chen, L. (2011) **A novel process for microencapsulation of fish oil with barley protein**, *Food Research International*, Vol. 44: 2735-2741

Wang, Y.; Bamdad, F.; Song, Y.; Chen, L. (2012b) **Hydrogel particles and other novel protein-based methods for food ingredient and nutraceutical delivery systems**, *Encapsulation Technologies and Delivery Systems for Food Ingredients and Nutraceuticals*, Chapter 14: 412-450

Watson, M. A.; Lea, J. M.; Bett-Garber, K. L. (2017) **Spray drying of pomegranate juice using maltodextrin/cyclodextrin blends as the wall material**, *Food Science & Nutrition*, Vol. 5: 820-826

Webster, D. (2003) **pH – Principles and Measurement**, *Encyclopedia of Food Sciences and Nutrition*: 4501-4507

Whelehan, M.; Marison, I. W. (2011) **Microencapsulation using vibrating technology**, *Journal of Microencapsulation*, Vol. 28 (8): 669-688

Wielinga, W. C. (2009) **Galactomannans**, *Handbook of Hydrocolloids*, Chapter 10: 228-251

Williams, P. A.; Phillips, G. O. (2009a) **Gum arabic**, *Handbook of Hydrocolloids*, Chapter 11: 252-273

Williams, P. A.; Phillips, G. O. (2009b) **Introduction to food hydrocolloids**, *Handbook of Hydrocolloids*, Chapter 1: 1-22

Wong, S. W.; Yu, B.; Curran, P.; Zhou, W. (2009) **Characterising the release of flavour compounds from chewing gum through HS-SPME analysis and mathematical modelling**, *Food Chemistry*, Vol. 114: 852-858

Woodard & Curran, Inc. (2006) **Waste Characterization**, *Industrial Waste Treatment Handbook*, Chapter 5: 83-126

Wu, B.-C.; McClements, D. J. (2015) **Engineering Hydrogel Microspheres for Healthy and Tasty Foods**, *Microencapsulation and Microspheres for Food Applications*, Chapter 7: 131-149

Wu, X. Y.; Lee, P. I. (2000) **Preparation and Characterization of Inulin Ester Microspheres as Drug Carriers**, *Journal of Applied Polymer Science*, Vol. 77: 833-840

Wu, Y.; Ding, W.; Jia, L.; He, Q. (2015) **The rheological properties of tara gum (*Caesalpinia spinosa*)**, *Food Chemistry*, Vol. 168: 366-371

Wüstenberg, T. (2015) **General overview of food hydrocolloids**, *Cellulose and Cellulose Derivatives in the Food Industry: Fundamentals and Applications*, First Edition, Chapter 1: 1-68

Xiao, Z.; Liu, W.; Zhu, G.; Zhou, R.; Niu, Y. (2014) **A review of the preparation and application of flavour and essential oils microcapsules based on complex coacervation technology**, *Journal of the Science of Food and Agriculture*, Vol. 94 (8): 1482-1494

Xing, F.; Cheng, G.; Yang, B.; Ma, L. (2004) **Microencapsulation of Capsaicin by the Complex Coacervation of Gelatin, Acacia and Tannins**, *Journal of Applied Polymer Science*, Vol. 91: 2669-2675

Xing, F.; Cheng, G.; Yi, K.; Ma, L. (2005) **Nanoencapsulation of Capsaicin by Complex Coacervation of Gelatin, Acacia, and Tannins**, *Journal of Applied Polymer Science*, Vol. 96: 2225-2229

Xu, L.; Xu, G.; Liu, T.; Chen, Y.; Gong, H. (2013) **The comparison of rheological properties of aqueous welan gum and xanthan gum solutions**, *Carbohydrate Polymers*, Vol. 92: 516-522

Xu, X.; Visser, R. G. F. ; Trindade, L. M. (2014) **Starch Modification by Biotechnology: State of Art and Perspectives**, *Starch Polymers*, Chapter 4: 79-102

Xue, J.; Zhang, Z. (2008) **Preparation and characterization of calcium-shellac spheres as a carrier of carbamide peroxide**, *Journal of Microencapsulation*, Vol. 25 (8): 523-530

Xue, J.; Zhang, Z. (2009) **Physical, Structural, and Mechanical Characterization of Calcium-Shellac Microspheres as a Carrier of Carbamide Peroxide**, *Journal of Applied Polymer Science*, Vol. 113: 1619-1625

Yalkowsky, S. H.; He, Y.; Jain, P. (2010) *Handbook of Aqueous Solubility Data*, Second Edition

Yan, C.; Zhang, W. (2014) **Coacervation processes**, *Microencapsulation in the Food Industry*, Chapter 12**:** 125-137

Yang, F.; Xia, S.; Tan, C.; Zhang, X. (2013) **Preparation and evaluation of chitosan-calcium-gellan gum beads for controlled release of protein**, *European Food Research and Technology*, Vol. 237: 467-479

Yang, J.; Gao, C.; Lü, S.; Liu, M.; Zhang, X.; Liu, Z. (2015) **Cationic Starch Nanoparticles**, *Microencapsulation and Microspheres for Food Applications*, Chapter 4: 57-77

Yang, Z.; Peng, Z.; Li, J.; Li, S.; Kong, L.; Li, P.; Wang, Q. (2014) **Development and evaluation of novel flavour microcapsules containing vanilla oil using complex coacervation approach**, *Food Chemistry*, Vol. 145: 272-277

Young, N. W. G.; O'Sullivan, G. R. (2011) **The influence of ingredients on product stability and shelf life**, *Food and Beverage Stability and Shelf Life*, Chapter 5: 132-183

Youssef, M. K.; Wang, Q.; Cui, S. W.; Barbut, S. (2009) **Purification and partial physicochemical characteristics of protein free fenugreek gums**, *Food Hydrocolloids*, Vol. 23: 2049-2053

Yu, F.; Li, Z.; Zhang, T.; Wei, Y.; Xue, Y.; Xue, C. (2017) **Influence of encapsulation techniques on the structure, physical properties, and thermal stability of fish oil microcapsules by spray drying**, *Journal of Food Processing Engineering*, Vol. 40 (6): e12576

Zajda, M.; Aleksander-Kwaterczak, U. (2019) **Wastewater Treatment Methods for Effluents from the Confectionery Industry – an Overview**, *Journal of Ecological Engineering*, Vol. 20 (9): 293-304

Zajic, J. E.; Panchal, C. J. (1976) **Bio-Emulsifiers**, *CRC Critical Reviews in Microbiology*, Vol. 5 (1): 39-66

Zhang, H. (2011) **The Basic Properties of Building Materials**, *Building Materials in Civil Engineering*, Chapter 2: 7-28

Zhang, K.; Zhang, H.; Hu, X.; Bao, S.; Huang, H. (2012) **Synthesis and release studies of microalgal oil-containing microcapsules prepared by complex coacervation**, *Colloids and Surfaces B: Biointerfaces*, Vol. 89: 61-66

Zhang, L.; Zeng, X.; Fu, N.; Tang, X.; Sun, Y.; Lin, L. (2018a) **Maltodextrin: A consummate carrier for spray-drying of xylooligosaccharides**, *Food Research International*, Vol. 106: 383-393

Zhang, Y.; Baiocco, D.; Mustapha, A. N.; Zhang, X.; Yu, Q.; Wellio, G.; Zhang, Z.; Li, Y. (2020) **Hydrocolloids: Nova materials assisting encapsulation of volatile phase change materials for cryogenic energy transport and storage**, *Chemical Engineering Journal*, Vol. 382: 123028

Zhang, Y.; Kong, H.; Fang, Y.; Nishinari, K.; Phillips, G. O. (2013) **Schizophyllan: A review on its structure, properties, bioactivities and recent developments**, *Bioactive Carbohydrates and Dietary Fibre*: 53-71

Zhang, Y.; Zhang, Z.; Ding, Y.; Pikramenou, Z.; Li, Y. (2019) **Converting Capsules to Sensors for Nondestructive Analysis: From Cargo-Responsive Self-Sensing to Functional Characterization**, *ACS Applied Materials & Interfaces*, Vol. 11 (9): 8693-8698

Zhang, Y.; Zhang, Z.; Li, X.; Li, W.; Shen, X.; Wang, H. (2018b) **Effect of welan gum on the hydration and hardening of Portland cement**, *Journal of Thermal Analysis and Calorimetry*, Vol. 131: 1277-1286

Zhang, Z.; Adams, M. (2014) **Mechanical Properties of Single Microparticles and their Compaction Behavior**, *American Pharmaceutical Review*, Vol. 17 (1)

Zhang, Z.; Saunders, R.; Thomas, C. R. (1999) **Mechanical strength of single microcapsules determined by a novel micromanipulation technique**, *Journal of Microencapsulation*, Vol. 16 (1): 117-124

Zhang, Z.-Q.; Pan, C.-H.; Chung, D. (2011) **Tannic acid cross-linked gelatin-gum arabic coacervate microspheres for sustained release of allyl isothiocyanate: Characterization and *in vitro* release study**, *Food Research International*, Vol. 44: 1000-1007

Zhivkov, A. M. (2013) **Electrical Properties of Carboxymethyl Cellulose**, *Cellulose – Fundamental Aspects*, Chapter 8: 197-226

Züge, L. C. B.; Haminiuk, C. W. I.; Maciel, G. M.; Silveira, J. L. M.; Scheer, A. de P. (2013) **Catastrophic inversion and rheological behavior in soy lecithin and Tween 80 based food emulsions**, *Journal of Food Engineering*, Vol. 116: 72-77

Zuidam, N. J.; Shimoni, E. (2010) **Overview of Microencapsulates for Use in Food Products or Processes and Methods to Make Them**, *Encapsulation Technologies for Active Food Ingredients and Food Processing*, Chapter 2: 3-30